SYNTHESIS AND MODIFICATION OF METAL OXIDE NANOSTRUCTURES FOR SENSING APPLICATIONS

Thesis Submitted to

Delhi Technological University

for the Award of Degree of

DOCTOR OF PHILOSOPHY
in
DEPARTMENT OF APPLIED PHYSICS

Submitted by

DEEPIKA SANDIL

Under the Supervision of

Dr. NITIN K. PURI

&

PROF. S.C. SHARMA

Delhi Technological University
Bawana Road, Delhi 110042
India

JUNE 2019

DEDICATED TO….

MY MOTHER IN-LAW

LATE SMT. MALTI RANI SHARMA

&

MY BELOVED PARENTS

ACKNOWLEDGEMENTS

*It is an honor and privilege to express my heartfelt gratitude to my research supervisor –**Dr. Nitin K. Puri**, Associate Professor, Department of Applied Physics, Delhi Technological University, without whose guidance and encouragement this research simply would not have been possible. His knowledge and experience coupled with his caring attitude and teaching acumen have always been a source of inspiration and motivation throughout my journey at DTU. I shall forever cherish my time working under his direction and hope to have lifelong association with him and the university that has become a second home to me. I would like to wholeheartedly thank and convey my gratitude to my research co-supervisor- **Prof. Suresh C. Sharma**, DRC Chairman, Department of Applied Physics, for his exceptional mentoring and continuous support during the course of my research endeavours.*

*I would also like to express my sincere thanks and deepest gratitude to **Prof. Bansi D. Malhotra**, Department of Biotechnology, Delhi Technological University, Delhi and **Dr. Saurabh Srivastava**, Assistant Professor at Rajkiya Engineering College, Ambedkar Nagar (Uttar Pradesh) for their valuable research insights, support, and encouragement throughout my research work. They have mentored me in more ways than one and were always fervent in lending support, personally and professionally. Their knowledge and wisdom has not only helped me academically but also in developing my personality as an individual.*

*I thank all the members of department of Biotechnology, DTU especially **Shine Augustine** for constant support and creating a pleasant working environment.*

*My heartfelt thanks and appreciation to friends and colleagues - **Kamal Arora, Gaurav Sharma, Ritika Khatri** and **Kanika Sharma** who have been a part of my research endeavours at the Advanced Sensor Laboratory (ASL). Special thanks to **Ms. Mukesh Kumari** for her guidance and support.*

*Besides this, I am thankful to **Prof. Rinku Sharma**, Head of the Department, Department of Applied Physics, and honourable **Prof. Yogesh Singh**, Vice Chancellor, DTU for their enduring support in executing the research work efficiently. I also thank all the faculty members of the department of Applied Physics,*

DTU. I am also thankful to all the technical and office staff of the department who supported me during my research work.

I express my kind regards and gratitude to the management of my workplace- ***Bhagwan Parshuram Institute of Technology****, BPIT, New Delhi, for their support and encouragement at every stage. I also thank* ***Mrs. Mamta Choudhary*** *for her abundant support.*

I thank my parents, ***Mr. Vinod Vats*** *and* ***Mrs. Shakuntla Vats*** *for showering me with unconditional love throughout my life. Their unwavering belief in my abilities have forever instilled confidence and given me a sense of assurance that shaped me as an individual. I thank my grandmother (****Smt. Phoolwati Devi),*** *my sister (****Sonal)****, my brothers (****Shailesh and Bharat****), and my nephew (****Kanishk)*** *for their love, support and encouragement which kept propelling me towards my goals.*

I dedicate this work to the biggest blessing in my life, my daughter – ***Navya*** *and my husband* ***Gautam*** *for standing beside me at every stage of my research journey. Also, I would like to thank my father-in-law (****Gian Chand Sharma****), sister-in-law (****Kavita****), and brother-in-law (****Gaurav****) and my niece (****Bhoomi****) and nephew (****Adhiraj****) for their unabated faith in me.*

Finally, I thank the almighty for being present around me always.

Thank you!!!

Deepika Sandil

ABSTRACT

Synthesis and Modification of Metal Oxide Nanostructures for Sensing Applications

Metal oxide semiconductors have been known as smart and advanced functional materials showing potential applications in various fields such as solar cells, smart windows, photocatalysis, and sensors etc. However, the confinement of dimensions of these materials in the nano range has remarkably tailored their physical and chemical properties making them novel in their characteristics. Based upon this, in recent years, tungsten trioxide (WO_3) evolved as one of the most researched materials due to its simple and economic synthesis approach, high chemical stability, and good electro chemical kinetics. WO_3 is found to exist in different polymorphs such as orthorhombic, monoclinic, tetragonal, and hexagonal phase which depends on synthesis parameters. These different crystal systems modify the electronic structure of WO_3 and thus influence its electronic properties and hence electrochemical kinetics.

In the present study, we have focused our attention towards the synthesis of different dimensional WO_3 nanostructures existing in different crystal systems. For a facile and cost-effective production, we have employed hydrothermal synthesis process for synthesis of different WO_3 nanostructures and composites. These WO_3 based nanostructures have found wide range of applications such as optical and electronic based nanodevices, photocatalysis, and biomedical sensing applications. Among all these, applications of WO_3 based nanostructures towards the development diagnostic biosensors have aroused much interest. For the biosensing applications, successful immobilization of bio-entities onto the diagnostic platform is crucial. As

interaction of nanostructure with the biological entities get highly influenced by its crystal phase, morphology, electronic properties, surface chemistry and functionalization of the surface. Our study further focuses on investigations of the biosensing applications of different WO_3 nanostructures based upon their electro-chemical behaviour. Among different biosensing applications, recently, cardiovascular diseases (CVDs) have raised major health burden leading to prime cause of death. Acute myocardial infarction (AMI) is one of the CVDs caused by the necrosis of myocardial tissues due to ischemia. The insufficient fact details regarding the diseases and its classification seems to delay the diagnosis process of the disease in the clinical laboratories. Learning the concentration of cardiac biomarkers plays a significant role in the diagnosis of AMI. Among other cardiac biomarkers, cardiac Troponin I (cTnI) is a highly cardiac specific muscle protein biomarker which shows significant increase in its value with the onset of myocardial necrosis.

Hence in this thesis, our main focus is on studying different WO_3 nanostructures, characterizations, and functionalization procedures to be used for the diagnosis of the AMI by detecting cardiac biomarker cTnI.

In this context, **Chapter 1** highlights the description of metal oxide nanostructures especially tungsten trioxide (WO_3) nanostructures in terms of their fundamental properties, different synthesis processes and its applications with the main emphasis in biosensing. Efforts have been put to present a comprehensive literature review on detection of cardiac troponin I using electrochemical sensing.

Chapter 2 briefs the different materials and chemicals used for the synthesis and modification of WO_3 nanostructures and the fabrication of nanostructured tungsten trioxide (nWO_3) based biosensors for cardiac detection employing electrochemical techniques. Further, the different analytical approach is employed for

the characterization of the nWO_3, modified nWO_3 electrodes, and immunoelectrodes. Endeavours have also been made to brief the protocols used for the surface functionalization and antibody immobilization.

Chapter 3 demonstrates the fabrication of 3-aminopropyl tri-ethoxy saline (APTES) conjugated ***tungsten trioxide nanoparticles*** (APTES/WO_3 NPs) based platform for cardiac Troponin I (cTnI) detection. The WO_3 NPs has been synthesized using hydrothermal synthesis route. The electrochemical response studies of the fabricated immunoelectrode show sensitivity as 26.56 Ω $ng^{-1}mL\ cm^{-2}$ in a wide linear detection range 1- 250 ng mL^{-1}. Also, the proposed platform shows the stability of 4 weeks.

Chapter 4 reports the development of 2-dimensional (2-D) based platform for the detection of cardiac biomarker cTnI. The synthesis and fabrication of ***tungsten trioxide nanosheet*** (WO_3 NS) based platform is reported for selective and quantitative detection of the cTnI biomarker. The fabricated immunoelectrode (anti-cTnI/APTES/WO_3 NS/ITO) exhibits improved sensitivity as 30.8 Ω ng^{-1} mL cm^{-2} along with good stability up to 5 weeks. These enhanced characteristics of the immunoelectrode can be attributed to the high loading of cTnI antibodies onto WO_3 NS matrix due to the enhanced active surface area provided by WO_3 NS. The proposed immunoelectrode platform also showed a better result with the spiked serum samples.

Chapter 5 describes the development of a sensitive and a label-free electrochemical immunosensing platform for the detection of a cTnI biomarker using ***tungsten trioxide nanorods*** (WO_3 NRs) as a matrix. The impedimetric response study of the proposed immunoelectrode shows extremely high sensitivity as 6.81($K\Omega$ $ng^{-1}mL\ cm^{-2}$). The excellent selectivity and good reproducibility of the proposed

immunoelectrode have been attributed to the 1-D WO_3 NRs which provide an efficient direct electrical conduction path between the electrodes and the immobilized biomolecules.

Chapter 6 illustrate the advantages of the integration of WO_3 nanorods onto electro-active material reduced graphene oxide (RGO for electrochemical detection of a cTnI biomarker using ***tungsten trioxide–reduced graphene oxide (WO_3-RGO) nanocomposite*** as a matrix. The synergistic behaviour between RGO and WO_3 nanorods has allowed the fabricated immunoelectrode to exhibit enhanced heterogeneous electron transfer rate constant (K_o = 2.4 $\times 10^{-4}$ cm s^{-1}) resulting in improved biosensor efficiency. The immunoelectrode exhibit good sensitivity as 58.24 mA/cm^2 per decade for an extended detection range 0.01- 250 ng mL^{-1} with the stability up to 30 days. The validation of fabricated immunoelectrode with cardiac patient samples has demonstrates the clinical application of the proposed biosensing platform too.

Chapter 7 summarizes and discusses the future scope of this thesis work.

LIST OF FIGURES

LIST OF TABLES

LIST OF PUBLICATIONS

1. **Deepika Sandil**, Saurabh Kumar, Kamal Arora, Saurabh Srivastava, B. D. Malhotra, S. C. Sharma, and Nitin K. Puri. "Biofunctionalized nanostructured tungsten trioxide based sensor for cardiac biomarker detection." *Materials Letters* 186 (2017): 202-205.
2. **Deepika Sandil**, Saurabh Srivastava, B. D. Malhotra, S. C. Sharma, and Nitin K. Puri. "Bio-functionalized tungsten trioxide-reduced graphene oxide nanocomposites for sensitive electrochemical immunosensing of cardiac biomarker." *Journal of Alloys and Compounds* 763 (2018): 102-110.
3. **Deepika Sandil**, Suresh C. Sharma, and Nitin K. Puri. "Protein-functionalized WO_3 nanorods–based impedimetric platform for sensitive and label-free detection of a cardiac biomarker." *Journal of Materials Research* (2019): 1-10
4. **Deepika Sandil**, and Nitin K. Puri. "2D Nanostructured Tungsten Trioxide Based Electrochemical Immunosensor for Cardiac Troponin I Detection." (**Communicated** in *New Journal of Chemistry, RSC (2019)*

LIST OF CONFERENCES

1. "Bio-functionalized reduced graphene oxide supported tungsten trioxide nanorods for cardiac biomarker detection" **Deepika Sandil**, Saurabh Srivastava, Nitin K. Puri., **17th International Conference on Thin Films** (ICTF 2017), November 13th – 17th, 2017, NPL, New Delhi (**Received Best Poster Award)**

2. "Synthesis and Fabrication of functionalized Nanostructured CuO platform for electrochemical Detection of cancer biomarker**" Deepika Sandil**, S.C. Sharma, Nitin K. Puri, **17th International Meeting on Chemical Sensors (**IMCS 2018), July 15th – 19th, 2018, Vienna, Austria .

LIST OF ACRONYMS

0-D	Zero dimensional
1-D	One dimensional
2-D	Two dimensional
3-D	Three dimensional
A	Ampere
Ab	Antibody
AFM	Atomic force microscopy
Ar	Argon
Ag	Antigen
Ag/AgCl	Silver/silver chloride
AMI	Acute myocardial infarction
Anti-cTnI	Cardiac Troponin I antibody
APTES	3- Aminopropyltriethoxysilane
BSA	Bovine serum albumin
CA	Contact angle
CEA	Carcinoembryonic antigen
CRP	C-reactive protein
CK-MB	Creatine Kinase isoenzyme
CV	Cyclic Voltammetry
cTn	Cardiac troponin
cTnI	Cardiac troponin I
CRP	C-reactive protein
CVD	Cardio vascular disease
DPV	Differential pulse voltammetry
e^-	Electron
EA	Ethanol amine
ELISA	Enzyme-linked immunosorbent assay
EIS	Electrochemical impedance spectroscopy
EDC	N-(3-Dimethylaminopropyl)-N-ethylcarbodiimide

eV	Electron volt
$[Fe(CN)_6]^{3-}$	Ferricyanide
$[Fe(CN)_6]^{4-}$	Ferrocyanide
FESEM	Field emission scanning electron microscope
FT-IR	Fourier transform infrared
HRTEM	High resolution transmission electron microscope
ITO	Indium tin oxide
Mb	Myoglobin
MO	Metal oxide
NHS	N-Hydroxy succinimide
PBS	Phosphate buffer saline
PLD	Pulse laser deposition
Pt	Platinum
R_{CT}	Charge transfer resistance
RGO	Reduced graphene oxide
RSD	Relative standard deviation
SEM	Scanning electron microscope
TEM	Transmission electron microscope
WO_3	Tungsten trioxide
nWO_3	Nanostructured tungsten trioxide
XRD	X-ray diffraction

TABLE OF CONTENTS

CHAPTER 1

Introduction and literature Review

This chapter discusses the importance of metal oxide based nanostructures and their different applications. Special emphasis has been given to tungsten trioxide (WO_3) nanostructures including their different synthesis processes. Further, this chapter discusses the detailed biosensing application of these WO_3 nanostructures having different morphologies. The chapter continues to discuss cardio vascular disease (CVD) and the role cardiac biomarkers towards the diagnosis of CVD. Thereafter we discussed the role of WO_3 nanostructures towards the development of biosensors.

1.1 Nanotechnology

Nanotechnology has been defined as an engineered science which involves the understanding and manipulation of structures in the dimension range of 1-100 nanometers (nm). These nano-dimensions based materials also known as nanomaterials exhibit many novel physicochemical characteristics such as high chemical stability, enhanced thermal and electrical conductivity, improved catalytic activity and many others [1-2]. Materials with such characteristics are thus capable of exploring new structures, systems, and devices [3-5]. This revolutionalized technology has benefited the society in every aspect i.e., fabrication of nanosensors that can constantly monitor the environmental changes, development of biosensors for the diagnosis and prognosis of various diseases, and many others [6-9].

Nanomaterials have been defined as the crystalline or amorphous compounds whose dimension lies in the range of 1–100 nm. These materials have significantly different features and characteristics relative to the same materials having bigger or larger dimensions. The properties at nanoscale become sensitive with respect to their sizes. This sensitiveness can be related to the availability of more percentage of surface atoms which enhanced the chemical reactivity at the material surface. The materials with enhanced chemical reactivity thus become potential for many industrial applications including catalysis and sensing [10-11]. To meet further challenges, the selection of the fabrication technique of functional nanomaterials with controlled morphology is required. The numerous works in this direction is still going in search of finding new economical methods of synthesizing nanomaterials along with superior characteristics. The different synthesis approach made by the researchers introduces the different class of nanomaterials, particularly based on the dimensions results in 0-dimensional (0-D), 1-dimensional (1-D), 2-dimensional (2-D), and 3-dimensional (3-D) nanomaterials as shown in **Figure 1.1**. These different dimensional nanomaterials exhibit variant morphologies and present potential in different fields.

Quantum dots and nanoparticles (less than 20 nm) are classified as 0-D structures in which movements of electrons are confined in all 3 dimensions. Nano-rods, nanofibres, and nanowires are the examples of 1-D structures in which electrons have free motion only in one direction while in rest two, its motion is confined. The 2-D structures including thin films, nanosheets, and nanoflowers exhibits electrons motion freely in the X-Y plane and have found its application in the fabrication of nanodevices. Further, in 3-D structures (multi-layers, and polycrystalline forms), electrons have free motion in all X, Y, Z directions and exhibits as a compact polycrystalline structure with nanosize crystals.

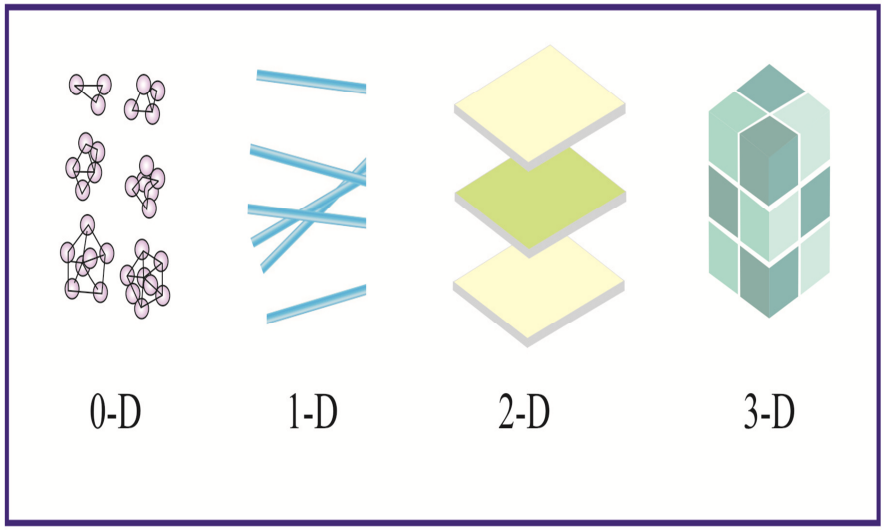

Figure 1.1: Classification of nanomaterials on the basis of dimensions

1.1.1 Metal Oxide Nanostructure

From the application point of view, the semiconductor based nanomaterials are the most promising class of nanomaterials. The distinctive electronic and electrical properties of the semiconductor make it a significant candidate for the exploration. Among different semiconductor based materials, metal oxides materials are more applicable in various fields due to their exceptional functional properties and most importantly, the thermal and chemical stability exhibited by these materials [12]. This can also be due to the large electro-negativity of O_2 which results in strong bonding. Nevertheless, nanostructuring of metal oxides

materials will definitely enhance the performance of the material due to the increased surface-to-volume ratio, high surface energy, spatial confinement, strong adherence to the surface [13]. The fabrication of metal oxide nanostructures with different morphologies and incorporation of other structures in their matrix will definitely improve their properties and can unlock new approach for their application in various fields.

Metal oxide-based nanomaterials exhibit a large variety of structural design and multiple morphologies with distinctive surface properties. The unique and tunable characteristics of these nanomaterials including thermal, optical, catalytic, electrical, and electrochemical made them an ideal candidate in various application fields such as super capacitors, environmental monitoring, fuel cells, solar cells, chemical sensors and biosensors [14-17]. Among many, tungsten trioxide (WO_3) nanostructures have been well studied and shown great interest due to its outstanding performances as an electrochromic material, a photo-catalytic applicant, anodic electrode material in Li-ion batteries, and field emitters [18-21]. The major key features including superior thermal stability, simple and ease synthesis of different morphologic structures, enhanced electrochemical kinetics and low cost and wide availability makes it an interesting candidate to explore.

1.2 Nanostructured Tungsten Trioxide (nWO_3)

Tungsten trioxide is an n-type transition metal oxide formed with filled oxygen (O) 2p orbitals and empty tungsten (W) 5d orbitals [22-23]. It is an efficient functional material exhibiting potential applications due to its stability in both physical and chemical states, the existence of cation intercalated states and structural flexibility [24-25]. However, studying WO_3 nanostructures has unlocked more potential due to its distinctive characteristics and properties with respect to its bulk form. The enhancement in the properties and characteristics of the nanostructured WO_3 (nWO_3) has been attributed to the: i) large surface to volume ratio; which provides large active surface area for the physicochemical interaction, and ii)

quantum confinement; which significantly improves the charge transportation, electrical and optical characteristics.

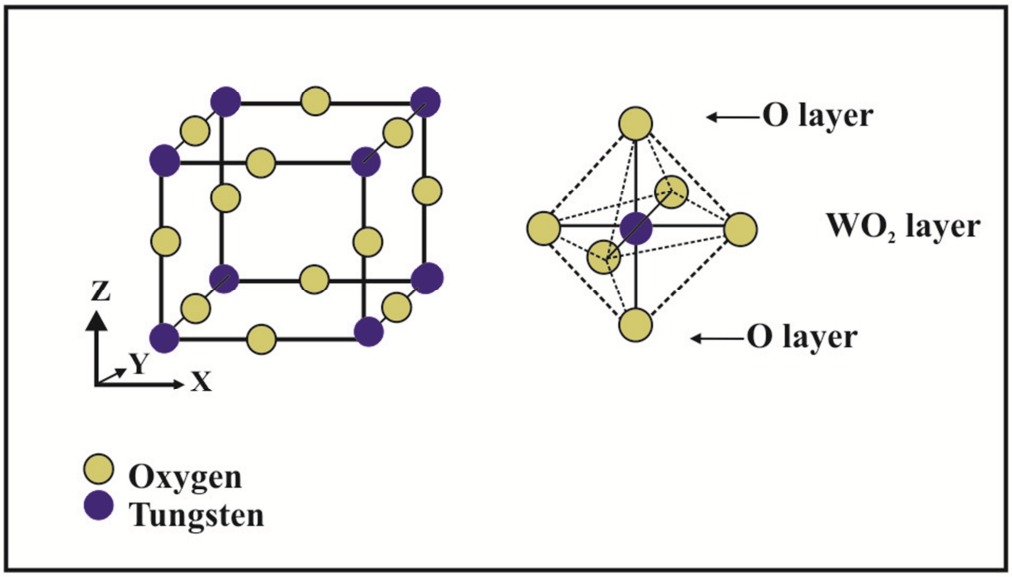

Figure 1.2: Primitive unit cell structure of WO_3

An ideal tungsten trioxide (WO_3) is a 3-D cubic network structure consisting of WO_6 octahedra unit linked with corner sharing configurations. This structure is identical to ReO_3 perovskite unit structure but not as symmetrical as ReO_3 due to its distorted structure [26]. **Figure 1.2** represent a primitive unit structure of WO_3, where cornered sites of the unit cell are occupied by W ions while O ions at the bisected site. The variation in the W─O bond length and position of W atom results in the existence of different phases of WO_3 which are stable within a defined temperature scale. These different phase structures of WO_3 are monoclinic II, monoclinic I, triclinic, orthorhombic, tetragonal, hexagonal and cubic. **Figure 1.3** represent one of the phase structure of WO_3 exhibiting tunnel-like structure (hexagonal or trigonal) which make it an ideal host for cations intercalation and diffusion process [27]. The formation of these phases is highly dependent on the morphology of the synthesized WO_3, which again depends on the synthesis approach and precursors employed. This led to the

discovery and study of the new synthesis approaches for the different phases and dimensions of WO_3 and its composites.

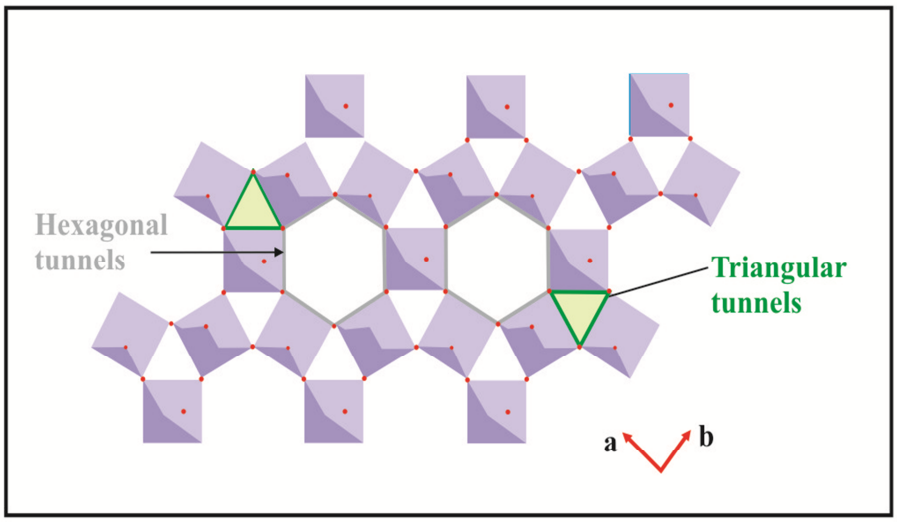

Figure 1.3: Phase structure of WO_3 exhibiting Tunnel like structure

The existence of sub or non-stoichiometric WO_3 structures has been studied well due to its oxygen deficient lattice units formed with the edge-sharing WO_6 octahedra units [28]. The non-stoichiometric lattice structure of WO_X ($2.1< x< 3$) can withhold the considerable O_2 deficiency by exhibiting partially reduced W^{5+} states which strongly influenced its energy band and conducting nature. Solonin et al. had reported the formation of non-stoichiometric phase at the initial stage of reduction of hexagonal phased WO_3 and studied its electronic structure [29]. This shows that WO_3 undergoes a structural change in a reduction process. The number of non-stoichiometric WO_X structures including $W_{18}O_{49}$, $W_{20}O_{58}$, and $W_{24}O_{68}$ are also well studied which are formed due to the corner sharing WO_6 and partial edge sharing [30]. Hence it can be concluded that WO_3 material can gain the additional merits features due to its sub-stoichiometric structures. Another most studied structure of WO_3 is the WO_3 hydrates (WO_3. nH_2O) which are formed during the chemical synthesis process. The water contents of these hydrates play a significant role in crystal lattice formation [31].

$WO_3.2H_2O$ (dehydrate), $WO_3.H_2O$ (monohydrate), $WO_3.0.5H_2O$ (semi-hydrate), and $WO_3.0.33\ H_2O$ is the most observed hydrates structures of WO_3.

1.2.1 Fundamental Properties of Nanostructured WO_3

The fundamental properties of nanostructured WO_3 are exceptionally unique and display distinctive characteristics. The electronic property of the WO_3 is one of the fundamental properties of WO_3 which shows modification with the change in its crystal structure. The energy band-gap (Eg) of WO_3 expressed as the difference between the energy levels of the valence band and the conduction band resulted from the filled oxygen (O) 2p orbitals and by the empty tungsten (W) 5d orbitals respectively [32]. The amorphous form of WO_3 structure, most distorted structure exhibits large Eg ~ 3.25 eV, while bulk WO_3 possess 2.62 eV (Eg) in monoclinic phase. The transformation of WO_3 from bulk state to nano state has shown quantum confinement effect which results in a blue shift in the band-gap with the reduction in grain size [33]. Experimentally, the measured band-gap energy of WO_3 lies in the range of 2.5–3.2 eV which is suitable for absorbing approximately 30 % of solar radiation. This characteristic of WO_3 makes it a potential candidate as a visible light photocatalyst [34]. Further, a pure stoichiometric WO_3 is found to be highly transparent to a visible spectrum of electromagnetic radiations while it exhibits yellowish colour for small band-gap energies. The amount of light absorbed by the WO_3 is generally expressed in terms of absorption coefficient (α) given by the **Equation 1.1**:

$$\alpha(\varepsilon) \sim (\varepsilon - Eg)\eta \qquad \textbf{(1.1)}$$

where ε denotes the photon energy (ε = hν, greater than Eg) and η represent the quantum efficiency. For indirect transitions, η = 2 and for direct transition η = ½. Moreover, the superior electrical conductivity characteristic of WO_3 is also well studied and has found its potential application in sensing applications. The electrical conductivity of an n-type WO_3

is strongly depend on the density of free electrons available in the conduction band which further depends on the presence of defects in the crystal [35]. The conductivity of the WO_3 can be modified with the variation in various factors such as a number of dopants, thickness of a film, grain size, and phase [36]. All these are related to structural modification which strongly depends on the synthesis route of WO_3 and its growth mechanism. Patel et al. has shown in his work that synthesis of WO_3 films using sputtering and thermal deposition techniques exhibits comparatively high electron mobility and carrier concentration as 6.5 cm^2 V^{-1} s^{-1} and 5×10^{19} cm^{-3} respectively [37]. Further, Rui et al. investigated in their work that 1-D non-stoichiometric WO_3 can exhibit high carrier mobility as 40 cm^2 V^{-1} s^{-1} [38]. Thus we conclude from above discussions that with the variation in structure of WO_3, enhanced electrical conductivity can be achieved.

1.3 Synthesis Techniques of Nanostructured WO_3

The synthesis of WO_3 and WO_3 nanostructures have been reported by employing different strategies. Broadly, there are two synthesis strategies which are preferred; first as a top-down strategy which involves physical approach such as sputtering or thermal evaporation, and second is a bottom-up strategy which involves both physical and chemical approach. For the fabrication of tungsten trioxide and its nanostructures of various dimensions (0-D, 1-D, and 2-D) and designing of miniaturized devices, bottom-up approach is generally preferred which make use of specific and non-covalent interaction for the synthesis of nanostructures [39]. Broadly, the most preferred physical techniques used for the synthesis of WO_3 include thermal evaporation, sputtering, and pulse laser deposition technique. While for the chemical synthesis route; sol-gel, electrodeposition, and hydrothermal technique are preferred. Both techniques have their respective advantages and disadvantages and have been used for desired applications

1.3.1 Physical Methods

1.3.1.1 Thermal Evaporation Process

Thermal evaporation technique is one of the diverse techniques of synthesizing crystalline nanostructures. The working process of this technique involves the heating of the source material in a high vacuum chamber of the thermal furnace which generate the vapour phase of the source and facilitates the deposition at the substrate at relatively low temperature as shown in **Figure 1.4**. For the synthesis WO_3 thin film, tungsten (W) metal or WO_3 can be considered as source material in condensed or powder form. The resulted deposited film can further be annealed to achieve the desired crystal phase or the stoichiometry. Different morphologies of WO_3 can also be obtained using thermal evaporation technique.

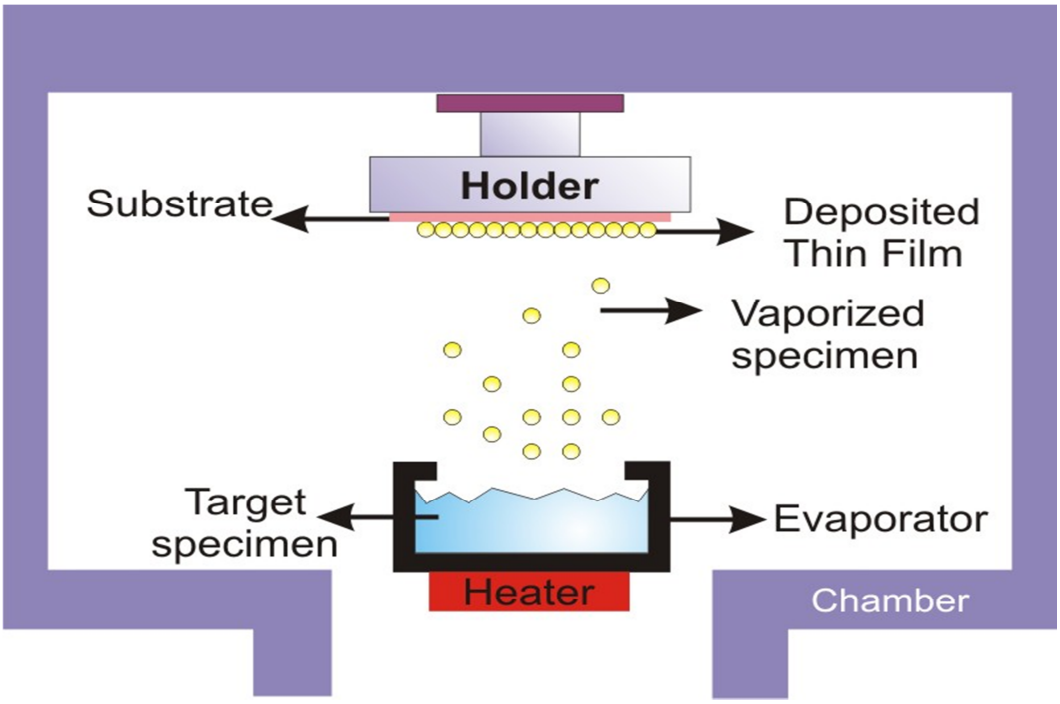

Figure 1.4: Schematic representation of thermal evaporation apparatus

For instance, Zhu et al. showed the formation of tree-shaped tungsten oxide using W foil as source material in an Argon (Ar) atmosphere [40]. Later, Kim et al. had reported the synthesis of WO_3 nanorods onto W substrate using WO_3 as a powder [41].

Further, it was reported that the diameters and the thickness of the 1-D WO_3 nanowires synthesized by a thermal evaporation technique can vary inversely with respect to substrate temperature and can increase by increasing O_2 pressure [42].

1.3.1.2 Sputtering Process

Sputtering is also one of the most studied methods of synthesis of thin films of WO_3. In this technique, the target material is vaporized from a solid target using a highly accelerated beam of inert gas ions causing ejection of atoms from the surface and deposition of a film on a substrate. The schematic of working of sputtering process is shown in **Figure 1.5.**

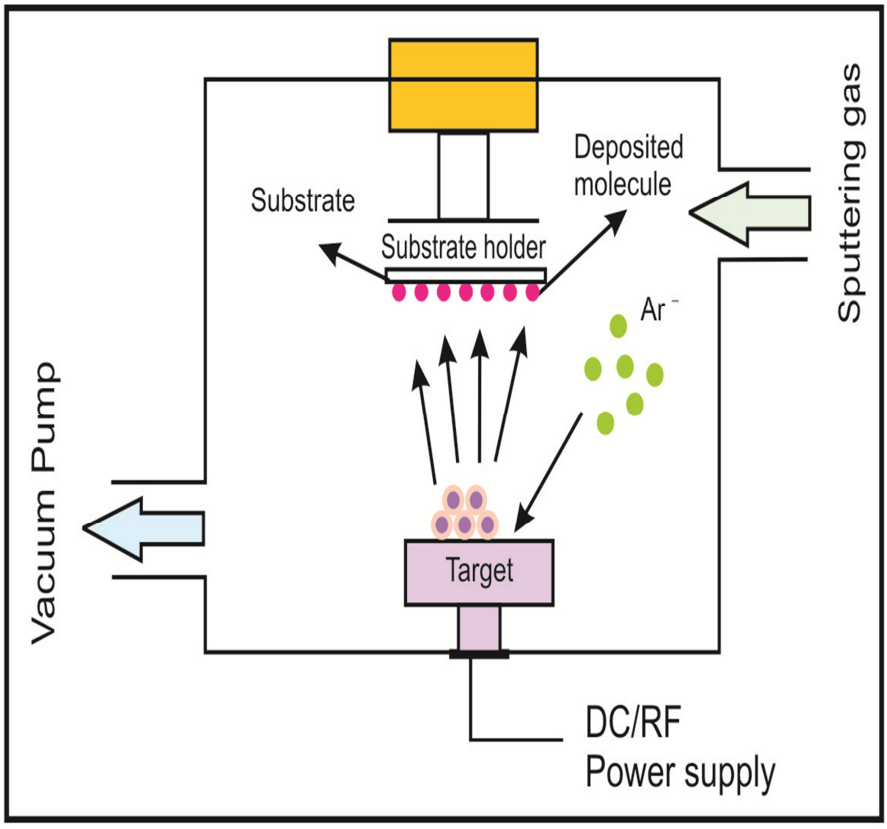

Figure 1.5: Schematic representation of DC/RF sputtering process

The high sputtering power and controlled processing system which involves temperature, gas type, and pressure precisely determine the thickness, crystallinity, grain size,

and morphology of the deposited film. In general, the thin film of WO_3 as obtained by sputtered method exhibits different composition and microstructure as made by the thermal evaporation method. And this is because of the dislodging of atoms from a target on bombardment with high energy in sputtering which results in breaking up of WO_3 molecular bonds when using oxide target. The thin films of WO_3 can be obtained by using reactive DC-magnetron sputtering or RF sputtering technique by considering metallic tungsten (W) or WO_3 as targets in O_2 affluent environment [43]. Akram et al. had reported the deposition of WO_3 thin films using RF sputtering in the atmosphere of Argon gas with 10 % O_2 mixture [44].

1.3.1.3 Pulse Laser Deposition (PLD) Process

PLD is a novel deposition process for the formation of a thin layer of oxides materials, especially for sensing applications. This process employs a high power pulse laser beam to excite the target surface in a vacuum chamber. The interaction between laser beam and the target results in the electronic excitation and physical ablation of the surface atoms due to chemical and mechanical energy involving in the vaporization process. The ablated atoms results in the formation of plasma which adiabatically get expand inside the chamber and later condensed at the substrate for the deposition. This technique also found its utility in the field of protective coating. **Figure 1.6** represents the schematic diagram of a pulsed laser deposition apparatus. The physical and the chemical parameters of the deposited film can be varied with the variation in the laser energy, its intensity, distance between target and substrate and also the carrier gas presence in the chamber. In literature, Mitsugi et al. has reported the study of WO_3 thin films synthesized by the PLD technique in the presence of O_2 pressure and revealed the formation of different crystal phases of WO_3 with the variation in O_2 pressure and substrate temperature [45].

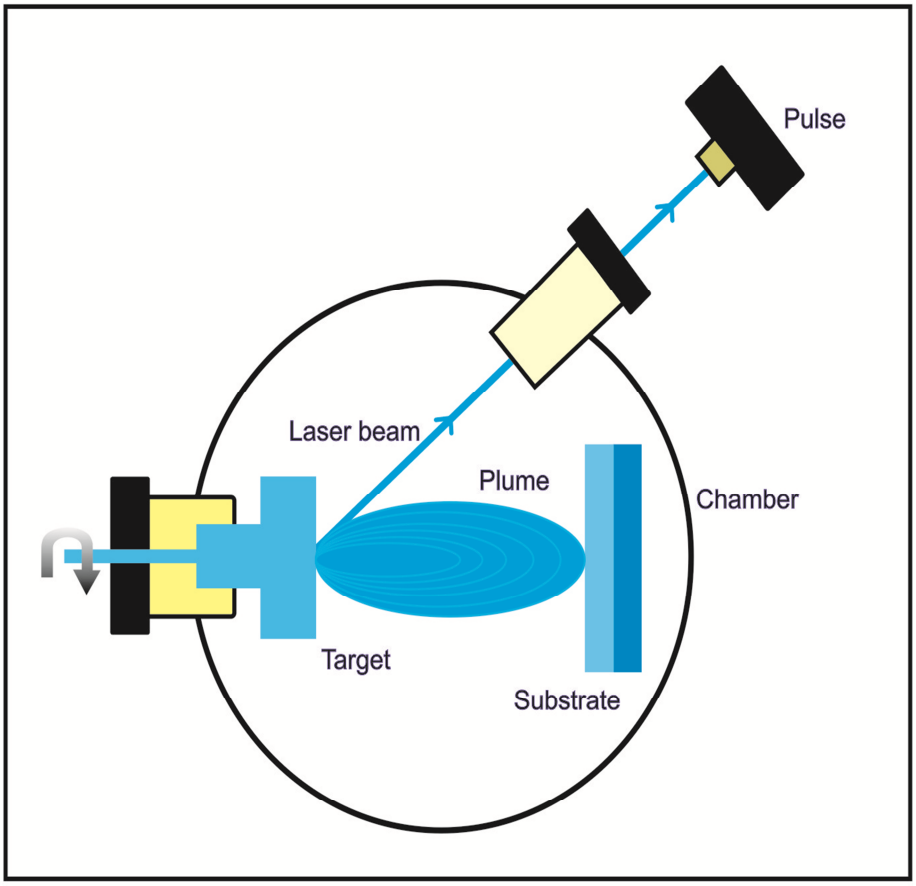

Figure 1.6: Schematic of Pulse laser deposition process

1.3.2 Chemical Methods

1.3.2.1 Sol-Gel Process

The sol-gel process is a powerful approach for the synthesis of thin films, especially of inorganic species. Typically this process involves the hydrolysis of a precursor solution which results in a formation of sol (suspended colloidal particles) and later gel formation from the aggregated sol molecules as shown in **Figure 1.7**. Later, the gel is thermally treated to produce the desired structure or phase. For the synthesis of WO_3, acidification of the precursor solution ($Na_2WO_4.2H_2O$) is preferred with spontaneous polymerization leading to the formation of sol and later gel formation during the aging process. The resultant product as hydrolysis of H_2WO_4 on condensation results in hydrous WO_3 crystalline product. However,

not always resultant is crystalline in nature; sometimes amorphous solids do exist, therefore post-annealing is required for further crystallization.

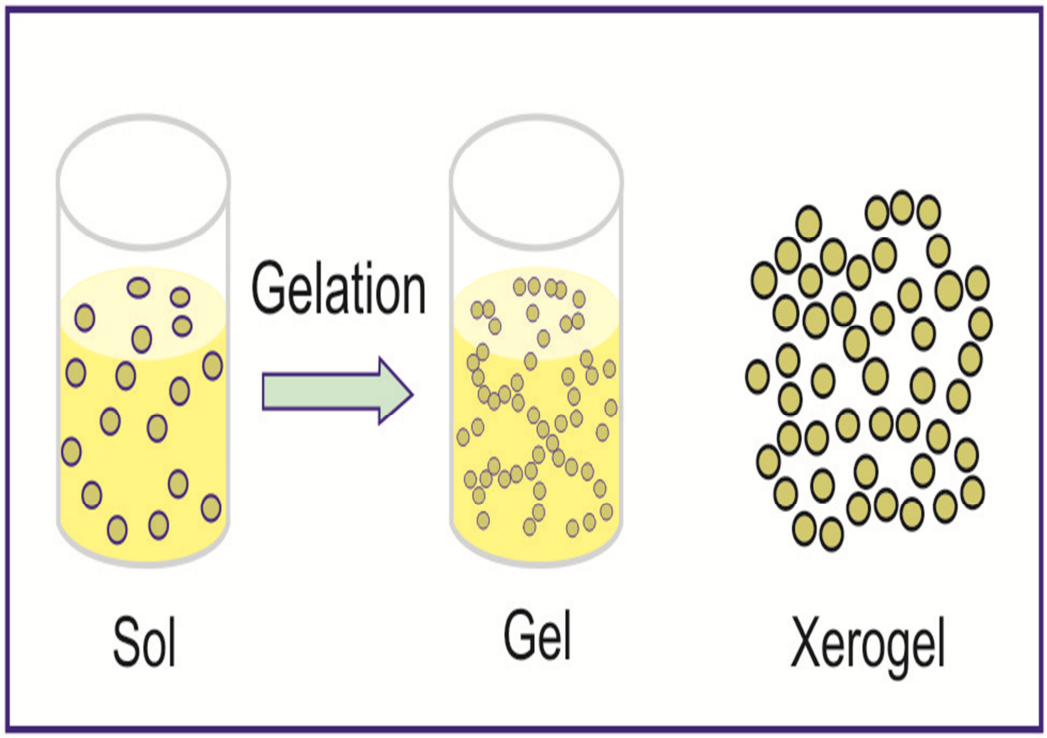

Figure 1.7: Schematic of Sol-Gel process

Spin coating or dip coating method is generally employed for the film deposition. Sanato et al. reported the synthesis of WO_3 via sol-gel technique and studied the change in the crystal structure with varying annealing temperature [46]. Researchers have also reported the synthesis of sol-gel based WO_3 using peroxotungstic acid as precursor solution and mesoporous network shaped morphology [47].

1.3.2.2 Electrochemical Deposition Process

The electrochemical deposition is a versatile technique in which the target material gets deposited onto any conducting substrate under the influence applied potential at room temperature as shown in **Figure 1.8**. The synthesis process is very efficient in producing thin films with desired thickness and morphology by varying applied potential field, pH value of

electrolyte and the deposition time. The main advantages of this technique include its low-cost, high purity, controllable thickness, and low-processing temperature.

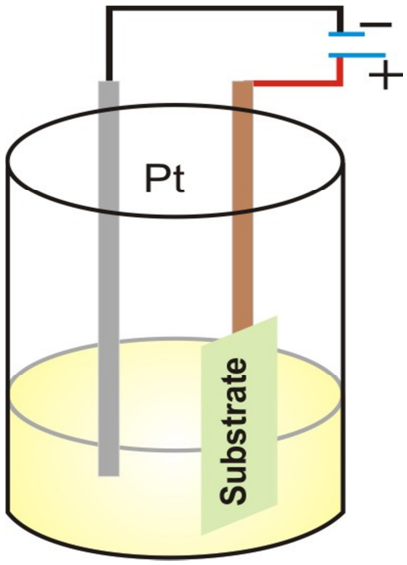

Figure 1.8: Schematic of electrochemical deposition technique

The electro-deposition of metal oxides films can be accomplished via different methods. For instance, Deepa et al. reported the fabrication of mesoporous WO_3 thin films using electrodeposition technique by employing sodium dodecyl sulfate [48]. Hussain et al. showed the synthesis of 1-D WO_3 by using anodized aluminium oxide membrane [49]. Also, Poongodi et al. demonstrated the formation of WO_3 nano-flakes using a peroxotungstic acid solution and employing a template-free electrodeposition technique [50].

1.3.2.3 Hydrothermal Process

Among all other chemical synthesis methods, the hydrothermal method is a simple and a cost-effective method in producing different morphologies of WO_3 along with large production. The synthesis process depends on the solubility of solvents in aqueous media (water) under high pressure. The procedure for the hydrothermal synthesis of WO_3 involves preparation of precursor solution using HCl and sodium tungstate and followed with

hydrothermal reactions. The hydrothermal reaction is performed using Teflon-lined stainless autoclave and an oven. The prepared precursor solution is poured into a Teflon chamber and then this sealed autoclave is placed in the oven for the nucleation and crystallites growth process. **Figure 1.9** represents the schematic diagram of the autoclave used in hydrothermal synthesis. To produce different morphologies and crystal phase of WO_3 nanostructures, additives play an important role in the growth mechanism. The ions of the additives get adsorbed onto the crystal surface of WO_3 and obstruct the growth of the crystal in particular direction resulting in the formation of confined structures.

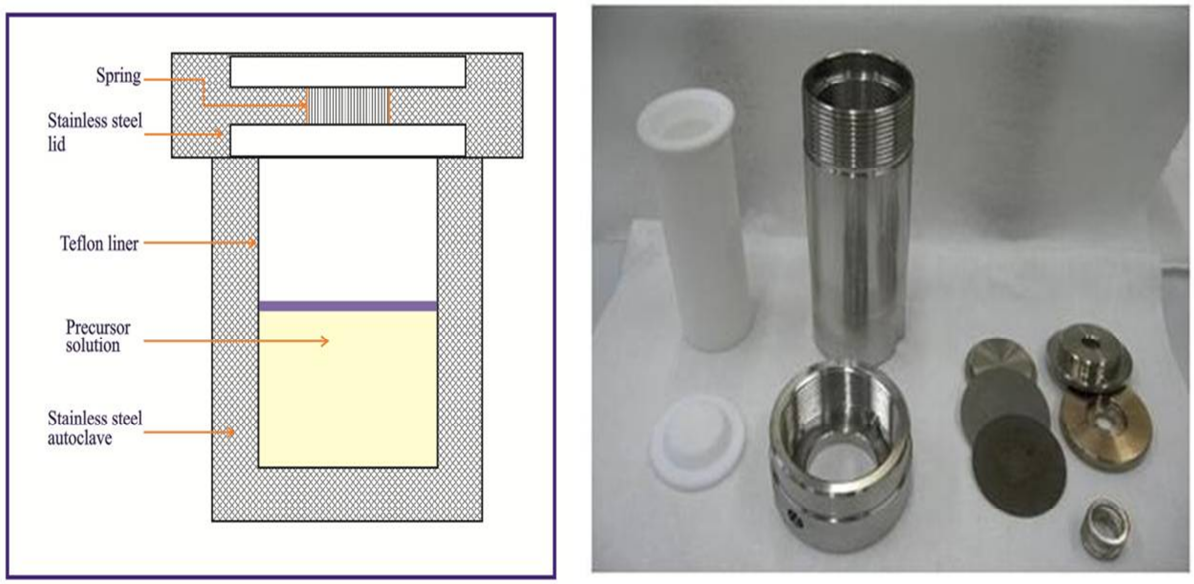

Figure 1.9: Schematic diagram of autoclave used for hydrothermal reaction

The synthesis of 1-D nanostructures, whose width and thickness lies in a nanoscale domain, while the length in micro-scale which shown their remarkable potential in gas sensing, field emission displays and photo–detectors can also be prepared using hydrothermal synthesis. Nguyen et al. reported the synthesis of hexagonal WO_3 nanorods using a wet chemical assisted hydrothermal method. The as-prepared nanorods were used for NH_3 gas sensing [51]. The synthesis of WO_3 nanostructures of the defined phase and morphology do depend on stabilizing cations and directing anions used in the hydrothermal reactions. It is

found that for 1-D WO_3 nanostructures, $NaSO_4$, NaCl, Li_2SO_4, HCl, and $H_2C_2O_4$ can be used as capping or directed agents while for 2-D WO_3 nanostructures, tartaric acid, HBF4, or p-aminobenzoic acid can be used as structure directing agents in hydrothermal synthesis. Song et al. reported the synthesis of orthorhombic phased WO_3 nanobelts using cetyl-trimethyl-ammonium bromide (CTAB) and sodium sulfate as capping agents [52]. While Su et al. produced both monoclinic and orthorhombic phase 2-D WO_3 using reducing agents (citric and tartaric acids) as capping agent [53]. Also, different structure directing additives such as oxalic acid, p-aminobenzoic acid, and potassium sulfate have reported to produced hexagonal phase WO_3. Further, the hydrothermal synthesis of 3-D WO_3 such as networks, arrays, or hierarchical structures can also be accomplished in the presence of malic acid or oxalic acid. For example, Zhang et al. reported the hydrothermal synthesis of the sphere like WO_3 structures and studied its gas sensing property [54].

All this literature survey ensures that different morphologies of WO_3 can be synthesized with a distinctive crystal phase using this facile and cost-effective hydrothermal technique. In the present work, we report the synthesis of different morphologies of WO_3 using precursor as $Na_2WO_4.2H_2O$ and different additive. **Figure 1.10** depicts schematic diagram representing hydrothermal technique employed to synthesized WO_3 nanostructures in this thesis work. For instance, to synthesize tungsten trioxide nanoparticles, we employed Oxalic acid as the structure directing agent. The $Na_2WO_4.2H_2O$ precursor solution was first acidified using HCl solution and then treated with oxalic acid. The resultant was then hydrothermally treated at 120 °C for 4 hours. The synthesis of tungsten trioxide nanosheet was accomplished with the employment of citric acid. The acidification of $Na_2WO_4.2H_2O$ precursor solution results in tungstite solution which was further treated with citric acid. The resultant solution was then hydrothermally treated at 150°C for 20 hours. At last, to synthesize tungsten trioxide nanorods, sodium chloride (NaCl) was used as a structure

directing agent in the hydrothermal synthesis process. The NaCl treated tungstite solution was hydrothermally treated at 180°C for 10 hours for the synthesis of nanorods structures. All these results were justified using different electron microscopic investigations such as scanning electron microscope, field emission scanning electron microscope and transmission electron microscope.

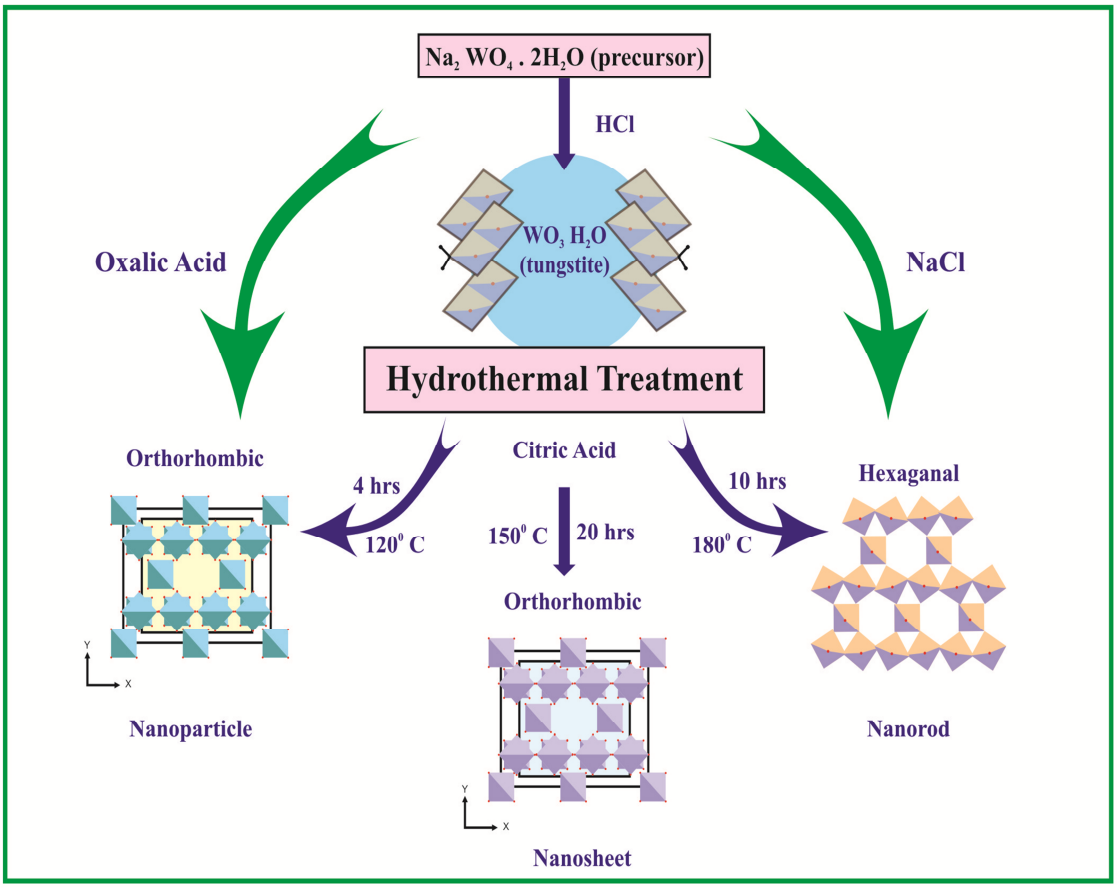

Figure 1.10: Schematic diagram of hydrothermally synthesized WO_3 nanostructures

1.4 Applications of Nanostructured Tungsten Trioxide (nWO_3)

Nanostructured tungsten trioxide (nWO_3) is one of the most investigated advanced functional nanomaterials as its exhibits promising properties including electrochromic, electrocatalytic and electrochemical properties. The significant advancement has been observed in its applications due to its improved thermal and environmental stability as

compared to other materials. Below in this section, we have discussed the potential applications of nWO_3 in various fields including electrochromic devices, gas sensing, photo-catalytic, and biosensing.

1.4.1 Electro-Chromic Devices

Tungsten trioxide (WO_3) is a well studied electrochromic material due to its reversible optical properties with the insertion and extraction of charges. And because of the high stability and reversible coloration effects, it is found to be a remarkable candidate for the development of electrochromic devices. The electrochromism phenomenon includes the intercalation of ions (H^+ or Li^+) into the WO_3 film from the electrolyte. With the application of the negative field, WO_3 get reduced (blue colour) and on the application of positive field the reduced state of WO_3 get oxidized again. In 1815, Berzelius was first who reported the change in colour of WO_3 when heated in H_2 gas atmosphere [55]. While in 1969, S.K. Deb demonstrated the coloration mechanism in WO_3 thin films with the application of 104 V cm^{-1} electric field [56].

WO_3 based electrochromic (EC) devices are studied in both amorphous and crystalline form. However, due to the low chemical stability and poor structure, amorphous WO_3 was failed to produce stable EC devices. While bulk crystalline WO_3 exhibited poor coloration efficiency and low charge density [57]. After observing these drawbacks of the WO_3 based EC devices, nWO_3 becomes an ideal candidate for the EC applications which present significant enhancement in the charge density, coloration time, and coloration efficiency. As we have discussed before, WO_3 can exhibit in different stable crystal phases including triclinic, orthorhombic, monoclinic, and hexagonal. Compared to others, it is found that hexagonal nWO_3 based EC devices have excellent charge densities due to the diversity of its structure (unique hexagonal shaped rings and trigonal cavities) which supported the facile cation intercalation [58].

1.4.2 Photocatalysis

The photocatalysis is a process in which light of suitable energy is illuminated onto the material surface which generates electron-hole pairs. This photo-generated charge carrier undergoes interfacial charge transfer process to produce superoxide and hydroxyl (OH^-) radicals that can efficiently be used for pollution degradation, organic synthesis, and water splitting. To achieve an efficient photocatalytic activity, good crystallinity, lower band gap energy, stability, and large active surface area is a priority as it can decrease the rate of recombination of charge carriers and also increase the population of the active site to harvest solar energy [59]. Although TiO_2 is a well-studied material as a photocatalyst due to its distinctive physicochemical and electronic properties but its wide energy band gap limited its activity for the utilization of solar spectrum radiations. This limitation led to the exploitation of WO_3 material to promote the photocatalytic reactions. Tungsten trioxide (WO_3), an n-type semiconductor can absorb about 30 % of solar energy due to its smaller and narrow energy band gap (2.4–2.8 eV) which makes it a potential candidate for photocatalysis process. Along with this, the other salient features such as non-toxicity, stability in acidic media, facile synthesis, photosensitivity, and corrosion resist of WO_3 makes it a favourable photocatalyst. The enhancement in the performance of a photocatalytic activity for WO_3 was observed by considering WO_3 in crystalline and various nanostructured forms [60-61]. Nanostructured WO_3 exhibits a large surface to volume ratio which provides a large surface area for photochemical reaction to occur. Also, the different dimensional WO_3 exhibits different characteristics which can further modify the performance. Zhu et al. in his work synthesized the WO_3 thin films and studied its photochemical behaviour [62]. While Szilagyi et al. investigated the photo-catalytic characteristics of tungsten trioxide nanofibres in his work [63]. Further, it was found that despite the strong adsorption within a visible spectrum, WO_3 was thermodynamically unable to reduce water to produce H_2 due to its positive conduction

band (CB) edge than the H_2/H_2O reduction potential. However, this was overcome with the application of the external field or doping with metal ions which had enhanced its photocatalytic performance in comparison to bare WO_3. Later, Xiang et al. had reported the enhanced performance of Au modified WO_3 nanorods as a photocatalyst [64].

1.4. 3 Gas Sensors

The monitoring of chemical gases with the application of sensors has become crucial for human health, environmental protection, and industrial processes. The sensor is a device that detects or senses any change in physical or chemical species and convert it into a detectable signal. Gas sensor, a subclass of chemical sensor is based on the detection of the change of the resistance of the sensing material due to adsorption of the gas molecules on the surface. The high diffusion coefficient of oxygen vacancies and chemical inertness of nWO_3 make it suitable for the gas sensing applications. Nanostructured WO_3 based gas sensors have presented enhanced sensor performance in respect of sensitivity, reproducibility, and low power consumption. All these salient features of the nWO_3 can be ascribed to its high crystalline structures, large active surface area, and transport mechanism of charge carriers when exposed to gas species. The use of metal additives (Pt, Au, and Pd) as catalysts on the sensing platform had also shown improved selectivity and sensitivity of the platform and also reduced the recovery and response duration [65]. Penza et al. had reported the enhanced sensing characteristics of WO_3 thin films activated with noble metals for NO_x [66].

1.4.4 Biomedical Applications

In recent time, intensive research on the biomedical application of nWO_3 has gained interest due to its fascinating properties such as high sensitivity, stability in aqueous media, photo-sensitiveness, and biocompatibility. In addition to electrochromic and photo-catalytic properties, nWO_3 also exhibits exceptional electrochemical potential.

nWO_3 modified electrodes reveal superior characteristics over the bulk electrodes including high electro-active surface area and rapid electron transfer kinetics which makes it an ideal candidate for both chemical and bio-sensing applications [67]. For instance, Santos et al. reported the development of WO_3 based pH sensor exhibiting outstanding sensitivity in extensive pH range (pH 5-7) [68]. Righettoni et al. presented the Si: WO_3 based sensor for the selective detection of acetone [69]. And Choi et al. had reported a highly sensitive and selective sensing platform for a diagnostic application using metal doped WO_3 nanofibres [70]. All these studies revealed the potential of WO_3 in the field of biomedical.

1.5 Cardiovascular Disease (CVD)

Despite the extensive efforts and great achievements in the preventive measures and medical treatment of cardiovascular disease (CVD), CVD is still the most prevalent cause of human death in all over the world. About 17 million lives have been claimed worldwide due to CVD. In this direction, World Health Organization (W.H.O) and World Heart Federation have come together to put efforts to reduce death ratio from CVD by 25% by the end of the year 2025 [71-72]. W.H.O presents different strategies on the prevention, monitoring, and management of the CVD globally. Cardiovascular disease which is a disease related to heart and the blood vessels where many factors such as unhealthy nutrition, stress, cholesterol, high blood pressure, and poor physical activity increases its risk severely. And with time, it has included both developed and undeveloped countries under its umbrella. In India, it is estimated that hypertension is directly responsible for 57% of all stroke deaths while 24% of all heart disease deaths [73]. In particular, there are different causes of death related to CVD. But ischemic heart disease (IHD) and ischemic stroke contribute majority in CVD deaths. Acute myocardial infarction (AMI) is one of the IHD and colloquially termed as "heart attack".

AMI is an event of myocardial necrosis caused due to (acute obstruction of a coronary artery) unstable ischemic syndrome. Over the past decade, the diagnosis of AMI as described by the W.H.O is based on three test condition procedures. First is a patient complaining about characteristic chest pain, second diagnosed electrocardiogram (ECG) variation, and third elevation of the concerned biochemical marker in the serum of the patients. Although ECG is in practice in identifying the existence of AMI, it is not a reliable test for early detection as sometimes it presented false ECG to a CVD patient. Thus analysing of cardiac biomarkers in the blood serum would be effectively more crucial in identifying CVD risk for the clinical applications. For the generalization, measurement of concentration of these CVD biomarkers in the bloodstream with the onset of disease would enable the early diagnosis of the disease. Further for the clinical applications, the choice of cardiac biomarkers for CVDs risk should exhibits salient characteristics such as high specificity and sensitivity, provide wide time window for the detection, and get quickly release into the bloodstream.

1.5.1 Cardiac Biomarkers

Cardiac biomarkers are defined as the protein molecules that are found in the bloodstream released from the heart muscle cell after the cardiac injury. The strength of the concentration of these biomarkers indicates the level of damage to the heart muscles. Since the last decade, these biomarkers have shown their support and potential for the clinical analysis of human patients with the suspected cardiac injury. The high selectivity and sensitivity and rapid release of these biomarkers in blood serum make them ideal for early diagnosis. Cardiac biomarkers are an important diagnostic tool to the patients complaining chest pain and suspected myocardial infarction (MI). Biomarkers namely Myoglobin, Creatine Kinase, and Troponin have been considered as specific cardiac biomarkers which get released into the blood circulation with the occurrence of myocardial necrosis.

1.5.1.1 Myoglobin

It is the first protein molecule which gets released rapidly after the damage of muscle cells due to its low molecular weight. But as skeletal muscle too contains Myoglobin, therefore its diagnosis is not very specific for the MI. The cut-off level for Myoglobin in blood serum is 100 ng mL^{-1}. The main advantage in the analysis of Myoglobin biomarker is that it appears in blood serum in only 30 minutes after the occurrence of injury, unlike other biomarkers Troponin and Creatine kinase which take 3-4 hours.

1.5.1.2 Creatine Kinase

Creatine Kinase (CK) is another cardiac protein molecule studied for the diagnosis of AMI. It is an isoenzyme made up of three enzymes including CK-MB, CK-MM, and CK-BB, which are found in both skeletal as well as cardiac tissues. Among these, enzyme CK-MB exists significantly in cardiac tissues but its concentration is very less compared to CK-MM concentration in myocardial muscle. The rapid increase in CK-MB level after myocardial damage, make it a sensitive biomarker for the early diagnosis of AMI. However, due to its poor specificity and a small window of detection, it is not considered as a significant biomarker for early diagnosis of AMI.

1.5.1.3 Troponin

Troponin (Tn) is a complex protein molecule which is associated with the muscle contraction in cardiac and skeletal muscle. Cardiac Troponin (cTn) is structurally different from that of skeletal troponin, hence considered as the potent and specific marker for the cardiac diagnosis. It is a combination of 3 subunit proteins (Troponin C, I, T) and together with tropomyosin is centred at the actin monomers contributing towards the formation of cardiac myofilaments (**Figure 1.11**). All three cTn serve different functions:

i) **Troponin C**: The function of Tn C is to generate the conformational variation in cTnI on binding with calcium ions.

ii) **Troponin I**: The main function of Tn I is to hold troponin-tropomyosin complex by binding to the actin.

iii) **Troponin T**: Tn T get bind to the tropomyosin and make an interlock to form a troponin-tropomyosin complex.

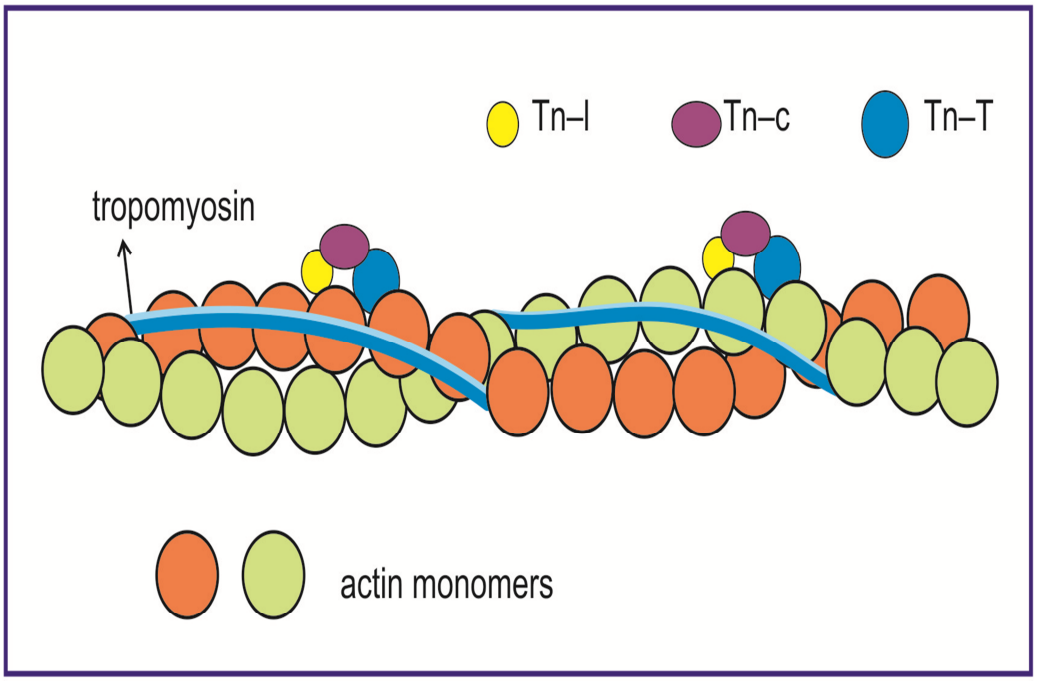

Figure 1.11: Schematic representation of cardiac myofilaments

Cardiac Troponin I (cTnI) is one of the three subunit complex protein with a molecular weight as 22.5 kDa. It is highly cardiac-specific protein molecule due to the presence of an additional amino acid residue on its N-terminal that does not exist in skeletal muscles. Hence it has increased specificity and considered as "gold standard" biomarker for AMI detection. The concentration of cTnI level begin to rise within 3-4 hours after the onset of MI and the elevated value remain to persist for up to 8-10 days, thus giving a wide window of detection for AMI. In general, a normal human has virtually nil level of troponin in blood serum (0.5 ng mL^{-1}) however with the rise in troponin level can provide prognostic information.

1.5.2 Detection of Cardiac Biomarkers

The analysis and diagnosis of cardiac biomarkers have been investigated by employing different techniques including enzyme-linked immunosorbent assay (ELISA) [74], radioimmunoassay [75], fluorescence [76], and electrochemiluminescence assay [77]. Among these, ELISA assay does ensure high diagnostic accuracy but has constraints such as long diagnostic time, needs experts for the performance and analysis and are expensive too. While other techniques, require labelling and special treatment for the sample preparation which leads to complex fabrication of sensor device and increased detection time. Hence for the diagnosis of cardiac disease, we need to develop a cost-effective, highly sensitive and a reliable sensor exhibiting excellent selectivity. Biosensor, in this regard provides the rapid and continuous measurement, low cost instrumentation, need small volume of reagents, ease fabrication, portable, and remarkable sensitivity and selectivity [78]. The advancement in biosensors has been accomplished with the utilization of new and label-free detection mechanism resulting in better diagnosis applications. This development in the designing and materialization of wide range of biosensors has surpassed the earlier used techniques including imaging, fluorescence, and other labelled techniques.

1.5.2.1 Fundamentals of Biosensor

A biosensor as defined by "The International Union of Pure and Applied Chemistry" (IUPAC) is an integrated device which produces analytical information using a bio-recognition element and a transducer element. The bio-recognition element (antibody, whole cells, DNA, etc) recognizes the specific target analyte and produce the physicochemical response and convert it into a measurable signal via transducer element. The measured output signal of a biosensor can be investigated using different transduction strategies such as optical, magnetic, thermometric, and electrochemical. These different transduction strategies provide label-free detection, high sensitivity, and fast response time, simplicity in processing,

low-cost, and convenient portability. All these characteristics make the biosensor as a suitable platform for clinical and non-clinical diagnostics applications. **Figure 1.12** represents the schematic diagram of working of biosensor. Broadly a biosensor consists of three main components:

i) a bio-recognition element,

ii) an immobilizing matrix and

iii) a transducer.

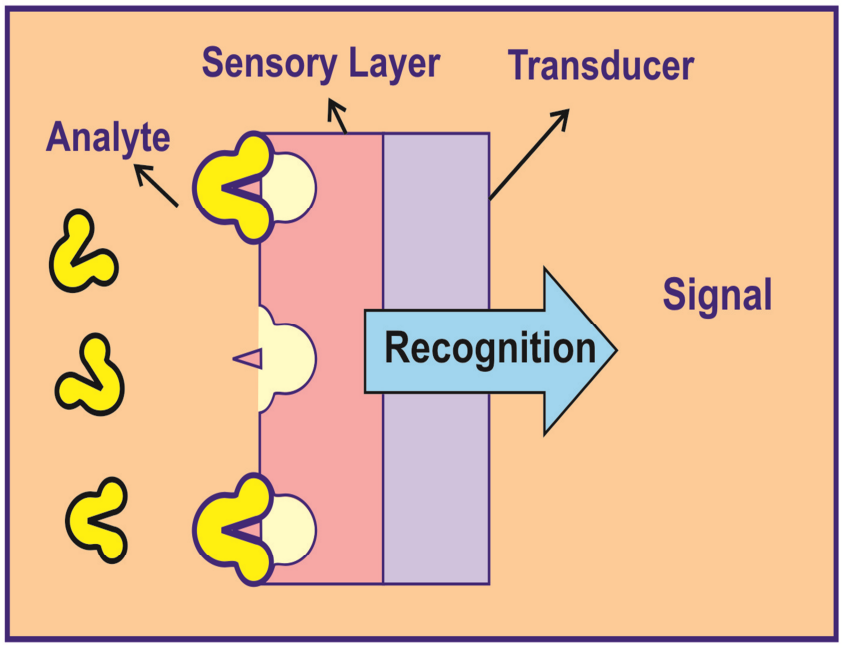

Figure 1.12: Schematic diagram of working of a biosensor

A biosensor employs an immobilizing matrix for the incorporation of the desired bio-recognition element onto the transducer surface. Among all others, an electrochemical biosensor incorporates the sensitivity of an electrochemical transducer along with the specificity of the bio-recognition element. The sensor immobilizes enzymes, proteins, antibodies, or tissues as a bio-recognition element onto the immobilizing matrix that binds selectively with the target analyte producing a measurable signal that is proportional to the concentration of analyte.

Further on the basis of the bio-recognition element, an electrochemical biosensor can be classified as an affinity biosensor and a bio-catalytic biosensor. A bio-catalytic biosensor employs enzymes, or whole cells as recognition element and binds selectively to the target analyte, thereby catalysis the reaction at the substrate and produce the electro-active products and measured via a transducer. A lot of work has been reported in the context of enzyme-based sensors for the detection of glucose and lactose [79-80]. Affinity biosensor depends on the selective interaction of the antibodies, signalling receptors, or nucleic acids (as bio-recognition elements) with their respective analyte to generate a measurable signal. Affinity biosensor further can be classified as label and label free immunosensor. The schematic representation of classification of biosensor is shown in **Figure 1.13.**

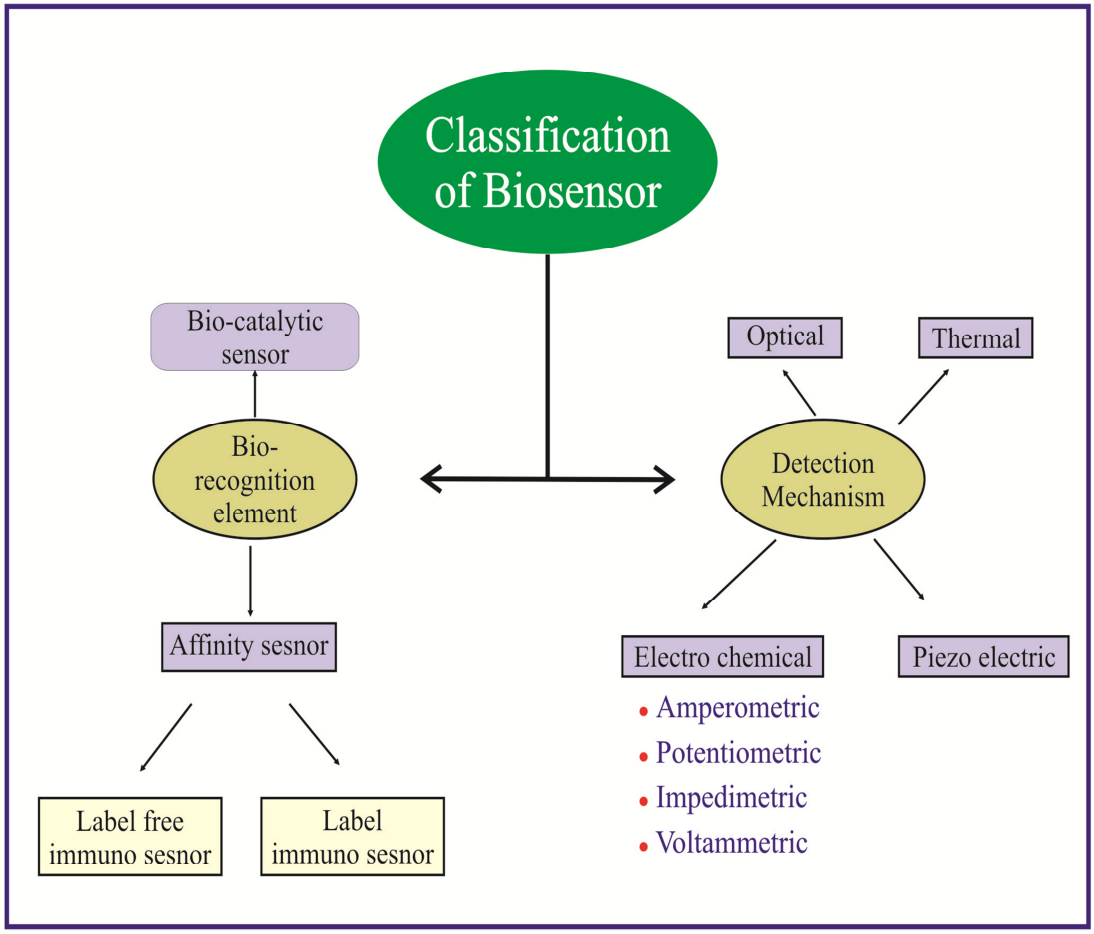

Figure 1.13: Schematic representation of classification of biosensor

The main characteristics of biosensor which defines its performance include sensitivity, reproducibility, stability, and selectivity are defined as:

1) **Sensitivity**: It is defined as the ratio of change in output response to the per unit change in input figure (concentration of antigen) which influence the output response. Therefore, considered as an important characteristic of a biosensor.

2) **Reproducibility:** It tells the capability of a biosensor to produce identical responses for the different identical fabricated biosensor platforms. It further ensures the reliability and robustness of the biosensor.

3) **Stability:** This characteristic of a biosensor tells how long the biosensor can produce a stable response under an ambient biosensing environment. Immobilization of bio-receptors and their bonding with analyte are the important factors which influence the stability of a biosensor.

4) **Selectivity:** It defined as the ability of a biosensor to detect the selective (target) analyte in the presence of other non-selective analytes. Bio-receptors play an important role in defining the selectivity of the fabricated biosensors. For example, considering affinity based biosensors such as immune sensors (antigen-antibody), selectivity depends highly on specific interaction between antibody and antigen only.

1.5.2.2 Immunosensor

Immunosensor is a biosensor which works on the principle of a specific interaction between antigen (Ag) and the antibody (Ab) biomolecules onto the surface of the transducer. Due to the strong interaction and the binding forces between the antigen and antibody, the immunosensor exhibits high sensitivity and selectivity which makes them considerable applicable in clinical diagnostics. The Ab-Ag immunoreactions onto the electrochemical transducer surface generate the variation in potential, conductance, capacitance, current, or in

impedance of the electrochemical cell system. Due to fast response time, compactness, cost-effectiveness, ease of fabrication, and need for small analyte volume, immunosensors have become clinical choice analytical tools [81]. The antibody biomolecule, a Y- shaped globular protein secreted from the body's immune system in response to alien elements in the body. In general, all antibodies exhibit the same structure and are 150 kDa in molecular weight. **Figure 1.14** represents the structure of antibody biomolecule consisting of 4 polypeptide chain. The two identical inner are a heavy chain (50,000 Da) while outer two are lighter chains (22,000 Da) and both two chains (heavy and light chain pair) are connected via disulfide bonds.

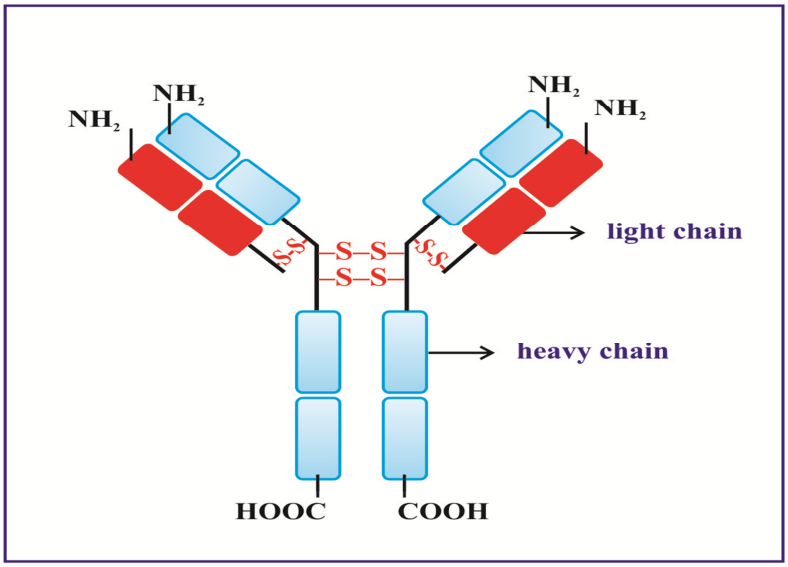

Figure 1.14: Structure of antibody biomolecule

Monoclonal and polyclonal are the two types of antibody that can be used accordingly depending on their field of application. Monoclonal antibody units are highly specific to a single epitope (domain of an antigen that interacts with antibody) of antigen, thus can minimize the cross-reactivity of the bio-species. However, polyclonal antibody can interact with multiple epitopes present on antigen showing heterogeneous response [82]. **Figure 1.15** represents the interaction of a monoclonal and polyclonal antibody with the antigen.

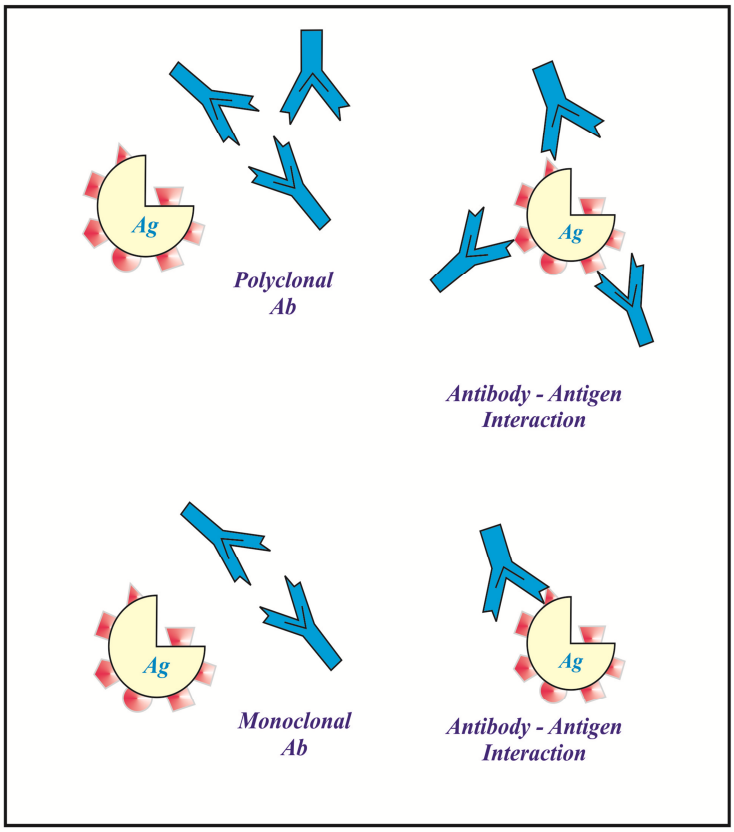

Figure 1.15: Schematic representation of the interaction of a monoclonal and polyclonal antibody with the antigen

1.5.3 Electrochemical Immunoassay for Cardiac Detection

As discussed above, an electrochemical immunoassay is based upon the exchange of charges on interaction between antibody and antigen which leads to the change in voltage or current at the transducing surface. In recent time, a number of cardiac Troponin I (cTnI) detection platform using nanostructures is reported. For instance, Qiao et al. reported the electrochemical sensing of cTnI biomarker using Aptamer-MoS_2 as matrix [83]. Zhang et al. used gold (Au) nanoparticles doped covalent organic framework and also labels (toluidine blue) for ultrasensitive electrochemical detection of cTnI [84]. Also, Ahammad et al. developed a sensitive biosensing platform using Au nanoparticles as a matrix. In their work, they used labelled antibody which was linked to Au nanoparticles via linker molecule [85].

Similarly other researchers have used Au nanoparticles as an amplification platform [86]. However, these entire platforms showed good sensitivity but they are not cost- effective, need special fabrication protocols and not economical too. The other characteristics of the proposed platforms have not been reported.

In the mean time, researchers have diverted their attention towards the incorporation of metal oxide nanostructures in the development of novel biosensor [87-88]. The oxide nanostructures are stable, catalytic, non-toxic, and functional biocompatible. The enhanced features of these nanostructures including facile electron transfer kinetics, stability in aqueous media and strong adsorption make them ideal candidate as an immobilizing matrix for the development of biosensors.

1.5.4 Role of Metal Oxide Nanostructures in Biosensor

The immobilizing matrix onto which biomolecules get immobilized plays a significant role in the development of the biosensors. The sensitivity and selectivity of the biosensor are the key characteristics which depend on the morphological and structural properties of the immobilizing matrix. In recent times, metal oxide (MO) nanostructures have shown great potential towards the enhancement in the performance of the biosensor as an immobilized matrix due to their distinctive electrical and optical properties. The MO nanostructure provides enhanced possibility for the excellent interfacing between biological recognition events and transducer and thus can present the designing of advanced biosensor device with novel characteristics and functions. Thus to fabricate an efficient and potent biosensor, selection of MO nanostructure is very crucial as it provides the ambient environment for the immobilizing of biomolecules [89-90]. And it is this interface binding known as nano-biointerface between MO nanostructure and the biomolecule which influence the performance of a biosensor. The variables such as an effective surface area, surface energy, roughness, presence of functional groups and other physical states of MO

nanostructure plays a significant role in the formation of an effective biointerface. An effective biointerface helps the biomolecules to retain its biological activity in the resultant compatible microenvironment along with high stability. Principally, the binding of biomolecules with MO nanostructures (immobilization) is accomplished via the physical or chemical method. Physical adsorption, encapsulation, confinement, and membrane entrapment are the commonly used physical method of immobilization. Whereas, covalent binding and covalent cross-linking are the chemical methods of immobilization which depends on the presence of functional entities. The details of these immobilization techniques have been discussed in **chapter 2**.

1.5.4.1 Nanostructured Tungsten Trioxide as Biosensor

Among the various novel MO nanostructures, nanostructured tungsten trioxide (nWO_3) as an immobilizing matrix has explored the various prospects and the future challenges in the development of the biosensing devices. This is mainly due to its high electrochemical properties, enhanced electro-active surface area, suitable narrow band-gap, and good electro catalytic activity. Interestingly, due to the good electrical and catalytic properties of nWO_3, it became a suitable applicant as "electronic wires" to enhance the electron transfer kinetics between redox centres in proteins and electrode surface [91]. Feng et al. utilized nWO_3 films to immobilize haemoglobin protein and investigated the interfacial electron transfer kinetics and the thermal stability of the immobilized protein [92]. Later, Sun et al. demonstrated the detection of glucose with high efficiency using WO_3 as a platform [93]. Hariharan et al. fabricated WO_3 based biosensor for L-dopa detection with high selectivity and sensitivity [94]. Hence, nWO_3 has significantly shown potential toward the development of biosensor as a good transduction material.

The efficiency of nWO_3 towards immobilization of biomolecules and retaining its biological activity might helps in enhancing the sensing characteristics of the biosensing

platform. Further, employing the label-free electrochemical technique for cardiac biomarker detection using WO_3 sensing platform can enhanced the sensitivity, stability and selectivity of the biosensor.

1.5.4.2 WO_3-RGO Nanocomposite

In recent time, the synthesis of nanocomposite resulting from integration of WO_3 with chemically active reduce graphene oxide (RGO) has shown enhanced characteristics in literature. For instance, Thangavel et al. reported the synthesis of WO_3-RGO nanocomposite for photocatalytic application highlighting the enhanced optical and thermal stability of the resultant nanocomposite [95]. Su et al. employed WO_3-RGO nanocomposite for NO_2 gas sensing at low concentration [96]. Prabhu et al. reported the green synthesis of WO_3-RGO nanocomposite which showed enhanced photo-electrochemical water splitting characteristics [97].

RGO has been well studied as an exceptional candidate for sensing applications. The presence of additional functional groups, large effective surface area, low cost and ease fabrication reveals its potential application in biosensing field too. The RGO based platforms have shown their applications in food toxin detection, enzymatic analysis, and for immunosensor development too. Reduced graphene oxide (RGO) is a reduced form of graphene oxide (GO) and exhibits in the form of sheet. RGO exhibits enhanced electrical conductivity unlike GO (insulator) due to the restored π conjugated system. The reduced graphene oxide resembles the pristine graphene in all respect including mechanical, electrical and thermal characteristics, as well as surface morphology [98-99]. The different reduction methods of GO includes electrochemical, chemical, and thermal reduction methods [100].

Further, RGO has shown tremendous performance in the development of sensors and especially electrochemical biosensors due to its distinctive characteristics which includes high electrochemical activity, abundant functional groups for covalent functionalization, and

enhanced chemical and electrical properties. The functionalization of RGO through covalent and non-covalent processes has shown the improvements in sensitivity and selectivity of biosensing platform and also in loading capacity of biomolecules [101]. In this respect, we have also explored RGO-WO_3 nanocomposite matrix for electrochemical detection of cardiac biomarker cTnI.

1.6 References

1. Faraji, N., Rainer Adelung, Y. K. Mishra, and J. Seidel. "Nanoscale electromechanical and electronic properties of free-standing ZnO nano-and micro-structured platelets." *Nanotechnology* 28, no. 40 (2017): 405701.
2. Navya, P. N., and Hemant Kumar Daima. "Rational engineering of physicochemical properties of nanomaterials for biomedical applications with nano-toxicological perspectives." *Nano Convergence* 3, no. 1 (2016): 1.
3. Choi, Suji, Hyunjae Lee, Roozbeh Ghaffari, Taeghwan Hyeon, and Dae-Hyeong Kim. "Recent advances in flexible and stretchable bio-electronic devices integrated with nanomaterials." *Advanced Materials* 28, no. 22 (2016): 4203-4218.
4. Ariga, Katsuhiko, Qingmin Ji, Waka Nakanishi, Jonathan P. Hill, and Masakazu Aono. "Nanoarchitectonics: a new materials horizon for nanotechnology." *Materials Horizons* 2, no. 4 (2015): 406-413.
5. Eranna, G. Metal oxide nanostructures as gas sensing devices. *CRC Press*, 2016.
6. Abeer, Syed. "Future medicine: nanomedicine." *JIMSA* 25 (2012): 187-192.
7. Alharbi, Khalid Khalaf, and Yazeed A. Al-sheikh. "Role and implications of nanodiagnostics in the changing trends of clinical diagnosis." *Saudi journal of biological sciences* 21, no. 2 (2014): 109-117.
8. Riu, Jordi, Alicia Maroto, and F. Xavier Rius. "Nanosensors in environmental analysis." *Talanta* 69, no. 2 (2006): 288-301.

9. Melker, Richard J., and Donn Michael Dennis. "Application of biosensors for diagnosis and treatment of disease." *U.S. Patent* 6,974,706, issued December 13, 2005.
10. Carabineiro, Sónia AC, and David T. Thompson. "Catalytic applications for gold nanotechnology." *In Nanocatalysis*, pp. 377-489. Springer, Berlin, Heidelberg, 2007.
11. Vashist, Sandeep Kumar, A. G. Venkatesh, Konstantinos Mitsakakis, Gregor Czilwik, Günter Roth, Felix von Stetten, and Roland Zengerle. "Nanotechnology-based biosensors and diagnostics: technology push versus industrial/healthcare requirements." *Bionanoscience* 2, no. 3 (2012): 115-126.
12. Carrier, Xavier, Sébastien Royer, and Eric Marceau. "Synthesis of metal oxide catalysts." In Metal Oxides in Heterogeneous Catalysis, pp. 43-103. *Elsevier,* 2018.
13. Yu, Xinge, Tobin J. Marks, and Antonio Facchetti. "Metal oxides for optoelectronic applications." *Nature materials* 15, no. 4 (2016): 383.
14. Zhi, Mingjia, Chengcheng Xiang, Jiangtian Li, Ming Li, and Nianqiang Wu. "Nanostructured carbon–metal oxide composite electrodes for supercapacitors: a review." *Nanoscale* 5, no. 1 (2013): 72-88.
15. Dey, Ananya. "Semiconductor metal oxide gas sensors: A review." *Materials Science and Engineering: B* 229 (2018): 206-217.
16. Kannan, Ramanujam, Ae Rhan Kim, Jong Seok Kim, and Dong Jin Yoo. "3D graphene-mixed metal oxide-supported carbonpalladium quantum dot nanoarchitectures–A facile bifunctional electrocatalyst for direct ethylene glycol fuel cells and oxygen evolution reactions." *International Journal of Hydrogen Energy* 41, no. 40 (2016): 18033-18043.
17. Liu, Xueqin, James Iocozzia, Yang Wang, Xun Cui, Yihuang Chen, Shiqiang Zhao, Zhen Li, and Zhiqun Lin. "Noble metal–metal oxide nanohybrids with tailored nanostructures for efficient solar energy conversion, photocatalysis and environmental remediation." *Energy & Environmental Science* 10, no. 2 (2017): 402-434.

18. Wen, Rui-Tao, Gunnar A. Niklasson, and Claes G. Granqvist. "Sustainable rejuvenation of electrochromic WO_3 films." *ACS applied materials & interfaces* 7, no. 51 (2015): 28100-28104.
19. Paik, Taejong, Matteo Cargnello, Thomas R. Gordon, Sen Zhang, Hongseok Yun, Jennifer D. Lee, Ho Young Woo et al. "Photocatalytic hydrogen evolution from substoichiometric colloidal WO_{3-x} nanowires." *ACS Energy Letters* 3, no. 8 (2018): 1904-1910.
20. Tong, Hui, Yingming Xu, Xiaoli Cheng, Xianfa Zhang, Shan Gao, Hui Zhao, and Lihua Huo. "One-pot solvothermal synthesis of hierarchical WO_3 hollow microspheres with superior lithium ion battery anode performance." *Electrochimica Acta* 210 (2016): 147-154.
21. Pal, Shreyasi, and Kalyan Kumar Chattopadhyay. "Tungsten oxide nanostructures for energy storage and field emission applications." *J. Eng. Technol. Res* 5 (2016): 97-101.
22. Gillet, M., K. Aguir, C. Lemire, E. Gillet, and K. Schierbaum. "The structure and electrical conductivity of vacuum-annealed WO_3 thin films." *Thin Solid Films* 467, no. 1-2 (2004): 239-246.
23. Cong, Shan, Fengxia Geng, and Zhigang Zhao. "Tungsten oxide materials for optoelectronic applications." *Advanced Materials* 28, no. 47 (2016): 10518-10528.
24. Granqvist, Claes G. "Electrochromic tungsten oxide films: review of progress 1993–1998." *Solar Energy Materials and Solar Cells* 60, no. 3 (2000): 201-262.
25. Ramana, C. V., Satoshi Utsunomiya, R. C. Ewing, C. M. Julien, and U. Becker. "Structural stability and phase transitions in WO_3 thin films." *The Journal of Physical Chemistry B* 110, no. 21 (2006): 10430-10435.

26. Zheng, Haidong, Jian Zhen Ou, Michael S. Strano, Richard B. Kaner, Arnan Mitchell, and Kourosh Kalantar-zadeh. "Nanostructured tungsten oxide–properties, synthesis, and applications." *Advanced Functional Materials* 21, no. 12 (2011): 2175-2196.
27. Huang, Kai, and Qing Zhang. "Rechargeable lithium battery based on a single hexagonal tungsten trioxide nanowire." *Nano Energy* 1, no. 1 (2012): 172-175.
28. Migas, D. B., V. L. Shaposhnikov, and V. E. Borisenko. "Tungsten oxides. II. The metallic nature of Magnéli phases." *Journal of Applied Physics* 108, no. 9 (2010): 093714.
29. Solonin, Yu M., O. Yu Khyzhun, and E. A. Graivoronskaya. "Nonstoichiometric tungsten oxide based on hexagonal WO_3." *Crystal Growth & Design* 1, no. 6 (2001): 473-477.
30. Al Mohammad, A., and M. Gillet. "Phase transformations in WO_3 thin films during annealing." *Thin Solid Films* 408, no. 1-2 (2002): 302-309.
31. Kuti, Lisa M., Surinderjit Singh Bhella, and Venkataraman Thangadurai. "Revisiting Tungsten Trioxide Hydrates (TTHs) Synthesis- Is There Anything New." *Inorganic chemistry* 48, no. 14 (2009): 6804-6811.
32. Gullapalli, S. K., R. S. Vemuri, and C. V. Ramana. "Structural transformation induced changes in the optical properties of nanocrystalline tungsten oxide thin films." *Applied physics letters* 96, no. 17 (2010): 171903.
33. Granqvist, Claes G. "Electrochromic tungsten oxide films: review of progress 1993–1998." *Solar Energy Materials and Solar Cells* 60, no. 3 (2000): 201-262.
34. Kumar, S. Girish, and KSR Koteswara Rao. "Tungsten-based nanomaterials (WO_3 & Bi_2WO_6): modifications related to charge carrier transfer mechanisms and photocatalytic applications." *Applied Surface Science* 355 (2015): 939-958.

35. Aguir, K., C. Lemire, and D. B. B. Lollman. "Electrical properties of reactively sputtered WO_3 thin films as ozone gas sensor." *Sensors and Actuators B: Chemical* 84, no. 1 (2002): 1-5.

36. Vemuri, R. S., K. Kamala Bharathi, S. K. Gullapalli, and C. V. Ramana. "Effect of structure and size on the electrical properties of nanocrystalline WO_3 films." *ACS applied materials & interfaces* 2, no. 9 (2010): 2623-2628.

37. Patel, K. J., C. J. Panchal, V. A. Kheraj, and M. S. Desai. "Growth, structural, electrical and optical properties of the thermally evaporated tungsten trioxide (WO_3) thin films." *Materials Chemistry and Physics* 114, no. 1 (2009): 475-478.

38. Huang, Rui, Jing Zhu, and Rong Yu. "Condensed Matter: Electronic Structure, Electrical, Magnetic, And Optical Properties: Synthesis and electrical characterization of tungsten oxide nanowires." *Chinese Physics B* 18 (2009): 3024-3030.

39. Whitesides, George M., and Bartosz Grzybowski. "Self-assembly at all scales." *Science* 295, no. 5564 (2002): 2418-2421.

40. Zhu, Yan Qiu, Weibing Hu, Wen Kuang Hsu, Mauricio Terrones, Nicole Grobert, Jonathan P. Hare, Harold W. Kroto, David RM Walton, and Humberto Terrones. "Tungsten oxide tree-like structures." *Chemical Physics Letters* 309, no. 5-6 (1999): 327-334.

41. Kim, Hyeyoung, Karuppanan Senthil, and Kijung Yong. "Photo-electrochemical and photocatalytic properties of tungsten oxide nanorods grown by thermal evaporation." *Materials Chemistry and Physics* 120, no. 2-3 (2010): 452-455.

42. Thangala, Jyothish, Sreeram Vaddiraju, Rahel Bogale, Ryan Thurman, Trevor Powers, Biswapriya Deb, and Mahendra K. Sunkara. "Large-Scale, Hot-Filament-Assisted Synthesis of Tungsten Oxide and Related Transition Metal Oxide Nanowires." *small* 3, no. 5 (2007): 890-896.

43. Deniz, Derya, David J. Frankel, and Robert J. Lad. "Nanostructured tungsten and tungsten trioxide films prepared by glancing angle deposition." *Thin Solid Films* 518, no. 15 (2010): 4095-4099.

44. Akram, Hossain, Hirokazu Tatsuoka, Michihiko Kitao, and Shoji Yamada. "Preparation and aging of sputtered tungstic oxide films." *Journal of applied physics* 62, no. 5 (1987): 2039-2043.

45. Mitsugi, Fumiaki, Eiichi Hiraiwa, Tomoaki Ikegami, Kenji Ebihara, and Raj Kumar Thareja. "WO_3 thin films prepared by pulsed laser deposition." *Japanese journal of applied physics* 41, no. 8R (2002): 5372.

46. Santato, Clara, Marek Odziemkowski, Martine Ulmann, and Jan Augustynski. "Crystallographically oriented mesoporous WO_3 films: synthesis, characterization, and applications." *Journal of the American Chemical Society* 123, no. 43 (2001): 10639-10649.

47. Yang, Bin, Yingjie Zhang, Elizabeth Drabarek, Piers RF Barnes, and Vittorio Luca. "Enhanced photoelectrochemical activity of sol−gel tungsten trioxide films through textural control." *Chemistry of Materials* 19, no. 23 (2007): 5664-5672.

48. Deepa, M., A. K. Srivastava, S. N. Sharma, and S. M. Shivaprasad. "Microstructural and electrochromic properties of tungsten oxide thin films produced by surfactant mediated electrodeposition." *Applied Surface Science* 254, no. 8 (2008): 2342-2352.

49. Hussain, Tajamal, Asma Tufail Shah, Khurram Shehzad, Adnan Mujahid, Zahoor Hussain Farooqi, Muhammad Hamid Raza, Mirza Nadeem Ahmed, and Zaib Un Nisa. "Formation of self-ordered porous anodized alumina template for growing tungsten trioxide nanowires." *International Nano Letters* 5, no. 1 (2015): 37-41.

50. Poongodi, S., Palaniswamy Suresh Kumar, D. Mangalaraj, N. Ponpandian, P. Meena, Yoshitake Masuda, and Chongmu Lee. "Electrodeposition of WO_3 nanostructured thin

films for electrochromic and H_2S gas sensor applications." *Journal of Alloys and Compounds* 719 (2017): 71-81.

51. Nguyen, Dac Dien, Duc Vuong Dang, and Duc Chien Nguyen. "Hydrothermal synthesis and NH_3 gas sensing property of WO_3 nanorods at low temperature." *Advances in Natural Sciences: Nanoscience and Nanotechnology* 6, no. 3 (2015): 035006.
52. Song, Xuchun, Yang Zhao, and Yifan Zheng. "Hydrothermal synthesis of tungsten oxide nanobelts." *Materials Letters* 60, no. 28 (2006): 3405-3408.
53. Su, Xintai, Feng Xiao, Yani Li, Jikang Jian, Qingjun Sun, and Jide Wang. "Synthesis of uniform WO_3 square nanoplates via an organic acid-assisted hydrothermal process." *Materials Letters* 64, no. 10 (2010): 1232-1234.
54. Zhang, Hejing, Tianmo Liu, Long Huang, Weiwei Guo, Dejun Liu, and Wen Zeng. "Hydrothermal synthesis of assembled sphere-like WO_3 architectures and their gas-sensing properties." *Physica E: Low-dimensional Systems and Nanostructures* 44, no. 7-8 (2012): 1467-1472.
55. Granqvist, Claes G. "Electrochromic tungsten oxide films: review of progress 1993–1998." *Solar Energy Materials and Solar Cells* 60, no. 3 (2000): 201-262.
56. Deb, Satyen K. "Opportunities and challenges in science and technology of WO_3 for electrochromic and related applications." *Solar Energy Materials and Solar Cells* 92, no. 2 (2008): 245-258.
57. Deepa, M., A. K. Srivastava, K. N. Sood, and S. A. Agnihotry. "Nanostructured mesoporous tungsten oxide films with fast kinetics for electrochromic smart windows." *Nanotechnology* 17, no. 10 (2006): 2625.
58. Balaji, Subramanian, Yahia Djaoued, André-Sébastien Albert, Richard Z. Ferguson, and Ralf Brüning. "Hexagonal tungsten oxide based electrochromic devices: spectroscopic

evidence for the Li ion occupancy of four-coordinated square windows." *Chemistry of Materials* 21, no. 7 (2009): 1381-1389.

59. Zhang, Huanjun, Guohua Chen, and Detlef W. Bahnemann. "Photoelectrocatalytic materials for environmental applications." *Journal of Materials Chemistry* 19, no. 29 (2009): 5089-5121.
60. Santato, Clara, Martine Ulmann, and Jan Augustynski. "Enhanced visible light conversion efficiency using nanocrystalline WO_3 films." *Advanced Materials* 13, no. 7 (2001): 511-514.
61. Berger, S., H. Tsuchiya, A. Ghicov, and P. Schmuki. "High photocurrent conversion efficiency in self-organized porous WO_3." *Applied Physics Letters* 88, no. 20 (2006): 203119.
62. Zhu, Tao, Meng Nan Chong, and Eng Seng Chan. "Nanostructured tungsten trioxide thin films synthesized for photoelectrocatalytic water oxidation: a review." *Chem Sus Chem* 7, no. 11 (2014): 2974-2997.
63. Szilágyi, Imre M., Balázs Fórizs, Olivier Rosseler, Ágnes Szegedi, Péter Németh, Péter Király, Gábor Tárkányi et al. "WO_3 photocatalysts: Influence of structure and composition." *Journal of catalysis* 294 (2012): 119-127.
64. Xiang, Q., G. F. Meng, H. B. Zhao, Y. Zhang, H. Li, W. J. Ma, and J. Q. Xu. "Au nanoparticle modified WO_3 nanorods with their enhanced properties for photocatalysis and gas sensing." *The Journal of Physical Chemistry C* 114, no. 5 (2010): 2049-2055.
65. Mizsei, J., Pekko Sipilä, and Vilho Lantto. "Structural studies of sputtered noble metal catalysts on oxide surfaces." *Sensors and Actuators B: Chemical* 47, no. 1-3 (1998): 139-144.

66. Penza, M., C. Martucci, and G. Cassano. "NO_x gas sensing characteristics of WO_3 thin films activated by noble metals (Pd, Pt, Au) layers." *Sensors and Actuators B: Chemical* 50, no. 1 (1998): 52-59.

67. Zahoor, Muhammad Tahir, Mashkoor Ahmad, Khan Maaz, Shafqat Karim, Khalid Waheed, Ghafar Ali, Shafqat Hussain, Syed Zahid Hussain, and Amjad Nisar. "Tungsten oxide multifunctional nanostructures: Enhanced environmental and sensing applications." *Materials Chemistry and Physics* 221 (2019): 250-257.

68. Santos, Lídia, Joana P. Neto, Ana Crespo, Daniela Nunes, Nuno Costa, Isabel M. Fonseca, Pedro Barquinha et al. "WO_3 nanoparticle-based conformable pH sensor." ACS *applied materials & interfaces* 6, no. 15 (2014): 12226-12234.

69. Righettoni, Marco, Antonio Tricoli, and Sotiris E. Pratsinis. "Si: WO_3 sensors for highly selective detection of acetone for easy diagnosis of diabetes by breath analysis." *Analytical chemistry* 82, no. 9 (2010): 3581-3587.

70. Choi, Seon-Jin, Inkun Lee, Bong-Hoon Jang, Doo-Young Youn, Won-Hee Ryu, Chong Ook Park, and Il-Doo Kim. "Selective diagnosis of diabetes using Pt-functionalized WO_3 hemi-tube networks as a sensing layer of acetone in exhaled breath." *Analytical chemistry* 85, no. 3 (2013): 1792-1796.

71. Deaton, Christi, Erika Sivaraja Froelicher, Lai Ha Wu, Camille Ho, Kawkab Shishani, and Tiny Jaarsma. "The global burden of cardiovascular disease." *European Journal of Cardiovascular Nursing* 10, no. 2_suppl (2011): S5-S13.

72. McAloon, Christopher J., Luke M. Boylan, Thomas Hamborg, Nigel Stallard, Faizel Osman, Phang B. Lim, and Sajad A. Hayat. "The changing face of cardiovascular disease 2000–2012: An analysis of the world health organisation global health estimates data." *International journal of cardiology* 224 (2016): 256-264.

73. Gupta, Rajeev. "Trends in hypertension epidemiology in India." *Journal of human hypertension* 18, no. 2 (2004): 73.

74. Heeschen, Christopher, Britta U. Goldmann, Lukas Langenbrink, Guido Matschuck, and Christian W. Hamm. "Evaluation of a rapid whole blood ELISA for quantification of troponin I in patients with acute chest pain." *Clinical chemistry* 45, no. 10 (1999): 1789-1796.

75. Cummins, Bernadette, Margaret Lucy Auckland, and Peter Cummins. "Cardiac-specific troponin-l radioimmunoassay in the diagnosis of acute myocardial infarction." *American heart journal* 113, no. 6 (1987): 1333-1344.

76. Song, Seung Yeon, Yong Duk Han, Kangil Kim, Sang Sik Yang, and Hyun C. Yoon. "A fluoro-microbead guiding chip for simple and quantifiable immunoassay of cardiac troponin I (cTnI)." *Biosensors and Bioelectronics* 26, no. 9 (2011): 3818-3824.

77. Kuster, Diederik WD, David Barefield, Suresh Govindan, and Sakthivel Sadayappan. "A sensitive and specific quantitation method for determination of serum cardiac myosin binding protein-C by electrochemiluminescence immunoassay." *JoVE (Journal of Visualized Experiments)* 78 (2013): e50786.

78. Ali, J., J. Najeeb, M. Asim Ali, M. Farhan Aslam, and A. Raza. "Biosensors: their fundamentals, designs, types and most recent impactful applications: a review." *J Biosens Bioelectron* 8, no. 1 (2017).

79. Wen, Dan, Shaojun Guo, Yizhe Wang, and Shaojun Dong. "Bifunctional nanocatalyst of bimetallic nanoparticle/TiO_2 with enhanced performance in electrochemical and photoelectrochemical applications." *Langmuir* 26, no. 13 (2010): 11401-11406.

80. Asif, Muhammad H., Syed M. Usman Ali, Omer Nur, Magnus Willander, Cecilia Brännmark, Peter Strålfors, Ulrika H. Englund, Fredrik Elinder, and Bengt Danielsson.

"Functionalised ZnO-nanorods based selective electrochemical sensor for intracellular glucose." *Biosensors and Bioelectronics* 25, no. 10 (2010): 2205-2211.

81. Lim, Syazana Abdullah, and Minhaz Uddin Ahmed. "Electrochemical immunosensors and their recent nanomaterial-based signal amplification strategies: a review." *RSC Advances* 6, no. 30 (2016): 24995-25014.
82. Leenaars, Marlies, and Coenraad FM Hendriksen. "Critical steps in the production of polyclonal and monoclonal antibodies: evaluation and recommendations." *Ilar Journal* 46, no. 3 (2005): 269-279.
83. Qiao, Xiujuan, Kunxia Li, Jinqiong Xu, Ni Cheng, Qinglin Sheng, Wei Cao, Tianli Yue, and Jianbin Zheng. "Novel electrochemical sensing platform for ultrasensitive detection of cardiac troponin I based on aptamer-MoS_2 nanoconjugates." *Biosensors and Bioelectronics* 113 (2018): 142-147.
84. Zhang, Tong, Ning Ma, Asghar Ali, Qin Wei, Dan Wu, and Xiang Ren. "Electrochemical ultrasensitive detection of cardiac troponin I using covalent organic frameworks for signal amplification." *Biosensors and Bioelectronics* 119 (2018): 176-181.
85. Ahammad, AJ Saleh, Yo-Han Choi, Kwangnak Koh, Jae-Ho Kim, Jae-Joon Lee, and Minsu Lee. "Electrochemical detection of cardiac biomarker troponin I at gold nanoparticle-modified ITO electrode by using open circuit potential." *Int. J. Electrochem. Sci* 6, no. 6 (2011): 1906-1916.
86. Shan, Meng, Min Li, Xiaoying Qiu, Honglan Qi, Qiang Gao, and Chengxiao Zhang. "Sensitive electrogenerated chemiluminescence peptide-based biosensor for the determination of troponin I with gold nanoparticles amplification." *Gold Bulletin* 47, no. 1-2 (2014): 57-64.

87. Liu, Jinping, Yuanyuan Li, Xintang Huang, and Zhihong Zhu. "Tin oxide nanorod array-based electrochemical hydrogen peroxide biosensor." *Nanoscale research letters* 5, no. 7 (2010): 1177.

88. Doong, Ruey-an, and Hui-mei Shih. "Array-based titanium dioxide biosensors for ratiometric determination of glucose, glutamate and urea." *Biosensors and Bioelectronics* 25, no. 6 (2010): 1439-1446.

89. Tang, Dianping, Yuling Cui, and Guonan Chen. "Nanoparticle-based immunoassays in the biomedical field." *Analyst* 138, no. 4 (2013): 981-990.

90. Solanki, Pratima R., Ajeet Kaushik, Ved V. Agrawal, and Bansi D. Malhotra. "Nanostructured metal oxide-based biosensors." *NPG Asia Materials* 3, no. 1 (2011): 17.

91. Deng, Zifeng, Yichun Gong, Yongping Luo, and Yang Tian. "WO_3 nanostructures facilitate electron transfer of enzyme: application to detection of H_2O_2 with high selectivity." *Biosensors and Bioelectronics* 24, no. 8 (2009): 2465-2469.

92. Feng, Jiu-Ju, Jing-Juan Xu, and Hong-Yuan Chen. "Direct electron transfer and electrocatalysis of hemoglobin adsorbed onto electrodeposited mesoporous tungsten oxide." *Electrochemistry communications* 8, no. 1 (2006): 77-82.

93. Sun, Qiang-Qiang, Maowen Xu, Shu-Juan Bao, and Chang Ming Li. "pH-controllable synthesis of unique nanostructured tungsten oxide aerogel and its sensitive glucose biosensor." *Nanotechnology* 26, no. 11 (2015): 115602.

94. Hariharan, V., S. Radhakrishnan, M. Parthibavarman, R. Dhilipkumar, and C. Sekar. "Synthesis of polyethylene glycol (PEG) assisted tungsten oxide (WO_3) nanoparticles for L-dopa bio-sensing applications." *Talanta* 85, no. 4 (2011): 2166-2174.

95. Thangavel, Sakthivel, Manikandan Elayaperumal, and Gunasekaran Venugopal. "Synthesis and properties of tungsten oxide and reduced graphene oxide nanocomposites." *Materials Express* 2, no. 4 (2012): 327-334.

96. Su, Pi-Guey, and Shih-Liang Peng. "Fabrication and NO_2 gas-sensing properties of reduced graphene oxide/WO_3 nanocomposite films." *Talanta* 132 (2015): 398-405.

97. Prabhu, S., L. Cindrella, Oh Joong Kwon, and K. Mohanraju. "Green synthesis of rGO-WO_3 composite and its efficient photoelectrochemical water splitting." *International Journal of Hydrogen Energy* 42, no. 50 (2017): 29791-29796.

98. Rozada, Rubén, Juan I. Paredes, María J. López, Silvia Villar-Rodil, Iván Cabria, Julio A. Alonso, Amelia Martínez-Alonso, and Juan MD Tascón. "From graphene oxide to pristine graphene: revealing the inner workings of the full structural restoration." *Nanoscale* 7, no. 6 (2015): 2374-2390.

99. Chua, Chun Kiang, and Martin Pumera. "Chemical reduction of graphene oxide: a synthetic chemistry viewpoint." *Chemical Society Reviews* 43, no. 1 (2014): 291-312.

100. Compton, Owen C., and SonBinh T. Nguyen. "Graphene oxide, highly reduced graphene oxide, and graphene: versatile building blocks for carbon-based materials." *small 6, no. 6* (2010): 711-723.

101. Pumera, Martin, Adriano Ambrosi, Alessandra Bonanni, Elaine Lay Khim Chng, and Hwee Ling Poh. "Graphene for electrochemical sensing and biosensing." *TrAC Trends in Analytical Chemistry* 29, no. 9 (2010): 954-965.

CHAPTER 2

Materials and Characterization Tools

This chapter briefs the various materials and chemicals used for the synthesis of different morphological tungsten trioxide nanostructures and reagents used for the fabrication of nanostructured WO_3 based biosensor. The different analytical approach used for the characterization of nWO_3, modified nWO_3 electrodes, and immunoelectrodes have also been detailed. Further, efforts have been made to brief the procedures and protocols employed for the biomolecules immobilization process.

2.1 Materials: Chemicals and Bio-chemicals

The chemicals such as sodium tungstate dehydrates ($Na_2WO_4.2H_2O$), Hydrochloric acid (HCl), oxalic acid ($C_2H_2O_4$), citric acid ($C_6H_8O_7$), sodium chloride (NaCl), and nitric acid (HNO_3) have been procured from Sigma Aldrich and used for the synthesis of different morphological nWO_3. The reagents namely 3-aminopropyltriethoxy saline (APTES), water soluble EDC [1-(3-(dimethylamino)-propyl)-3-ethylcarbodiimide hydrochloride], N-hydroxysuccinimide (NHS), ethanolamine (EA) have been procured from Sigma-Aldrich and used for the functionalization and immobilization process respectively. Further, sodium monophosphate (NaH_2PO_4), sodium diphosphatedihydrate ($Na_2HPO_4.2H_2O$), potassium ferrocyanide [$K_4\{Fe(CN)_6\}.3H_2O$], and potassium ferricyanide [$K_3\{Fe(CN)_6\}$] have been procured from fisher scientific and used for the preparation of phosphate buffer solution (PBS). The biomolecules cardiac Troponin I (cTnI) as antigen and cardiac Troponin I antibody (anti-cTnI) have been obtained from Ray Biotech, Inc. (India). All these reagents and chemicals have been used without any further purification. Milli-Q water having a resistivity of 18.3 MΩ was used for the preparation of all buffers and solutions. The prepared PBS solution then used for dilution of biomolecules (antigen and antibody) and washing of abricated immunoelectrodes.

2.2 Characterization Tools: Structural and Spectroscopic Tools

The properties of nanomaterial vary significantly with size and shape, hence accurate measurement of dimensions of nanomaterials is crucial toward its applications. The characterization of functionalized and unfunctionalized materials and its composites has been performed at different stages. To study the size, shape, and morphology of nanostructures, we employed electron microscopy techniques, while spectroscopy techniques have been used to study functionalization processes and composite. Further, we used electrochemical analyzer to study electrochemical behavior of the fabricated electrodes and immunoelectrodes.

In the following sections the different characterization tools employed for the study of materials and the fabricated electrodes have been described. Further, we brief the surface functionalization processes and immobilization procedures used in this work.

2.2.1 Scanning Electron Microscope (SEM)

Scanning electron microscope (SEM) is an advanced model of microscope which uses electrons rather than light to study the three-dimensional structure of the solid sample. The high-resolution image produced by SEM display the topographical, compositional, and morphological information of the solid sample. A scanning electron microscope employs the electromagnetic "lenses" to focus an electron beam onto a specimen to create an image by recording the interactions of the electron beam with the specimen surface, which can be a metal, metal oxide, ceramic or the biological specimen. In addition to topographical information, SEM can detect and analyze surface fractures, examine surface contaminations, provide details in microstructures, identify crystalline structures, and can provide qualitative chemical analyses too [1].

Figure 2.1 represents the schematic of the construction of the scanning electron microscope. The main component of SEM is electron gun, placed at the top of the column structure which produces the electrons and can accelerate them to up to 30 keV using electrostatic potential. The electromagnetic lenses and the passages placed below generate a focus electron beam. A high vacuum environment is sustained inside the chamber to avoid the scattering of an electron beam. The solid specimen consisting of periodic structure acts as a diffraction grating for the incident electron beam and results in the scattering of electron beams in various directions. For the visual investigation of the surface of the sample, two types of signals especially secondary electrons and backscattered electrons are used. Secondary electrons (SE) results from the inelastic collision and are characterized by low energy signals (50 eV). From these signals, we reveal the surface structure with a high

resolution. The backscattered electrons (BSE) which result from an elastic collision helps in studying topographical variance and atomic number variance with up to 1 micron of resolution [2]. In addition to these signals, the X-ray signals are also generated from the specimen which is used to determine elemental composition using energy dispersive X-ray spectroscopy (EDS).

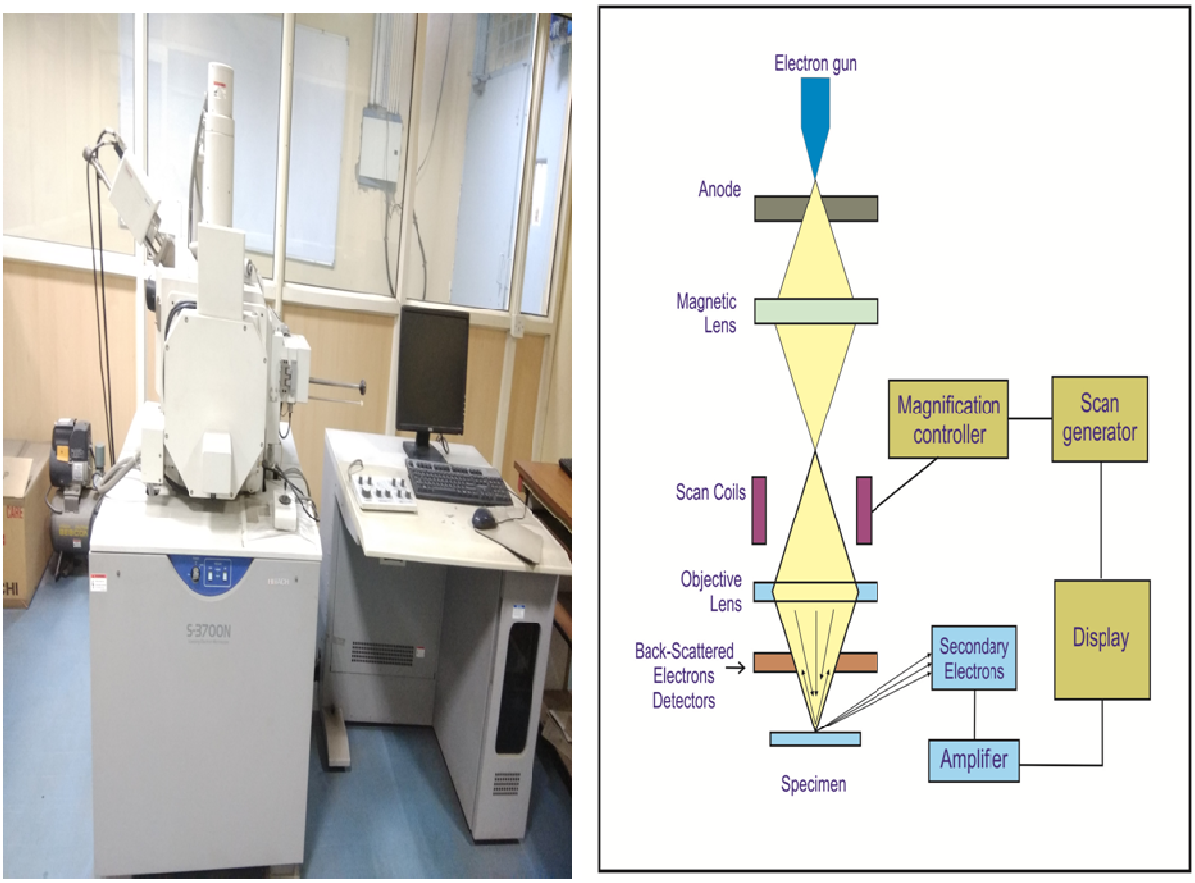

Figure 2.1: Set-up of a scanning electron microscope (SEM) and schematic representation of SEM

2.2.2 Field Emission-Scanning Electron Microscope (FE-SEM)

FE-SEM is an advanced analytical model of SEM which provides topographical and elemental information by scanning the specimen surface with a high energy electron beam in a raster scan pattern. The main difference between FE-SEM and SEM is the electron generating system. FE-SEM uses field emission gun as a source of electrons that produce an

extremely focused and low-energy beam which enhanced the spatial resolution. The system operates at low potentials which helps to minimize the charging effect on non-conductive specimens and avoids damage of sensitive specimens. **Figure 2.2** represents the interaction of electrons beam with the specimen. The high energy electrons beam on striking the specimen generates the secondary electrons. Another important feature of FE-SEM is "In-lens detectors" it uses for secondary electrons. The secondary electrons get caught by these detectors and produce the electronic signal which is amplified to produce a scanned image. A backscattered electron "In-Lens detectors" provides a pure backscattered signal without secondary electron contamination and low accelerating potential. Also, it results in higher Z-contrast and can select the electrons according to their energy.

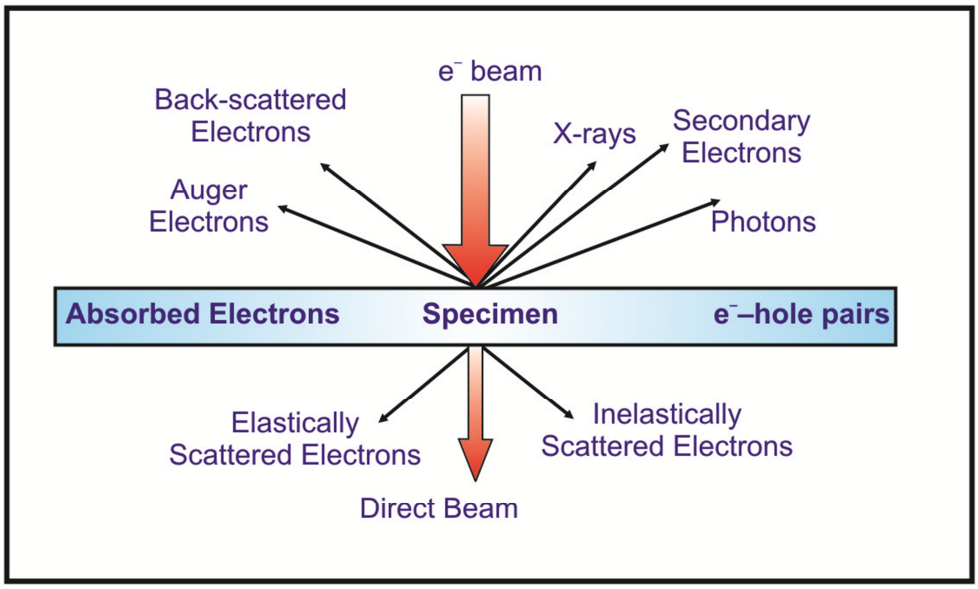

Figure 2.2: Interaction of electrons beam with the specimen

Along with these electrons, X-rays are also emitted on the interaction of electrons beam with the specimen. These X-rays get collected by detectors and produce electronic signals. These signals are very useful in the identification of elements present in the specimen. The unique atomic profile of each element makes X-rays to give qualitative

information of elements using energy dispersive X-ray analysis (EDAX). The morphologies of WO_3 and its composite (RGO-WO_3) were examined using FE-SEM (TESCAN) system.

2.2.3 Transmission Electron Microscope (TEM)

To study the high-resolution morphological images of the specimen and the crystallinity of it, a powerful analytical tool was employed known as transmission electron microscope (TEM). TEM gives detail information at the atomic-scale level of the specimen. It utilizes high energetic electrons beam to provide morphological, compositional and crystallographic information. A unique nanometer-size electron probe of TEM helps in identifying and quantifying the electronic and chemical structures of nanomaterial specimen. This system operates in two approaches: convergent and parallel beam approach. The objective lens along with the specimen chamber represents the heart of the TEM where an electrons beam gets transmitted through the thin specimen and interacts with it [3]. For the good TEM image, the thickness of the specimen lies in the range of 100- 200 nm as beyond this thickness, electrons could not readily penetrate through the specimen. The imaging system which consists of an objective lens and other lenses helps in producing magnified images or the diffraction pattern (DP). The intensity distribution of electrons after transmittance is imaged with a three-stage lens system onto a fluorescent screen [4].

A schematic of the transmission electron microscope is shown in **Figure 2.3**. As TEM utilizes a smaller wavelength electron beam, it produces a high resolution and magnified image. The TEM can be operated in different modes such as HR-TEM, SAED, or simple TEM to study morphology, particle dimensions, growth direction and lattice parameters of the material. The sample preparation for TEM analysis was done by dispersing the powder specimen in acetone using high power ultrasonicater (500 W, 20 kHz). The dispersed specimen was then drop-casted onto the carbon-coated Cu-grid. The different morphologies of WO_3 were examined using a JEOL JEM-2100.

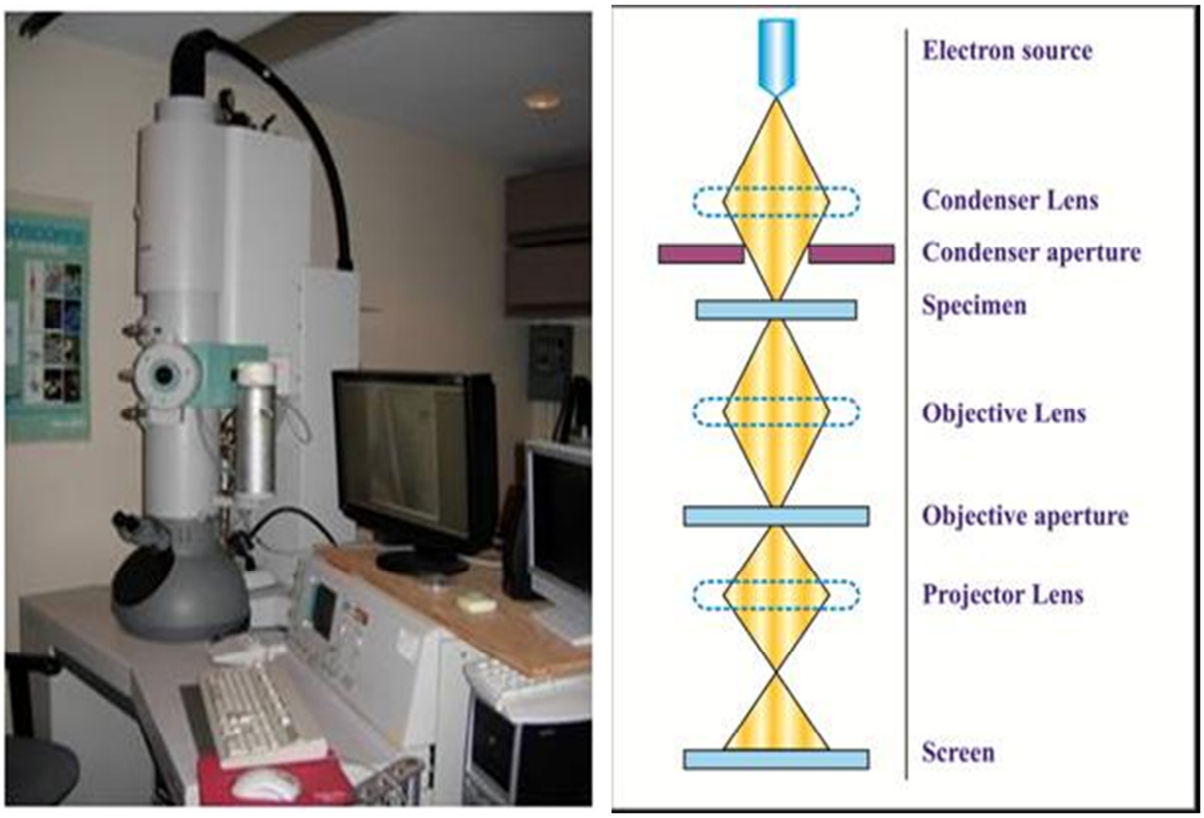

Figure 2.3: Set-up of transmission electron microscope (TEM) and the schematic representation of TEM

2.2.4 X-Ray Diffraction (XRD)

X-ray diffractometer is a measuring instrument used for different X-ray diffraction applications which involves phase analysis, structure determination, and stress measurement. X-ray diffraction (XRD) is a rapid and non-destructive analyses technique based on simple constructive interference between X-ray radiations after incident onto the specimen surface. The working principle of XRD is based on Bragg's law ($2d \sin\theta = n\lambda$) as shown in **Figure 2.4**. The crystalline specimen acts as a 3-D diffraction grating for the incident wavelength (λ). As X-rays have a wavelength comparable to the inter-atomic spacing (d), they will get diffracted and produce diffraction pattern [5]. The resultant characteristic X-ray diffraction pattern provides the unique "fingerprint" of the crystals present in the specimen.

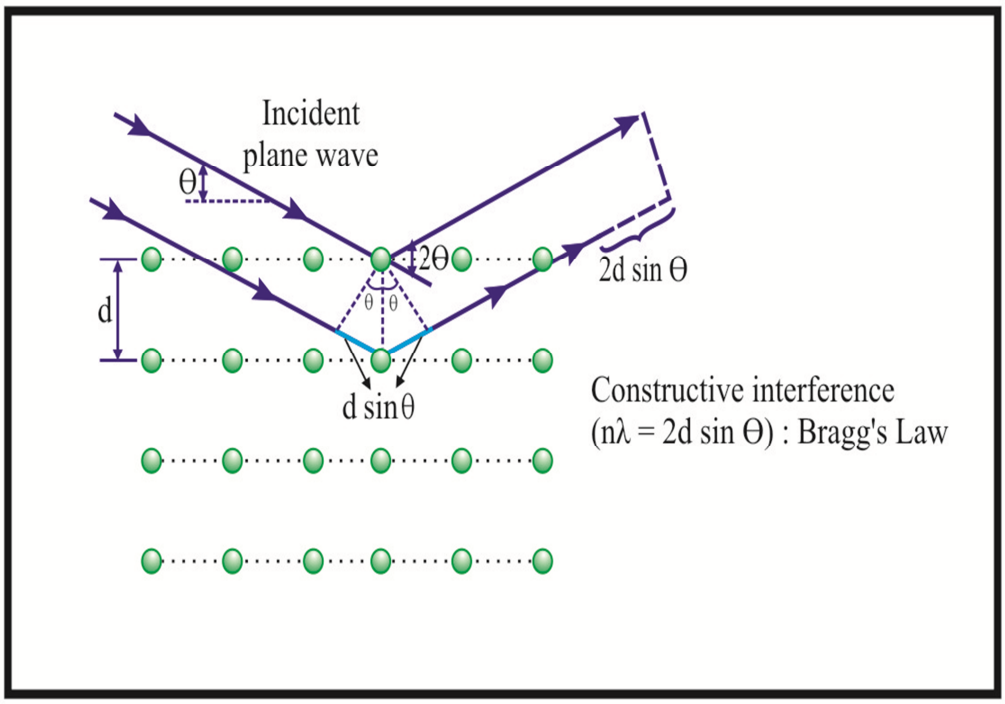

Figure 2.4: Schematic of X-ray diffraction satisfying Bragg's equation

In our case, we obtained X-ray diffraction patterns for the different morphologies of nanostructured WO_3 and its composite RGO-WO_3 recorded in the range of 10° to 80° using Bruker-D8 advanced XRD at the scan speed of 0.01 deg./sec. The obtained XRD spectra were analyzed using the JCPDS-ICDD powder diffraction database.

Further studying the FWHM of the different diffracted peaks, crystallite size can also determine using Debye Scherrer's **Equation**.

$$\mathbf{D = (0.89 \times \lambda)/ (\beta \times \cos\theta)}$$

Here, D represents the crystallite size, λ as a wavelength of Cu Kα (0.154 nm), β as FWHM and θ as diffraction angle [6]. **Figure 2.5** represents the setup of X-ray diffraction (XRD) used for the structural analysis.

Figure 2.5: Set-up of X-ray diffraction (XRD)

2.2.5 Atomic Force Microscope (AFM)

Atomic force microscope (AFM) is an appliance which produces a 3-D high-resolution image with a lateral resolution in few nanometers and vertical resolution less than 1 nm. It is a kind of scanning probe microscope which gives a topographical image of a specimen surface using interactions between a tip and a specimen. AFM mainly consists of a cantilever with a small tip at the free end, a photodiode, a laser, and a scanner as shown in **Figure 2.6.** A tip of the cantilever plays an important role in imaging [7]. It is generally made up of silicon or silicon nitride and is 3 – 15 microns in length while cantilever is 100-500 microns in length. A 3-D image is deduced by recording the cantilever motion along Z-direction as a function of the sample's X and Y location.

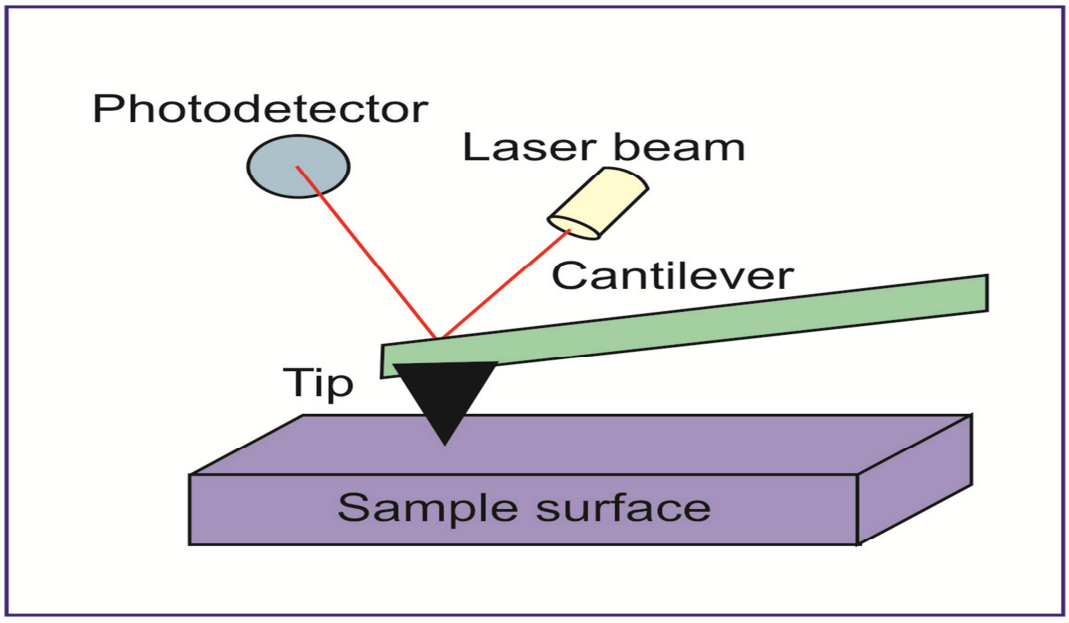

Figure 2.6: Schematic representation of atomic force microscopy (AFM)

AFM has different imaging approaches known as contact modus, non-contact modus, and tapping modus AFM [8]. The AFM in ***contact modus*** produces frictional forces during the scanning, as the tip is in contact with specimen surface and thus it is not suitable for the soft samples analysis. While in ***non-contact modus,*** the tip is not in contact with specimen surface but oscillates above the surface during scanning. Thus, the feedback loop is used to monitor the changes in amplitude due to the attractive Van der Waals forces and can obtain monitored topographical image of the surface. This modus is therefore well suited for the soft samples; however, the resolution gets compromised. Last, in ***tapping modus***, a stiff cantilever is employed which oscillates close to resonance frequency at a tip-specimen separation. This results in a small part of oscillation to lie in the repulsive regime of the Lennard–Jones potential. The tip-specimen interaction, therefore, varies from long-range attraction force to weak repulsion force. Thus, the tip intermittently touches the specimen while scanning and causes changes in the amplitude and the phase of oscillation. Hence, this modus of imaging produces a high-resolution 3-D image. In this work, we employed this appliance for the

characterization of a fabricated electrode at the different stage of functionalization and immobilization.

2.2.6 Raman Spectrometer

Raman spectrometer is a spectroscopic technique which utilizes the scattered light to obtain details of molecular vibrations containing information of symmetry, bonding, and structure of the molecules. Hence, it provides significant and subjective information of the individual compound of the specimen. In principle, this spectroscopy is based on inelastic scattering of monochromatic light (***Raman Effect***) [9]. When highly monochromatic light is incident on the substance, then three types of phenomena can be possible as shown in **Figure 2.7** First is ***Rayleigh scattering*** in which frequency of the scattered beam light is equivalent to the incident beam light. Second is ***anti-stokes Raman scattering***, in this frequency of the scattered beam light is higher than that of the incident beam light. And third ***Stokes Raman scattering,*** in this frequency of the scattered beam light is lower than that of incident beam light.

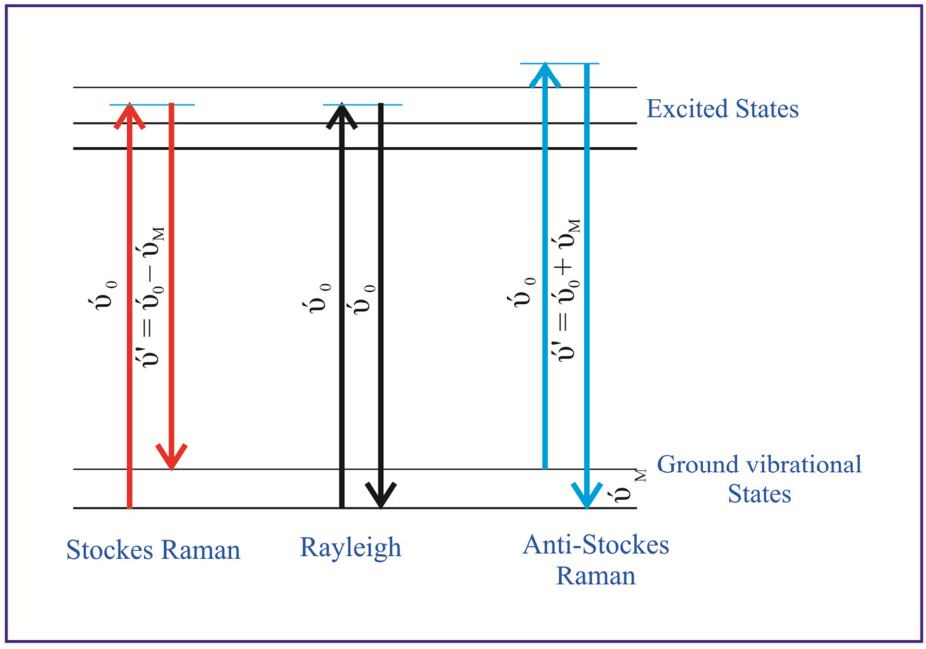

Figure 2.7: Energy level transitions in Raman scattering

In general, this spectroscopy deals with the study of changes in the molecular bonds polarizability of the specimen. The interaction of light with a molecule induces a deformation of its electron cloud resulting in a change of polarizability [10]. And these molecular bonds carrying specific energy transitions corresponding to changes in polarizability give rise to Raman active modes. A Raman spectrometer consists of 4 basic components including a laser light which serves as the excitation source, a wavelength selector, specimen illumination system, and the detector (photodiode array, CCD). In this work, we studied the Raman spectra to characterize the molecular structure of the WO_3-RGO nanocomposite. The films were deposited on the corning glass substrate and the spectra were obtained using 514 nm (excitation wavelength) as the light source (Argon laser).

2.2.7 Fourier Transform –Infrared (FT-IR) Spectrophotometer

Fourier transform infrared spectrophotometer is a powerful and non-destructive appliance which utilizes an infrared light region of the electromagnetic spectrum for interaction with the specimen. Generally, the molecules present in the specimen absorb this range of light radiations and give details specifically to the bonds present in the molecules [11]. In our work, we employed this appliance to study the formation or attachment of functional groups or biomolecules during different stages of preparation of electrodes and immunoelectrodes. The spectroscopy deals with the study of change in electric dipole moment of the molecules resulting from the absorption of a specific wavelength by the specimen molecule. Hence, the absorbed IR radiations correspond to the identification of the specimen.

In FT-IR spectrometers, beams are produced via interferometer. Generally, a Michelson interferometer is employed in FT-IR spectrometer which employs a beamsplitter to produce two beams of different path length which on recombination produces interferences and forms an interferogram. The resultant interferogram consists of time domain which gets

converted into a spectrum by using Fourier transform. And the first FT-IR spectrum was produced by Perkin Elmer, U.S.A. The absorption spectrum in FT-IR identifies the presence of chemical bonds and the functional group present in the specimen. **Figure 2.8** represents the setup of FTIR.

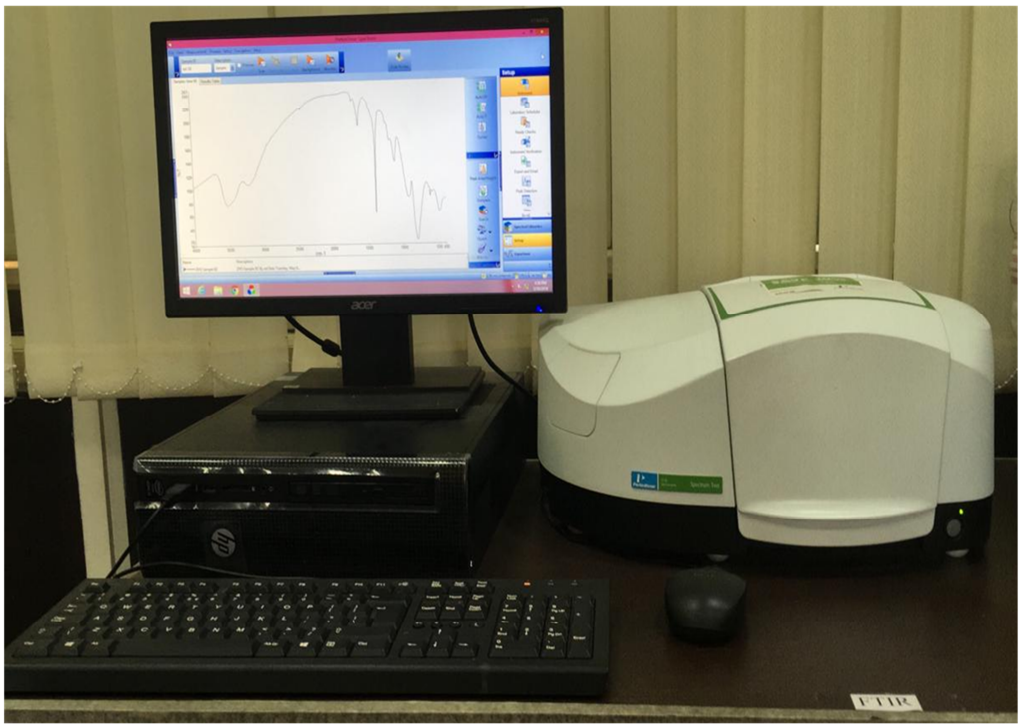

Figure 2.8: Set-up of Fourier transform –infrared (FT-IR)

In our work, we investigated the IR measurements using Potassium bromide (KBr) approach. In this approach, a very small amount of the powder specimen was dispersed in KBr and pellet was prepared to obtain spectra in transmission mode. The spectrum was obtained for the wave number range corresponding to mid-range of infrared (4000–400 cm^{-1}) and plotted against the transmittance values. We obtain FT-IR spectra at different stages of functionalization and immobilization of biomolecules onto the functionalized WO_3 based electrodes.

2.2.8 Contact Angle Measurement

The contact angle (CA) measurement illustrates the hydrophobic and hydrophilic characteristics of the modified surface. Going to its history, **Thomas Young** was the first person who explains the relation between contact angle and the wettability [12]. As wettability measurements can directly address the surface properties including adhesiveness, hydrophilicity, and hydrophobicity. Hence, by studying the wetting properties of modified surfaces, one can represent fundamental characteristics of the surface. Also with the advance in its studies, researchers have also put forward relation between the roughness and hydrophobicity and others too. The most common technique employed for contact angle measurement is the **static sessile drop technique**. In this technique, measurement is performed by putting a drop of liquid onto a solid surface and simultaneously will capture an image of that drop. Later, we will draw a tangent to the drop at its base using a goniometer from which we can measure CA [13].

2.3 Electrochemical Techniques

Electrochemical techniques are viable characterization tools based on the principle of electrochemistry and deals with the study of oxidation and reduction reactions. In recent times, electrochemical techniques have contributed to the development of efficient and sensitive biosensors as a transducer [14]. In such electrochemical biosensors, the reactions are monitored electrochemically either by generating a measurable current, potential, or impedance. As electrochemistry is a surface technique, it offers certain advantages in detection such as ease of fabrication of electrodes, small sample volumes, and simplicity in construction. Based on the measurement parameters such as potential, current, or impedance, the electrochemical techniques can be categories as Voltammetry, Amperometry, and electrochemical impedance spectroscopy [15-16].

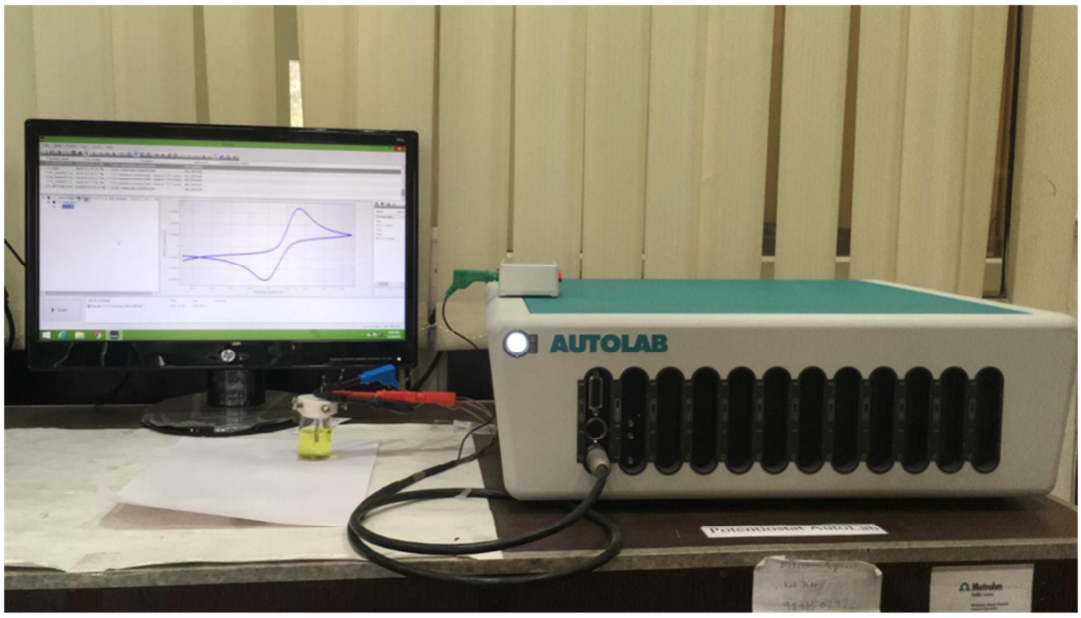

Figure 2.9: Set-up of electrochemical instrument autolab potentiostat (Eco Chemie, Netherlands)

In this work, we have used a three electrode electrochemical cell system consisting of a fabricated electrode, Ag/AgCl, and platinum (Pt) wire as working electrode, a reference electrode and as counter electrode respectively. The cell was further connected to an instrument a**utolab potentiostat** (Eco Chemie, Netherlands) as shown in **Figure 2.9** for the measurements. The Autolab potentiostat controls the voltage between the working electrode and the reference electrode and then measures the current flow through the cell. The impedance spectroscopy, cyclic voltammetry (CV), and differential pulse voltammetry (DPV) are the electrochemical analytical tools which were employed as the transduction mechanism in the fabrication of the biosensor platform.

2.3.1 Cyclic Voltammetry (CV)

Cyclic voltammetry (CV) is a most widely studied technique in the electrochemical analysis which presents details of the thermodynamics processes, electron transfer dynamics, and the other electrochemical properties of the electro-active species. In CV, the current is

measured in response to the cycled voltage applied at the working electrode at a fixed scan rate. In general, when a low voltage is applied to the cell, the response current (reaction rates) is determined by measuring charge transfer between the working electrode and the electrolyte solution. This results in an increase of current with an increase in voltage. The current increases till the voltage reach the oxidation potential of the given analyte and after it, start falling due to the deficiency of the charges close to the electrode surface. At this point, opposite polarity voltage is applied and this will produce a reduction peak similar in shape as that of the oxidation peak [17-18]. Generally, for the quasi-reversible reaction, non-symmetric peaks are observed and for the irreversible process, we do not observe the peak in the measurable potential region. Thus observing the CV curve, information about redox potential and the nature of the electrochemical processes can be justified. The different parameters which we can examine from the CV include anodic and cathodic peak current (Iap, Icp), and anodic and cathodic peak potential (Epa, Epc) is shown in **Figure 2.10**.

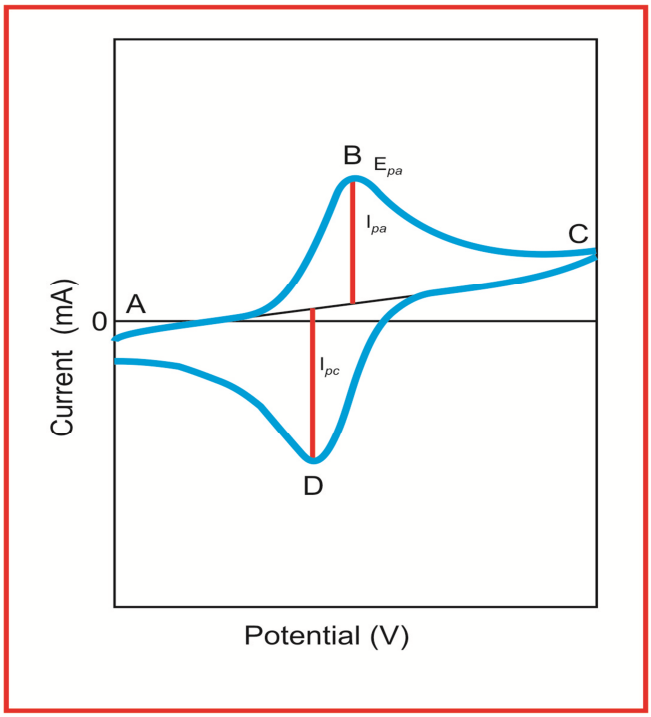

Figure 2.10: Schematic representation of cyclic voltammogram (CV)

In our work, we studied the cyclic voltammograms for the examination of fabricated electrodes and immunoelectrodes and verified scan rate study too.

2.3.2 Electrochemical Impedance Spectroscopy (EIS)

For a sensitive detection, electrochemical impedance spectroscopy (EIS) is considered as ideal spectroscopy for the study of interfacial kinetics at the electrode surface. The impedance measurement can be faradic or non-faradic in respect of the investigation of measurements performed in the presence or absence of the redox probe respectively. The EIS is a faradic impedance technique which deals with the electron transfer kinetics at the interface by overcoming different obstruction made by solution resistance and polarization resistance. The impedance (Z) is measured by applying small amplitude voltage perturbation (10 mV) and detecting the corresponding current. The measured impedance is a complex quantity, therefore, its value is described as a combination of real (Z_R) and imaginary (Z_I) impedance [19]. The faradaic impedance spectrum, plotted between Z_I and Z_R is known as ***Nyquist plot*** and since the impedance measurement is obtained in a broad range of frequencies, therefore it is termed as electrochemical impedance spectroscopy (EIS). As shown in **Figure 2.11**, a Nyquist plot is consists of a semi-circle region and a straight line. The semi-circle region which corresponds to the electron transfer kinetics at the electrode surface observed at higher frequencies domain while the straight line which represents the diffusion limited process observed at low frequencies domain [20]. In recent time, investigation of immuno-interactions in biosensing using the EIS technique has shown tremendous potential toward the development of biosensors. Such biosensors are known as electrochemical immunosensors which examine the variation in the faradic current as observed due to steric obstruction made by the bio-molecular interactions.

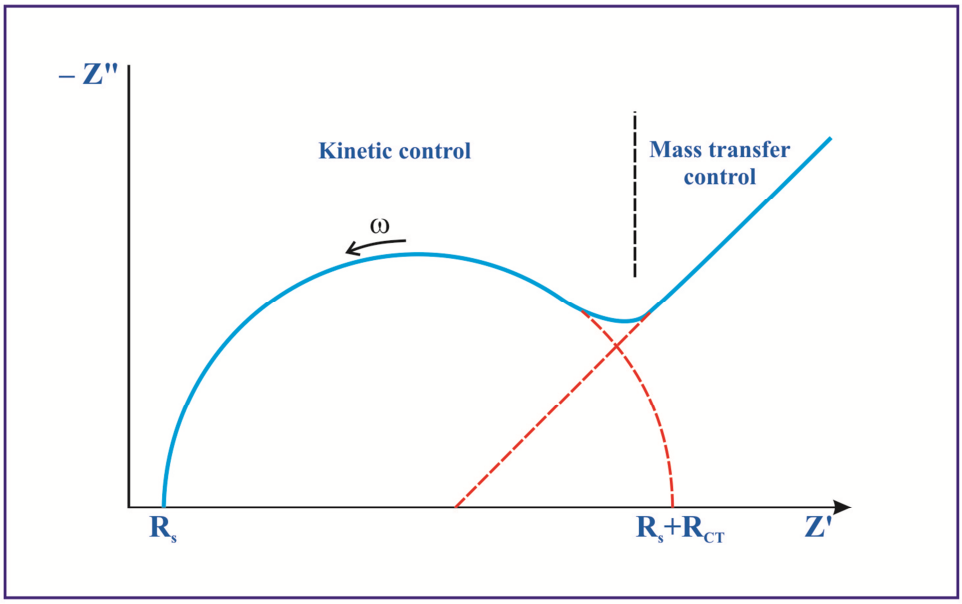

Figure 2.11: EIS impedance spectrum (Nyquist plot)

2.3.3 Differential Pulse Voltammetry (DPV)

Differential pulse voltammetry (DPV) is a voltammetry technique in which potential waveform is made up of small pulses of single-valued amplitude superimposed on a staircase waveform. The current is examined twice for each pulse period. The current is measured first at the beginning of the applied pulse, and later at the end of the pulse. And the measured current difference between the two currents (ΔI) is plotted against potential and referred to as differential pulse voltammogram. When the potential is at around the redox potential, the ΔI reaches the maximum value, and it decreases to zero for diffusion process [21]. Thus this technique discriminates the faradaic current from the capacitive current. The current response of differential pulse voltammetry depicts the symmetric peak and height of this current is directly related to the concentration of the analyte.

In DPV, we actually measured Δi/ΔE value and effect of the charging current is minimized which make it more sensitive with respect to other voltammetry techniques. In this

work, we employed this technique to study the response of RGO-WO_3 based immunoelectrode towards cTnI detection in **chapter 6**.

2.4 Surface Functionalization and Antibody Immobilization Chemistries

2.4.1 Surface Functionalization

The biological recognition phenomenon in electrochemical biosensing produces a quantitative signal, which is equivalent to the concentration of the analyte in the given volume. Thus, the biomolecule immobilization process plays a crucial role in the performance of the biosensor. And the substrate material such as nanomaterials, electrodes, etc., should be modified to introduce functional species such as amino, ethoxy, or carboxyl groups on the substrate material that can bind to biomolecules with high activity, great bonding strength, good orientation, and excellent long-term stability.

The process of generating a silane group is known as Silanization. The silanization provides the means to tailor surface properties such as hydrophilicity, hydrophobicity, charge, etc. and also biocompatible microenvironment. To accomplish the grafting of silane molecules, the substrate surface is chemically activated with hydroxyl groups which result in the formation of covalent Si─OH bonds onto the substrate surface. The surface modification using functionalized molecules also known as coupling agents such as phenyl terminated, amine terminated, and thiol terminated silanes have been well studied for the fabrication of the bioanalytical platforms [22]. Sagiv et al. were the first to report the strong bounded chemisorbed monolayer using silane agents [23]. Amino-silane **APTES (3- Aminopropyl-triethoxysilane**) is the most studied coupling agent for the surface functionalization process. The APTES molecule consists of three hydrolyzable ethoxy groups and one amine (─ NH_2) group in which ethoxy groups contributes toward the silanization process and amine groups contributes towards further functionalization process via covalent bonding [24-25]. APTES

as a functionalization agent offers various advantages toward the development of an efficient biosensing platform such as:

i) High antibody loading,

ii) Leach proof antibody biomolecules binding,

iii) Long term stability, and

iv) An enhanced specific activity of biomolecules

2.4.2 Electrophoretic Deposition (EPD) Technique

The fabrication of thin films and coating can be accomplished by employing an electrophoretic deposition (EPD) technique. In this technique, colloidal particles suspended in the media get electrophoretic deposits on the electrode (ITO) substrate with the application of the electric field. The main driving force in EPD is the mobility and charge of the colloidal particles [26]. Depending on the nature of the particle such as positive or negative, deposition can be cathodic or anodic respectively.

In EPD, the characteristics of films and deposition kinetics depend on various parameters. These parameters are as follow:

i) **Deposition time**: For a constant applied potential difference, the force influencing electrophoresis phenomenon decreases with deposition time. The reason behind this is the creation of an insulating layer at the substrate. However, at the initial stage of deposition, there exhibits a linear relationship between deposition time and mass.

ii) **Applied potential:** The applied potential field plays an important role in the rate of deposition of colloidal particles and also the structure of the deposit [27]. For a uniform film deposition, moderate fields should be applied (25- 100 V/cm) while at relatively high fields (> 100 V/cm) the films get deteriorates.

iii) **Concentration:** The concentration of the colloidal particles in the suspension does affect the rate of deposition of a film onto the substrate.

iv) **Substrate:** The conductivity of the substrate plays an important role in the uniformity of the deposited films [28-29]. If the substrate has low conductivity, the deposition rate decreases and results in the non-uniformity of the film.

2. 4.3 Substrate

Indium tin oxide (ITO) is a well-studied electrode material in the various fields of applications. The high electrical conductivity and optoelectronic characteristics serve it as a good conducting substrate for the development of sensor devices [30]. The exclusive physical and electrochemical properties of ITO make it a very stable and ideal electrode substrate. In recent time, ITO has been contributing to the fabrication of electro-analytical sensors due to its excellent surface characteristics and electron transfer kinetics [31-33]. Towards the development of electrochemical biosensors, ITO as a substrate had been in practice. Prior to the immobilization of bio-entities, the ITO surfaces get modified with functionalized molecules (silane reagents) for the stable and control immobilization of bio-entities. 3-Aminopropyl-triethoxysilane (APTES) as a functionalized alkyl silanes was used to functionalized the ITO surface which provides free NH_2 groups onto the surface for the covalent binding with COOH groups of antibody biomolecules.

2.4.4 Immobilization Techniques

The most crucial step in the preparation of the immunosensor platform is the immobilization of antibodies biomolecules onto the electrode surface. The performance of an immunosensor is highly dependent on the characteristics of the immobilized antibodies as it further dictates the stability, sensitivity, reproducibility, and other bioanalytical variables [34-35]. The supportive matrix should be bio-friendly, non-toxic, strong mechanical stability and highly reactive functional groups. For immobilization of antibody biomolecules onto the matrix, choose of an appropriate technique is required to prevent the denaturation of

biomolecules. As such there are four principal techniques for the immobilization of antibody biomolecules namely, adsorption, and encapsulation as physical methods and cross-linking, and covalent bonding as chemical methods.

2.4.4.1 Physical Adsorption

The physical adsorption is a simple and fast method of immobilization of biomolecules. In this technique, immobilization of antibody biomolecules is accomplished by the non-covalent interactions such as weak van der Waals forces, electrostatic, hydrophobic, and hydrogen bonds. This adsorption technique is weak and non-specific, but it enables a large number of reasonable binding. The main advantages of this immobilization technique are:

i) Requires no reagents and adopt easy protocols for the adsorption.

ii) No conformational changes in the biomolecules.

iii) The reversible process such that the matrix can be regenerated with fresh biomolecules.

However, this technique has its own drawback that the adsorbed proteins biomolecules can leach away from the surface of the adsorbed surface is exposed to the high liquid flow.

2.4.4.2 Physical Encapsulation

Physical encapsulation is an irreversible method of immobilization where the biomolecules get entrapped in support either in polymer membranes or in a lattice structure of a material and retain the biomolecule. As a result, biomolecules get physically restricted within a confined space or network. The biomolecules do not chemically interact with the polymer matrix; therefore it avoids the denaturation of the biomolecules. Hence, encapsulation improves the mechanical stability of the immobilized matrix and minimizes the leaching. The main advantages of the method are

i) Encapsulation of a large number of biomolecules in it.

ii) Chemically inactive.

iii) Thermally stable

iv) Low-temperature process and optically clear.

v) Creates an optimal microenvironment for the biomolecules.

2.4.4.3 Cross-Linking

Cross-linking is a chemical method of immobilization which involves the covalent attachment of the antibody biomolecules onto a matrix via a linker molecule. The formation of an intermolecular cross-linkage between the protein biomolecules and the matrix is accomplished by the means of bi- or multifunctional reagents. Generally, glutaraldehyde is used as cross-linker reagent due to its availability in large quantity and economical. The covalent attachment provides a stronger attachment than physical adsorption and also provides the biomolecules with high catalytic activity.

2.4.4.4 Covalent Binding

Covalent binding is one of the most widely used immobilization technique resulting in the formation of strong chemical bonds between biomolecules and the matrix. For the strong covalent binding, the direction of the antibody biomolecule is very crucial as it determines the stability of the immobilized matrix. In this phenomenon, the binding between biomolecules and the matrix is very strong and avoids leakage of the biomolecules even in the presence of high ionic strength. The main advantages of this method are as follow

i) It increases the shelf life of the immunosensor.

ii) Enhances thermal stability of biomolecules when coupled with other support.

iii) High loading of the antibody biomolecules

iv) Antibody modification is not required

In this study, we have used 3-aminopropyltriethoxy saline (APTES) as a functionalized agent which can generate free amino groups onto the matrix and will

covalently bind with carboxyl groups (COOH) of antibodies. Also, to activate the –COOH groups of antibody, we have used EDC-NHS hetero-bifunctional cross-linking. The EDC-NHS chemistry generates the activated surface after the formation of an amide bond between amine functionalized (APTES) matrix and the carboxyl group of the antibody.

2.5 References:

1. Egerton, Ray F. *Physical principles of electron microscopy*. New York: Springer, 2005.
2. Bozzola, John J., and Lonnie Dee Russell. *Electron microscopy: principles and techniques for biologists*. Jones & Bartlett Learning, 1999.
3. Guo, Yizhu, Sandra Gonzalez, and Ana R. Guadalupe. "Transmission Electron Microscopy Characterization and Application of Sol-Gel Membranes." *Microscopy and Microanalysis* 5, no. 6 (1999): 445-451.
4. Ding, Yong, and Zhong Lin Wang. "Structure analysis of nanowires and nanobelts by transmission electron microscopy." (2004): 12280-12291.
5. Jenkins, Ron, and Robert L. Snyder. *Introduction to X-ray powder diffractometry*. No. 543.427 JEN. 1996.
6. Cullity, B. D. "Elements of X-ray diffraction, Addition-Wesley Publ. Co." *Inc., New York* (1978): P102.
7. Eaton, Peter, and Paul West. *Atomic force microscopy*. Oxford university press, 2010.
8. Hinterdorfer, Peter, and Yves F. Dufrêne. "Detection and localization of single molecular recognition events using atomic force microscopy." *Nature methods* 3, no. 5 (2006): 347.
9. Pelletier, M. J. "Quantitative analysis using Raman spectrometry." *Applied spectroscopy* 57, no. 1 (2003): 20A-42A.
10. Lewis, Ian R., and Howell Edwards. *Handbook of Raman spectroscopy: from the research laboratory to the process line*. CRC Press, 2001.

11. Smith, Brian C. *Fundamentals of Fourier transform infrared spectroscopy*. CRC Press, 2011.
12. Strobel, Mark, and Christopher S. Lyons. "An essay on contact angle measurements." *Plasma Processes and Polymers* 8, no. 1 (2011): 8-13.
13. Zhao, Tianyi, and Lei Jiang. "Contact angle measurement of natural materials." *Colloids and Surfaces B: Biointerfaces* 161 (2018): 324-330.
14. Huang, Ying, Jin Xu, Junjie Liu, Xiangyang Wang, and Bin Chen. "Disease-Related Detection with Electrochemical Biosensors: A Review." *Sensors* 17, no. 10 (2017): 2375.
15. Thévenot, Daniel R., Klara Toth, Richard A. Durst, and George S. Wilson. "Electrochemical biosensors: recommended definitions and classification." *Analytical Letters* 34, no. 5 (2001): 635-659.
16. BHARDWAJ, TANU. "Review on biosensor technologies." *Journal Impact Factor* 6, no. 2 (2015): 36-62.
17. Kissinger, Peter T., and William R. Heineman. "Cyclic voltammetry." *Journal of Chemical Education* 60, no. 9 (1983): 702.
18. Heinze, Jürgen. "Cyclic voltammetry—"electrochemical spectroscopy". New analytical methods (25)." *Angewandte Chemie International Edition in English* 23, no. 11 (1984): 831-847.
19. Bahadır, Elif Burcu, and Mustafa Kemal Sezgintürk. "A review on impedimetric biosensors." *Artificial cells, nanomedicine, and biotechnology* 44, no. 1 (2016): 248-262.
20. Reece, C. "An introduction to electrochemical impedance spectroscopy." *Jefferson Lab* (2005).
21. Brown, Alan P., and Fred C. Anson. "Cyclic and differential pulse voltammetric behavior of reactants confined to the electrode surface." *Analytical Chemistry* 49, no. 11 (1977): 1589-1595.

22. Vashist, Sandeep Kumar, Edmond Lam, Sabahudin Hrapovic, Keith B. Male, and John HT Luong. "Immobilization of antibodies and enzymes on 3-aminopropyltriethoxysilane-functionalized bioanalytical platforms for biosensors and diagnostics." *Chemical reviews* 114, no. 21 (2014): 11083-11130.
23. Sagiv, Jacob. "Organized monolayers by adsorption. 1. Formation and structure of oleophobic mixed monolayers on solid surfaces." *Journal of the American Chemical Society*102, no. 1 (1980): 92-98.
24. Vuori, Leena, Markku Hannula, Kimmo Lahtonen, Petri Jussila, Harri Ali-Löytty, Mika Hirsimäki, Rainer Pärna, Ergo Nõmmiste, and Mika Valden. "Controlling the synergetic effects in (3-aminopropyl) trimethoxysilane and (3-mercaptopropyl) trimethoxysilane coadsorption on stainless steel surfaces." *Applied Surface Science* 317 (2014): 856-866.
25. Terracciano, M., I. Rea, J. Politi, and L. De Stefano. "Optical characterization of aminosilane-modified silicon dioxide surface for biosensing." *Journal of the European Optical Society-Rapid publications* 8 (2013).
26. Besra, Laxmidhar, and Meilin Liu. "A review on fundamentals and applications of electrophoretic deposition (EPD)." *Progress in materials science* 52, no. 1 (2007): 1-61.
27. Sarkar, Partho, and Patrick S. Nicholson. "Electrophoretic deposition (EPD): mechanisms, kinetics, and application to ceramics." *Journal of the American Ceramic Society* 79, no. 8 (1996): 1987-2002.
28. Ma, Jan, and Wen Cheng. "Deposition and packing study of sub-micron PZT ceramics using electrophoretic deposition." *Materials Letters* 56, no. 5 (2002): 721-727.
29. Basu, Rajendra N., Clive A. Randall, and Merrilea J. Mayo. "Fabrication of dense zirconia electrolyte films for tubular solid oxide fuel cells by electrophoretic deposition." *Journal of the American Ceramic Society* 84, no. 1 (2001): 33-40.

30. Chopra, K. L., S. Major, and D. K. Pandya. "Transparent conductors—a status review." *Thin solid films* 102, no. 1 (1983): 1-46.
31. Sun, Xiuhua, and Kevin D. Gillis. "On-chip amperometric measurement of quantal catecholamine release using transparent indium tin oxide electrodes." *Analytical chemistry*78, no. 8 (2006): 2521-2525.
32. Zhang, Jingdong, Miyako Kambayashi, and Munetaka Oyama. "Seed mediated growth of gold nanoparticles on indium tin oxide electrodes: electrochemical characterization and evaluation." *Electroanalysis: An International Journal Devoted to Fundamental and Practical Aspects of Electroanalysis* 17, no. 5-6 (2005): 408-416.
33. Muthurasu, A., and V. Ganesh. "Electrochemical characterization of Self-assembled Monolayers (SAMs) of silanes on indium tin oxide (ITO) electrodes–Tuning electron transfer behaviour across electrode–electrolyte interface." *Journal of colloid and interface science* 374, no. 1 (2012): 241-249.
34. Prieto-Simon, B., M. Campas, and J-L. Marty. "Biomolecule immobilization in biosensor development: tailored strategies based on affinity interactions." *Protein and peptide letters* 15, no. 8 (2008): 757-763.
35. Ferreira, Marystela, Pablo A. Fiorito, Osvaldo N. Oliveira Jr, and Susana I. Córdoba de Torresi. "Enzyme-mediated amperometric biosensors prepared with the Layer-by-Layer (LbL) adsorption technique." *Biosensors and Bioelectronics*19, no. 12 (2004): 1611-1615.

CHAPTER 3

Functionalized Tungsten Trioxide Nanoparticles Based Platform for Cardiac Troponin I (cTnI) Detection

In this chapter, we demonstrate the fabrication of 3-aminopropyl tri-ethoxy saline (APTES) conjugated ***tungsten trioxide nanoparticles*** *(APTES/WO_3 NPs) based platform for cardiac Troponin I (cTnI) detection. The tungsten trioxide nanoparticles are synthesized using hydrothermal synthesis route. The fabricated APTES/WO_3 NPs/ITO electrode and antibody immobilized electrode (anti-cTnI/APTES/WO_3 NPs/ITO) were characterized using atomic force microscope (AFM), Fourier transform infrared spectrometer (FT-IR) and electrochemical impedance spectroscopy (EIS). The electrochemical response studies of the fabricated immunoelectrode shows sensitivity as 26.56 Ω $ng^{-1}mL\ cm^{-2}$ in a wide linear detection range 1- 250 ng mL^{-1}. Also, the proposed platform shows the stability of 30 days.*

The work presented in this chapter is published as:

"Bio-functionalized nanostructured tungsten trioxide based sensor for cardiac biomarker detection"

Materials Letters 186 (2017) 202-205

3.1 Introduction

Cardiac markers have the most dynamic applications owing to the increasing number of people suffering from cardiovascular diseases (CVDs) and rising demand for instant diagnosis of these diseases. Early and accurate diagnosis of CVD can provide appropriate, timely and cost-effective treatment and hence prevention action. Acute myocardial infarction (AMI) is one of the cardiovascular diseases, caused by necrosis of myocardial tissue due to ischemia. Amongst the various biomarkers, cardiac Troponin I (cTnI) is a cardiac-specific biomarker that releases with the onset of myocardial necrosis. Compared to other biomarkers such as C-reactive protein (CRP), Myoglobin (Mb), and Creatine-kinase-MB, cTnI has more specificity and sensitivity towards AMI detection [1]. The level of cTnI in normal subjects is around 1 ng mL^{-1} that can increase up to 550 ng mL^{-1} in AMI patients [2]. Hence rapid and sensitive detection of cTnI with good detection ranges urgently required for the early treatment of AMI. The different analysis techniques which have been in used for cTnI detection includes enzyme-linked immunosorbent assay [3], fluoro-immunoassay [4], chemiluminescent immunoassays and aptamer-based biosensors [5-6]. Although these techniques do provide good sensitivity but the instrumentation expenditure and cumbersome operation limits infeasibility. Hence biosensor can be an appropriate appliance for the early diagnosis of cardiac disease.

With the advancement in nanotechnology, the development of immunosensor based on the electrochemical technique for biomarker measurement has proven to be effective in point-of-care diagnostics. Surveyed literature has shown that the fusion of biological molecules and nanostructured metal oxides can be documented to play a pivotal role in the conception of nano-scale instruments used in clinical diagnosis and electronic devices [7]. Among the various nanostructured metal oxides, tungsten trioxide nanoparticles (WO_3 NPs) exhibit apposite physical and chemical properties [8]. Tungsten trioxide nanoparticles

modified electrode do exhibit enhanced electrochemical kinetics, reduced over potential, and large electro-active surface areas unlike bulk working electrodes. Therefore, the main focus behind this chapter is to investigate the applicability of WO_3 NPs for the development of diagnostic protein based biosensor. The enhanced electrical, tunable conductivity and catalytic behaviour of WO_3 NPs render it as more feasible to be deployed as "electronic wires" that could enhance transfer of electrons between electrode surfaces and redox centres in protein biomolecules [9]. Further, the accentuated surface-to-volume ratio and electrical sensitivity allow WO_3 NPs to be used as a label or tracer in electrochemical analysis. These distinctive features of WO_3 NPs can therefore enhance its biosensing applications. The study conducted by Hariharan et al. reported the WO_3 based biosensor for L- dopa detection with high selectivity and sensitivity [10]. Later, Sun et.al utilized WO_3 for glucose detection with high efficiency [11]. Hence in this chapter, we have demonstrated the conception of a basic; label-free immunosensor based on nanostructured tungsten trioxide nanoparticles that can detect the presence of Troponin I, a prominent myocardial infarction biomarker. The proposed detection strategy is elementary, cost-effective and is based on immobilizing an antibody of cTnI on a 3–aminopropyltriethoxy saline (APTES) functionalized WO_3 NPs /ITO electrode.

3.2 Experimental Section

3.2.1 Synthesis and Functionalization of WO_3 NPs

The tungsten trioxide nanoparticles have been synthesized using a facile low-temperature hydrothermal process with a modification [12]. Firstly, we prepared a 0.5M sodium tungstate ($Na_2WO_4.2H_2O$) solution in a 30 mL of Milli-Q water and then stirred it briskly for a few seconds. For the acidification, we added 6M HCl to the solution dropwise, till the pH of the solution reaches the value 1. Afterward, we added 1.5 gm of oxalic acid to the above solution and kept on stirring for 45 minutes. For the hydrothermal treatment, the

stirred solution got transferred to a 50 mL Teflon-lined vessel and then placed in a stainless steel autoclave. The autoclave is then placed in an oven at 120 °C for 4 hours for the hydrothermal reaction. Thereafter as the autoclave cooled naturally to room temperature, we collected the sample after centrifuging it for 6-7 times with Milli-Q water. The resultant sample (WO_3 NPs) is used for further characterization and functionalization process.

For the functionalization of WO_3 NPs, we prepared a 100 mg of WO_3 NPs solution in a 20ml of isopropanol and then sonicated effectually for attaining a well-dispersed suspension. This is followed by addition of 200 µL of 98% APTES and stirring at 300 rpm for 48 hours (2 days) continuously [13]. The resultant functionalized WO_3 nanoparticles got filtered and washed thoroughly with Milli-Q water to remove the unbound APTES molecules.

3.2.2 Fabrication of Antibody Immobilized APTES/WO_3 NPs/ITO Immunoelectrode

The fabrication of a thin film of APTES functionalized WO_3 NPs onto the pre-hydrolyzed ITO glass substrate has been accomplish through electrophoretic deposition (EPD) technique. The electrophoretic deposition (EPD) is an advantageous technique due to its low cost; ease of processing; uniform deposits, control of deposited films thickness and micro structural homogeneous nature [14]. Before deposition, we prepared a colloidal suspension of 10 mg of functionalized WO_3 NPs in a 2mL C_2H_2OH and Milli-Q water solution. For electrophoretic deposition, we utilized a two-electrode cell consisting of hydrolyzed ITO glass and platinum wire as anode and cathode respectively. A constant DC potential of 56V has been applied between the electrodes having separation of 1cm placed inside the cell containing a colloidal suspension of APTES functionalized WO_3 NPs for 90 seconds. The prepared electrode (APTES/WO_3 NPs/ITO) then treated with Milli-Q water and set to dry at room temperature (25°C) overnight.

For the purpose of immobilizing cTnI antibody biomolecules onto the fabricated electrode, an anti-cTnI solution has been prepared in a phosphate buffer solution (pH =7.4). Prior immobilization, the antibody solution got activated with EDC-NHS chemistry where EDC and NHS act as an activator and coupling agent, respectively [15]. Afterward, this solution (20µL) is evenly spread onto APTES functionalized electrode through drop casting and set for incubation under humid conditions for 7 hours at room temperature (25°C). Thereafter, the electrode is treated with PBS to eliminate unbounded antibody biomolecules. Lastly, instead of BSA (bovine serum albumin), we used ethanol-amine (EA) for obstructing the non-specific sites of the fabricated electrode. The resultant fabricated EA/anti-cTnI/APTES/WO_3 NPs/ITO immunoelectrode is used for sensing study and contained at 5°C when not used. The schematic of the fabrication of APTES functionalized WO_3 NPs based biosensor for cTnI detection is shown in **Figure 3.1**

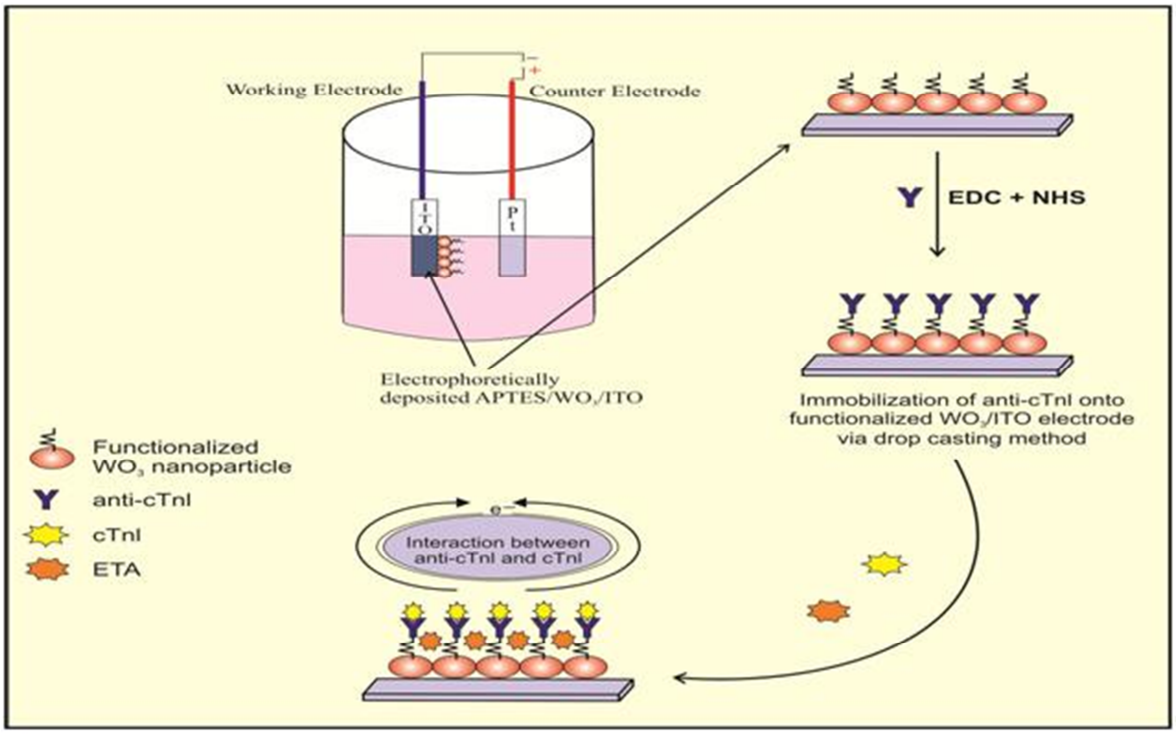

Figure 3.1: Schematic illustrations of the fabrication of WO_3 NPs based immunoelectrode

3.3 Results and Discussions

3.3.1 Microscopic and Structural Studies

The XRD study has been carried out to investigate crystallinity and phase of the synthesized tungsten trioxide nanoparticles (WO_3 NPs) as shown in **Figure 3.2**. The presence of intense characteristic peak at 24.22° and other diffraction peaks at 28.56°, 33.99°, 41.39°, 50.09°, 55.6°, and 61.58° are well indexed to (200), (112), (220), (222), (114), (420) and (134) planes, respectively (**JCPDS 71-0131**). These peaks revealed the presence of orthogonal phase in WO_3 NPs with a good crystalline structure. The average crystallite size (D) of WO_3 nanoparticles was estimated as 20 nm using Debye-Scherer equation (**Equation 3.1**)

$$\boldsymbol{D = \frac{0.9\,\lambda}{\beta\, Cos\theta}} \qquad \textbf{(3.1)}$$

where λ (1.540Å) corresponds to X-ray wavelength, β and θ represent full width at half maximum and Bragg's angle respectively.

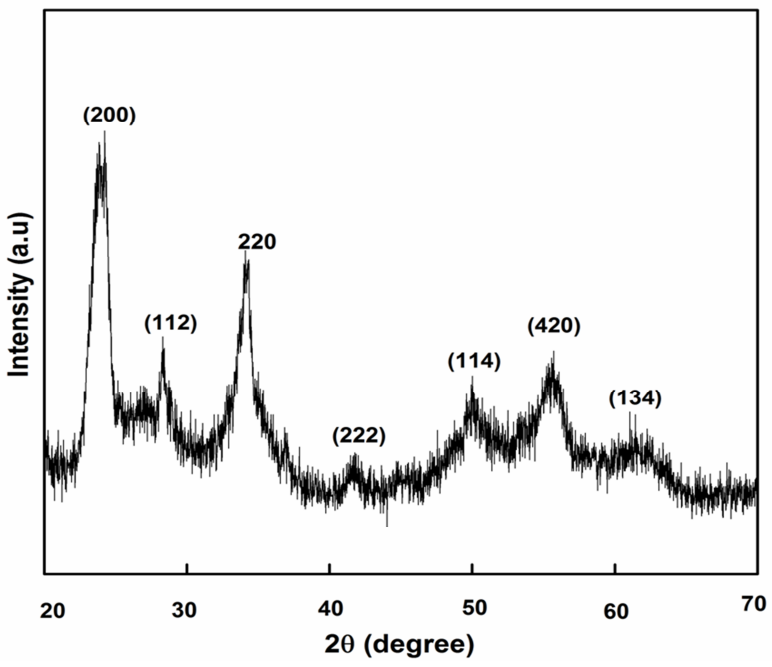

Figure 3.2: Powder X-ray diffraction (XRD) pattern of tungsten trioxide nanoparticles (WO_3 NPs)

The micrograph depicting the morphological structure of the as-synthesized WO_3 NPs sample as shown in **Figure 3.3** has been examined using scanning electron microscopy**.** The micrograph depicts the spherical shaped WO_3 nanoparticles existing unevenly in diameters.

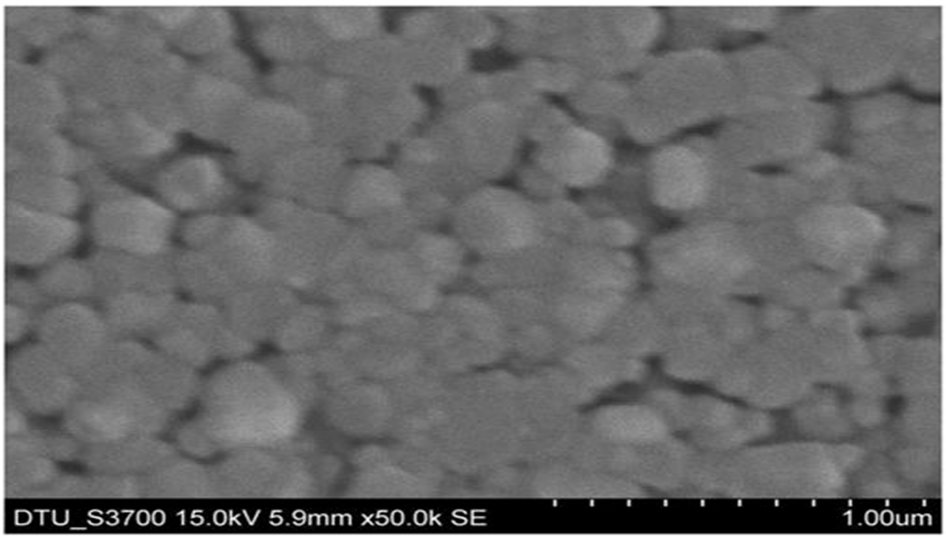

Figure 3.3: Scanning electron microscope (SEM) micrograph of as-synthesized WO_3 NPs

As topography and surface roughness of the electrode is documented to play a significant role in determining the conformation of the adsorbed protein layer [16]. Therefore, we have analyzed the topographical images of the fabricated electrodes. **Figure 3.4** represents the topographical image of 3-D height plots for the electrodes as analyzed using an atomic force microscope (AFM).

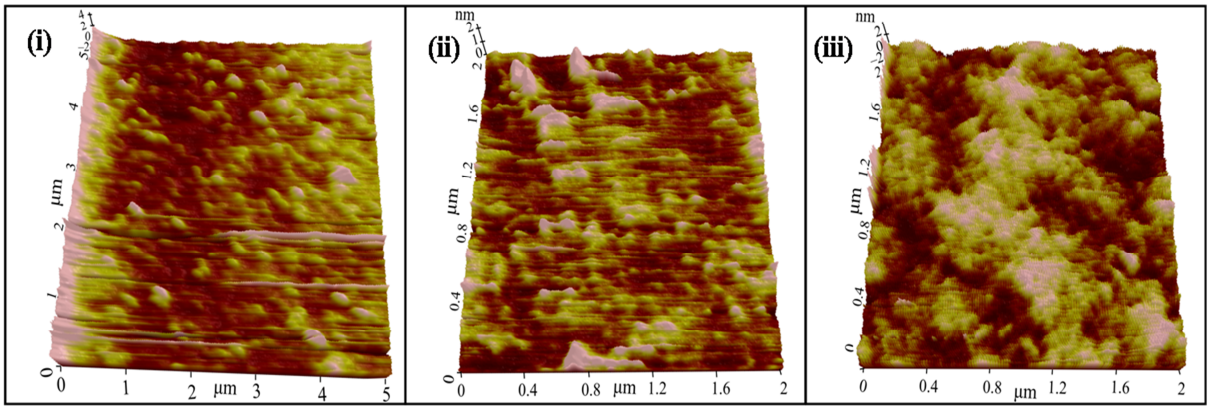

Figure 3.4: Atomic force micrograph (AFM) of (i) WO_3 NPs/ITO electrode, (ii) APTES/WO_3 NPs/ITO, and (iii) anti-cTnI/APTES/WO_3 NPs/ITO immunoelectrode.

The analysis of micrographs revealed that the average surface roughness of WO_3 NPs/ITO electrode (0.307 nm) decreased to 0.120 nm after modification with APTES. This decrease indicated the creation of a uniform layer attributed to intermolecular interaction between APTES and tungsten trioxide nanoparticles. However, post immobilization of antibody biomolecules (anti-cTnI) onto functionalized electrode surface, the average roughness increased to 5.9 nm which indicates the attachment of the antibody molecules.

3.3.2 Spectroscopic Studies

Fourier transform infrared (FT-IR) spectrometer has been used to investigate the formation of various chemical bonds at the different stages of functionalization and immobilization processes. **Figure 3.5** represent the Fourier transform infrared (FT-IR) spectra of the (i) WO_3 NPs, (ii) APTES/WO_3 NPs, and (iii) anti-cTnI/APTES/WO_3 NPs. The peak seen at 1410 cm^{-1} (**curve i)** represents stretching vibration of ν (W-O) whereas a broad peak at 770 cm^{-1} corresponds to ν (W-O_{inter}-W) stretching vibration of the bridging O_2 [17]. In **curve ii**, we observed peak at 3421 cm^{-1} resulted due to asymmetric (N-H) stretching vibration of NH_2 whereas peaks observed at 1614 cm^{-1} and 1422 cm^{-1} corresponds to δ(-NH_2) and δ (Si-CH_2) respectively present in APTES [18]. Further, peak at 2932 cm^{-1} has been attributed to a methylene group (-CH_2) which indicated that silane agent has been grafted onto the surface successfully and the peak at 1122 cm^{-1} is due to stretching mode of Si-O-Si [14]. All these results suggest that APTES has been successfully anchored on the WO_3 surface. In the FT-IR spectra of antibody immobilized APTES/WO_3 NPs/ITO electrode (**curve iii**), we observed peaks at 3462 cm^{-1}, 1636 cm^{-1} and 733 cm^{-1} which has been attributed to the amide B, amide I, and amide IV respectively [19]. The peaks observed at 2927 cm^{-1} (-CH_2) and at 1101 cm^{-1} (Si-O-Si) have been found to be shifted after antibody immobilization. All these results indicated the successful grafting of APTES molecules and immobilization of antibody biomolecules onto the WO_3 NPs based platform surface.

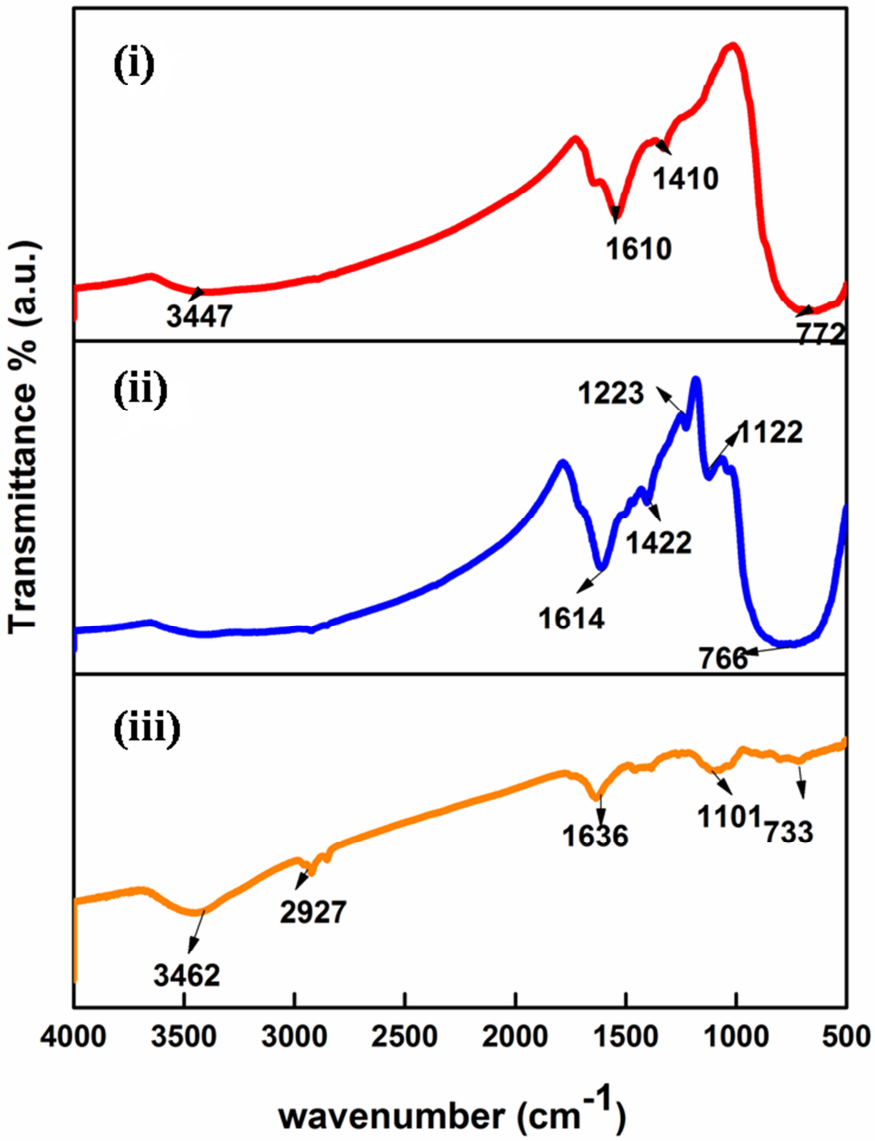

Figure 3.5: FT-IR spectra of (i) WO_3 NPs, (ii) APTES/WO_3 NPs, and (iii) anti-cTnI/APTES/WO_3 NPs

3.3.3 Electrochemical Studies

Electrochemical impedance spectroscopy (EIS) technique has been utilized to determine the interfacial properties between the fabricated electrode and electrolyte boundaries. **Figure 3.6 (A)** shows the Nyquist plot obtained for bare ITO electrode, APTES/WO_3 NPs/ITO, and anti-cTnI/APTES/WO_3 NPs/ITO electrodes in the PBS (pH 7.4) containing 5mM $[Fe(CN)_6]^{3-/4-}$ in the frequency range 10^7-10^{-2} Hz at a biasing potential of 10

mV. The charge transfer process in these electrodes is investigated by measuring charge transfer resistance (R_{CT}) at the electrode/electrolyte interface. The magnitude of R_{CT} for ITO electrode (434.07 Ω) increased to 543.15 Ω for APTES/WO_3 NPs/ITO electrode. This increased showed that the ITO electrode got modified with APTES functionalized WO_3 nanoparticles. And after the antibody immobilization, R_{CT} of anti-cTnI/APTES/WO_3 NPs/ITO electrode further increased to 589.36 Ω indicating the insulating nature of the antibody molecules.

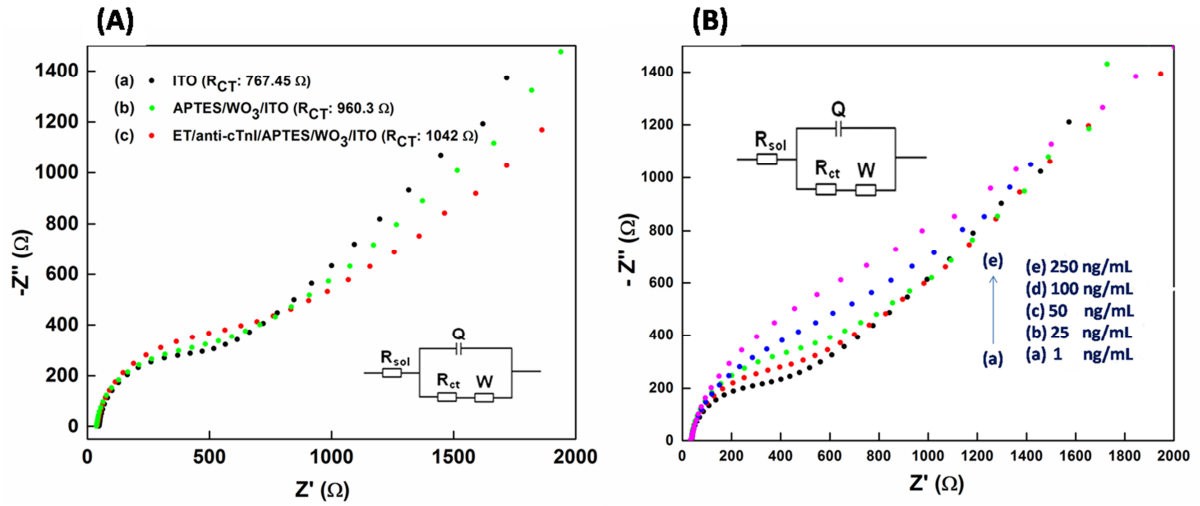

Figure 3.6: (A) EIS studies of the different electrodes (a) ITO, (b) APTES/WO_3 NPs/ITO, (c) EA/anti-cTnI/APTES/WO_3 NPs/ITO. (B) Response study of the fabricated electrode as a function of cTnI concentration (1 – 250 ng mL^{-1})

The heterogeneous electron transfer rate constant (k_o) of the APTES/WO_3 NPs/ITO and anti-cTnI/APTES/WO_3 NPs/ITO electrodes has been compared using **Equation 3.2**

$$k_o = \frac{RT}{n^2F^2AR_{CT}S} \qquad (3.2)$$

In the equation above, R as gas constant; T as absolute temperature (K); A denotes the specific electrode area (cm^2); S denotes the bulk concentration of redox molecules; n as the number of electrons per molecule transferred at the redox probe and F as Faraday constant signifies. The magnitude of k_o value of the APTES/WO_3 NPs/ITO electrode is

estimated as 3.93×10^{-4} cm s^{-1} which decreases to 3.623×10^{-4} cm s^{-1} after antibody attachment over the electrode. This indicates that electron transfer kinetics get hindered with the immobilization of antibody biomolecules due to its insulating characteristics.

The response study of the as-fabricated immunoelectrode (EA/anti-cTnI/APTES/WO_3 NPs/ITO) has been analyzed with respect to the cTnI antigen concentration (1-250 ng mL^{-1}) using EIS technique **[Figure 3.6 (B)]**. The value of R_{CT} has been evaluated from the diameter of the Nyquist plot while fitting the curve under the Randles circuit. The studies revealed that R_{CT} of the immunoelectrode increased linearly with respect to cTnI concentration (1-250 ng mL^{-1}). This is most likely due to the creation of electrically insulated antibody-antigen pairs that inhibit electron transfers via $[Fe(CN)_6]^{3-/4-}$. The linear variation of the R_{CT} value obtained from the calibration plot **[Figure 3.7 (A)]** obeys **Equation (3.3)** having the regression coefficient (R^2) as 0.99.

$$\mathbf{R_{ct}\ (\Omega) = 618.70\ (\Omega) + 6.64\ (\Omega\ ng^{-1}\ mL) \times [concentration\ (ng\ mL^{-1})]} \qquad \mathbf{(3.3)}$$

The APTES/WO_3 NPs/ITO based immunoelectrode exhibits high sensitivity of 26.56 Ω $ng^{-1}mL\ cm^{-2}$ within the linear range of 1-250 ng mL^{-1}. Furthermore, we also conducted an experiment to investigate electrochemical responses of APTES/WO_3 NPs/ITO electrode towards cTnI without immobilizing anti-cTnI (control experiment). However, we have not found any significant changes in the R_{CT} value with the variation in concentrations of cTnI as shown in **Figure 3.7 (A)**. These results showed that the response exhibited by the fabricated sensor is completely attributable to the specific immunoreactions between anti-cTnI and cTnI molecules only. Further, the limit of detection is also evaluated as 16 ng mL^{-1} using $3\sigma/m$ as standard criteria, where σ is the standard deviation value and m indicates the slope of the calibration plot**. Figure 3.7 (B)** compares the R_{CT} response of anti-cTnI/APTES/WO_3 NPs/ITO immunoelectrode in presence of serum sample (containing 100 ng mL^{-1} cTnI) and

standard sample (100 ng mL^{-1} cTnI). The estimated low RSD value (2.65%) indicated that the anti-cTnI/APTES/WO_3 NPs/ITO immunoelectrode could be utilized for real sample analysis. Storage integrity of the fabricated immunoelectrode has been too investigated through observing the EIS response and measuring the R_{CT} value at a regular interval of five days up to 40 days with 50 ng mL^{-1} cTnI concentration **[Figure 3.8 (A)]**. The analysis of data revealed that R_{CT} exhibits 92% of its initial response for up to 30 days, thereafter it decreased to 80% at the end of 40 days. This indicated that the fabricated biosensor has storage integrity up to 4 weeks.

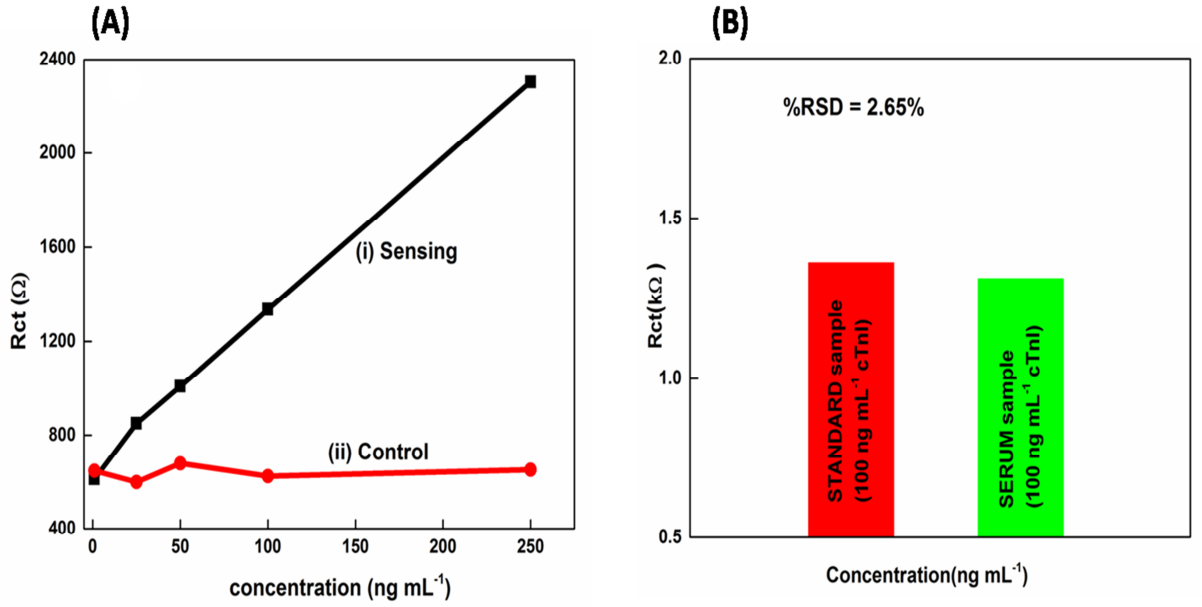

Figure 3.7: (A) Representation of the calibration plot obtained between R_{CT} value and the cTnI concentration along with control studies. (B) The response of the fabricated immunoelectrode in the presence of serum sample and the standard sample

Further, the limit of detection is also evaluated as 16 ng mL^{-1} using 3σ/m as standard criteria, where σ is the standard deviation value and m indicates the slope of the calibration plot**. Figure 3.7 (B)** compares the R_{CT} response of anti-cTnI/APTES/WO_3 NPs/ITO immunoelectrode in presence of serum sample (containing 100 ng mL^{-1} cTnI) and standard sample (100 ng mL^{-1} cTnI).

The estimated low RSD value (2.65%) indicated that the anti-cTnI/APTES/WO_3 NPs/ITO immunoelectrode could be utilized for real sample analysis. Storage integrity of the fabricated immunoelectrode has been too investigated through observing the EIS response and measuring the R_{CT} value at a regular interval of five days up to 40 days with 50 ng mL^{-1} cTnI concentration **[Figure 3.8 (A)]**. The analysis of data revealed that R_{CT} exhibits 92% of its initial response for up to 30 days, thereafter it decreased to 80% at the end of 40 days. This indicated that the fabricated biosensor has storage integrity up to 4 weeks.

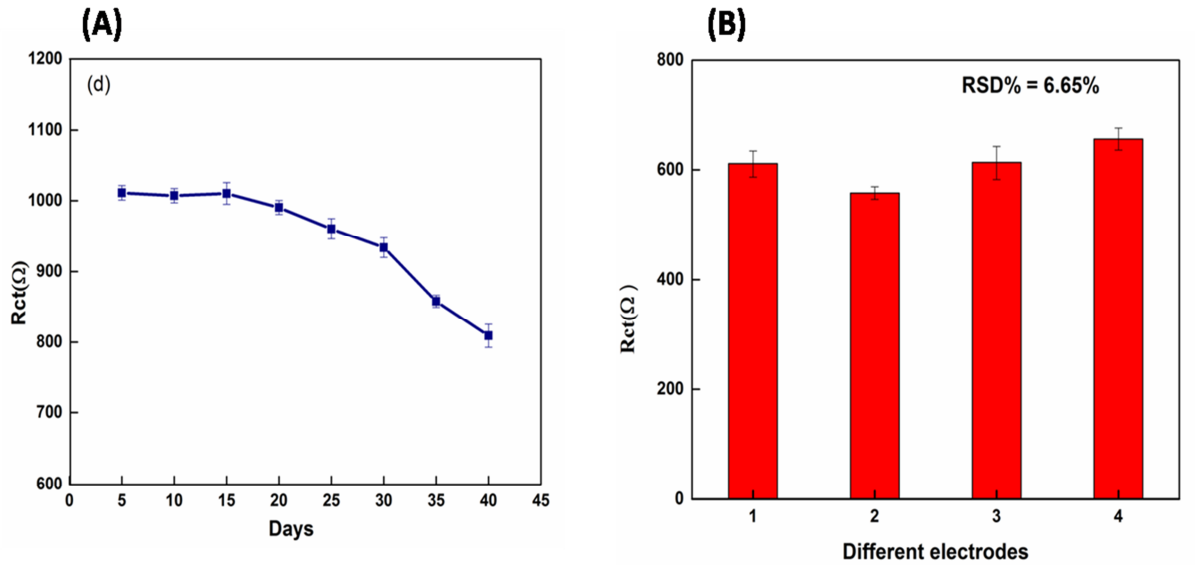

Figure 3.8: (A) Stability study of the fabricated immunoelectrode and (B) Reproducibility study of the immunoelectrode studied on 4 identical electrodes fabricated under the same conditions

At last, we investigated the reproducibility of the EA/anti-cTnI/APTES/WO_3 NPs/ITO electrode by studying the R_{CT} value of the 4 different immunoelectrodes fabricated under ideal conditions **[Figure 3.8 (B)]**. The change in the R_{CT} value of the different immunoelectrodes has been estimated by evaluating relative standard deviation (RSD %). The RSD % value found as 6.65 % is within an acceptable error range, thus suggesting an excellent reproducibility of the proposed immunoelectrode.

The characteristics of the fabricated biosensor along with some those reported in the literature for cTnI detection is shown in **Table 3.1**. The APTES/WO_3 NPs/ITO based biosensor exhibits a much higher sensitivity (26.56 Ω $ng^{-1}mL\ cm^{-2}$), good stability (4 weeks), and an extended linearity (1- 250 ng mL^{-1}) than some of the other sensors reported in the literature.

Electrode	**Detection Technique**	**Detection range ng mL^{-1}**	**Sensitivity/ Stability (St)**	**References**
Fluoro-microbead guiding chip	Optical immunoassay	0.1-100	Improved sensitivity	[20]
ABEI-Au N.Ps	(ECL) Immunosensor	0.0025-10	Enhanced sensitivity	[21]
PDMS-Au NPs	Colorimetric detection	0.01-10	…..	[22]
Conducting paper	CV	1-100	5.5 $\mu A/ngmL^{-1}cm^{-2}$	[23]
CNF- based NEA	EIS	5.0 -100	Increased sensitivity	[6]
APTES/WO_3 NPs/ ITO	**EIS**	**1-250**	**26.56 Ω mL ng^{-1} cm^{-2} St: 30 days**	**Present Work**

Table 3.1: Characteristics of the Tungsten trioxide nanoparticles based biosensor along with those reported in literature.

3.4 Conclusions

In summary, we have successfully synthesized and functionalized nanostructured tungsten trioxide nanoparticles (WO_3 NPs). Thin films of APTES/WO_3 NPs/ITO have been fabricated via electrophoretic deposition technique and followed with covalent immobilization of antibody of cTnI for the detection of cTnI using EIS technique.

In comparison with other reported Troponin biomarker detection methods including biosensors, the proposed biosensor is simple and label-free. It exhibits a wider detection range as 1- 250 ng mL^{-1}, sensitivity as 26.56 Ω $ng^{-1}mL\ cm^{-2}$, storage stability as 30 days and detection limit as 16 ng mL^{-1}. These results can be contributed towards the successful functionalization of WO_3 NPs surface for the building of immunoassay platform leading to the sensitive detection of cardiac biomarker cTnI. Thus, this work demonstrates the potential of WO_3 NPs based matrix for the development of facile and cost-effective diagnostic biosensor for the clinical applications. In the next chapter, we will focus on the enhancement in the characteristics of the fabricated platform by tailoring the dimensions of WO_3 in order to build a resourceful biosensor device.

3.5 References

1. Han, Xu, Shanghao Li, Zhili Peng, Abdelhameed M. Othman, and Roger Leblanc. "Recent development of cardiac troponin I detection." *Acs Sensors* 1, no. 2 (2016): 106-114.
2. Periyakaruppan, Adaikkappan, Ram P. Gandhiraman, M. Meyyappan, and Jessica E. Koehne. "Label-free detection of cardiac troponin-I using carbon nanofiber based nanoelectrode arrays." *Analytical chemistry* 85, no. 8 (2013): 3858-3863.
3. Cho, Il-Hoon, Eui-Hwan Paek, Young-Kee Kim, Joo-Ho Kim, and Se-Hwan Paek. "Chemiluminometric enzyme-linked immunosorbent assays (ELISA)-on-a-chip biosensor based on cross-flow chromatography." *Analytica chimica acta* 632, no. 2 (2009): 247-255.
4. Wu, Alan HB, Noelle Fukushima, Robert Puskas, John Todd, and Philippe Goix. "Development and preliminary clinical validation of a high sensitivity assay for cardiac

troponin using a capillary flow (single molecule) fluorescence detector." *Clinical Chemistry* 52, no. 11 (2006): 2157-2159.

5. Shan, Meng, Min Li, Xiaoying Qiu, Honglan Qi, Qiang Gao, and Chengxiao Zhang. "Sensitive electrogenerated chemiluminescence peptide-based biosensor for the determination of troponin I with gold nanoparticles amplification." *Gold Bulletin* 47, no. 1-2 (2014): 57-64.
6. Qiao, Xiujuan, Kunxia Li, Jinqiong Xu, Ni Cheng, Qinglin Sheng, Wei Cao, Tianli Yue, and Jianbin Zheng. "Novel electrochemical sensing platform for ultrasensitive detection of cardiac troponin I based on aptamer-MoS_2 nanoconjugates." *Biosensors and Bioelectronics* 113 (2018): 142-147.
7. Solanki, Pratima R., Ajeet Kaushik, Ved V. Agrawal, and Bansi D. Malhotra. "Nanostructured metal oxide-based biosensors." *NPG Asia Materials* 3, no. 1 (2011): 17.
8. Zheng, Haidong, Jian Zhen Ou, Michael S. Strano, Richard B. Kaner, Arnan Mitchell, and Kourosh Kalantar-zadeh. "Nanostructured tungsten oxide–properties, synthesis, and applications." *Advanced Functional Materials* 21, no. 12 (2011): 2175-2196.
9. Deng, Zifeng, Yichun Gong, Yongping Luo, and Yang Tian. "WO_3 nanostructures facilitate electron transfer of enzyme: application to detection of H_2O_2 with high selectivity." *Biosensors and Bioelectronics* 24, no. 8 (2009): 2465-2469.
10. Hariharan, V., S. Radhakrishnan, M. Parthibavarman, R. Dhilipkumar, and C. Sekar. "Synthesis of polyethylene glycol (PEG) assisted tungsten oxide (WO_3) nanoparticles for L-dopa bio-sensing applications." *Talanta* 85, no. 4 (2011): 2166-2174.
11. Sun, Qiang-Qiang, Maowen Xu, Shu-Juan Bao, and Chang Ming Li. "pH-controllable synthesis of unique nanostructured tungsten oxide aerogel and its sensitive glucose biosensor." *Nanotechnology* 26, no. 11 (2015): 115602.

12. Ahmadi, Majid, Reza Younesi, and Maxime JF Guinel. "Synthesis of tungsten oxide nanoparticles using a hydrothermal method at ambient pressure." *Journal of Materials Research* 29, no. 13 (2014): 1424-1430.
13. Kumar, Suveen, Saurabh Kumar, Sachchidanand Tiwari, Shine Augustine, Saurabh Srivastava, Birendra Kumar Yadav, and Bansi Dhar Malhotra. "Highly sensitive protein functionalized nanostructured hafnium oxide based biosensing platform for non-invasive oral cancer detection." *Sensors and Actuators B: Chemical* 235 (2016): 1-10.
14. Ata, M. S., Y. Liu, and I. Zhitomirsky. "A review of new methods of surface chemical modification, dispersion and electrophoretic deposition of metal oxide particles." *Rsc Advances* 4, no. 43 (2014): 22716-22732.
15. Xiao, Fei, Ningdan Zhang, Hongjie Gu, Min Qian, Jing Bai, Wen Zhang, and Litong Jin. "A monoclonal antibody-based immunosensor for detection of Sudan I using electrochemical impedance spectroscopy." *Talanta* 84, no. 1 (2011): 204-211.
16. Roach, Paul, David Farrar, and Carole C. Perry. "Surface tailoring for controlled protein adsorption: effect of topography at the nanometer scale and chemistry." *Journal of the American Chemical Society* 128, no. 12 (2006): 3939-3945.
17. Tong, Maosong, Guorui Dai, Yuanda Wu, Xiuli He, and Dingsan Gao. "WO_3 thin film prepared by PECVD technique and its gas sensing properties to NO_2." *Journal of materials science* 36, no. 10 (2001): 2535-2538.
18. Majoul, N., S. Aouida, and B. Bessaïs. "Progress of porous silicon APTES-functionalization by FTIR investigations." *Applied Surface Science* 331 (2015): 388-391.
19. Srivastava, Saurabh, Shiju Abraham, Chandan Singh, Md Azahar Ali, Anchal Srivastava, Gajjala Sumana, and Bansi D. Malhotra. "Protein conjugated carboxylated gold@ reduced graphene oxide for aflatoxin B 1 detection." *Rsc Advances* 5, no. 7 (2015): 5406-5414.

20. Song, Seung Yeon, Yong Duk Han, Kangil Kim, Sang Sik Yang, and Hyun C. Yoon. "A fluoro-microbead guiding chip for simple and quantifiable immunoassay of cardiac troponin I (cTnI)." *Biosensors and Bioelectronics* 26, no. 9 (2011): 3818-3824.

21. Shen, Wen, Dayong Tian, Hua Cui, Di Yang, and Zhiping Bian. "Nanoparticle-based electrochemiluminescence immunosensor with enhanced sensitivity for cardiac troponin I using N-(aminobutyl)-N-(ethylisoluminol)-functionalized gold nanoparticles as labels." *Biosensors and Bioelectronics* 27, no. 1 (2011): 18-24.

22. Wu, Wen-Ya, Zhi-Ping Bian, Wei Wang, and Jun-Jie Zhu. "PDMS gold nanoparticle composite film-based silver enhanced colorimetric detection of cardiac troponin I." *Sensors and Actuators B: Chemical* 147, no. 1 (2010): 298-303.

23. Jagadeesan, Kishore Kumar, Saurabh Kumar, and Gajjala Sumana. "Application of conducting paper for selective detection of troponin." *Electrochemistry Communications* 20 (2012): 71-74.

CHAPTER 4

2-D Nanostructured Tungsten Trioxide Based Biosensor for Cardiac Biomarker Detection

In this chapter, we report the development of a two dimensional (2-D) based matrix for detecting the cardiac biomarker. The high specific surface area of 2-D nanomaterial provide more surfaces for the functionalization process leading to the enhancement in the characteristics of the fabricated biosensor platform. In this context, we work towards the synthesis and fabrication of a matrix based on ***tungsten trioxide nanosheet (WO_3 NS)*** *for the electrochemical sensing of troponin I (cTnI) – the aforementioned biomarker. Selective and quantitative detection of cTnI antigen has been accomplished by immobilizing troponin I antibody (anti-cTnI) onto APTES-functionalized WO_3 NS platform. The developed WO_3 NS based platform provided a large surface area for high loading of antibody biomolecules and improved sensitivity with extended linear detection range and good stability.*

The work presented in this chapter is communicated as:

"2D Nanostructured Tungsten Trioxide based Biosensor for Cardiac Biomarker Detection"

New Journal of Chemistry (2019)

4.1 Introduction

Nanostructured tungsten trioxide (nWO_3), n-type metal-oxide nanostructure possesses multifunctional characteristics with photocatalytic, electrochromism, photo-chromism and sensing applications [1-4]. The different morphologies exhibited by nWO_3 which include nanoplates, nanorods, hollow sphere, and many others have shown tremendous enhancement in the performance of the devices [5-7]. Incidentally, the 2-D nano-morphological materials exhibit superior thermal and electronic properties and high mechanical strength along with large specific surface area. Also due to their layered structures, they can promote high adsorption into interplanar sites and possess high quantum effects [8]. Thus employing these unique properties of 2-D materials with highly favourable advantages, we can design a potential platform for the biosensing applications.

As discussed earlier, acute myocardial infarction (AMI) is a necrosis of myocardial cells resulting from the acute obstruction of the coronary heart arteries [9]. However, by learning the concentration of cardiac biomarkers can be significant in detecting AMI [10]. Among all cardiac biomarkers, cardiac biomarker Troponin I (cTnI) has shown remarkable increase in its level with the onset of myocardial necrosis. The unique molecular structure of cTnI show traces of amino acid residues on its N-terminal, which do not occur on its skeletal form. Consequently, this makes it a promising analyte for cardiac specificity in diagnosis of AMI [11-12]. Further, it has been found that with the onset of AMI, cTnI get released into the blood serum from the death cell of cardiac muscles and remain elevated for 8-10 days. Thus these following observation and unique amino sequence of cTnI make it a potential diagnostic marker for early diagnosis of AMI. For a rapid and facile diagnosis of AMI, a compact analytical device "biosensor" has been considered as an efficient and sensitive platform for the diagnosis of AMI. And for the enhancement in sensitivity of the biosensors, immunoassays based on electrochemical detection techniques are preferred due to

simplification in processing, low-cost, portability and real-time analysis [13-14]. Therefore, 2-D WO_3 can be Hence in this chapter, we have employed 2-D tungsten trioxide based platform for the electrochemical sensing of cTnI. The proposed platform can be a promising platform towards the development of biosensors, offering a great prospect in biological recognition events and signal transduction mechanism of it.

4.2 Experimental Section

4.2.1 Synthesis of WO_3 Nanosheets (WO_3 NS)

WO_3 NS have been synthesized using a wet chemical method employing $Na_2WO_4.2H_2O$ as a precursor as reported earlier with modification [15]. Briefly, 0.05 M of precursor solution is first prepared by dissolving 0.5 gm of $Na_2WO_4.2H_2O$ in 30 mL of deionized water. Thereafter, we added 0.3 gm of citric acid to the precursor solution and stirred well for 10 minutes. Later, 6 M HCl is added drop-wise to the solution (for acidification) till the pH of the solution reached 1 and stirred for further 30 minutes till the formation of a yellowish precipitate. For hydrothermal reaction, the resultant precipitate has been transferred into a Teflon-lined autoclave and kept in the oven for 20 hours at 150°C. After the autoclave cooled down to room temperature, we extract the resultant yellow coloured product using centrifugation operated at 10000 rpm.

4.2.2 Functionalization and Fabrication of APTES/WO_3 NS/ITO Electrode

The functionalization of WO_3 NS has been accomplished by using amino-silane coupling agent 3-Aminopropyl-triethoxysilane (APTES). This amino-silane provides an active platform for the bio-immobilization onto the surface of nanomaterials [16]. Firstly, a colloidal suspension of WO_3 NS is prepared in isopropanol solution using ultrasonication. Then we poured 250 μL of APTES drop-wise to this solution and stirred at 280 rpm for 36 hours at room temperature. Thereafter, we filtered the suspension and rinsed with Milli-Q

water to remove the unattached APTES molecules and used the final product as APTES functionalized WO_3 NS for the fabrication of electrode.

The fabrication of APTES functionalized WO_3 NS thin film onto hydrolyzed indium tin oxide (ITO) substrate has been accomplished using electrophoretic deposition (EPD) method. For the film deposition, a colloidal suspension of APTES functionalized WO_3 NS (1 mg mL^{-1}) is prepared in acetonitrile and placed in a two-electrode cell [17]. Platinum wire acted as the counter electrode and a hydrolyzed ITO glass substrate acted as a working electrode. Both are aligned parallel to each other with 1 cm apart inside the cell containing colloidal suspension. The desired film got deposited onto the ITO substrate at an optimized D.C potential of 50 V for 1.5 minutes. The resultant electrode (APTES/WO_3 NS/ITO) is then washed with Milli-Q water and used after drying.

4.2.3 Fabrication of Antibody Immobilized APTES/WO_3 NS/ITO Immunoelectrode

Cardiac Troponin I antibody (anti-cTnI) solution of concentration 50 μg mL^{-1} has been used for the immobilization of antibody biomolecules. Before immobilization, –COOH groups of antibodies have been activated using EDC (0.4M) and NHS (0.1M) in 1:1 ratio. Thereafter, 20 μL of prepared solution got evenly spread onto APTES/WO_3 NS/ITO surface and placed in a humid chamber at room temperature (24°C) for 6 hours followed with washing with PBS solution. The amino terminal (-NH_2) of APTES functionalized electrode would bound covalently with the –COOH group terminal of the anti-cTnI forming amide bond (OC-NH). This has been confirmed later using FT-IR spectroscopy. Further, to desist active sites, that are non-specific, we treated the anti-cTnI/APTES/WO_3 NS/ITO electrode with ethanolamine (EA, 0.01 M). To achieve this, 20 μL of EA is drop-casted over the electrode surface and kept undisturbed for 3 hours and then rinsed with PBS solution. Finally, the resultant fabricated EA/anti-cTnI/APTES/WO_3 NS/ITO electrode is placed in a

refrigerator when not in use (at 5°C). The step-by-step fabrication of the WO_3 NS based immunoelectrode is schematically displayed in **Figure 4.1.**

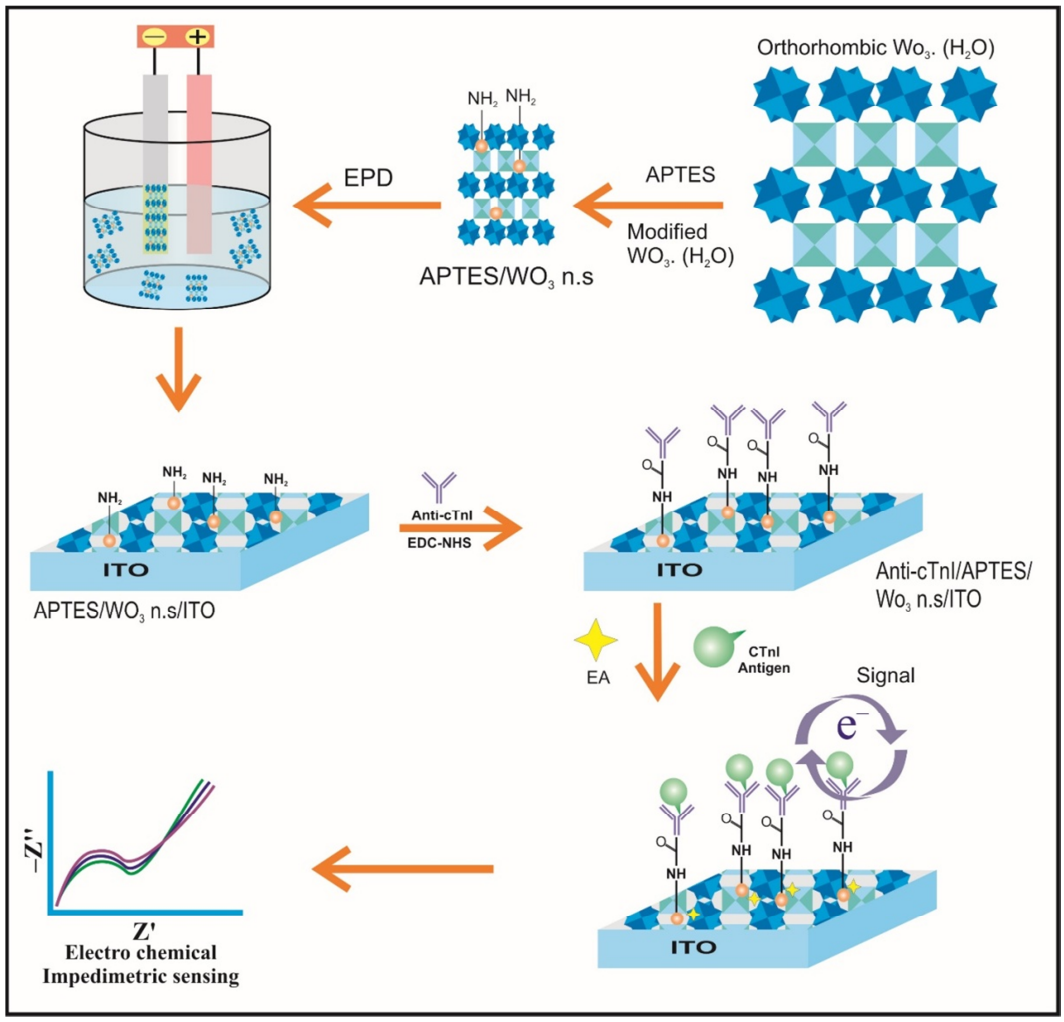

Figure 4.1: Schematic of step-wise fabrication of WO_3 NS based immunoelectrode

4.3 Results and Discussions

4.3.1 Structural and Morphological Characterization

The X-ray diffraction (XRD) pattern shown in **Figure 4.2** has been obtained for the as-synthesized WO_3 nanostructures. The accentuated characteristic peaks observed at 16.5° and 25.6° correspond to the (020) and (111) reflected planes of $WO_3.H_2O$. The other diffracted peaks observed at 23.7°, 30.4°, 34.1°, 34.9°, 37.6°, 38.8°, 42.6°, 46.4°, 49.6°, 52.6°, 56.1°, 57.2°, 61.6°, and at 62.9° are well indexed to (120), (031), (200), (002), (140),

(022), (122), (231), (202) (222), (311), (113), (331), and (260) reflection planes, respectively. These planes are well-matched with **JCPDS card no.: (084-0886)** indicating purity and crystallinity of the synthesized $WO_3.H_2O$.

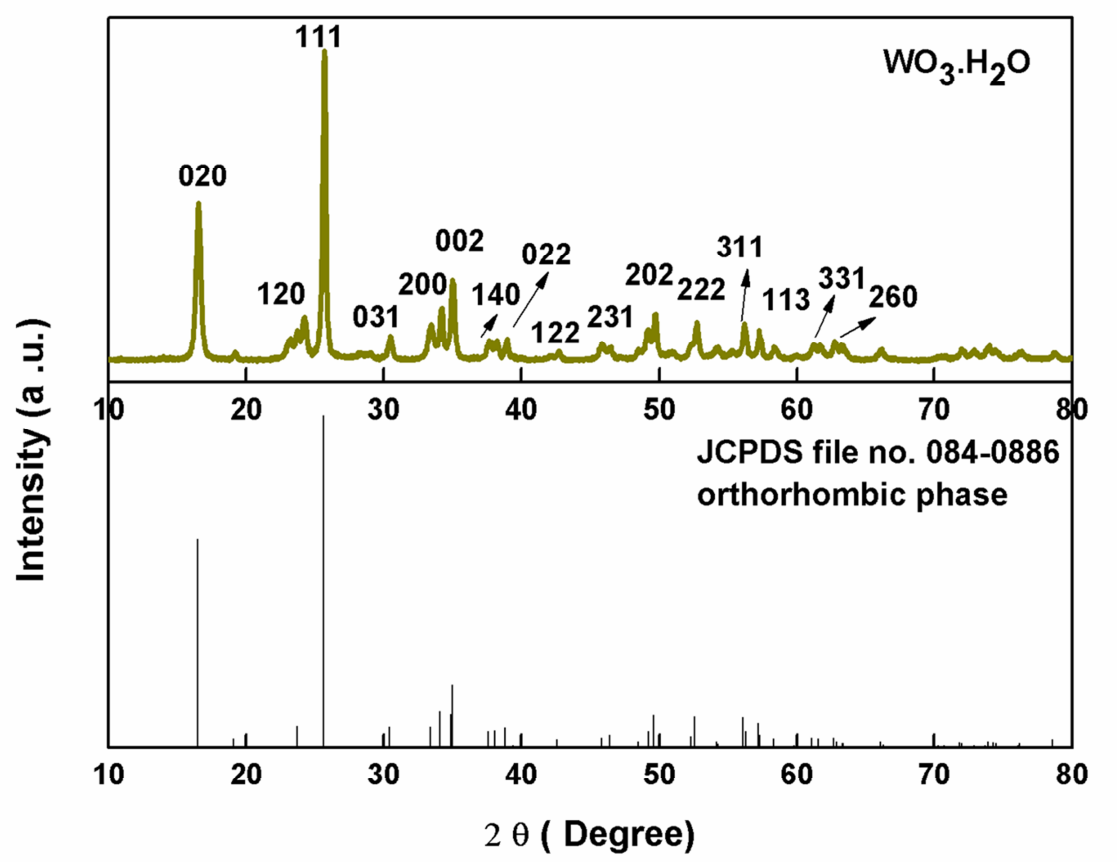

Figure 4.2: X-ray diffraction of synthesized WO_3 NS

Figure 4.3 represents the scanning electron micrograph and transmission electron micrograph of synthesized nanostructured tungsten trioxide. **Figure 4.3 (i)** depicts the formation of stacked nanoplates obtained at 0.5µm scale using SEM. Further, TEM micrograph **[Figure 4.3 (ii)]** shows the existence of square-shaped nanosheets having lateral dimensions ranging from 90 to 180 nm. The high-resolution transmission electron microscopy (HR-TEM) micrograph **[Figure 4.3 (iii)]** displays lattice fringes of WO_3 nanosheets with an interplanar spacing of 3.5Å (corresponding with 111 planes) depicting the high crystallinity of the synthesized tungsten trioxide nanosheets (WO_3 NS).

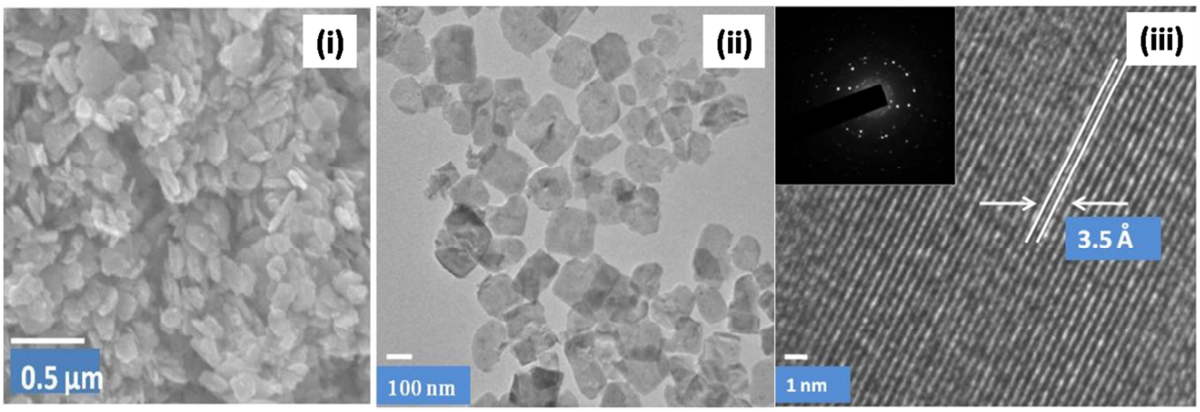

Figure 4.3: (i) Scanning electron micrograph (SEM), (ii) Transmission electron micrograph (TEM), and (iii) High-resolution transmission electron micrograph (HR-TEM) of WO_3nanosheet. (Inset SAED)

4.3.2 Spectroscopic Investigation

Figure 4.4 depicts the FT-IR spectra of the synthesized WO_3 NS before and after functionalization and immobilization process. The spectrum obtained for WO_3 NS **[curve i]** showed the characteristic band at 688 cm^{-1} corresponding to stretching ν(W─O_{inter}─W) vibration of the corner-sharing WO_6 octahedron in the WO_3 and the peak at 946 cm^{-1} corresponds to the W═O vibration. The bending vibration experienced at 1625 cm^{-1} concurs with the W─OH in-plane vibrations [18-19]. The sharp peak observed at 3425 cm^{-1} corresponds to the stretching mode of ν (O─H) due to the adsorption of water molecules. All these vibration features indicated that synthesized WO_3 NS contains no impurity. The peaks corresponding to the APTES **[curve ii]** observed at 3400 cm^{-1}, and at 2935 cm^{-1} have been attributed to N─H stretching vibration and the presence of C─H bonds of aldehydes groups existent on the surface of APTES molecules. Further, the peaks observed at 1631 cm^{-1}, 1565 cm^{-1}, and at 1130 cm^{-1} correspond to N─H bending vibration of primary amide ─NH_2 groups, bending vibration corresponding to secondary amide groups and stretching mode of Si─O─Si [20]. After the immobilization of cTnI antibody on APTES functionalized WO_3 NS surface

[**curve iii**], the observed characteristic band at about 3460 cm^{-1} indicates the presence of amide A band of protein molecules. The peaks present at 1650 cm^{-1} and 1556 cm^{-1} correspond to amide I band associated with C═O stretching vibration and the amide II band associated with N ─H bending vibration and C─N stretching vibration respectively [21]. Hence, from FT-IR analysis we can confirmed the successful surface functionalization with the presence of primary amide groups (─NH_2) and immobilization of antibody of cardiac troponin I with amide bond formation.

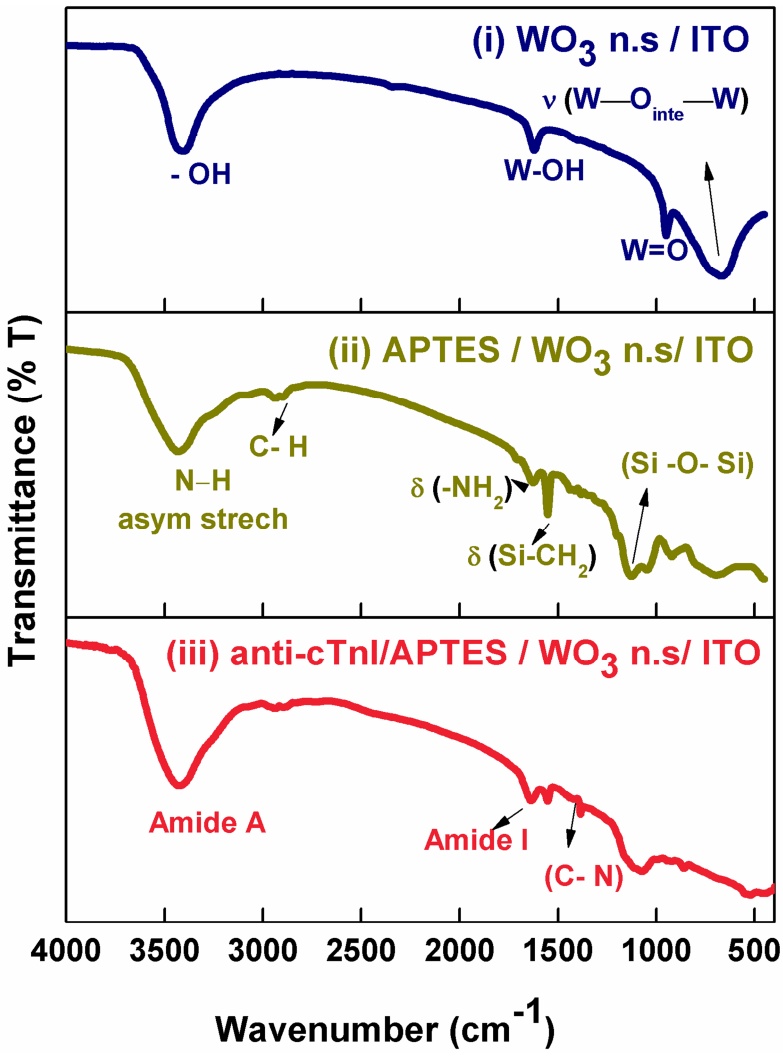

Figure 4.4: Fourier transform infrared (FT-IR) spectra of (i) WO_3 NS/ITO, (ii) APTES/WO_3 NS/ITO, and (iii) Anti-cTnI/APTES/WO_3 NS/ITO

4.3.3 Electrochemical Investigations

To investigate the electrochemical kinetics of the fabricated electrode, we employed autolab Potentiostat to perform all electrochemical measurements at room temperature. To perform the experiments, we used a conventional three-electrode cell with the fabricated immunoelectrode acting as the working electrode; platinum wire acting as a counter electrode, and silver/silver chloride acting as a reference electrode. Standard phosphate buffer saline (7.4 pH) solution with 5mM $[Fe\ (CN)_6]^{3-/4-}$ as redox agent is used as the electrolyte solution. And for a sensitive electron transfer kinetics towards the surface modifications, we preferred $[Fe\ (CN)_6]^{3-/4-}$ as a redox couple.

4.3.3.1 Cyclic Voltammetry Investigations

Figure 4.5(A) depicts the cyclic voltammetry (CV) evaluation of the APTES/WO_3 NS/ITO electrode at different stages of modification. The measurements have been investigated in the scale of -0.8 V to +0.8 V at a scan rate of 50 mV s^{-1}. The curves represented well-defined redox peaks due to the oxidation and reduction of $[Fe\ (CN)_6]^{3-/4-}$ in the presence of the working electrode. The oxidation peak-current (I_a) and peak-to-peak potential separation (ΔE) of the APTES/WO_3 NS/ITO electrode are found as 0.546 mA and 0.433V respectively. The ratio of oxidation peak current (I_a) to reduction peak current (I_c) found as 1.10 showed the reversible process of the redox species. However, after the immobilization, the oxidation peak-current declined (0.480 mA) due to the insulating nature of the antibody. The current further declined to 0.411 mA with the application of EA on the antibody functionalized surface. This decrease indicates the fact that EA has blocked most of the un-immobilized active sites present on the immunosensor surface which might have hindered the permeability of redox agent $[Fe(CN)_6]^{3-/4-}$.

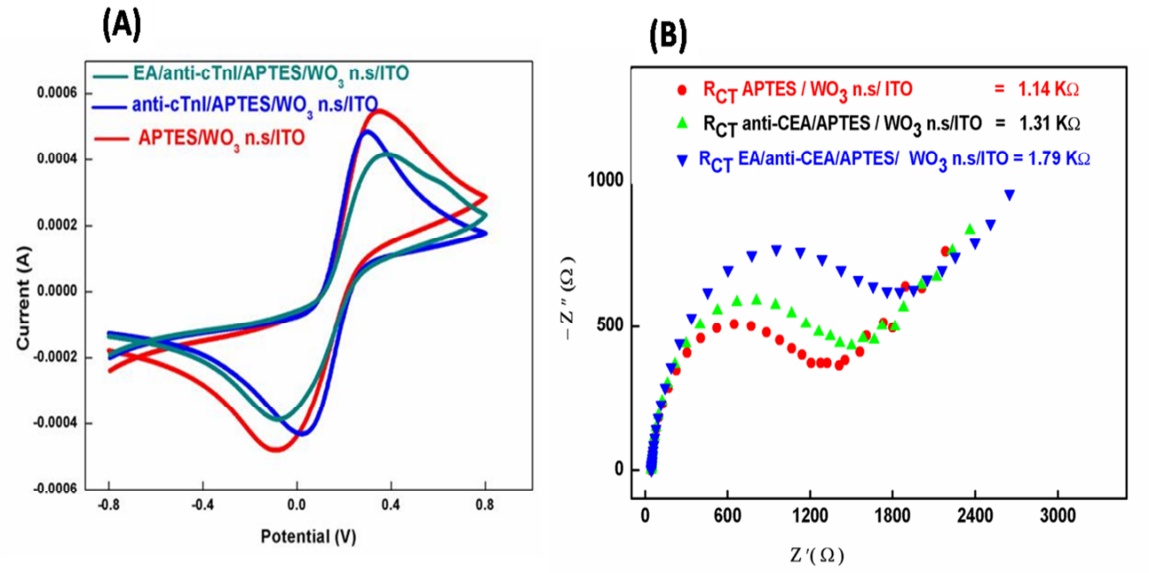

Figure 4.5: (A) Cyclic voltammograms (CVs) of the fabricated electrodes at different stages of modification. (B) Electrochemical impedance spectra (EIS) of fabricated electrodes obtained in a frequency range 0.01- 10^5 Hz operated at a fix biasing potential 0.01 V (Inset: Randles equivalent circuit)

4.3.3.2 Electrochemical Impedance Spectroscopy (EIS) Investigations

EIS technique is used to investigate electron transfer kinetics at the bio-interface site using a three-electrode system in the frequency range of 0.01 to 10^5 Hz. **Figure 4.5 (B)** depicts the Nyquist plot of (i) APTES/WO_3 NS/ITO; (ii) anti-cTnI/APTES/WO_3 NS/ITO, and (iii) EA/anti-cTnI/ APTES/WO_3 NS/ITO electrodes studied at the biasing potential of 0.01 V. The impedance spectra (Nyquist plot) consist of a semi-circle portion and a linear portion obtained at high frequencies and low frequencies region respectively. The value of charge transfer resistance (R_{CT}) at the electrode surface is analyzed using the diameter of the semicircle in the Nyquist plot, whereas the linear portion signifies the mass transfer limited process.

The APTES/WO_3 NS/ITO electrode exhibited the R_{CT} value of 1.14 KΩ which increased to 1.31 KΩ and 1.79 KΩ respectively for anti-cTnI/APTES/WO_3 NS/ITO and EA/anti-cTnI/APTES/WO_3 NS/ITO electrode. The increased in R_{CT} value signified the insulating nature of antibody biomolecules and obstruction of non-specific active sites due to the application of ethanolamine (EA) onto antibody immobilized surface. All these results confirm the fabrication of the EA/anti-cTnI/APTES/WO_3 NS/ITO electrode.

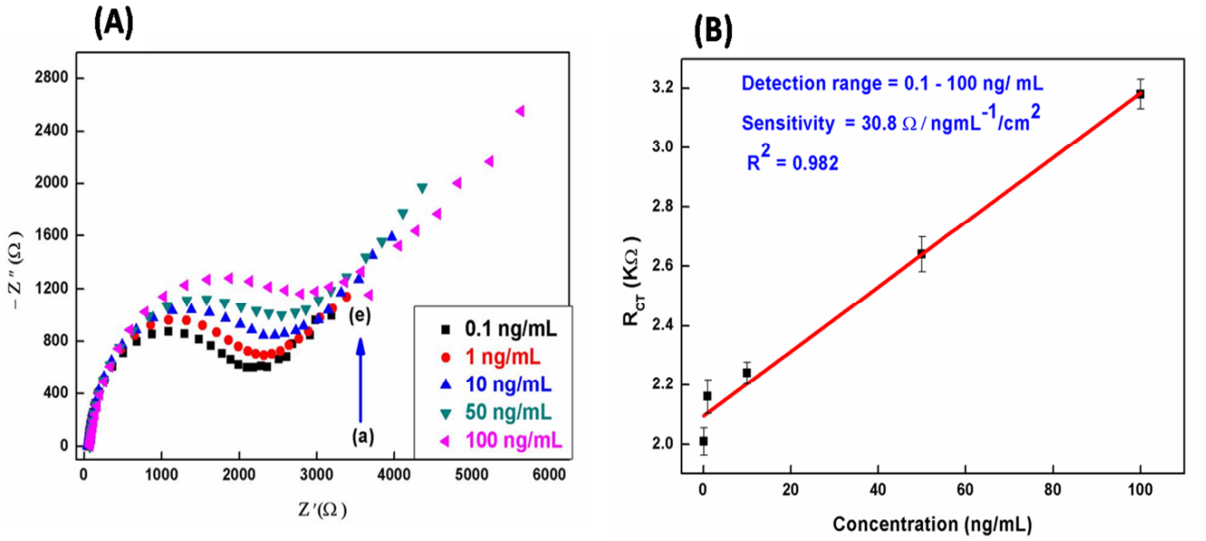

Figure 4.6: (A) Electrochemical response studies of the EA/anti-cTnI /APTES/WO_3 NS/ ITO immunoelectrode as a function of cTnI concentration (0.1 – 100 ng mL^{-1}). (B) Calibration curve plot of the immunoelectrode with respect to R_{CT} value as a function of cTnI concentration

Figure 4.6 (A) depicts the impedance spectra (Nyquist plot) of the fabricated immunoelectrode in response to the different concentration of cardiac troponin I (cTnI, 0.1 to 100 ng mL^{-1}). All the measurements have been carried out in the presence of a PBS solution (5mM $[Fe(CN)_6]^{3-/4-}$ as a redox agent) with an incubation time of 12 minutes before every measurement. An increase in semi-circle's diameter and hence the value of R_{CT} is observed with the rise of cTnI antigen concentration. The rise in R_{CT} value has been attributed to the

formation of cTnI and anti-cTnI insulated immuno-complex which obstructs interfacial electron (e^-) transfer at the electrode surface. **Figure 4.6 (B)** reveals the linearity change in the value of R_{CT} with respect to change in the concentration of cTnI antigen (0.1 to 100 ng mL^{-1}). The calibration plot is fitted between cTnI concentration and the R_{CT} value obeying E**quation 4.1**

$$\mathbf{R_{CT}\ (K\Omega) = 2.09\ (K\Omega) + 0.010\ (K\Omega\ ng^{-1}\ mL) \times [concentration\ (ng\ mL^{-1})];} \quad \mathbf{(4.1)}$$

with $R^2 = 0.982$

The sensitivity of the fabricated immunoelectrode (EA/anti-cTnI/APTES/WO_3 NS/ITO) as calculated from the slope of the calibration plot found to be **30.8 Ω mL ng^{-1} cm^{-2}** with regression coefficient as 0.982. Further, the limit of detection (LOD) is evaluated using 3σ/m as standard criteria, where σ is the standard deviation value and m indicates the slope of the calibration plot. The estimated value of LOD is found as 0.1 ng mL^{-1}.

4.3.4 Performance of the Fabricated Immunoelectrode

The integrity of the immunoelectrode is further verified through selectivity, reproducibility, and stability studies. To investigate the selectivity of the EA/anti-cTnI/APTES/WO_3 NS/ITO electrode, the interference study has been conducted in the presence of various interfering biomarkers such as Carcinoembryonic (CEA, 20 ng mL^{-1}), C-reactive protein (CRP, 1000 ng mL^{-1}), Myoglobin (Mb, 100 ng mL^{-1}) and cardiac troponin I (cTnI, 50 ng mL^{-1}) as shown in **Figure 4.7 (A)**. 10 minutes of incubation is preferred before each measurement. The value of the R_{CT} exhibited by the immunoelectrode in presence of the various interfering biomarkers have been noted as 1.79 KΩ (blank), 1.81 KΩ (CEA), 1.88 KΩ (CRP), 1.92 KΩ (Mb), and 2.62 KΩ in presence of the cTnI antigen. These results show that the fabricated immunoelectrode is highly specific to cTnI antigen and observed negligible variation in R_{CT} value in the presence of interfering biomarkers.

The stability of the immunoelectrode has been analyzed for a period of the total of 6 weeks and over regular intervals of one week. The EIS response is investigated in the PBS solution by investigating the change in R_{CT} value with 0.1 ng ml^{-1} concentration of cTnI antigen **[Figure 4.7 (B)]**. The immunoelectrode exhibits excellent stability up to 5 weeks with 90% response of R_{CT} value, after which the response decreases to 88% at the end of 6 weeks. The immunoelectrode displayed adequate stability till the end of the duration of analysis.

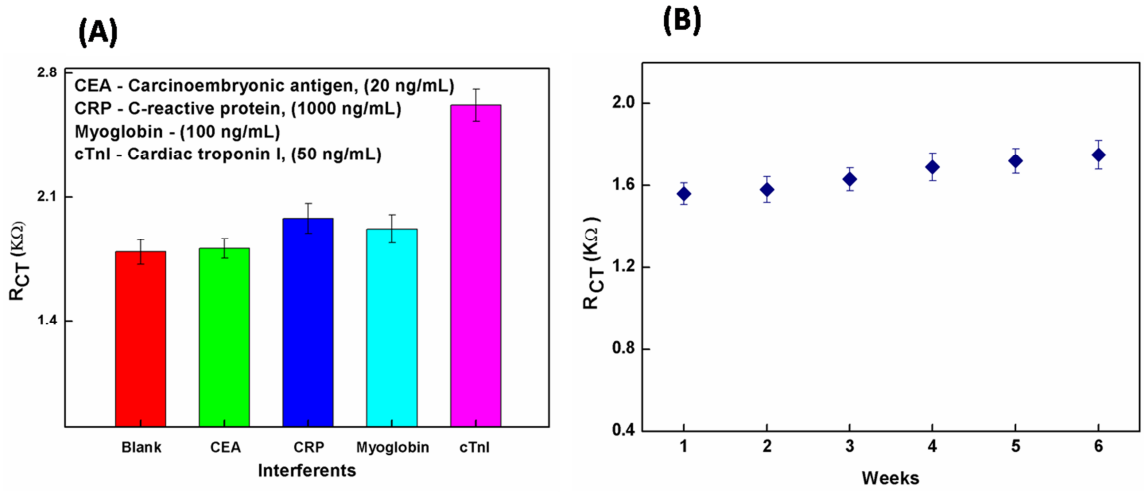

Figure 4.7: (A) Selectivity study of the EA/anti-cTnI/APTES/WO_3 NS/ITO immunoelectrode in the presence of different interferents. (B) Stability study of EA/anti-cTnI/APTES/WO_3 NS/ITO immunoelectrode in the presence of cTnI (0.1 ng mL^{-1}) obtained at a regular interval of 1 week

The reproducibility of the immunoelectrode has been affirmed by studying EIS measurements on 5 different immunoelectrode fabricated under similar condition. The measurements are investigated in the presence of cTnI (0.1ng mL^{-1}) concentration with each measurement measured 4 times for each electrode and errors bars were included accordingly **[Figure 4.8 (A)]**. The low relative standard deviation % value (**RSD %, 1.68%)** showed

good reproducibility of the fabricated immunoelectrode. Further to validate the performance of the fabricated immunoelectrode in cardiac detection diagnosis, EIS response studies of the immunoelectrode is performed with serum obtained through as the pathological laboratory (Dr. Lal path lab, Delhi). The R_{CT} levels of the fabricated immunoelectrode in the presence of spiked sera with cTnI antigen (50 and 100 ng mL^{-1}) is compared with the standard sample solution **[Figure 4.8 (B)]**. The results of the electrochemical response studies show that there is no significant change in the R_{CT} value of the spiked sera and the standard solution. Hence, the developed immunoelectrode provide a promising platform for the diagnosis of the cTnI biomarker in clinical immunoassays.

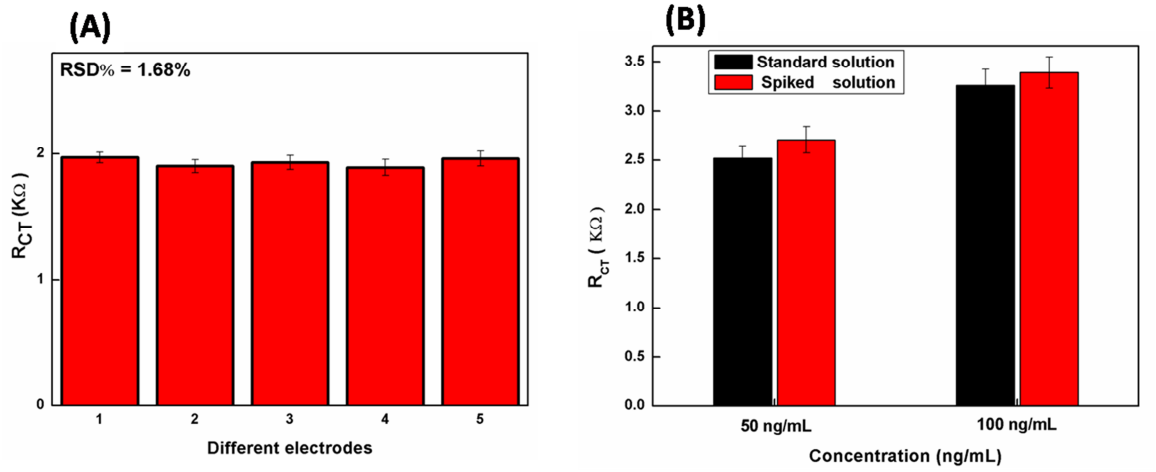

Figure 4.8: (A) EIS response of five different EA/anti-cTnI /APTES/WO_3 NS/ITO immunoelectrode fabricated under a similar condition in the presence of 0.1 ng mL^{-1} cTnI antigen. (B) Response study of the fabricated immunoelectrode presence of spiked sera with cTnI antigen (50 and 100 ng mL^{-1}) was compared with the standard sample solution.

Thus, all these results validate that the as-prepared EA/anti-cTnI/APTES/WO_3 NS/ITO immunoelectrode can be favourable clinical therapy and an improved diagnostic platform for the early detection of AMI, which may pay a way towards the higher survival rate of the patients.

4.4 Conclusion

A facile and a sensitive electrochemical immunoelectrode have been fabricated for the diagnosis of AMI by detecting a specific biomarker – cardiac Troponin I (cTnI), through 2-D WO_3 NS platform. TEM and SEM studies revealed the formation of large surfaced tungsten trioxide nanosheets (WO_3 NS). Fourier transform infrared (FT-IR) as well as cyclic voltammetry studies revealed the successful functionalization with APTES and immobilization of anti-cTnI biomolecules onto WO_3 NS matrix. The electrochemical impedance spectroscopy (EIS) studies show an enhancement in impedance signal of the immunoelectrode in the detection range 0.1 to 100 ng mL^{-1}. The immunoelectrode exhibits improved sensitivity as 30.8 Ω mL ng^{-1} cm^{-2} along with good stability up to 5 weeks as compared to nanoparticles as platform. Also, the value of limit of detection as estimated is 0.1 ng mL^{-1}. These enhanced characteristics have been attributed to the high loading of cTnI antibodies on WO_3 NS matrix due to the enhanced active surface area provided by WO_3 NS. The proposed immunoelectrode platform also showed a good result with the spiked serum samples. Hence, owing to rapid electron transfer kinetics; strong adsorption capability; and high surface-to-volume ratio, the proposed platform (WO_3 NS) puts a step forward towards the development of an integrated biosensor for the electrochemical detection of cardiac biomarkers. More efforts are needed to enhance the fabricated sensor performance to be able to commercialize in the clinical laboratories.

4.5 References:

1. Chen, Di, and Jinhua Ye. "Hierarchical WO_3 hollow shells: dendrite, sphere, dumbbell, and their photocatalytic properties." *Advanced Functional Materials* 18, no. 13 (2008): 1922-1928.

2. Lee, S-H., Rohit Deshpande, Phil A. Parilla, Kim M. Jones, Bobby To, A. Harv Mahan, and Anne C. Dillon. "Crystalline WO_3 nanoparticles for highly improved electrochromic applications." *Advanced Materials* 18, no. 6 (2006): 763-766.
3. Huang, Rong, Yi Shen, Li Zhao, and Minyan Yan. "Effect of hydrothermal temperature on structure and photochromic properties of WO_3 powder." *Advanced Powder Technology* 23, no. 2 (2012): 211-214.
4. Righettoni, Marco, Antonio Tricoli, and Sotiris E. Pratsinis. "Si: WO_3 sensors for highly selective detection of acetone for easy diagnosis of diabetes by breath analysis." *Analytical chemistry*82, no. 9 (2010): 3581-3587.
5. Zhao, Y. M., and Y. Q. Zhu. "Room temperature ammonia sensing properties of $W_{18}O_{49}$ nanowires." *Sensors and Actuators B: Chemical* 137, no. 1 (2009): 27-31.
6. You, L., Y. F. Sun, J. Ma, Y. Guan, J. M. Sun, Y. Du, and G. Y. Lu. "Highly sensitive NO_2 sensor based on square-like tungsten oxide prepared with hydrothermal treatment." *Sensors and Actuators B: Chemical* 157, no. 2 (2011): 401-407.
7. Lee, Choong-Yong, Sun-Jung Kim, In-Sung Hwang, and Jong-Heun Lee. "Glucose-mediated hydrothermal synthesis and gas sensing characteristics of WO_3 hollow microspheres." *Sensors and actuators B: chemical* 142, no. 1 (2009): 236-242.
8. Balendhran, Sivacarendran, Sumeet Walia, Hussein Nili, Jian Zhen Ou, Serge Zhuiykov, Richard B. Kaner, Sharath Sriram, Madhu Bhaskaran, and Kourosh Kalantar-zadeh. "Two-dimensional molybdenum trioxide and dichalcogenides." *Advanced Functional Materials* 23, no. 32 (2013): 3952-3970.
9. Thygesen, Kristian, Joseph S. Alpert, Allan S. Jaffe, Maarten L. Simoons, Bernard R. Chaitman, and Harvey D. White. "Third universal definition of myocardial infarction." *Circulation*126, no. 16 (2012): 2020-2035.

10. Babuin, Luciano, and Allan S. Jaffe. "Troponin: the biomarker of choice for the detection of cardiac injury." *Cmaj* 173, no. 10 (2005): 1191-1202.
11. Thygesen, Kristian, Johannes Mair, Hugo Katus, Mario Plebani, Per Venge, Paul Collinson, Bertil Lindahl et al. "Recommendations for the use of cardiac troponin measurement in acute cardiac care." *European heart journal*31, no. 18 (2010): 2197-2204.
12. Han, Xu, Shanghao Li, Zhili Peng, Abdelhameed M. Othman, and Roger Leblanc. "Recent development of cardiac troponin I detection." *Acs Sensors* 1, no. 2 (2016): 106-114.
13. Skládal, Petr. "Advances in electrochemical immunosensors." *Electroanalysis* 9, no. 10 (1997): 737-745.
14. Wan, Ying, Yan Su, Xinhua Zhu, Gang Liu, and Chunhai Fan. "Development of electrochemical immunosensors towards point of care diagnostics." *Biosensors and Bioelectronics* 47 (2013): 1-11.
15. Li, Feng, Chao Li, Linghui Zhu, Wenbin Guo, Liang Shen, Shanpeng Wen, and Shengping Ruan. "Enhanced toluene sensing performance of gold-functionalized $WO_3 \cdot H_2O$ nanosheets." *Sensors and Actuators B: Chemical* 223 (2016): 761-767.
16. Vashist, Sandeep Kumar, Edmond Lam, Sabahudin Hrapovic, Keith B. Male, and John HT Luong. "Immobilization of antibodies and enzymes on 3-aminopropyltriethoxysilane-functionalized bioanalytical platforms for biosensors and diagnostics." *Chemical reviews* 114, no. 21 (2014): 11083-11130.
17. Ata, M. S., Y. Liu, and I. Zhitomirsky. "A review of new methods of surface chemical modification, dispersion and electrophoretic deposition of metal oxide particles." *Rsc Advances* 4, no. 43 (2014): 22716-22732.

18. Zhao, Weiwei, Bin Cui, Hongjin Qiu, Ping Chen, and Yaoyu Wang. "Multifunctional Fe_3O_4@ WO_3@ $mSiO_2$–APTES nanocarrier for targeted drug delivery and controllable release with microwave irradiation triggered by WO_3." *Materials Letters* 169 (2016): 185-188.
19. Tong, Maosong, Guorui Dai, Yuanda Wu, Xiuli He, and Dingsan Gao. "WO_3 thin film prepared by PECVD technique and its gas sensing properties to NO2." *Journal of materials science* 36, no. 10 (2001): 2535-2538.
20. Majoul, N., S. Aouida, and B. Bessaïs. "Progress of porous silicon APTES-functionalization by FTIR investigations." *Applied Surface Science* 331 (2015): 388-391.
21. Srivastava, Saurabh, Shiju Abraham, Chandan Singh, Md Azahar Ali, Anchal Srivastava, Gajjala Sumana, and Bansi D. Malhotra. "Protein conjugated carboxylated gold@ reduced graphene oxide for aflatoxin B 1 detection." *Rsc Advances* 5, no. 7 (2015): 5406-5414.

CHAPTER 5

Protein Functionalized WO_3 Nanorods based Impedimetric Platform for Cardiac Detection

In this chapter, we work towards the development of an efficient electrochemical sensing platform using ***tungsten trioxide nanorods (WO_3 NRs)*** *as an immobilized matrix. As dimensionality plays an important role in tailoring properties of nanostructures and hence its applications, therefore in this chapter we report the synthesis of 1-D WO_3 NRs based platform towards the development of cardiac biosensors. The 1-D WO_3 nanostructures might provide an efficient direct electrical conduction path between the electrodes and the immobilized biomolecules resulting in the enhanced sensitivity of the biosensing platform. Thin film of APTES functionalized WO_3 NRs has been deposited on ITO coated glass substrate (0.5cm× 1 cm) using electrophoretic deposition technique. The impedimetric response study of proposed immuno-sensor demonstrates high sensitivity [6.81(KΩ $ng^{-1}mL\ cm^{-2}$)] and good reproducibility.*

The work presented in this chapter is published as:

"**Protein-functionalized WO_3 nanorods-based impedimetric platform for sensitive and label-free detection of a cardiac biomarker**"

Journal of Materials Research (2019) 1331-1340

5.1 Introduction

In recent times, nanotechnology-based research has uncovered a multitude of novel materials suitable for the designing of biosensors. Amongst the numerous nanomaterials, metal oxide–based nanomaterials have been considered significant due to their great efficacy, non-toxicity, functional biocompatibility, and catalytic behaviour [1-3]. Among different morphologies, one-dimensional (1-D) materials such as nanowires, nanorods, and nanofibres possess distinct features, such as enhanced electronic properties, unique catalytic activities, and high surface area. Such excellent properties of 1-D material make it a promising platform for the development of biosensors by providing high signal-to-noise ratio, higher sensitivity, large surface area, and shorter response time [4-7]. Recently, Augustine et al. have developed the 1-D metal-oxide based platform for cancer detection [8]. Zhao et al. had developed ZnO nanowires based electrochemical biosensor for L-lactic acid amperometric detection [9]. All these results indicate that 1-D metal-oxide based materials can be ideal candidates for the development of sensitive biosensors.

Nanostructured tungsten trioxide (nWO_3) an n-type semiconductor has gained increasing attention because of the potential applications in multiple areas including electrochromic devices, photo-oxidation, solar cell devices, and sensors [10-13]. It is a member of the transition metal oxide family with electronic conformations of d^0 and d^{10}, which exhibits stimulating characteristics and steadiness important for the sensing uses. High electro-active surface area, fast electron transfer kinetics, and enhanced electrochemical properties are some of the important characteristics of nWO_3 that makes it an ideal candidate as a sensing electrode [14-16]. Owing to these exclusive electrochemical properties, nWO_3 can be considered as an ideal platform for sensing applications. Zhou et al. demonstrated the used of Na-doped tungsten trioxide nanorods (WO_3 NRs) for the detection of BPA [17].

Santos et al. fabricated nitrite biosensor based on WO_3 nanoparticles [15]. Indeed, the versatile properties of nWO_3, such as high sensitivity, biocompatibility, and reversible kinetics, make nWO_3 as a promising platform for the construction of biosensing electrodes. WO_3 nanostructures, such as nanorods, nanofibres, and nanobelts, have shown remarkable performance by providing high electrical and thermal electron transport kinetics due to the quantum confinement along with flexibility that can enable the physical manipulation of its structure. Also, the electrical conductivity of these highly confined structures becomes very sensitive to the presence of ions and other carriers [18].

For clinical applications, biosensor has been considered as an alternative and efficient platform for the detection of diseases. Being a compact and analytical device, biosensor offers simplicity in processing, real time analysis, and good sensitivity [19]. The working of biosensor illustrates the exquisite specificity and sensitiveness of biomolecules in conjunction with a physicochemical transducer, which carries out the bio-interaction measurements with real-time, ease, and simple-to-use formats. Among the various studied biosensors, such as optical, electrical, and electrochemical, the electrochemical immunosensor has been gaining significant attention as a label-free, fast, portable, and reliable analytical tool for clinical diagnostics and environmental monitoring [20-22]. The electrochemical immunosensor is based on specific antigen-antibody interaction and considered as a most sensitive detection tool in diagnosis because of its fast driven analysis, simplicity in its functioning, precise measurement, and ease of fabrication. For successful development of an electrochemical immunosensor, the immobilization of biomolecules and amplification of response signal are the primary requisite [23]. Nanostructured tungsten trioxide in this context has been preferred as an immobilized matrix due to their strong adherence behaviour, chemical stability, and high catalytic activity. Here in this chapter, we report the synthesis of WO_3 NRs using a facile hydrothermal method and demonstrate the application of WO_3 NRs based

immunosensing platform for the label-free electrochemical detection of cardiac biomarker Troponin I (cTnI). The structural and electrochemical characteristics of the fabricated platform are further characterized using various spectroscopic techniques.

5.2 Experimental Section

5.2.1 Synthesis of WO_3 nanorods (WO_3 NRs)

Tungsten trioxide nanorods (WO_3 NRs) have been synthesized using a hydrothermal method [24]. Firstly, 0.5 M sodium tungstate ($Na_2WO_4.2H_2O$) solution is prepared in Milli-Q water with constant stirring. To the resultant solution, we added 6 M HCl drop-wise for the acidification. Thereafter, we mixed 1.2 gm of NaCl in the solution with continuous stirring for 20 minutes. The resultant solution is hydrothermally treated using a stainless steel autoclave. The hydrothermal reaction is performed at 180 °C for about 10 hours. After this reaction period, the stainless steel autoclave cooled naturally and the sample got retrieved by centrifuging it 4-5 times with Milli-Q water. The as-synthesized sample is used for further characterization and functionalization process.

5.2.2 Functionalization and Fabrication of APTES/WO_3 NRs/ITO Electrodes

The activation of functional groups onto the surface of synthesized WO_3 NRs is necessary for the immobilization of the biomolecules entities namely antibodies. For this, we employed 3-aminopropyl-triethoxysilane (APTES), an amino-silane compound which customarily provides active amino groups ($–NH_2$) that can covalently bond with carboxyl groups (–COOH) of the antibody biomolecules [25]. In brief, we first prepared a well-dispersed suspension of WO_3 NRs in 2-propanol solvent through ultrasonication. To this solution, we added APTES solution (98%, 250 µL) and stirred it at 280 rpm for 40 hours at room temperature (24 °C). The resultant functionalized WO_3 NRs are used for preparation of electrodes. To accomplish this task, we prepared thin film of APTES functionalized WO_3

NRs onto the ITO substrate using electrophoretic deposition (EPD) process. For EPD, we first prepared a highly dispersed colloidal suspension of functionalized WO_3 NRs (1mg mL^{-1}) in acetonitrile solvent and operated at an optimized DC potential (48 V) for 120 seconds. Finally, the as-prepared electrode (APTES/WO_3 NRs/ITO) is treated with Milli-Q water to confirm the integrity of the prepared film.

5.2.3 Fabrication of Antibody Immobilized APTES/WO_3 NRs/ITO Immunoelectrode

The immobilization of cardiac troponin I antibody (anti-cTnI) onto the surface of the APTES functionalized WO_3 NRs electrode is accomplish by using EDC-NHS chemistry. A fresh mixture solution (20 µL) of anti-cTnI and EDC-NHS is prepared and got uniformly spread onto the APTES/WO_3 NRs/ITO electrode. The $–NH_2$ groups of APTES molecules can get covalently bounded with –COOH groups of anti-cTnI which have been activated using EDC and NHS chemistry, resulting in the formation of a strong amide bond (OC–NH).

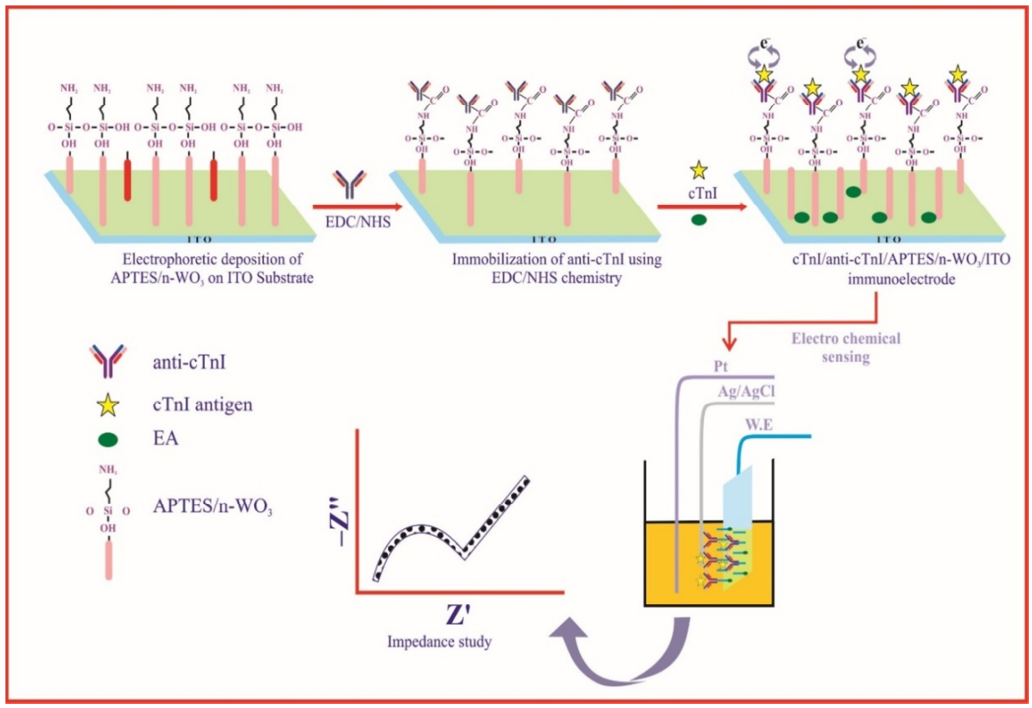

Figure 5.1: A step-wise fabrication of immunosensor and immobilization of antibodies on APTES modified WO_3 NRs electrode.

Lastly to obstruct the non-active sites present onto the immunoelectrode, we used EA solution (0.01 M). The resultant immunoelectrode is treated with the PBS solution and kept at 5 °C. A step-wise fabrication of immunoelectrode and immobilization of antibodies onto the APTES functionalized WO_3 NRs electrode is shown in **Figure 5.1.**

5.3 Results and Discussion

5.3.1 Microscopic and Structural Studies

The crystallinity of the hydrothermally synthesized WO_3 NRs has been studied using X-ray diffraction (XRD) pattern, as shown in **Figure 5.2**. The high-intense diffracted peaks observed at two-theta value 23.1°, 28.22°, 36.75°, 49.8°, and 56.2° corresponds to (002), (200), (202), (220), (204) crystal planes of WO_3 of hexagonal phase, respectively.

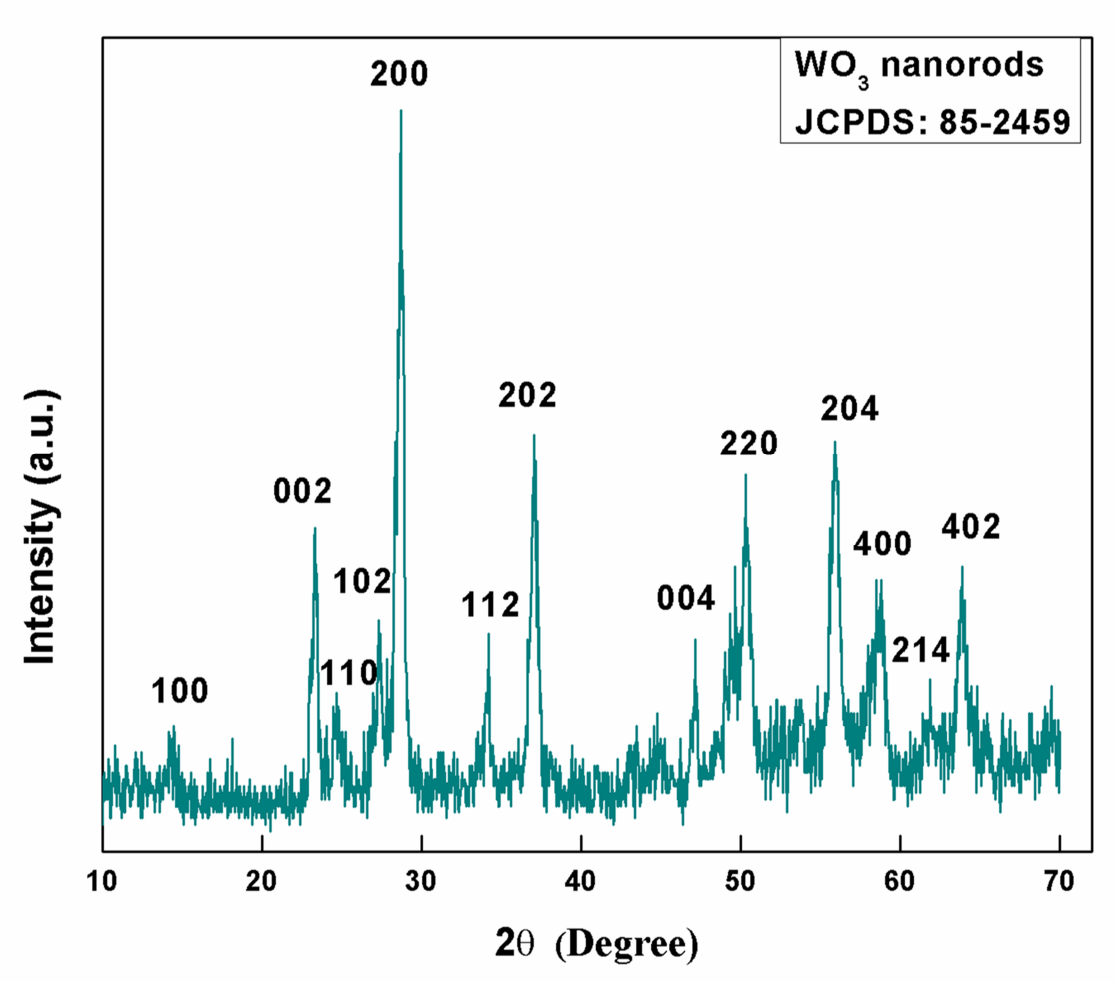

Figure 5.2: XRD pattern of hydrothermally synthesized WO_3 NRs

The other major diffracted peaks observed at 14.01°, 24.3°, 27.2°, 33.8°, 47.4°, 58.12°, 61.98°, and 63.45° correspond to (100), (110), (102), (112), (004), (400), (214) and (402) crystal planes respectively. All these planes well matched with the hexagonal phased WO_3 (**JCPDS 85-2459)** without the presence of undesired phases.

The estimated average crystallite size of WO_3 NRs is found as 68 nm that has been calculated using the Debye-Scherrer's equation given as **Equation 5.1**:

$$\boldsymbol{D = \frac{0.9\,\lambda}{\beta\, Cos\theta}} \qquad \textbf{(5.1)}$$

where λ (1.540Å) corresponds to X-ray wavelength, β and θ represent full width at half maximum and Bragg's angle respectively.

Figure 5.3 represents the micrographs depicting the morphological structure of the synthesized WO_3 sample, as examined under a field emission scanning electron microscope (FESEM) and Transmission electron microscope (TEM). FESEM micrograph observed at low magnification [**Figure 5.3 (i)]** revealed that the synthesized sample has a morphological structure of nanorods grown in large scale, and at high magnification **[Figure 5.3 (ii)]**, we observed the existence of nanorods bundles with inhomogeneous distribution. The estimated diameter of these nanorods has been found as 50 ± 30 nm. The selected area electron diffraction **[Figure 5.3 (iii)]** pattern showed that the synthesized WO_3 NRs are single crystalline and grown along [002], [112], and [204] directions. The TEM image [**inset, Figure 5.3 (iii)]** also revealed the existence of bundles of rods with variable length ranging from hundreds of nanometers to few micrometers and that of diameter in the range of 50 nm to 100 nm.

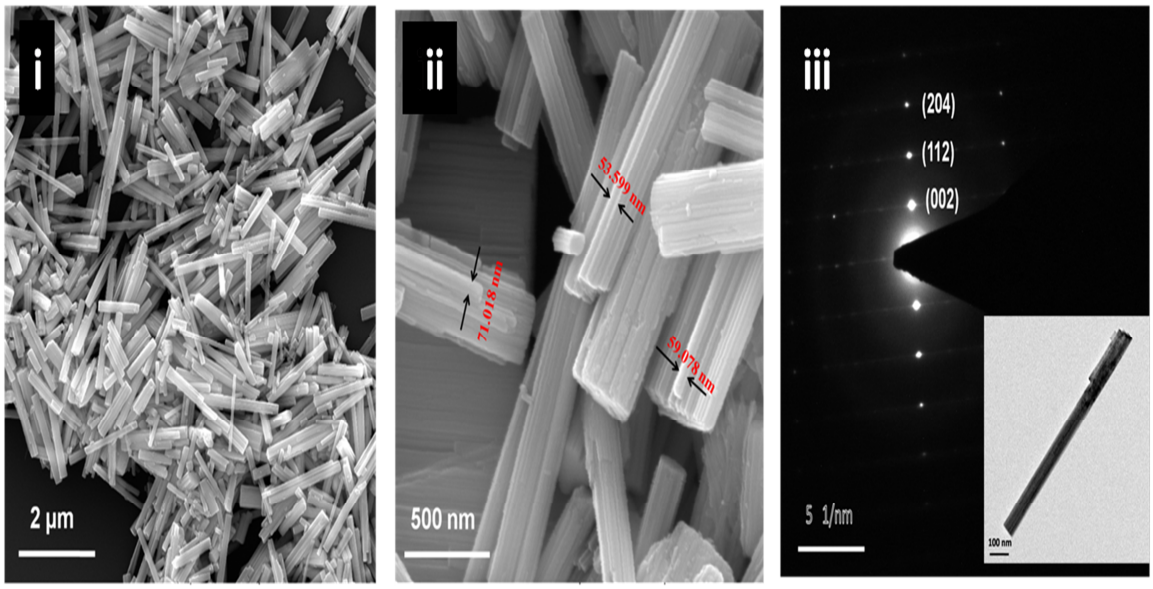

Figure 5.3: FESEM micrograph of WO_3 NRs (i) at 2 µm scale, (ii) at 500 nm scale, and (iii) SAED image of WO_3 NRs. (Inset: TEM image of WO_3 NRs)

5.3.2 Spectroscopic Analysis

Fourier transform infrared (FT-IR) spectroscopic study is performed to investigate the presence of chemical bonds at the different stages of functionalization and immobilization process. **Figure 5.4** represents the FT-IR spectra obtained at different modified stages of the electrode. The APTES/WO_3 NRs/ITO electrode spectrum **(curve i)** exhibited characteristic bands of WO_3 at 1408 cm^{-1} and 823 cm^{-1}, which corresponded to ν (W–O) and ν (W–O_{inter}–W) stretching vibration of the oxygen, respectively [26-27]. The bands observed at 1623 cm^{-1} and 3437 cm^{-1} indicate the presence of free –NH_2 groups in APTES molecule [28-29]. The additional bands observed at 2942 cm^{-1} and 1109 cm^{-1} can be assigned to C–H bonds present in the APTES molecule surface and stretching mode of Si–O–Si, respectively [30]. After covalent immobilization of anti-cTnI **(curve ii**), the bands observed at 1249 cm^{-1} and 1384 cm^{-1} indicate the formation of an amide bond (C–N) between amino groups of APTES and –COOH groups of anti-cTnI.

Furthermore, we observed bands at 1567 cm^{-1} and 1643 cm^{-1} that can assigned to N–H bending of amide II and amide I of carbonyl stretching mode [31]. All these results indicate successful immobilization of antibody biomolecule (anti-cTnI) onto the functionalized matrix. Lastly, with the incorporation of EA onto the immobilized matrix (**curve iii**), we observed no changes in the band's position; rather the intensity of the bands got reduced due to the insulating nature of EA.

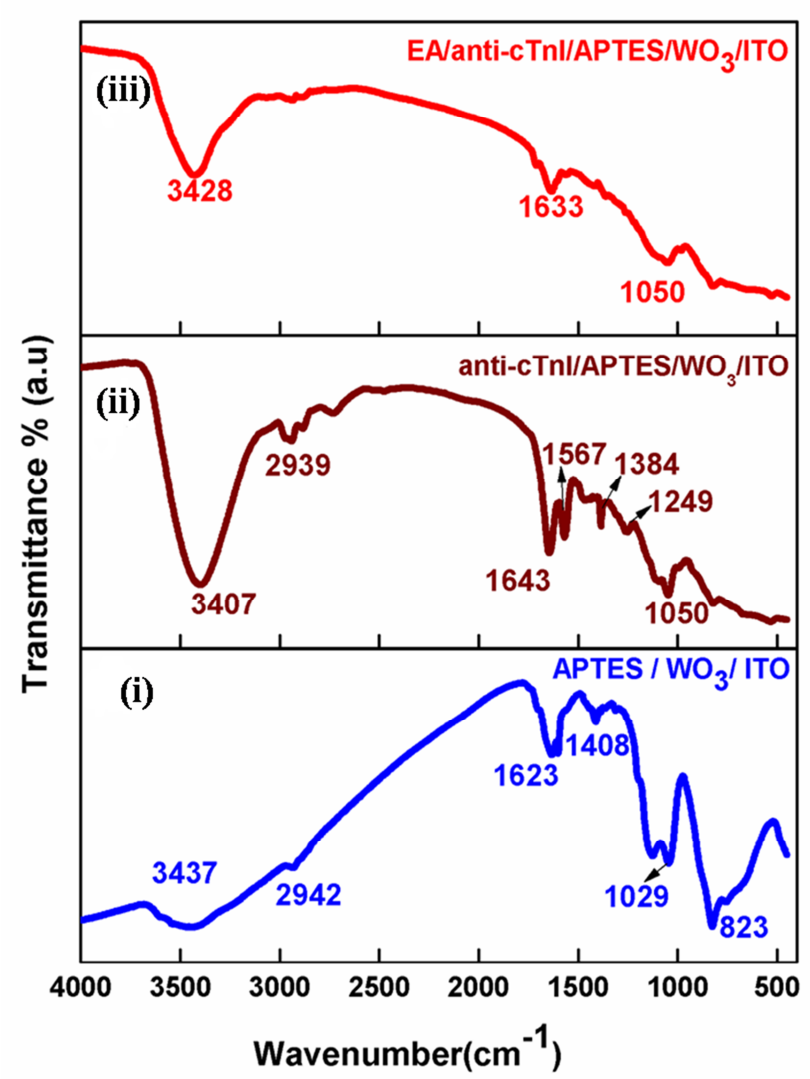

Figure 5.4: FT-IR spectra of (i) APTES/WO_3 NRs/ITO electrode, (ii) anti-cTnI/APTES/WO_3 NRs/ITO immunoelectrode, and (iii) EA/anti-cTnI/APTES/WO_3 NRs/ ITO immunoelectrode.

5.3.3 Electrochemical Characterizations

The electrochemical characteristics of the fabricated sensing platform have been investigated using cyclic voltammetry (CV) and electrochemical impedance spectroscopic (EIS) techniques. The CV has been widely studied in determining the qualitative information of electrochemical kinetics of the sensing electrode. The cyclic voltammograms have been studied at the scan rate of 50 mV s^{-1} in a PBS solution (pH 7.4) coupled with five milli-molar $[Fe(CN)_6]^{3-/4-}$ is shown in **Figure 5.5 (A).** The magnitude of the oxidation peak current to the reduction peak current ($\mathbf{i_a/i_c}$ **= 1.05)** for APTES/WO_3NRs/ITO electrode showed the reversible process of the redox probe. Furthermore, on immobilization of antibody biomolecules, the anodic peak current for immunoelectrode (anti-cTnI/APTES/WO_3 NRs/ITO, **0.303 mA**) got decreased in magnitude with respect to functionalized electrode (APTES/WO_3NRs/ITO, **0.347 mA**). This showed the insulating nature of the immobilized antibodies of cTnI which might has obstructed the electron transfer kinetics at the electrode surface. Further, the incorporation of EA molecules onto immunoelectrode surface resulted in the decrease in peak current value **(0.230 mA**). This decrease in current can be justified as all non-active sites present on the antibody immobilized surface got blocked by the EA molecules. All these results indicate the successful fabrication of immunosensing platform. Furthermore, the EIS study is also carried out to study the interfacial properties between the fabricated electrode surface and the electrolyte in the frequency range of 0.01– 10^5 Hz. The experimental data of EIS is modeled using an equivalent circuit known as the Randles circuit. The circuit consists of Warburg impedance (Z_W), double-layer capacitance (C_{dl}), solution resistance (R_S), and the electron transfer resistance (R_{CT}).

Figure 5.5 (B) represents the EIS spectra (Nyquist plot) of functionalized and the antibody immobilized electrodes that have been obtained on an autolab potentiostat/

galvanostat system. From the EIS spectra, the R_{CT} value of APTES/WO_3 NRs/ITO electrode is found as **2.15 KΩ**, which increased to **2.34 KΩ** after antibody immobilization.

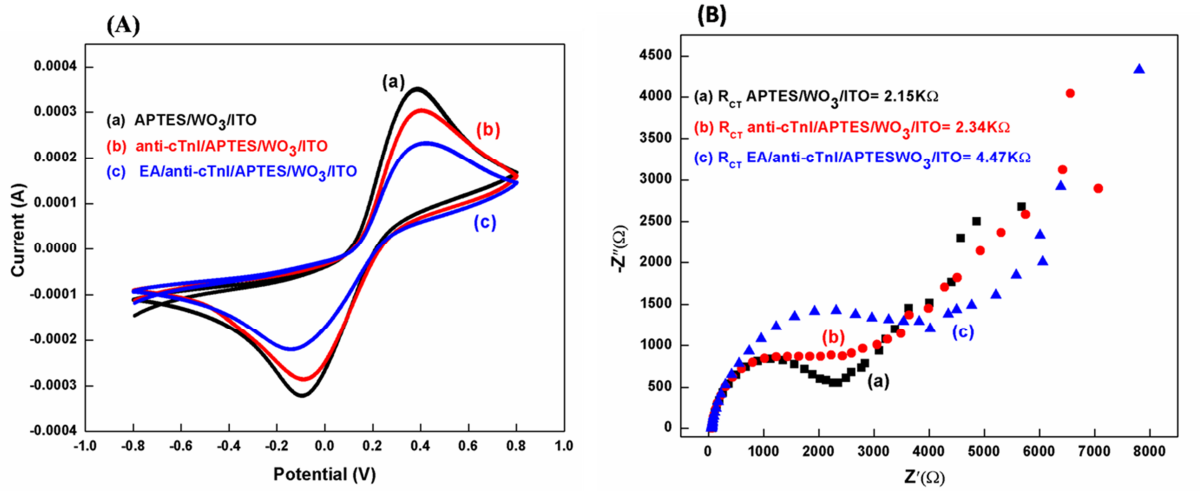

Figure 5.5: (A) Cyclic voltammograms (CV) of the different modified electrodes obtained at the scan rate of 50 mV s^{-1}, and (B) The EIS study of the modified electrodes obtained in the frequency range 0.01–10^5 Hz.

This increased impedance revealed the insulating nature of the antibody. Furthermore, with the incorporation of EA molecules that covered the non-specific sites of the immunoelectrode, the charge transfer phenomenon again got hindered, resulting in the increase in R_{CT} value to **4.47 KΩ**. Moreover, these electrodes have been also characterized by evaluating heterogeneous electron transfer constant (K_O) using **Equation (5.2):**

$$K_O = \frac{RT}{n^2F^2AR_{CT}C} \qquad (5.2)$$

where T represents as temperature, R as gas constant, n as total number of electrons transferring constant, F as the Faraday's constant, C as the bulk concentration of the redox couple, and A as the effective surface area. The value of K_O estimated for APTES/WO_3NRs/ITO electrode (**9.91 × 10^{-5} cm s^{-1}**) was found to be high compared with that of EA/anti-cTnI/APTES/WO_3NRs/ITO immunoelectrode (**4.47×10^{-5} cm s^{-1}**), thus demonstrating faster electron transfer kinetics at the interface of the electrode.

The characteristics of the fabricated immunoelectrode have been further investigated at different scan rates using cyclic voltammetry technique. **Figure 5.6 (A)** depicts the scan rate study as investigated in the broad range of 40 – 160 mV s^{-1}. The magnitude of both anodic peak current (I_{pa}) and cathodic peak current (I_{pc}) of the response revealed the linear correlation with the square root of scan rate value [**Figure 5.6(B)**], indicating a diffusion-controlled process of the electrochemical reaction [**Equations (5.3) and (5.4)].**

$$I_{pa} = 0.022\ mA + [0.0287 mA(s / mV) \times \{scan\ rate\ (mV/s)\}^{1/2}], \quad R^2 = 0.0990 \quad (5.3)$$

$$I_{pc} = -0.0528\ mA + [-0.0225 mA(s / mV) \times \{scan\ rate\ (mV/s)\}^{1/2}], \quad R^2 = 0.0989 \quad (5.4)$$

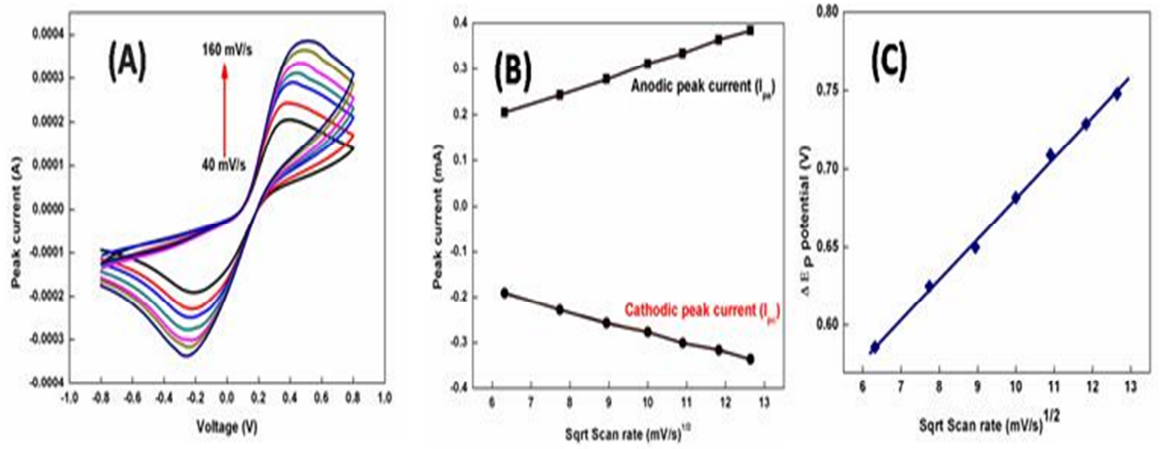

Figure 5.6: (A) Scan rate study of the fabricated immunoelectrode obtained in the range of 40–160 mV/s using CV. (B) Variation of peak currents (Ipa and Ipc) with respect to the scan rate. (C) Variation of redox peak potential difference with respect to the square root of scan rate.

Further, we observed that with an increase in scan rate, oxidation peak potential (V_{pa}) get positive shifted while reduction peak potential (V_{pc}) get negative shifted. This showed linearity between redox peak potential shifts ($\Delta E = V_{pa} - V_{pc}$) and the square root of the scan rate as depicted from **Equation (5.5)**. Lastly from **Figure 5.6 (C),** we observed appreciable linearity for the electron transfer kinetics at the electrode interfacial surface.

$$\Delta E\ (V) = 0.422\ V + [0.025\ V(s / mV) \times \{scan\ rate\ (mV/s)\}^{1/2}, \quad R^2 = 0.997 \quad (5.5)$$

5.3.4 Electrochemical Response Investigations

The investigation of the electrochemical response studies of the fabricated immunoelectrode as a function of cTnI concentration (0.01–10 ng mL^{-1}) has been performed by employing EIS technique. **Figure 5.7(A)** represents the Nyquist plot carried out with PBS (50 mM, pH 7.4) containing 5mM $[Fe(CN)_6]^{3-/4-}$ as a redox coupling agent (inset: Randles circuit). The transportation of electrochemically produced charge at the interface of electrode and electrolyte has been modeled by measuring the variation in resistance. The value of charge transfer resistance (R_{CT}) has been evaluated using NOVA software.

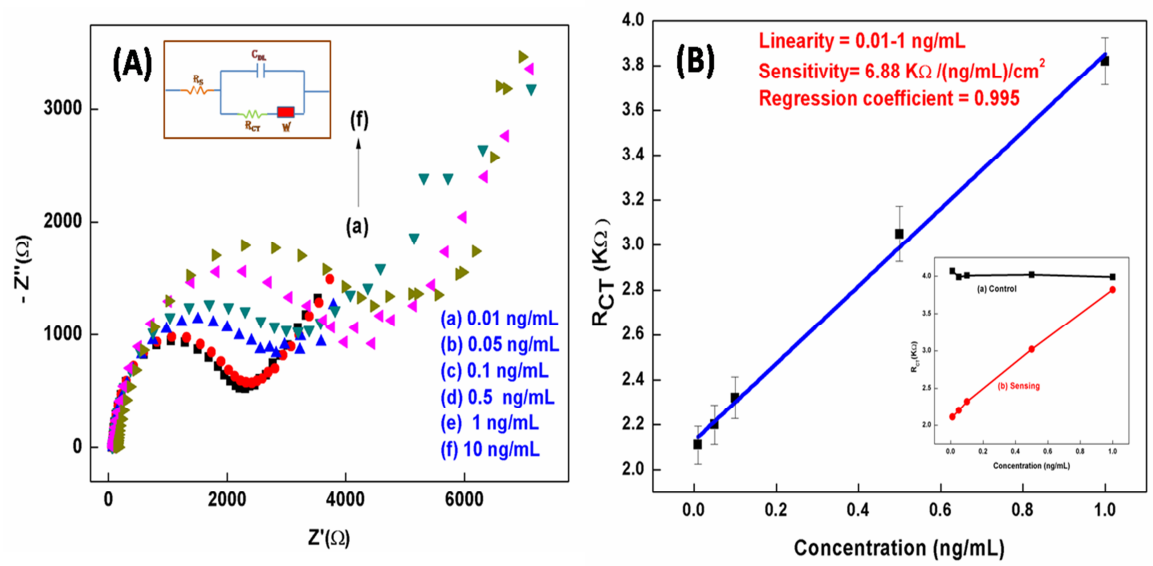

Figure 5.7: (A) EIS response study of the fabricated immunoelectrode studied as the function of cTnI concentration (0.01–10 ng/mL);(inset shows Randles equivalent circuit), and (B) representation of calibration plot obtained between R_{CT} and cTnI antigen concentration; inset shows sensing along with control study.

The R_{CT} value of the EA/anti-cTnI/APTES/WO_3 NRs/ITO immunoelectrode increased with the increase in cTnI concentration. This increase in impedance revealed the development of insulating antigen-antibody complex resulting from the specific key–lock interaction of the anti-cTnI and cTnI, which might have hindered the electron motion. The calibration plot has been obtained between R_{CT} value and the cTnI concentration as shown in

Figure 5.7 (B). The value of R_{CT} varies linearly with the cTnI concentration up to 1 ng mL^{-1} and obeys **Equation (5.6).**

$$\mathbf{R_{CT} = 2.12\ (K\Omega) + 1.723\ (K\Omega\ mL/ng) \times [concentration\ (ng/mL)],\quad R^2 = 0.995} \qquad \mathbf{(5.6)}$$

The analysis of the response study revealed that the APTES/WO_3 NRs/ITO–based immunoelectrode exhibits good sensitivity as **6.81 [KΩ mL/ (ng.cm^2)]** in a linear detection range of 0.01–1 ng mL^{-1}. The high sensitivity exhibited by the immunoelectrode can be ascribed to the existence of WO_3 NRs in the sensing platform that perhaps provided the enhanced charge conduction channel for the electron transfer kinetics. Moreover, a controlled study is conducted to study the electrochemical impedance response of APTES/WO_3 NRs/ ITO immunoelectrode toward the cTnI antigen without using anti-cTnI [**Figure 5.7(B), inset**]. It has been found that there is no significant variation in the magnitude of R_{CT} value in response to the different concentration of cTnI antigen. Hence, we can conclude that the fabricated immunosensor is highly sensitive and specific to the immuno interactions (cTnI-anti-cTnI). The proposed immunosensor is able to sensed cTnI concentration as low as 0.01 ng mL^{-1}.

The reproducibility of the fabricated immunoelectrode is further investigated by measuring the R_{CT} values for the four different fabricated immunoelectrodes prepared under ideal conditions in the presence of 0.5 ng mL^{-1} cTnI antigen. However, no noticeable change in the R_{CT} value is observed, as seen in **Figure 5.8 (A)**. The reproducibility of the immunoelectrode has been estimated by evaluating relative standard deviation (RSD %). The calculated mean value of R_{CT} for these four electrodes **(2.19 KΩ**) with RSD of **4.14%** lies within an acceptable error range, suggesting an excellent reproducibility of the immunoelectrode.

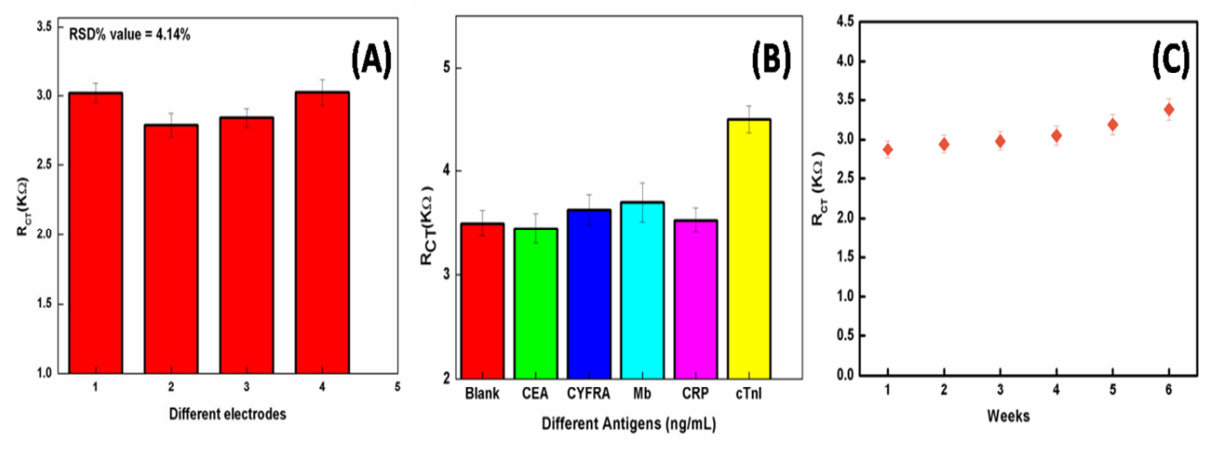

Figure 5.8: (A) Reproducibility study of the immunoelectrodes fabricated under identical conditions, (B) Interference study of the immunoelectrode in the presence of different interferents. (C) Shelf life study of the EA/anti-cTnI/APTES/WO_3 NRs/ITO immunoelectrode.

The selectivity study of the fabricated immunoelectrode is too investigated in the presence of other interfering biomarkers, such as C-reactive protein, Myoglobin, cytokeratin-19 antigen, and carcinoembryonic antigen, using EIS measurements. **Figure 5.8 (B)** shows the interference study of the immunoelectrode, where no significant change in the R_{CT} value is observed among different interferents concerning blank immunoelectrode. However, after the addition of cTnI antigen, we observed remarkable change in the R_{CT} value, which signifies the high specificity of the fabricated immunoelectrode for the cTnI biomarker.

Furthermore, we also conducted the shelf life study of the fabricated immunoelectrode by measuring R_{CT} value in the presence of 0.5 ng mL^{-1} cTnI antigen at the regular interval of 7 days **[Figure 5.8 (C)]**. The increase in R_{CT} value has been found as 7.3% up to 5 weeks after which the R_{CT} increased to more than 20% at the end of 6 weeks. Thus, the fabricated immunoelectrode retained its biological activity for up to 5 weeks. Hence, all these results indicated that the EIS technique for detection of biomarkers proved to be an efficient, simple, and fast response technique. In **Table 5.1**, the sensing characteristics of the fabricated immunosensor have been compared with those of the reported in the literature.

Sensing platform	Detection technique	Detection range	Sensitivity (S)	Detection limit	Reference
Gold nano dumb Bells	EIS	0.05-500 ng mL^{-1}	-	8 pg mL^{-1}	32
Carbon nanofibres	EIS	0.25-10 ng mL^{-1}	-	0.2 ng mL^{-1}	33
ZrO_2 n.ps	CV	0.1 – 100 ng mL^{-1}	3.9 μA mL/(ng/cm^2)	0.1 ng mL^{-1}	34
WO_3 NRs	**EIS**	**0.01-10** ng mL^{-1}	**6.81 KΩ mL/(ng/cm^2)**	**0.01 ng mL^{-1}**	**Present work**

Table 5.1: Sensing characteristics of the WO_3 NRs based platform compared to other reported platforms towards cTnI detection

5.4 Conclusion

We have developed an efficient and a label-free electrochemical sensing platform for detection of a cardiac biomarker using WO_3 NRs as an immobilized matrix. The APTES functionalized WO_3 NRs got deposited onto ITO electrode using electrophoretic deposition (EPD) technique, and subsequently, the functionalized WO_3 NRs have been used as an immobilized matrix for the covalent binding of anti-cTnI biomolecules. The variation in impedance signal of the fabricated immunosensor is observed on the formation of immunocomplex between anti-cTnI and cTnI antigen. The experimental results of the impedimetric studies revealed enhanced sensitivity [6.81 KΩ mL ng^{-1} cm^{-2}] and good reproducibility with long term stability (5 weeks). The enhanced characteristics of the proposed immunosensor can be attributed to the 1-D WO_3 nanostructures which might has provided an efficient electrical conduction path between the electrodes and the immobilized antibody biomolecules resulting in enhanced sensitivity of the biosensing platform. Hence,

these results direct us toward the realization of integrated and portable diagnostic tool based on WO_3 NRs as matrix.

5.5 References:

1. Walcarius, Alain, Shelley D. Minteer, Joseph Wang, Yuehe Lin, and Arben Merkoçi. "Nanomaterials for bio-functionalized electrodes: recent trends." *Journal of Materials Chemistry B* 1, no. 38 (2013): 4878-4908.
2. Zarur, Andrey J., and Jackie Y. Ying. "Reverse microemulsion synthesis of nanostructured complex oxides for catalytic combustion." *nature* 403, no. 6765 (2000): 65.
3. Solanki, Pratima R., Ajeet Kaushik, Ved V. Agrawal, and Bansi D. Malhotra. "Nanostructured metal oxide-based biosensors." *NPG Asia Materials* 3, no. 1 (2011): 17.
4. Wang, Fengyun, Longfei Song, Hongchao Zhang, Linqu Luo, Dong Wang, and Jie Tang. "One-dimensional metal-oxide nanostructures for solar photocatalytic water-splitting." *Journal of Electronic Materials* 46, no. 8 (2017): 4716-4724.
5. Fang, Xiaosheng, Linfeng Hu, Changhui Ye, and Lide Zhang. "One-dimensional inorganic semiconductor nanostructures: a new carrier for nanosensors." *Pure and Applied Chemistry* 82, no. 11 (2010): 2185-2198.
6. Solanki, Pratima R., Jay Singh, Bharti Rupavali, Sachchidanand Tiwari, and Bansi D. Malhotra. "Bismuth oxide nanorods based immunosensor for mycotoxin detection." *Materials Science and Engineering: C* 70 (2017): 564-571.
7. Galvin, Paul, Narayanasamy Padmanathan, Kafil M. Razeeb, James F. Rohan, Lorraine C. Nagle, Amelie Wahl, Eric Moore, Walter Messina, Karen Twomey, and Vladimir Ogurtsov. "Nanoenabling electrochemical sensors for life sciences applications." *Journal of Materials Research* 32, no. 15 (2017): 2883-2904.

8. Augustine, Shine, Amish G. Joshi, Birendra Kumar Yadav, Anurag Mehta, Pragati Kumar, Venkatesan Renugopalakrishanan, and Bansi D. Malhotra. "An emerging nanostructured molybdenum trioxide-based biocompatible sensor platform for breast cancer biomarker detection." *MRS Communications* 8, no. 3 (2018): 668-679.
9. Zhao, Yanguang, Xiaoqin Yan, Zhuo Kang, Xiaofei Fang, Xin Zheng, Lanqing Zhao, Hongwu Du, and Yue Zhang. "Zinc oxide nanowires-based electrochemical biosensor for L-lactic acid amperometric detection." *Journal of Nanoparticle Research* 16, no. 5 (2014): 2398.
10. Yan, Chaoyi, Wenbin Kang, Jiangxin Wang, Mengqi Cui, Xu Wang, Ce Yao Foo, Kenji Jianzhi Chee, and Pooi See Lee. "Stretchable and wearable electrochromic devices." *ACS nano*8, no. 1 (2013): 316-322.
11. Szilágyi, Imre M., Balázs Fórizs, Olivier Rosseler, Ágnes Szegedi, Péter Németh, Péter Király, Gábor Tárkányi et al. "WO_3 photocatalysts: Influence of structure and composition." *Journal of catalysis* 294 (2012): 119-127.
12. D. Sandil, S. Kumar, K. Arora, S. Srivastava, B. Malhotra, S. Sharma and N.K. Puri: Biofunctionalized nanostructured Tungsten trioxide based sensor for cardiac biomarker detection *Mater. Lett.* 186, 202 (2017).
13. Zheng, Haidong, Yasuhiro Tachibana, and Kourosh Kalantar-zadeh. "Dye-sensitized solar cells based on WO_3." *Langmuir*26, no. 24 (2010): 19148-19152.
14. Shi, Jichao, Gujin Hu, Yan Sun, Ming Geng, Jie Wu, Yufeng Liu, Meiying Ge, Junchao Tao, Meng Cao, and Ning Dai. "WO_3 nanocrystals: synthesis and application in highly sensitive detection of acetone." *Sensors and Actuators B: Chemical* 156, no. 2 (2011): 820-824.

15. Santos, Lídia, Célia M. Silveira, Elamurugu Elangovan, Joana P. Neto, Daniela Nunes, Luís Pereira, Rodrigo Martins et al. "Synthesis of WO_3 nanoparticles for biosensing applications." *Sensors and Actuators B: Chemical* 223 (2016): 186-194.
16. Cai, Ze-Xing, Hua-Yao Li, Jun-Chao Ding, and Xin Guo. "Hierarchical flowerlike WO_3 nanostructures assembled by porous nano flakes for enhanced NO_2 gas sensing." *Sensors and Actuators B: Chemical* 246 (2017): 225-234.
17. Zhou, Yuanzhen, Lehui Yang, Shanghui Li, and Yuan Dang. "A novel electrochemical sensor for highly sensitive detection of bisphenol A based on the hydrothermal synthesized Na-doped WO_3 nanorods." *Sensors and Actuators B: Chemical* 245 (2017): 238-246.
18. Liu, Jincheng, Olivier Margeat, Walid Dachraoui, Xianjie Liu, Mats Fahlman, and Jorg Ackermann. "Gram-Scale Synthesis of Ultrathin Tungsten Oxide Nanowires and their Aspect Ratio-Dependent Photocatalytic Activity." *Advanced Functional Materials* 24, no. 38 (2014): 6029-6037.
19. Ali, J., J. Najeeb, M. Asim Ali, M. Farhan Aslam, and A. Raza. "Biosensors: their fundamentals, designs, types and most recent impactful applications: a review." *J Biosens Bioelectron*8, no. 1 (2017).
20. Ko, Sungho, Bumjun Kim, Seong-Sik Jo, Se Young Oh, and Je-Kyun Park. "Electrochemical detection of cardiac troponin I using a microchip with the surface-functionalized poly (dimethylsiloxane) channel." *Biosensors and Bioelectronics* 23, no. 1 (2007): 51-59.
21. Prakash, M. Durga, Shiv Govind Singh, Chandra Shekhar Sharma, and V. Siva Rama Krishna. "Electrochemical Detection of Cardiac Biomarkers Utilizing Electrospun Multiwalled Carbon Nanotubes Embedded SU-8 Nanofibers." *Electroanalysis* 29, no. 2 (2017): 380-386.

22. Ronkainen, Niina J., H. Brian Halsall, and William R. Heineman. "Electrochemical biosensors." *Chemical Society Reviews* 39, no. 5 (2010): 1747-1763.
23. Malhotra, Bansi D., Saurabh Srivastava, Md Azahar Ali, and Chandan Singh. "Nanomaterial-based biosensors for food toxin detection." *Applied biochemistry and biotechnology* 174, no. 3 (2014): 880-896.
24. Wang, Jinmin, Eugene Khoo, Pooi See Lee, and Jan Ma. "Controlled synthesis of WO_3 nanorods and their electrochromic properties in H_2SO_4 electrolyte." *The Journal of Physical Chemistry C* 113, no. 22 (2009): 9655-9658.
25. Zhao, Weiwei, Bin Cui, Hongjin Qiu, Ping Chen, and Yaoyu Wang. "Multifunctional Fe_3O_4@ WO_3@ $mSiO_2$–APTES nanocarrier for targeted drug delivery and controllable release with microwave irradiation triggered by WO_3." *Materials Letters* 169 (2016): 185-188.
26. Tong, Maosong, Guorui Dai, Yuanda Wu, Xiuli He, and Dingsan Gao. "WO_3 thin film prepared by PECVD technique and its gas sensing properties to NO_2." *Journal of materials science* 36, no. 10 (2001): 2535-2538.
27. Sandil, Deepika, Saurabh Srivastava, B. D. Malhotra, S. C. Sharma, and Nitin K. Puri. "Biofunctionalized tungsten trioxide-reduced graphene oxide nanocomposites for sensitive electrochemical immunosensing of cardiac biomarker." *Journal of Alloys and Compounds* 763 (2018): 102-110.
28. Majoul, N., S. Aouida, and B. Bessaïs. "Progress of porous silicon APTES-functionalization by FTIR investigations." *Applied Surface Science* 331 (2015): 388-391.
29. Ata, M. S., Y. Liu, and I. Zhitomirsky. "A review of new methods of surface chemical modification, dispersion and electrophoretic deposition of metal oxide particles." *Rsc Advances* 4, no. 43 (2014): 22716-22732.

30. Srivastava, Saurabh, Shiju Abraham, Chandan Singh, Md Azahar Ali, Anchal Srivastava, Gajjala Sumana, and Bansi D. Malhotra. "Protein conjugated carboxylated gold@ reduced graphene oxide for aflatoxin B 1 detection." *Rsc Advances* 5, no. 7 (2015): 5406-5414.
31. Kumar, Suveen, Saurabh Kumar, Sachchidanand Tiwari, Shine Augustine, Saurabh Srivastava, Birendra Kumar Yadav, and Bansi Dhar Malhotra. "Highly sensitive protein functionalized nanostructured hafnium oxide based biosensing platform for non-invasive oral cancer detection." *Sensors and Actuators B: Chemical* 235 (2016): 1-10.
32. Negahdary, M., M. Behjati-Ardakani, N. Sattarahmady, H. Yadegari, and H. Heli. "Electrochemical aptasensing of human cardiac troponin I based on an array of gold nanodumbbells-Applied to early detection of myocardial infarction." *Sensors and Actuators B: Chemical* 252 (2017): 62-71.
33. Periyakaruppan, Adaikkappan, Ram P. Gandhiraman, M. Meyyappan, and Jessica E. Koehne. "Label-free detection of cardiac troponin-I using carbon nanofiber based nanoelectrode arrays." *Analytical chemistry* 85, no. 8 (2013): 3858-3863.
34. Kumar, Suveen, Saurabh Kumar, Shine Augustine, and Bansi D. Malhotra. "Protein functionalized nanostructured zirconia based electrochemical immunosensor for cardiac troponin I detection." *Journal of Materials Research* 32, no. 15 (2017): 2966-2972.

CHAPTER 6

Bio-Functionalized WO_3-RGO Nanocomposite for Electrochemical Sensing of Cardiac Biomarker

In this chapter, we demonstrate the fabrication of a facile and efficient biosensing platform for electrochemical detection of human cardiac biomarker Troponin I (cTnI) using ***tungsten trioxide-reduced graphene oxide (WO_3-RGO) nanocomposite*** *as a matrix. The WO_3-RGO nanocomposite is functionalized with 3-aminopropyl tri-ethoxy saline (APTES) for the activation of amino groups ($-NH_2$) that can covalently bind to the antibodies of cTnI. The fabricated immunoelectrode has been studied using contact angle measurement, FTIR and electrochemical methods. The synergistic behavior between RGO and WO_3 nanorods has allowed the immunoelectrode to exhibit enhanced heterogeneous electron transfer rate constant ($K_o = 2.4 \times 10^{-4}$ cms^{-1}) resulting in improved biosensor efficiency. Furthermore, the validation of immunoelectrode with cardiac patient samples demonstrates the clinical application of this nano-biosensing framework for detection of other biomarkers as well.*

The work presented in this chapter is published as:

"Bio-functionalized tungsten trioxide-reduced graphene oxide nanocomposites for sensitive electrochemical immunosensing of cardiac biomarker"

Journal of Alloys and Compounds 763 (2018) 102-110

6.1 Introduction

The novel and distinguishable properties and ease synthesis processes have been observed as the uniqueness of tungsten trioxide (WO_3) nanostructures among other metal oxide nanostructures. The enhanced electrical and catalytic characteristics of WO_3 nanostructures have made it an appropriate subject as an immobilizing matrix for the development of electrochemical sensors for the detection of biomarkers [1-2]. The strong adherence to the substrate, non-toxicity, chemically stable, simple synthesis and narrow band gap (Eg = 2.4-2.8 eV) are few of the advantages of WO_3 nanostructures which has enabled its variety of research in wide field of biomedical applications especially in biosensing. However, for the enhancement in the performance of the biosensors, nanocomposites or hybrid nanostructures have shown great potential in the development of biosensing devices [3]. In a recent time, graphene is one of the widely studied nanomaterials in the field of biosensing. Chemical vapour deposition (CVD), graphite intercalation method and reduction of graphene oxide are few of the synthesis techniques of graphene [4-6]. However, among all these, chemically reduction of graphene oxide to produce graphene nanosheets also known as reduced graphene oxide (RGO) is most appropriate and captivating due to its high yield production, ease synthesis and low cost [4]. RGO, a 2-D array of carbon atoms exhibits sp^2 bonds that contribute toward its unique properties including good electrical conductivity, larger surface area, and high electrochemical activity [7]. RGO has been found to exhibits covalently bonded oxygen rich functional groups such as carboxylic groups, hydroxyl and epoxy groups and carbonyl groups [8]. The presence of these functional groups has enlightened its hydrophilic characteristics and chemical reactivity [9-10]. These characteristics of RGO makes it suitable candidate as a functional element or as a substrate for the immobilization of other molecules. Hence incorporation of semiconducting material such as RGO with the nanostructured metal oxides would be promising in the biomedical

applications [11-13]. Nanocomposites based on RGO exhibits striking features such as high specific surface area, high mechanical strength, enhanced thermal and electrical characteristics and high electron transfer kinetics [13-14]. In this context, RGO can be considered as a promising supportive matrix. In recent time, a lot of work has been reported toward the development of improved sensing platform for the diagnosis of chemical and biological species based on the WO_3-RGO hybrid structures. For instance, Sun et al. had reported the development of photo-electrochemical sensing platform for the diagnosis of cysteine using functionalized WO_3-RGO modified electrode [15]. Zhu et al. had fabricated RGO-WO_3 nanocomposite for the photocatalytic degradation of sulfamethoxazole [16]. And similarly, researchers have also employed WO_3-RGO based platform for the gas sensing applications with improved characteristics [17-18]. All these results indicates that WO_3-RGO nano-composite based platform can be a promising platform towards the enhancement in the performance of biosensor for the detection of cardiac biomarker cardiac Troponin I (cTnI).

In this chapter, we report the synthesis of WO_3-RGO nano-composite using in-situ hydrothermal synthesis process. For the first time, the synthesized nanocomposite has been utilized as an immobilized platform for fabrication of simplistic and label-free electrochemical immuno-sensor for the analysis of cTnI. The proposed mechanism delivers improved sensitivity, wide detection range, and good stability which have been investigated comprehensively.

6.2 Experimental Section

6.2.1 Preparation of Graphene Oxide (GO)

The graphene oxide (GO) has been prepared using a modified Hummer's method [4, 19]. Firstly, a solution of concentrated H_2SO_4 / H_3PO_4 has been prepared in a ratio of 9:1. To this, 3 gm of graphite flakes has been added along with 18 gm of $KMnO_4$. The temperature of the resultant solution raised as the process leads to exothermic in nature. After this, the

solution has been subjected to the magnetic stirrer for 15 hours at 50 °C. The resultant reaction has been subsequently quenched on the addition of about 250 mL of ice along with 3mL of 30% H_2O_2. At last, the solution got centrifuged with the multiple washing with Milli-Q water until the pH 7 achieved after which it got dried at 70 °C resulting in graphite oxide. Finally, the prepared graphite oxide on dispersion in Milli-Q water is converted into graphene oxide using ultra-sonication treatment for 1 hour.

6.2.2 Preparation of Reduced Graphene Oxide (RGO)

The as-synthesized graphene oxide has been chemically reduced to reduced graphene oxide (RGO) by employing sodium borohydride. For this, 10 mL of aqueous suspension of GO solution (1 mg mL^{-1}) has been prepared. To this, 100 mg of sodium borohydride has been added and the resultant solution got subjected to stirring for 3 hours at 65 °C. The change in color of the solution has been observed from brown to black which indicated the reduction of GO to RGO. To obtain the RGO, the resultant solution got cooled down to room temperature and centrifuged at 1200 rpm using Milli-Q water.

6.2.3 Preparation of WO_3-RGO Nanocomposite

The preparation of WO_3-RGO nanocomposite has been accomplished using in-situ hydrothermal process. First we prepared a graphene oxide (GO) solution in 20 mL Milli-Q water followed with half an hour ultrasonication. To this solution, we added 0.1M of $NaWO_4.2H_2O$ and 0.225 gm of NaCl and stirred firmly for an hour to get the well dispersed solution. For acidification, HCl solution has been added such that the pH of the resultant solution reached to 2 values. Later, for the hydrothermal treatment, the solution has been placed in an autoclave and kept at temperature of 180 °C for 24 hours. After this, the resultant as prepared WO_3-RGO nanocomposite sample got collected through the multiple washing with Milli-Q water and ethanol followed by drying at 70 °C.

6.2.4 Functionalization and Fabrication of the WO_3-RGO Nanocomposite Based Immunoelectrode

The as-prepared WO_3-RGO nanocomposite is functionalized with APTES for providing active amino groups (─NH_2) that can covalently bind to the antibodies. For the functionalization process, we added 100 mg of WO_3-RGO nanocomposite sample to the 30 mL of isopropanol followed with ultra-sonication resulting in a suspended solution. To this, we added 200 μL of 3-aminopropyl tri-ethoxy saline (APTES) dropwise and kept for stirring for 45 hours at room temperature (27˚C). With the completion of stirring, the unbounded APTES molecules got removed by filtering the suspension followed with thoroughly washing with Milli-Q water. Thus, we successfully obtained APTES functionalized WO_3-RGO nanocomposite sample. After this, we obtained thin films of APTES functionalized WO_3-RGO nanocomposite onto the pre-hydrolyzed ITO electrode at optimized potential 45 V for 90 seconds using electrophoretic deposition (EPD) technique.

To fabricate the immunoelectrode, cTnI antibodies are covalently attached to the APTES/WO_3-RGO nanocomposite/ITO electrode using EDC-NHS chemistry. For this, we prepared a fresh anti-cTnI solution (50 μg mL^{-1}) in a PBS solution. Before immobilization, the carboxyl groups occurring in antibodies are stimulated using EDC-NHS technique. The EDC and NHS works as the coupling agent and activator respectively. The prepared mixture solution (30 mL) got uniformly applied to APTES-modified electrode through drop casting. The resultant antibody immobilized APTES/WO_3-RGO nanocomposite/ITO electrode existed in a humid chamber for 6 hours followed with the treatment with PBS solution. Lastly, we used EA solution (0.1 mg mL^{-1}) onto the anti-cTnI/APTES/WO_3-RGO nanocomposite/ITO electrode to obstruct non-specific active sites on the electrode. The as prepared immuno-electrodes got treated with Phosphate buffer saline solution and stored at 5˚C.

6.2.5 Electrochemical Measurement Procedures

All electrochemical measurements including electrochemical impedance spectroscopy (EIS) and differential pulse voltammetry (DPV) have been carried out using an electrochemical Autolab Potentiostat consisting of a three-electrode system. The PBS (50 mM, pH 7.4) solution consisting of 5mM $[Fe(CN)_6]^{3-/4-}$ as redox couple is used for all the electrochemical measurements. For EIS measurements, we studied the impedance spectrum obtained between frequencies 10^5 to 10^{-1} Hz for an input potential of 10 mV. While for the DPV measurements, we studied the response of the fabricated immunoelectrode in the potential range of - 0.8 to + 0.8 V at a scan rate of 50 mV s^{-1}. A step-by-step fabrication procedure of EA/anti-cTnI/APTES/WO_3-RGO nanocomposite/ITO immunoelectrode is shown in **Figure 6.1.**

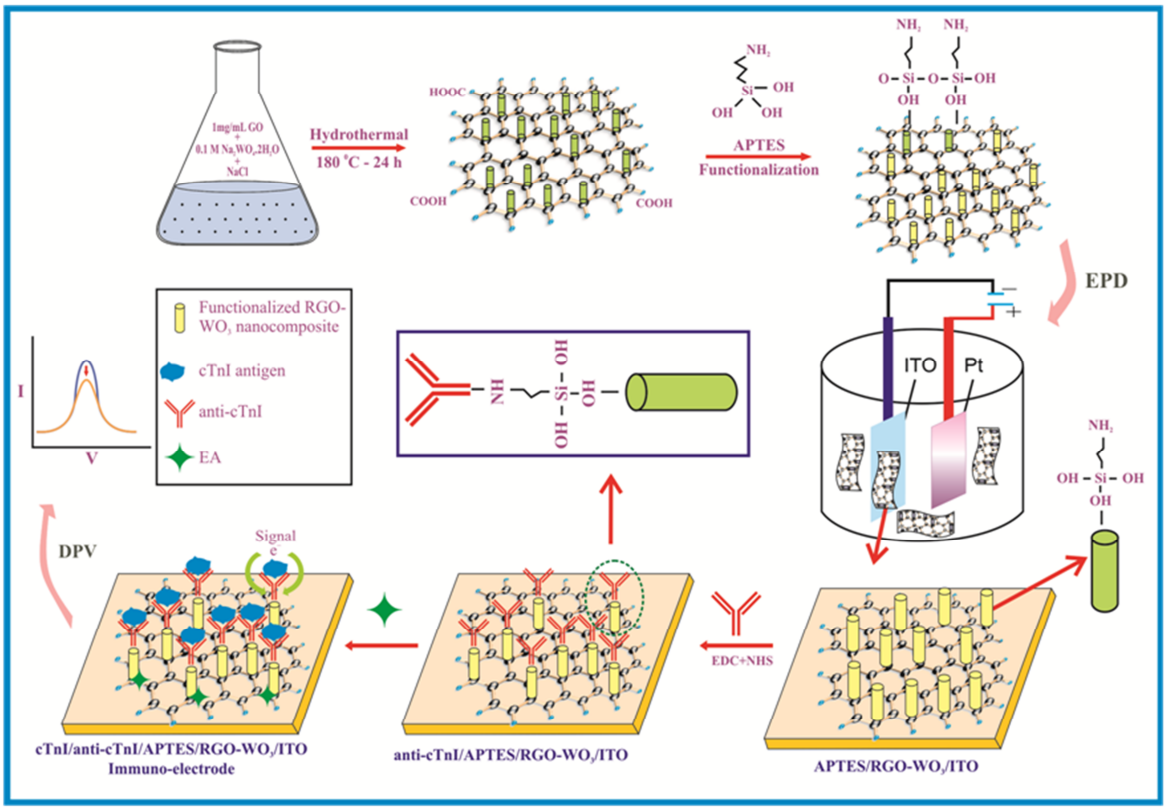

Figure 6.1: Schematic of fabrication of EA/anti-cTnI/APTES/WO_3-RGO nanocomposite/ITO based immunoelectrode for cTnI detection

6.3 Results and Discussions

6.3.1 Crystallographic and Morphological Studies

The investigation of the crystallinity and the integrity of the phase purity of the as prepared GO, RGO and RGO-WO_3 nanocomposite have been analyzed using powder XRD in the range of 5° - 80°. **Figure 6.2 (a)** exhibits an intense peak at 11.7° which corresponded to the (002) plane ($\mathbf{d_{002}}$**= 7.5 Å**) of GO which shifted to 23.4° on reduction of GO to RGO ($\mathbf{d_{002}}$ **= 3.79 Å**) **[Figure 6.2 (b)]**. The decline in the interplanar spacing of RGO as opposed to GO has been observed due to the removal of oxide clusters which has allowed graphene sheets to packed more tightly. The XRD pattern of as- prepared RGO-WO_3 nanocomposite **[Figure 6.2(c)]** showed strong diffraction peaks at 2θ =14.3° and 28.1° corresponding to (100) and (200) planes respectively. The other peaks seen at 34.2°, 37°, 44.8°, 49.6°,52.2° and 59.01° indexed to (111), (210), (002), (220), (310) and (400) crystal lattice planes, respectively. All these planes have been well matched with a hexagonal WO_3 crystal structure **(JCPDF 75-2187)** without the presence of any undesired phases.

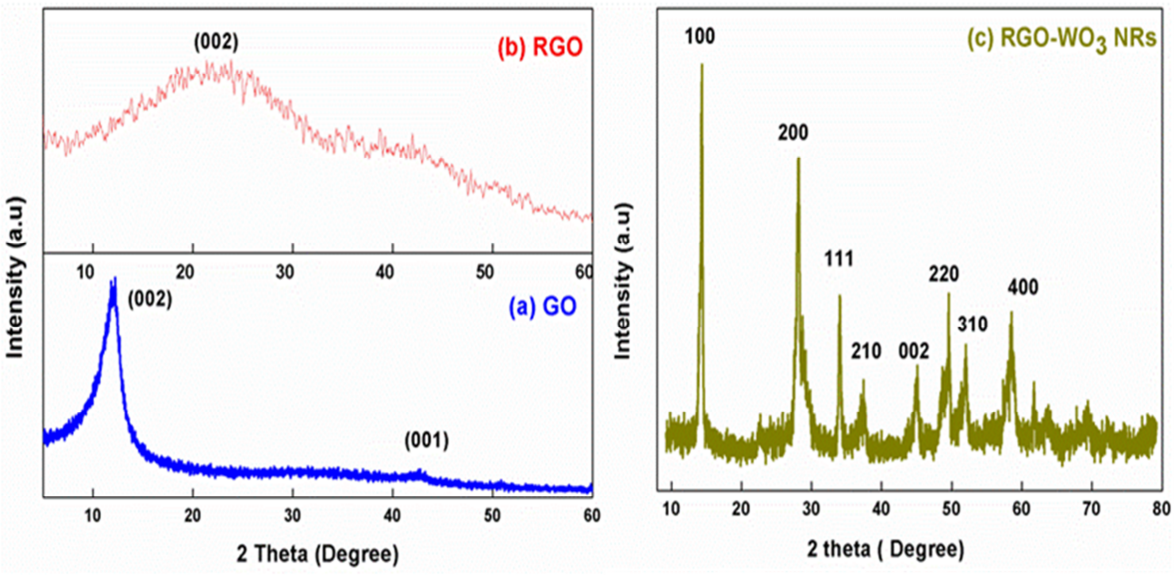

Figure 6.2: XRD pattern of GO, RGO, and WO_3-RGO nanocomposite

These high intense peaks of the nanocomposite indicated the good crystallinity of the synthesized structure. Also, no additional peak is emerged at $2\theta = 23.4°$ in the XRD spectrum of the nanocomposite which suggested that all RGO sheets have been homogeneously dispersed in the nanocomposite.

The morphological and structural analyses of WO_3 and WO_3-RGO nanocomposite have been studied using FE-SEM and TEM. **Figure 6.3 (i)** indicates that the proposed hydrothermal synthesis route resulted in the formation of the uniform 1-D nanostructure of WO_3 NRs with a smooth surface and existed in the form of bundles with an average diameter as 54 nm. The average size of the nanorods as estimated by FESEM is in close agreement with the TEM image of the WO_3 NRs **[Inset, Figure 6.3 (i)]**.

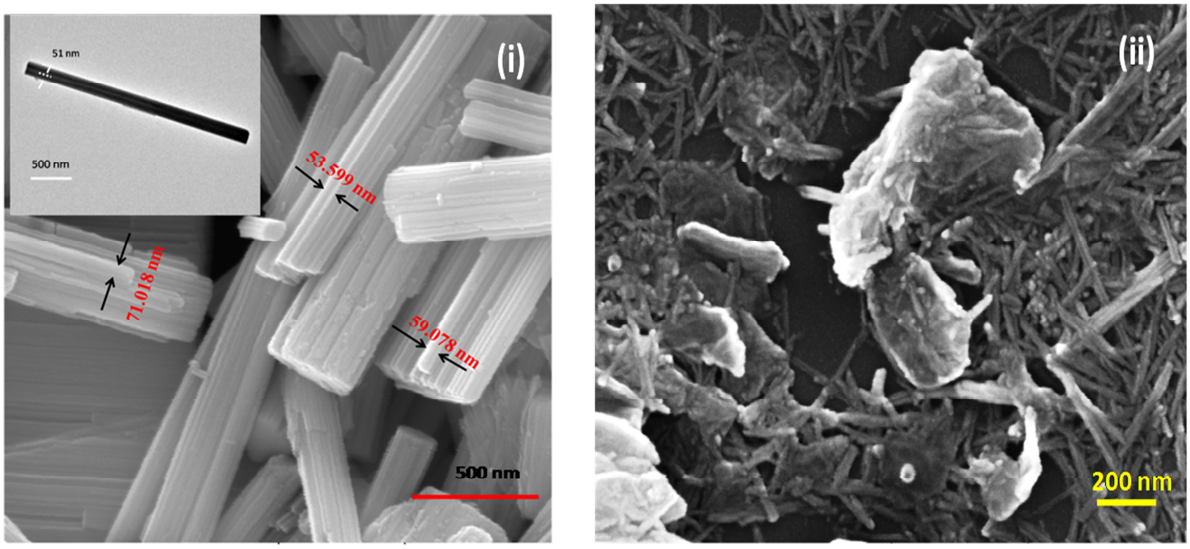

Figure 6.3: (i) FESEM image of WO_3 NRs, inset TEM image of WO_3 NRs; (ii) FESEM image of WO_3-RGO nanocomposite

However, for the in-situ grown WO_3-RGO nanocomposite, the RGO affected the width and uniformity of the 1-D structure of WO_3 **[Comparing Figure 6.3 (i) and (ii)]**. The FE-SEM image depicted the existence of mono-dispersed WO_3 NRs instead of bundles of rods. Further, we observed few of the WO_3 NRs surfaced at the RGO sheets while some of the NRs got trapped between RGO sheets**.**

6.3.2 Spectroscopic Studies

The grafting of the WO_3-RGO nanocomposite surface through the APTES and antibody immobilization have been investigated by studying FTIR spectrum of the WO_3-RGO nanocomposite, APTES/WO_3-RGO nanocomposite, and anti-cTnI/APTES/WO_3-RGO nanocomposite **[Figure 6.4 (A)]**. The FTIR spectrum of WO_3-RGO nanocomposite **[curve (i)]** exhibited two distinct peaks observed at 1205 cm^{-1} and 1724 cm^{-1} attributed to C─OH vibrations of a hydroxyl group and C═ O vibration of the carboxylic/carbonyl group respectively, exhibited by RGO. Peaks observed at 962 cm^{-1} and 1610 cm^{-1} represented the C─H stretching vibrations and aromatic C═C stretching vibrations, whereas the characteristic peaks of WO_3 seen at 1410 cm^{-1} and 766 cm^{-1}correspond to W─O and W─O─W stretching vibration of the bridging O_2 respectively [20]. The peaks seen at 3440 cm^{-1} and 1623 cm^{-1} in **curve (ii)** have been attributed to the asymmetric stretching and bending of NH_2 present in the APTES. Further, peak observed at 1408 cm^{-1} attributed to the bending vibrations (Si─CH_2) present in APTES. All these peaks revealed that APTES has been successfully grafted onto WO_3-RGO nanocomposite surface [21]. The intensities of Infrared (IR) peaks got suppressed after the immobilization of cTnI antibodies onto the APTES/WO_3-RGO nanocomposite/ITO **[curve (iii)]**. The appearance of the additional band at 3462 cm^{-1}, 1636 cm^{-1} and 705 cm^{-1} indicated the presence of N─H stretching of the amide A, amide I and amide IV, respectively which confirmed the successful binding of antibody onto APTES/WO_3-RGO nanocomposite/ITO electrode [22].

Raman spectroscopy is also studied to investigate the interaction betweenWO_3 NRs and RGO sheets. **Figure 6.4 (B)** represents the Raman spectra of RGO, WO_3 NRs andWO_3-RGO nanocomposite obtained in the range of 200 cm^{-1} to 3000 cm^{-1}. C**urve (i)** depicts **t**he Raman spectra of RGO which exhibited well-defined peaks at 1349 cm^{-1} and at 1598 cm^{-1} respectively and are attributable to the presence of characteristic D-band and G-band in RGO

[23]. C**urve (ii)** depicts the Raman spectra of WO_3 NRs which exhibited peaks at 813 cm^{-1}, 760 cm^{-1} and 933 cm^{-1} corresponded to the stretching vibrations of W─O; W─O─W and W═O, respectively. Also, the peaks observed at 242 cm^{-1} and 329 cm^{-1}indicated the presence of bending vibration of O─W─O [24]. It is noteworthy that the peaks observed in WO_3 NRs have been shifted and broaden in case of WO_3-RGO nanocomposite **[curve (iii)]** along with the presence of D and G band. The observed peaks have been attributed towards the formation of C─O─W bonds during hydrothermal treatment which further confirmed the decoration of WO_3 NRs on the RGO sheets surface.

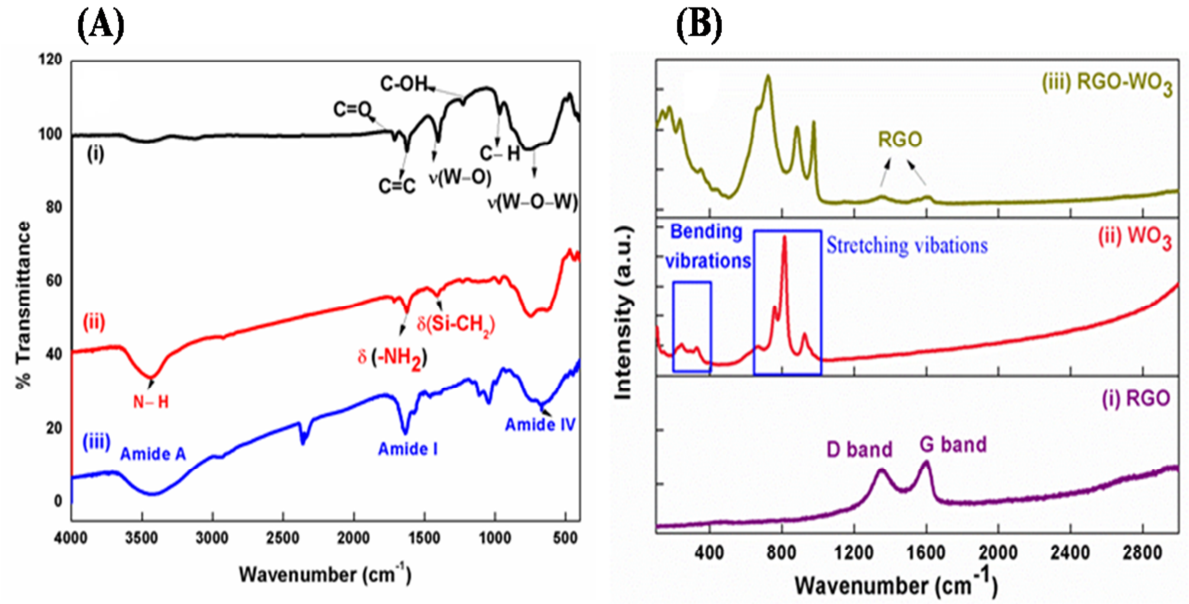

Figure 6.4: (A) FT-IR spectra of (i) RGO-WO_3 NRs, (ii) APTES/RGO-WO_3 NRs and (iii) anti-cTnI/APTES/RGO-WO_3 NRs and (B) Raman spectra of (i) RGO, (ii) WO_3 NRs and (iii) RGO-WO_3 NRs

6.3.3 Contact Angle Measurement Studies

The investigation of the hydrophilic and hydrophobic character of the WO_3-RGO nanocomposite/ITO electrode have been analysed by studying contact angle measurement. The static sessile drop method is employed to determine the contact angle of the electrode at different stages of surface modification. For the study of drop image, image analysis

mechanism is deployed to calculate contact angle (θ) value, by the shape of the drop. The initial contact angle value of the hydrolyzed ITO glass electrode (66.54°) **[Figure 6.5 (i)]** found to declined to 31.50° **[Figure 6.5 (ii)]** after the deposition of WO_3-RGO nanocomposite due to the presence of oxygenated hydrophilic groups like ─OH and ─COOH in the WO_3-RGO nanocomposite matrix.

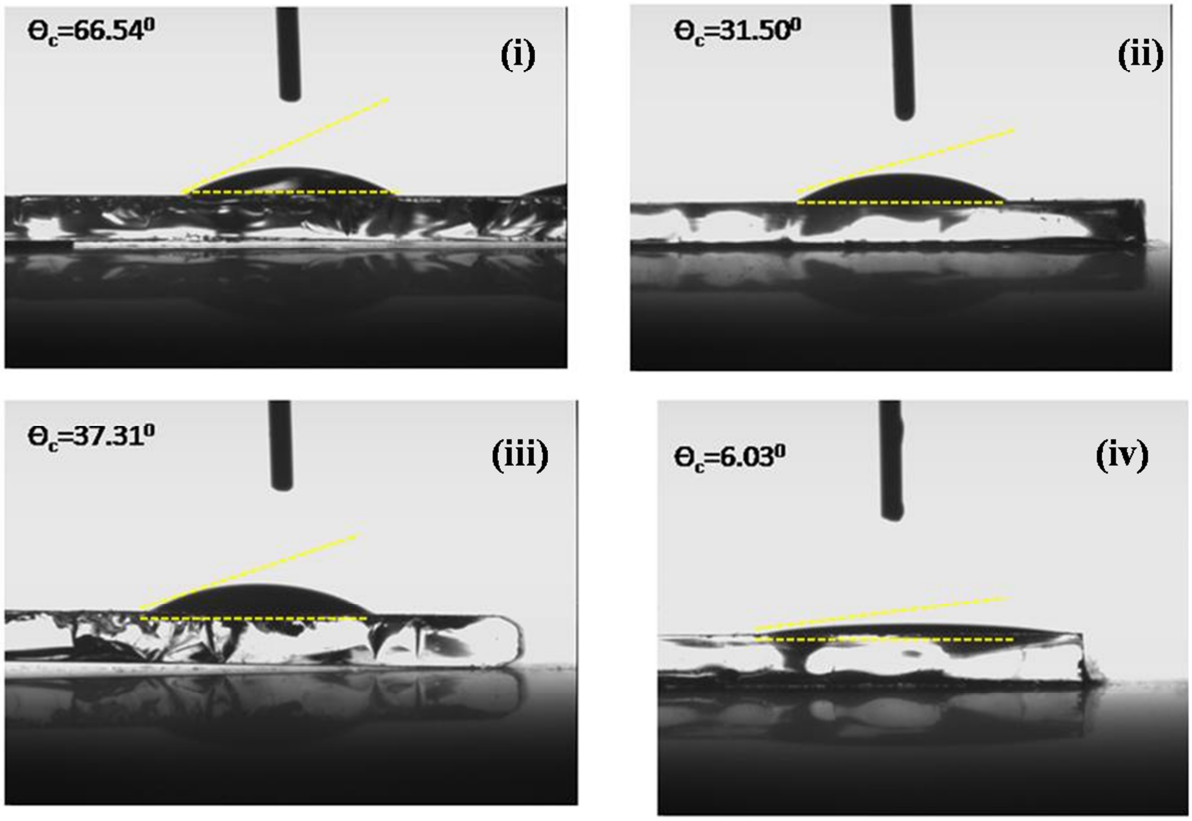

Figure 6.5: Contact angle measurement of (i) hydrolyzed ITO glass, (ii) RGO-WO_3 NRs/ITO, (iii) APTES/RGO-WO_3 NRs/ITO and (iv) anti-cTnI/APTES/RGO-WO_3 NRs/ITO

However, after functionalization with APTES, the contact angle found to increased to ~37° **[Figure 6.5 (iii)]**. This increase of contact angle value indicated the existence of hydrophobic alkyl structures in APTES molecules which imparts a hydrophobic character to the surface of the matrix. Finally, after covalent immobilization of antibody molecules on the functionalized surface, the contact angle value declined to 6.03° **[Figure 6.5 (iv)]** showing

the hydrophilicity nature of the antibody molecules. Thus, all these results indicated the successful immobilization of antibody over the functionalized matrix APTES/WO_3-RGO nanocomposite.

6.3.4 Electrochemical Characterization

The electrochemical properties of WO_3 NRs and in-situ grown WO_3-RGO nanocomposite have been investigated by electrochemical impedance spectroscopy (EIS) studies conducted in frequencies ranging from 10^5 to 10^{-1} Hz at potential measuring 10^{-2} V. The diameter of the semi-circle as shown in the Nyquist plot **[Figure 6.6 (A)]** measures the magnitude of R_{CT} that pertains to the di-electric characteristics at the electrode/electrolyte interface [25]. All these studies have been carried out using Nova (software), provided with the autolab system. The charge transfer resistance value measured for WO_3-RGO nanocomposite (R_{CT} = 887 Ω) is small as compared to that of WO_3 NRs (R_{CT} = 1350 Ω). This decrease in resistance has been attributed to the excellent electrical conductivity of the RGO in the nanocomposite matrix that enhanced the electron transfer kinetics at the electrode and solution interface. Further, we calculated the electron transfer rate constant (K_o) value of the fabricated nanocomposite electrode using **Equation (6.1)**

$$K_O = \frac{RT}{n^2F^2AR_{CT}C} \quad (6.1)$$

The value of K_o for the nanocomposite has been found as 2.54×10^{-4} cm s^{-1} as compared to WO_3 NRs (1.8×10^{-4}cms^{-1}). This showed that WO_3-RGO nanocomposite displayed better charge transfer properties as compared to WO_3 NRs and can give superior analytical performance in electrochemical biosensing device.

The electrochemical impedance spectra (EIS) study for the different modified electrodes has been investigated as shown in **Figure 6.6 (B)**. The WO_3 NRs exhibited

maximum R_{CT} value as 1.35 KΩ. However, the significant reduction in the R_{CT} value is observed for WO_3-RGO nanocomposite (887 Ω). This implied RGO in the nanocomposite array exhibited enhanced electrochemical conductivity. After immobilization of the antibody, the as-functionalized matrix (anti-cTnI/APTES/RGO-WO_3NRs/ITO) exhibited an elevated R_{CT} (905 Ω) as compared to WO_3-RGO nanocomposite due to the insulation offered by the antibody molecules. Lastly, after the attachment of ethanolamine (EA), which covered the bulk of the non-specific active sites, the charge transfer process further blocked, resulting in a higher R_{CT} (1.6 KΩ) of the nanocomposite electrode.

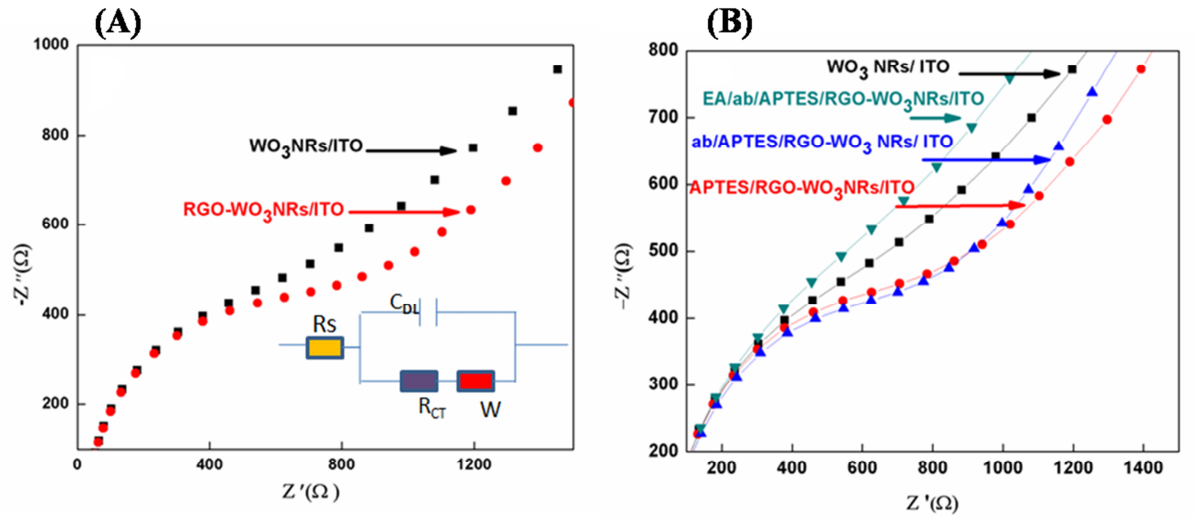

Figure 6.6: Electrochemical impedance spectroscopy (EIS) of (a) WO_3 NRs/ITO and RGO-WO_3 NRs/ITO electrodes (Inset: Randles circuit) and (b) EIS spectra of different modified electrodes in PBS solution (50mM, pH 7.4)containing 5mM $[Fe(CN)_6]^{3-/4-}$

6.3.5 Electrochemical Sensing Studies

The variation in the response current of the as-fabricated electrode has been studied as a function of cTnI (concentration 0.01 to 250 ng mL^{-1}) using DPV technique **[Figure 6.7 (A)]**. All responses have been carried out with PBS (pH 7.4) containing 5mM $[Fe(CN)_6]^{3-/4-}$ as a redox coupling agent. For each measurement, we used 20 mL of antigen into the

electrochemical cell with 10 minutes of incubation. The response graph showed the declined in peak current with the increased in cTnI concentration (0.01- 250 ng mL^{-1}). The decreased in response current remarked the creation of electrically insulating antigen-antibody complexes formed by the specific interaction of cardiac Troponin I antigen and its antibody that might have blocked the electron transfer via $[Fe(CN)_6]^{3-/4-}$ [34]. In **Figure 6.7 (B)**, the plot represents the response peak current against different cTnI concentrations.

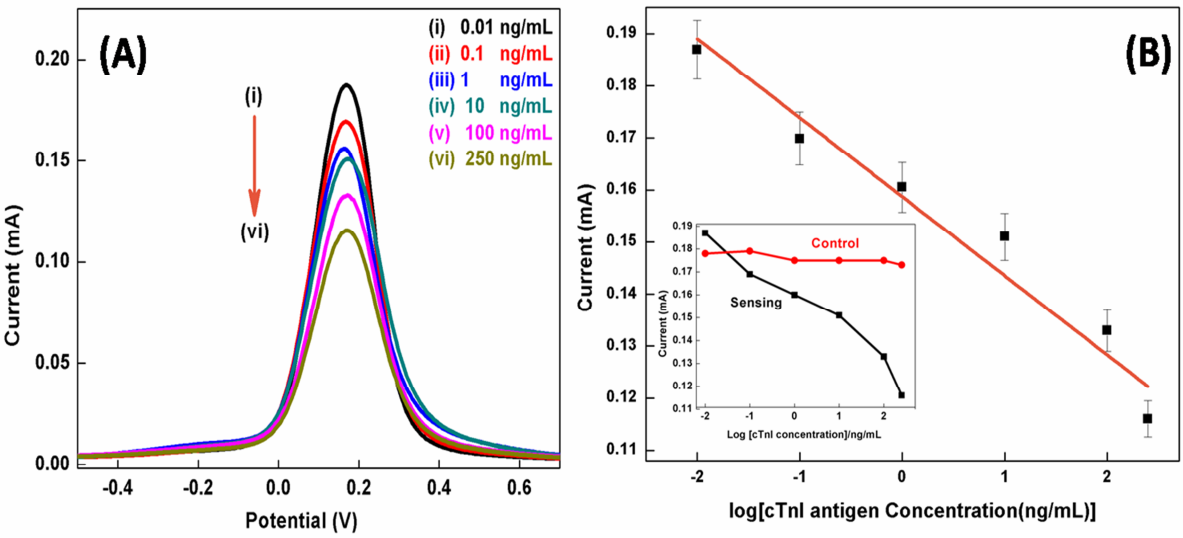

Figure 6.7: (A) DPV responses of the EA/anti-cTnI/APTES/RGO-WO_3 NRs/ITO immunoelectrode obtained as a function of cTnI concentrations (0.01-250 ng mL^{-1}). (B) Calibration plot between the DPV peak current and the logarithm of cTnI concentrations (0.01-250 ng mL^{-1}); (inset : control study)

The DPV peak current (I) exhibited a linear behaviour against logarithmic cTnI concentrations in the linearity range of 0.01-250 ng mL^{-1}, obeying **Equation (2).**

$I = 0.1587\ (mA) - 0.01456\ (mA) \times \log [cTnI\ concentration\ (ng\ mL^{-1})]$ **(6.2)**

The sensitivity of 58.24 mA/cm^2per decade is estimated from the slope of the calibration curve with regression coefficient as 0.989. Further, the immunoelectrode detected the cTnI concentration as small as 0.01 ng mL^{-1}. A control experiment [**Inset, Figure 6.7(B)**] has been

performed in the presence of cTnI concentrations (0.01 - 250 ng mL^{-1}), to check for any non-specific adsorption of the antigen molecule to the electrode surface, in absence of antibodies. However, no remarkable variation observed in the current response revealing that cTnI antigen specifically interacted with the immunoelectrode.

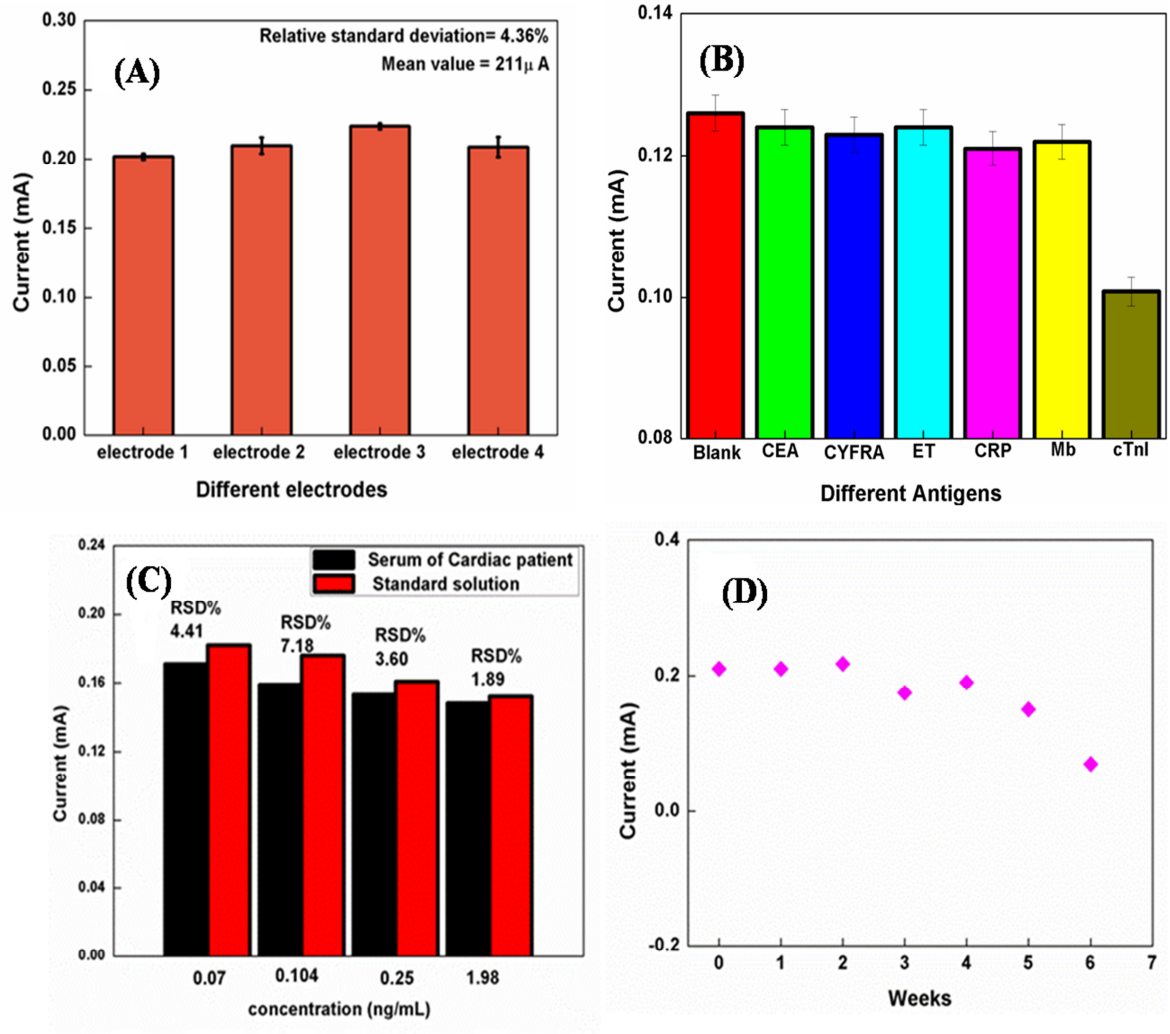

Figure 6.8: (A) Electrochemical current response of different EA/anti-cTnI/APTES/RGO-WO_3 NRs/ITO electrode fabricated under identical conditions with cTnI (0.01 ng mL^{-1}), (B) Electrochemical current response of the immunoelectrode in the presence of different interferents, (C) Real sample analysis study and (D) Shelf life studies of EA/anti-cTnI/APTES/RGO-WO_3 NRs/ITO immunoelectrode.

The reproducibility of the immunoelectrode is examined by measuring DPV current variation in presence of cTnI (0.01 ng mL^{-1}) on four independently fabricated

immunoelectrode prepared under identical conditions [**Figure 6.8 (A)**]. The relative standard deviation (RSD) has been calculated to evaluate the reproducibility of the electrodes. It is found that the immunoelectrode showed good reproducibility for four different electrodes with low value of RSD% of 4.36% with an average current of 200 mA. The low value of RSD% obtained for each electrode comes within the acceptable error range under the tested conditions, suggesting a good reproducibility.

For a clinical purpose, a sensor must exhibits high specificity for the target biomolecule compared to other interfering protein biomarkers present in the blood serum. Hence, the specificity of the fabricated immunoelectrode is evaluated using different interferents such as Carcinoembryonic antigen (CEA), Cytokeratin-19 antigen (CYFRA), Endotheline one protein (ET), C-reactive protein (CRP) and Myoglobin (Mb) as shown in **Figure 6.8 (B)**. The magnitude of DPV current response for the EA/anti-cTnI/APTES/WO_3-RGO nanocomposite/ITO immunoelectrode [**shown as blank in Figure 6.8 (B)]** observed as 0.209 mA. After that, the response of the immunoelectrode evaluated in the presence of interferents mentioned, each with concentration 50 ng mL^{-1} and 10 min incubation. Although we observed some signal variation but no prominent alteration in the current response in the presence of each interferent as compared to the blank electrode is observed. However on the addition of cTnI protein, a remarkable reduction of current is observed. This specificity of the immunoelectrode has been attributed to the fact that all other protein biomarkers to bind with anti-cTnI antibody functionalized on the APTES/RGO-WO_3 nanocomposite surface.

Further for clinical application, we investigated the developed immunosensor for cTnI detection using human serum samples obtained from the pathology laboratory (Dr. Lal path lab, Rohini, Delhi). The DPV current response has been studied for four different real samples and those for standard samples of the same concentrations. The results as shown in **Figure 6.8 (C)** revealed low RSD% value for the current response obtained for real and

standard samples. Hence, all these results indicate that the developed detection strategy can be preliminarily applicable for the determination of cTnI in human serum for routine clinical diagnosis.

Further, we also monitored the shelf life of the fabricated immunosensor by noting DPV current response in presence of 0.01 ng mL^{-1} cTnI at a regular intermission of 1 week **[Figure 6.8 (D)]**. The immunoelectrode retained its activity up to four weeks with the decrease in current as 8% when stored in refrigerated conditions at 4 °C, implying that cTnI antibody has been immobilized on APTES/WO_3-RGO nanocomposite/ITO matrix with its bioactivity well preserved. A comparative analysis of presently fabricated immunoelectrode with previously reported electrode materials is shown in **Table 6.1**.

Sensing platform	**Detection technique**	**Detection range**	**Sensitivity (S)**	**Detection limit**	**Reference**
Conducting paper	CV	1-100 ng mL^{-1}	5.5 μA mL ng^{-1} cm^{-2}	-	[26]
Porous GO/GCE	EIS	0.1-10 ng mL^{-1}	-	0.07 ng mL^{-1}	[27]
Pt/Graphene sheet/GCE	EIS	0.01-10 ng mL^{-1}	80 Ω / cm^2 per decade	4.2 pg mL^{-1}	[28]
Au/GO/GCE	Ampero-metric	0.05-3.0 ng mL^{-1}	-	0.05 ng mL^{-1}	[29]
APTES/WO_3-RGO nanocomposite	**DPV**	**0.01-250 ng mL^{-1}**	**58.24 μA/cm^2 per decade**	**0.01 ng mL^{-1}**	**Present work**

Table 6.1: Comparative analysis of WO_3-RGO nanocomposite based immunosensor with previously reported electrode materials

6.4 Conclusions

In summary, a hydrothermally synthesized tungsten trioxide and reduced graphene oxide (WO_3-RGO) nanocomposite-based electrochemical immunosensor is successfully fabricated and presented for the detection of a cardiac biomarker. A thin film of APTES/WO_3-RGO nanocomposite/ITO has been obtained using electrophoretic deposition, succeeded by covalent immobilization of cTnI antibody for the label-free electrochemical detection (of cTnI) through DPV technique. The heterogeneous electron transfer kinetics of WO_3-RGO nanocomposite found to be superior as opposed to bare WO_3 resulting in enhanced performance of the immunosensor. The electrochemical measurements showed that the planned immunosensor exhibited heightened sensitivity of 58.24 mA/cm^2 per decade in a detection range of 0.01- 250 ng mL^{-1}. The superior performance has been attributed to: (i) strong covalent coupling of antibody molecules to WO_3-RGO nanocomposite matrix through APTES which leads to the high stability of the device, (ii) large oxygen moieties present in WO_3 leading to increased antibody loading capacity resulting in wider detection range and lastly, (iii) strong synergistic effect between WO_3-RGO nanocomposite that has enhanced the electron transfer kinetics. The study of real sample analysis has also revealed an excellent correlation between the current response of standard and real samples of cardiac Troponin I (cTnI). Thus all these features result in high sensing performance of the proposed electrochemical immunosensor**.**

6.5 References:

1. Anithaa, A. C., N. Lavanya, K. Asokan, and C. Sekar. "WO_3 nanoparticles based direct electrochemical dopamine sensor in the presence of ascorbic acid." *Electrochimica Acta* 167 (2015): 294-302.

2. Santos, Lídia, Célia M. Silveira, Elamurugu Elangovan, Joana P. Neto, Daniela Nunes, Luís Pereira, Rodrigo Martins et al. "Synthesis of WO_3 nanoparticles for biosensing applications." *Sensors and Actuators B: Chemical* 223 (2016): 186-194.
3. Pandey, Prem C., Arvind Prakash, and Ashish Kumar Pandey. "Studies on electrochemical and peroxidase mimetic behavior of Prussian blue nanoparticles in presence of Pd-WO_3-SiO_2 Nanocomposite; bioelectro-catalytic sensing of H_2O_2." *Electrochimica Acta* 127 (2014): 132-138.
4. Chua, Chun Kiang, and Martin Pumera. "Chemical reduction of graphene oxide: a synthetic chemistry viewpoint." *Chemical Society Reviews* 43, no. 1 (2014): 291-312.
5. Kim, Keun Soo, Yue Zhao, Houk Jang, Sang Yoon Lee, Jong Min Kim, Kwang S. Kim, Jong-Hyun Ahn, Philip Kim, Jae-Young Choi, and Byung Hee Hong. "Large-scale pattern growth of graphene films for stretchable transparent electrodes." *nature* 457, no. 7230 (2009): 706.
6. Geng, Jianxin, Byung-Seon Kong, Seung Bo Yang, and Hee-Tae Jung. "Preparation of graphene relying on porphyrin exfoliation of graphite." *Chemical Communications* 46, no. 28 (2010): 5091-5093.
7. Bagri, Akbar, Cecilia Mattevi, Muge Acik, Yves J. Chabal, Manish Chhowalla, and Vivek B. Shenoy. "Structural evolution during the reduction of chemically derived graphene oxide." *Nature chemistry* 2, no. 7 (2010): 581.
8. Li, Fen, Xue Jiang, Jijun Zhao, and Shengbai Zhang. "Graphene oxide: A promising nanomaterial for energy and environmental applications." *Nano energy* 16 (2015): 488-515.
9. Choi, Hyun-Jung, Sun-Min Jung, Jeong-Min Seo, Dong Wook Chang, Liming Dai, and Jong-Beom Baek. "Graphene for energy conversion and storage in fuel cells and supercapacitors." *Nano Energy* 1, no. 4 (2012): 534-551.

10. Zhu, Yanwu, Shanthi Murali, Weiwei Cai, Xuesong Li, Ji Won Suk, Jeffrey R. Potts, and Rodney S. Ruoff. "Graphene and graphene oxide: synthesis, properties, and applications." *Advanced materials* 22, no. 35 (2010): 3906-3924.
11. Hu, Changyuan, Tiewen Lu, Fei Chen, and Rongbin Zhang. "A brief review of graphene–metal oxide composites synthesis and applications in photocatalysis." *Journal of the Chinese Advanced Materials Society* 1, no. 1 (2013): 21-39.
12. Nia, Pooria Moozarm, Woi Pei Meng, Farnaz Lorestani, M. R. Mahmoudian, and Y. Alias. "Electrodeposition of copper oxide/polypyrrole/reduced graphene oxide as a nonenzymatic glucose biosensor." *Sensors and Actuators B: Chemical* 209 (2015): 100-108.
13. Vashist, Sandeep Kumar, and John HT Luong. "Recent advances in electrochemical biosensing schemes using graphene and graphene-based nanocomposites." *Carbon* 84 (2015): 519-550.
14. Halder, Arnab, Minwei Zhang, and Qijin Chi. "Electroactive and biocompatible functionalization of graphene for the development of biosensing platforms." *Biosensors and Bioelectronics* 87 (2017): 764-771.
15. Sun, Bing, Kun Zhang, Lijian Chen, Lintong Guo, and Shiyun Ai. "A novel photoelectrochemical sensor based on PPIX-functionalized WO_3–rGO nanohybrid-decorated ITO electrode for detecting cysteine." *Biosensors and Bioelectronics* 44 (2013): 48-51.
16. Zhu, Wenyu, Faqian Sun, Ronn Goei, and Yan Zhou. "Facile fabrication of RGO-WO_3 composites for effective visible light photocatalytic degradation of sulfamethoxazole." *Applied Catalysis B: Environmental* 207 (2017): 93-102.
17. Su, Pi-Guey, and Shih-Liang Peng. "Fabrication and NO_2 gas-sensing properties of reduced graphene oxide/WO_3 nanocomposite films." *Talanta* 132 (2015): 398-405.

18. Shi, Jinjin, Zhixuan Cheng, Liping Gao, Yuan Zhang, Jiaqiang Xu, and Hongbin Zhao. "Facile synthesis of reduced graphene oxide/hexagonal WO_3 nanosheets composites with enhanced H2S sensing properties." *Sensors and Actuators B: Chemical*230 (2016): 736-745.
19. Srivastava, Saurabh, Shiju Abraham, Chandan Singh, Md Azahar Ali, Anchal Srivastava, Gajjala Sumana, and Bansi D. Malhotra. "Protein conjugated carboxylated gold@ reduced graphene oxide for aflatoxin B 1 detection." *Rsc Advances* 5, no. 7 (2015): 5406-5414.
20. An, Xiaoqiang, C. Yu Jimmy, Yu Wang, Yongming Hu, Xuelian Yu, and Guangjin Zhang. "WO_3 nanorods/graphene nanocomposites for high-efficiency visible-light-driven photocatalysis and NO_2 gas sensing." *Journal of Materials Chemistry* 22, no. 17 (2012): 8525-8531.
21. Radu, Gabriel-Lucian, Georgiana-Ileana Truica, Ramona Penu, Veronica Moroeanu, and Simona Carmen Litescu. "Use of the Fourier transform infrared spectroscopy in characterization of specific samples." *UPB Scientific Bulletin B: Chemical and Materials Science* 74, no. 4 (2012): 137-148.
22. Ali, Md Azahar, Chandan Singh, Kunal Mondal, Saurabh Srivastava, Ashutosh Sharma, and Bansi D. Malhotra. "Mesoporous few-layer graphene platform for affinity biosensing application." *ACS applied materials & interfaces* 8, no. 12 (2016): 7646-7656.
23. Krishnamoorthy, Karthikeyan, Murugan Veerapandian, Rajneesh Mohan, and Sang-Jae Kim. "Investigation of Raman and photoluminescence studies of reduced graphene oxide sheets." *Applied Physics A* 106, no. 3 (2012): 501-506.
24. Vargas-Consuelos, C. Ingram, Kyungah Seo, Marco Camacho-López, and Olivia A. Graeve. "Correlation between particle size and Raman vibrations in WO_3 powders." *The Journal of Physical Chemistry C* 118, no. 18 (2014): 9531-9537.

25. Cell, Main. "Electrochemical Impedance Spectroscopy (EIS): A Powerful and Cost-Effective Tool for Fuel Cell Diagnostics."
26. Jagadeesan, Kishore Kumar, Saurabh Kumar, and Gajjala Sumana. "Application of conducting paper for selective detection of troponin." *Electrochemistry Communications* 20 (2012): 71-74.
27. Kazemi, Sayed Habib, Elham Ghodsi, Siamak Abdollahi, and Samad Nadri. "Porous graphene oxide nanostructure as an excellent scaffold for label-free electrochemical biosensor: Detection of cardiac troponin I." *Materials Science and Engineering: C* 69 (2016): 447-452.
28. Singal, Shobhita, Avanish K. Srivastava, Ashok M. Biradar, and Ashok Mulchandani. "Pt nanoparticles-chemical vapor deposited graphene composite based immunosensor for the detection of human cardiac troponin I." *Sensors and Actuators B: Chemical* 205 (2014): 363-370.
29. Liu, Guozhen, Meng Qi, Yin Zhang, Chaomin Cao, and Ewa M. Goldys. "Nanocomposites of gold nanoparticles and graphene oxide towards an stable label-free electrochemical immunosensor for detection of cardiac marker troponin-I." *Analytica chimica acta* 909 (2016): 1-8.

CHAPTER 7

Conclusion and Scope of Future Work

The work presented in this thesis deals with the synthesis, characterization and application of the tungsten trioxide (WO_3) nanostructures and it's composite for the cardiac detection. The versatile features owe by the WO_3 nanostructures such as variety of polymorphic transformation, good electron transport kinetics, chemical stability, high catalytic activity, ease of functionalization and strong adsorption capability opens its application path toward the electrochemical sensing mechanism. Thin films of different WO_3 nanostructures were fabricated onto the ITO electrode using electrophoretic deposition technique (EPD). Employing EPD for the thin film deposition offers advantages in terms of uniformity, simple processing, low cost, controlled thickness, and homogeneity. Prior EPD, WO_3 nanostructures were functionalized using 3-aminopropyl tri-ethoxy saline (APTES) for the covalent immobilization of cardiac Troponin I antibody (anti-cTnI). The fabricated APTES functionalized WO_3 based ITO electrode presents a potential platform to the immobilization of anti-cTnI biomolecules for the detection of cardiac biomarker Troponin I.

7.1 Summary

Chapter 1 introduces the characteristic features of WO_3 nanostructures, its synthesis and applications of WO_3 nanostructures with special emphasis on its potential and utility in the development of biosensors. Besides this, efforts have been made to give detailed literature of the WO_3 in biosensing and also the salient features of antibodies employed for the fabrication of immunosensor platform.

Chapter 2 briefs the details of the various experimental techniques such as SEM, FESEM, X-Ray Diffractometer, FT-IR spectroscopy, AFM, and Raman spectroscopy that have been employed to characterize functionalized and un-functionalized WO_3 nanostructures based electrodes. Further, the electrochemical techniques such as CV, EIS, and DPV were employed to study electrochemical behaviour of the WO_3 based electrodes and immunoelectrodes. The EIS technique was used to study the electrochemical response of the fabricated immunoelectrode as a function of cTnI concentration. Also efforts have also been made to explain the procedures and protocols employed to immobilize antibody biomolecules of cTnI.

Chapter 3 discusses the fabrication of APTES conjugated Tungsten trioxide nanoparticles (APTES/n-WO_3) based platform for cTnI detection. The electrochemical response studies of the fabricated immunoelectrode show sensitivity as 26.56 Ω $ng^{-1}mL$ cm^{-2} in a wide linear detection range 1- 250 ng mL^{-1}. Also, the proposed platform shows the stability of 30 days.

Chapter 4 reports the development of a 2-D WO_3 based matrix for the detection of cTnI biomarker. The performance of the fabricated immunosensor (anti-cTnI/APTES/WO_3 NS/ITO) has been investigated with the measurement of charge transfer resistance (R_{CT}) with

respect to concentrations of cTnI antigen. The immunoelectrode exhibits good sensitivity as 30.8 Ω mL $ng^{-1}cm^{-2}$ along with good stability up to 6 weeks. The enhanced characteristics of the fabricated immunoelectrode can be attributed to the high loading of cTnI antibodies on WO_3 NS matrix due to the enhanced active surface area provided by WO_3 NS.

Chapter 5 deals with the development of an efficient electrochemical sensing platform for cTnI detection using WO_3 nanorods as an immobilized matrix. As dimensionality plays an important role in tailoring properties of nanostructures and hence its applications, therefore in this chapter we exploit 1-D WO_3 NRs based platform towards the development of cardiac biosensors. The 1-D WO_3 nanostructures provide an efficient direct electrical conduction path between the electrodes and the immobilized biomolecules resulting in the enhanced sensitivity of the biosensing platform. The electrochemical response study of the proposed platform (anti-cTnI/APTES/WO_3 NRs/ITO) demonstrates high sensitivity [6.81 KΩ mL ng^{-1} cm^{-2}] with respect to WO_3 nanosheets and nanoparticles as morphology.

Chapter 6 illustrates the advantages of the integration of nanostructured WO_3 onto the electro-active material RGO for the enhancement in biosensor's characteristics. The high active surface area of RGO might perhaps provide more electro-active sites and thus enhanced electron transfer kinetics suitable for the enhancement in the characteristics of the electrochemical biosensor. The WO_3-RGO nanocomposite based immunosensor shows the remarkable sensitivity (58.24 mA cm^{-2} per decade) in a broad linear detection range of 0.01-250 ng mL^{-1}.

Chapter 7 represents the summary of the complete research work performed throughout the thesis tenure, and also the major outcomes. Besides this, it also briefs the future scope of the present research work.

The sensing characteristics of all the fabricated nanostructured WO_3 based electrodes used in the present thesis work has been summarized in **Table 7.1**

Fabricated Electrode	Sensitivity	Detection Limit (ng mL^{-1})	Detection Range (ng mL^{-1})	Stability
WO_3 NPs	26.56 Ω mL ng^{-1} cm^{-2}	16	1-250	4 weeks
WO_3 NS	30.8 Ω mL ng^{-1} cm^{-2}	0.1	0.1-100	5 weeks
WO_3 NRs	6.81 KΩ mL ng^{-1} cm^{-2}	0.01	0.01-10	5 weeks
WO_3-RGO nanocomposite	58.24 μA cm^{-2} per decade	0.01	0.01-250	4 weeks

Table 7.1: Sensing characteristics of fabricated different nanostructured WO_3 based immunoelectrode for cTnI detection.

7.2 Major Outcomes

- A facile and a cost-effective hydrothermal synthesis process used for the different WO_3 nanostructures (nanoparticles, nanosheet, nanorods) and its composite (WO_3-RGO).
- Upto the best of my knowledge, this is the first extensive research work reporting WO_3 based biosensor for the detection of cardiac biomarker (cTnI) due to its enhanced electrochemical activity.
- Electrophoretic deposition technique has been employed for the deposition of thin film of APTES modified WO_3 nanostructures. Further, covalent immobilization of cardiac troponin I antibodies (anti-cTnI) on APTES functionalized WO_3 matrix has been achieved using EDC –NHS chemistry.
- The analysis of the electrochemical characteristics of the fabricated sensing platforms has been investigated using cyclic voltammetry (CV) and electrochemical impedance

spectroscopic (EIS) techniques. The electrochemical impedance spectroscopic (EIS) study carried out to study the interfacial properties between the fabricated electrode surface and the electrolyte in the frequency range of 0.01 Hz to 10^5 Hz.

- The transportation of electrochemically produced charge at the interface of electrode and electrolyte has been modeled by measuring the change in resistance. The charge transfer resistance (R_{CT}) which corresponds to the diameter of the semicircle of the Nyquist plot has been measured using NOVA software.
- The R_{CT} value of the immunosensor increased with the increase in cTnI concentration. This increase in impedance revealed the formation of insulating antigen-antibody complex produced due to the specific key-lock interaction of the anti-cTnI and cTnI that might have hindered the electron motion.
- The performance of the fabricated immunosensor was studied by investigating sensitivity, selectivity, reproducibility, and stability studies.
- Among different morphologies, WO_3 NRs based platform has shown outstanding sensitivity and detection limit.
- Compared with reported work, electrochemical measurements are much facile and simpler and easier to miniaturize which makes them more suitable for POC (point of care) detection.

7.3 Future Prospects

The present studies reveal that tungsten trioxide (WO_3) based nanostructures can efficiently be utilized for the development of high performance electrochemical biosensors with enhanced sensitivity, stability, and selectivity. A lot of scope is still there to design novel composite structures with WO_3 nanomaterial by incorporating nanostructured polymers, carbon based nanomaterials and other oxides. The unique physical and chemical properties owe by these materials can produce synergistic effect on incorporating with WO_3

nanostructures and would eventually presents the new class of nano-based materials with the advancement in applications including biosensors. Briefly, we have planned to accomplish following work in near future:

- First, we have aimed to work on WO_3/CuO nanocomposite which can provide enhanced porous structure. The resultant structure will be investigated for different electrochemical measurements and thereafter can contribute towards the enhancement in performance of the composite structure for the electrochemical detection of biomarkers.
- Further, to enhance the performance of tungsten trioxide based platform towards biosensing, we can employ a conducting polymer poly (3,4-ethylenedioxythiophene) also known as PEDOT to develop a hybrid nanocomposite. The proposed hybrid nanocomposites will combine the advantages of PEDOT, namely the good conductivity and electrical transports kinetics, with the sensitivity and selectivity of metal oxide materials.
- Lastly, it will also be beneficial to explore the application of WO_3 based matrices towards the detection of other biomarkers especially lung cancer. The main challenges in the diagnosis of this disease are its non-specific symptoms such as coughing, and shortness of breath and being silence at early stage. Thus, developing an effective diagnosis platform for the lung cancer biomarkers using WO_3 based matrix would be more economical and cost effective treatment and will definitely improve survival rate.

Deepika Sandil

Assistant Professor
Contact +91-9910918434
Email: vats.deepika@gmail.com

Objective

Pursuing research in Physics, especially in the field of nanoscience and technology to create sustainable and economically viable solutions for enriching human life

Academic Qualifications

- Submitted PhD thesis on the topic entitled **"Synthesis and modification of metal oxide nanostructures for sensing applications"** in Department of Applied Physics from **Delhi Technological University**
- **M.Tech** in Nanoscience with Ist Div from Delhi Technological University (2011-13)
- **M.Sc.** in Physics (Electronics) with Ist Div from Delhi University (2005-07)
- **B.Sc** Physics Hons. with Ist Div from Delhi University (2002-05)

Professional Experience

* **Working as Assistant Professor in Department of Applied Physics at BPIT College, Rohini (IP University) since 2007**

Responsibilities:

- Theory and practical classes for Applied Physics -I and Applied Physics -II of B.Tech first year students
- Senior member of B.Tech coordinator committee responsible for liaison with the university

List of Publications in International Journals

1. **D Sandil,** S Kumar, K Arora, S. Srivastava, B D Malhotra, S C Sharma and N K Puri, Biofunctionalized Nanostructured Tungsten Trioxide Based Sensor for Cardiac Biomarker Detection. ***Materials Letters***, 2017, 186, 202-205. (Impact factor 2.4)

2. K Arora**, D Sandil,** G Sharma, S. Srivastava, N K Puri, Effect of low pressure hydrogen environment on crystallographic properties of PdO nanoparticles, ***International Journal of Hydrogen Energy***, 2016 , Volume 41, 22155-22161

3. "Biofunctionalized tungsten trioxide-reduced graphene oxide nanocomposites for sensitive electrochemical immunosensing of cardiac biomarker" **D Sandil**, S. Srivastava, B. D. Malhotra, S. C. Sharma, N K Puri (2018), **Journal of Alloys and Compounds**, 763, 102-110.

4. "Protein functionalized WO3 nanorods based impedimetric platform for sensitive and label-free detection of a cardiac biomarker" **D Sandil**, S. C. Sharma, N K Puri, **Journal of Materials Research** (2019): 1-10

Workshops/Seminars Attended

1. Two days National Conference on **"Recent advances in Materials and Field Theory"** from 28th -29th December, 2016 at BPIT, Delhi.
2. One week TEQUIP-11 FDP on **"Advances in Microelectronics and plasma diagnostics"** from 29th Aug. to 2nd Sep.,2016 at D.T.U., Delhi.
3. Two days National Seminar on **"Applications of Radioisotope and radiation technology in food, environment, healthcare and industry"** from 8th -9th August, 2016 at Shriram Institute for industrial research, Delhi.
4. One day National Seminar on **"Frontiers in applied science and Technology"** on 22nd March, 2016 at D.T.U.
5. One day National Seminar on **"Recent Advances in Physics (NSRAP-2015)"** on 16th February 2015 at D.T.U., Delhi.
6. **"Bringing the Nanoworld Together"** Seminar at ITT Delhi, from 27th to 28th November 2014

Materials Letters 186 (2017) 202–205

Contents lists available at ScienceDirect

Materials Letters

journal homepage: www.elsevier.com/locate/matlet

Biofunctionalized nanostructured tungsten trioxide based sensor for cardiac biomarker detection

Deepika Sandil[a], Saurabh Kumar[b], Kamal Arora[a], Saurabh Srivastava[a,*], B.D. Malhotra[b,*], S.C. Sharma[a], Nitin K. Puri[a,*]

[a] Advanced Sensor Laboratory, Department of Applied Physics, Delhi Technological University, Delhi 110042, India
[b] Department of Biotechnology, Delhi Technological University, Main Bawana Road, Delhi 110042, India

ARTICLE INFO

Keywords:
Nanostructured tungsten trioxide
Troponin
Immunosensor
Electrophoretic deposition

ABSTRACT

We report results of the studies relating to the technological development of 3-aminopropyl tri-ethoxy saline (APTES) conjugated tungsten trioxide nanoparticles (APTES/n-WO_3) based sensor for cardiac Troponin I (cTnI) detection. The APTES/n-WO_3 nanoparticles were deposited onto indium tin oxide (ITO) coated glass electrode via electrophoretic deposition technique and were subsequently functionalized with troponin antibodies (anti-cTnI). The n-WO_3/ITO and anti-cTnI/APTES/n-WO_3/ITO electrodes were characterized using X-ray diffraction (XRD), UV–vis spectroscopy, Fourier transform infrared (FT-IR) spectroscopy, atomic force microscopy (AFM) and electrochemical impedance spectroscopy (EIS) respectively. This immunosensor exhibited a wider linear detection range (1–250 ng mL^{-1}) with good sensitivity (26.56 Ω $ng^{-1}mL\ cm^{-2}$).

1. Introduction

The fusion of biological molecules and nano-structured metal oxides is known to play an important role towards the development of nano-scale devices in clinical diagnostics and electronic applications [1]. Among the various nanostructured metal oxides, nanostructured tungsten trioxide (n-WO_3) has been found to have interesting physical and chemical properties [2]. n-WO_3 exhibits good electrical conductivity and catalytic behavior, that may perhaps make them suitable for application as “electronic wires” to enhance electron transfer between redox centers in proteins and electrode surfaces [3]. Besides this, the high surface-to-volume ratio and electrical properties of n-WO_3 can be used as labels or tracers for electrochemical analysis. The n-WO_3 has been predicted to have biosensing applications. Hariharan et al. employed WO_3 based biosensor for L- dopa detection with high selectivity and sensitivity [4]. Sun et.al utilized WO_3 for the glucose detection with high efficiency; thus, holding great promises for applications in bioelectronics [5]. There is thus a good scope to explore WO_3 for the efficient detection of other important bio-analytes.

Acute myocardial infarction (AMI) is a major cause of death caused by necrosis of myocardial tissue due to ischemia. Among the various biomarkers, cardiac Troponin I (cTnI) has been recognized as a principle biomarker with high specificity and great selectivity for the cardio vascular diseases. The level of cTnI in normal subjects is around 1 ng mL^{-1} that may increase to 550 ng mL^{-1} in AMI patients [6]. Hence rapid and sensitive detection of cTnI with good detection range is urgently required for the early treatment of AMI. In the present work, we demonstrate the development of a simple and label-free immunosensor to detect myocardial symptomatic biomarker Troponin-I using nanostructured tungsten trioxide. The proposed detection strategy is simple, economical and is based on direct immobilization of an antibody over 3–aminopropyl triethoxy saline (APTES) functionalized n-WO_3/ITO electrode. The results of the present studies exhibit good sensitivity, broad detection range and high storage stability.

2. Experimental

All chemicals of analytical grade were purchased from Sigma-Aldrich. The XRD (Bruker D-8 Advance), FT-IR (Nicolet 380) and AFM (Park system XE-100) were used for characterization of materials and electrodes. The electrochemical studies were carried out on an Autolab Potentiostat/Galvanostat (Metrohm, Netherlands) using a three- electrode system. De-ionized water (18.2 MΩ) was used for preparation of solutions.

The details of synthesis of nanostructured tungsten trioxide (n-WO_3) and its functionalization with APTES have been given in the Supplementary information sheet. [12] Thin films of APTES functionalized n-WO_3 over ITO (APTES/n-WO_3/ITO) electrode were prepared by electrophoretic deposition (EPD) technique. The anti-cTnI antibodies were immobilized over APTES/n-WO_3/ITO electrode. The fabrica-

* Corresponding authors.
E-mail addresses: saurabhnpl@gmail.com (S. Srivastava), bansi.malhotra@gmail.com (B.D. Malhotra), nitin.phy@dce.edu (N.K. Puri).

http://dx.doi.org/10.1016/j.matlet.2016.09.107
Received 20 June 2016; Received in revised form 29 August 2016; Accepted 26 September 2016
Available online 28 September 2016

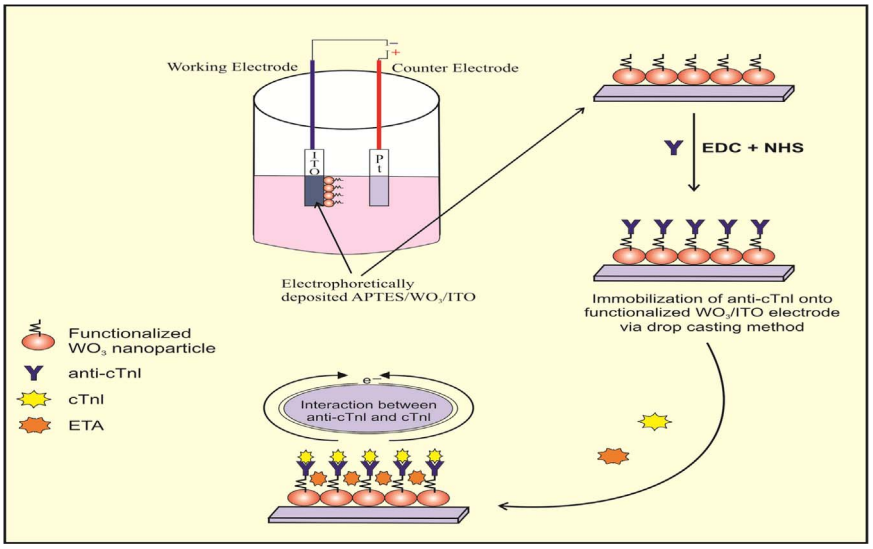

Scheme 1. Schematic of fabrication of the anti-cTnI/APTES/n-WO3/ITO bioelectrode for Troponin-I detection.

tion of APTES/n-WO_3/ITO electrode and anti-cTnI/APTES/n-WO_3/ITO bioelectrode has been given in the Supplementary information sheet [12]. The Schematic of fabrication of immunoelectrode has been demonstrated in Scheme 1.

3. Results and discussion

The XRD studies were carried out to investigate crystallinity and phase of the n-WO_3 powder and shown in Fig. 1(i). The presence of intense characteristic peak at 24.22° and other diffraction peaks at 28.56°, 33.99°, 41.39°, 50.09°, 55.6° and 61.58° are well indexed to (200), (112), (220), (222), (114), (420) and (134) planes, respectively (JCPDS 71-0131) .These peaks reveal the presence of orthogonal phase in WO_3 with good crystalline structure. The average crystallite size *D* of WO_3 nanoparticles was estimated to be 20 nm using Debye-Scherer equation.

$$D=\frac{0.9\lambda}{\beta Cos\theta} \quad (1)$$

Fig. 1(ii) shows Fourier transform infrared spectra (FT-IR) of the (a) n-WO_3, (b) APTES/n-WO_3, (c) anti-cTnI/APTES/n-WO_3. The band seen at 1410 cm^{-1} [Fig. 1(ii, a)] represents stretching vibration of ν (W-O) whereas broad band at 770 cm^{-1} corresponds to ν (W-O_{inter}–W) stretching vibration of the bridging O_2 [7]. In Fig. 1(ii, b), band seen at 3421 cm^{-1} is due to asymmetric (N-H) stretching vibration of NH_2 whereas peaks at 1614 cm^{-1} and 1422 cm^{-1} corresponds to δ(–NH_2) and δ (Si-CH_2) respectively present in APTES [8–10]. The peak at 2932 cm^{-1} is attributed to methylene group (–CH_2) indicating that silane agent was grafted onto the surface successfully and the peak at 1122 cm^{-1} is due to stretching mode of Si-O–Si [9]. These results

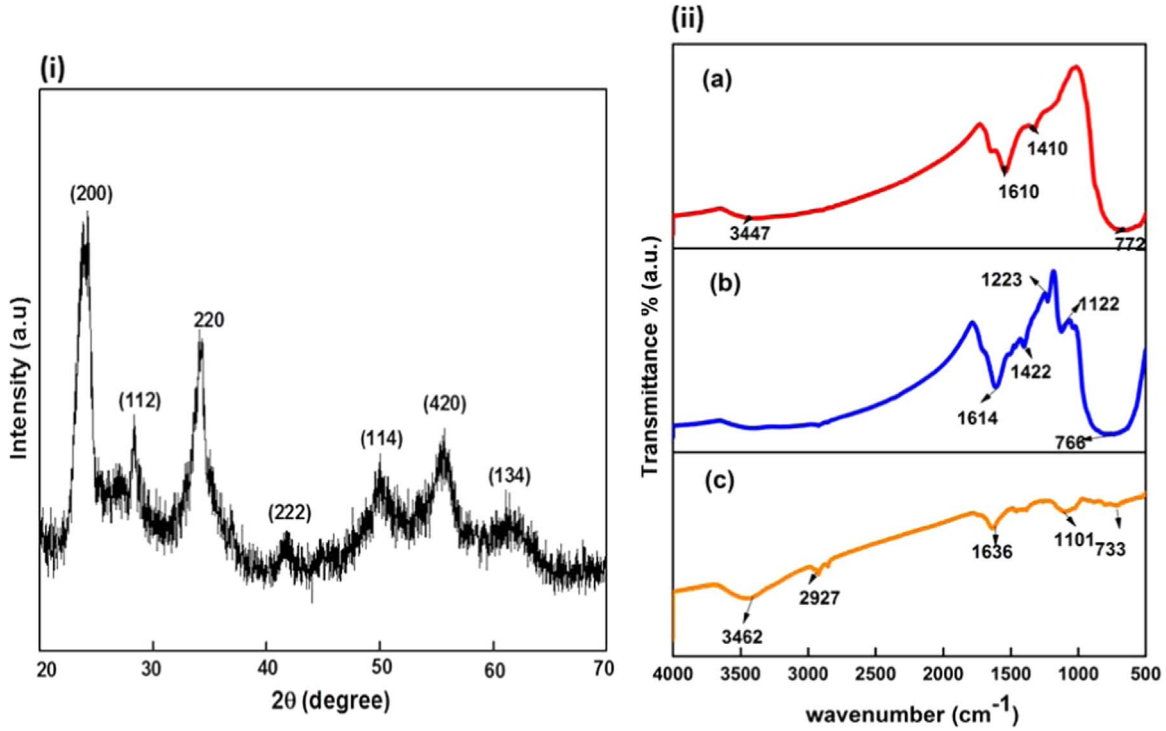

Fig. 1. (i): X-ray diffraction pattern obtained for the WO_3 nanoparticles. **(ii):** FT-IR spectra of **(a)** n-WO_3, **(b)** APTES/n-WO_3 and **(c)** anti-cTnI/APTES/n-WO_3.

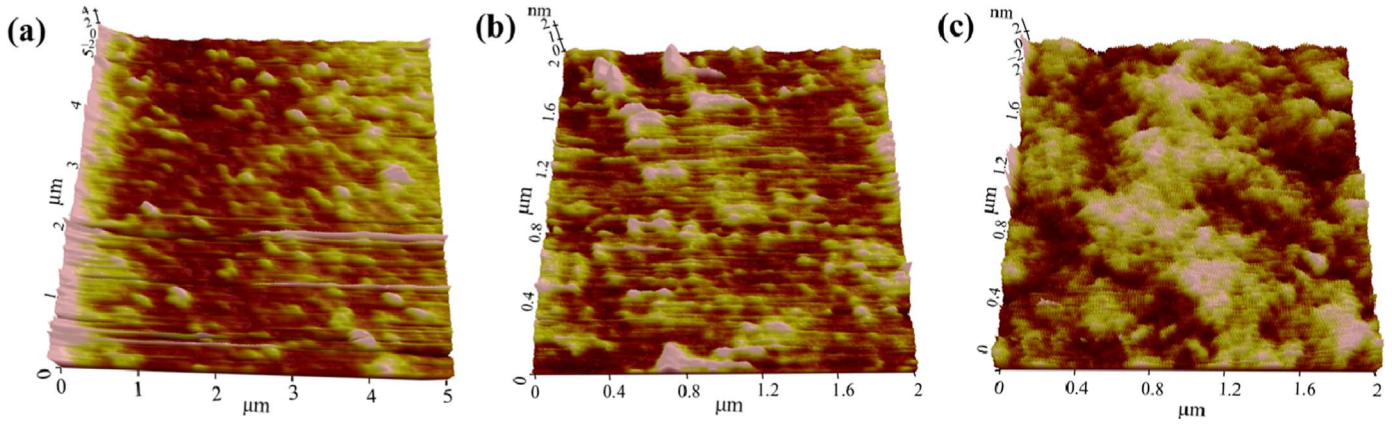

Fig. 2. AFM image of **(a)** n-WO_3/ITO electrode, **(b)** APTES/n-WO_3/ITO electrode and **(c)** anti-cTnI/APTES/n-WO_3/ITO bioelectrodes.

suggest that APTES was successfully anchored on the WO_3 surface. In the FT-IR spectra of antibody immobilized APTES/n-WO_3 /ITO electrode (Fig. 1ii c), the bands seen at 3462 cm^{-1}, 1636 cm^{-1} and 733 cm^{-1} can be attributed to the amide B, amide I and amide IV respectively indicating successful immobilization of the antibody on the electrode. The bands observed at 2927 cm^{-1} (–CH_2) and at 1101 cm^{-1} (Si-O–Si) were found to be shifted after antibody immobilization.

Topography and surface roughness of the electrode are known to play an important role in determining the conformation of the adsorbed protein layer [10]. Fig. 2 represents the topographical image of 3-D height plots for the electrodes. It can be seen that the average surface roughness of n-WO_3/ITO electrode (0.307 nm; Fig. 2a) decreased to 0.120 nm (Fig. 2b) after modification with APTES suggesting the formation of a uniform layer due to intermolecular interaction between APTES and n-WO_3/ITO surfaces. Finally after immobilization of anti-cTnI on APTES/n-WO_3/ITO electrode surface (Fig. 2c), average roughness increased to 5.9 nm indicating attachment of the antibody molecules.

Electrochemical impedance spectroscopy (EIS) technique was utilized to determine the interfacial properties between the electrode–electrolyte boundaries. Fig. 3(a) shows the Nyquist plot obtained for bare ITO electrode, APTES/n-WO_3/ITO and anti-cTnI/APTES/n–WO_3/ITO electrodes in the PBS (pH 7.0) containing 5 mM $[Fe(CN)_6]^{4-/3-}$ in the frequency range 10^7–10^{-2} Hz at a biasing potential of 10 mV. The charge transfer process in these electrodes was investigated by measuring charge transfer resistance (R_{ct}) at the electrode/electrolyte interface. It was observed that magnitude of R_{ct} for ITO electrode (434.07 Ω) increased to 543.15 Ω for APTES/n-WO_3/ITO electrode indicating modification of the ITO electrode with APTES modified WO_3 nanoparticles. And after the antibody immobilization, R_{ct} of anti-cTnI/APTES/n-WO_3/ITO electrode further increased to 589.36 Ω indicating insulating nature of the antibody molecules.

Electrochemical response studies of the anti-cTnI/APTES/n-WO_3/ITO immunoelectrode were conducted as a function of cTnI concentration (1–250 ng mL^{-1} using EIS technique (Fig. 3b). R_{ct} was evaluated from the diameter of the Nyquist plot while fitting the curve under Randles circuit. It was found that R_{ct} of the immunoelectrode (anti-cTnI/APTES/n-WO_3/ITO) increased linearly as a function of cTnI concentration (1–250 ng mL^{-1}). This could perhaps be due to the formation of electrically insulating antigen–antibody complexes produced from the specific interaction of the cTnI and antibody that may block the electron transfer via $[Fe(CN)_6]^{3-/4-}$ [11]. The linear variation of the R_{ct} value obtained from the calibration plot (Fig. 3c) obeys Eq. (2)

$$R_{ct}(\Omega) = 618.70(\Omega) + 6.64(\Omega\ ng^{-1}\ mL)*[concentration\ (ng\ mL^{-1})] \quad (2)$$

with regression coefficient (R^2) =0.99.

The APTES/n-WO_3/ITO based immunosensor exhibits high sensitivity of 26.56 Ω ng^{-1} mL cm^{-2} in the linear detection range of 1-250 ng mL^{-1}. Furthermore, a control experiment was performed to investigate the electrochemical response of APTES/n-WO_3/ITO electrode towards cTnI without using anti-cTnI. We did not observe any significant change in magnitude of R_{ct} with respect to different concentration of cTnI. This result indicated that the sensor response was due to the immunoreactions between anti-cTnI and cTnI molecules only. Fig. S2 compares R_{ct} response of anti-cTnI/APTES/n-WO_3/ITO immunoelectrode in presence of serum sample (containing 100 ng mL^{-1} cTnI) and standard sample (100 ng mL^{-1} cTnI) [12]. The estimated low RSD value (2.65%) indicated that the anti-cTnI/APTES/n-WO_3/ITO immunoelectrode could be utilized for real sample analysis. The storage stability of the anti-cTnI/APTES/n-WO_3/ITO immunoelectrode was investigated by observing the EIS response and measuring the R_{ct} value at a regular interval of five days up to 40 days in presence of 50 ng mL^{-1} cTnI concentration (Fig. 3d). The R_{ct} value was found to be 92% of its initial response for up to 30 days, thereafter it further decreased to 80% at the end of 40 days. This indicated the storage stability of the fabricated biosensor as 30 days. The reproducibility and selectivity studies of the fabricated biosensor has been demonstrated in the Supplementary information sheet [12] Table I shows the characteristics of the fabricated biosensor along with some those reported in the literature for cTnI detection [see Supplementary information sheet] [12]. The APTES/n-WO_3/ITO based biosensor exhibits a much higher sensitivity (26.56 Ω ng^{-1} mL cm^{-2}), good stability (30 days), and an extended linearity (1–250 ng mL^{-1}) than some of the other sensors reported in the literature.

4. Conclusion

In summary, we have successfully synthesized and functionalized nanostructured tungsten trioxide (n-WO_3). Thin films of APTES/n-WO_3/ITO have been fabricated via electrophoretic deposition technique and followed by covalent immobilization of antibody of cTnI for the detection of cTnI using EIS technique. In comparison with other reported Troponin biomarker detection methods including biosensors, the proposed biosensor is simple and label free. It exhibits a wider detection range as 1–250 ng mL^{-1}, sensitivity as 26.56 Ω ng^{-1} mL cm^{-2}, storage stability as 30 days and detection limit as 16 ng mL^{-1}. This may be attributed to high antibody loading properties and rapid electron transfer kinetics of n-WO_3. This superior sensing performance of the n-WO_3 based immunosensor reveals its potential for electrochemical biosensing applications. Efforts should be made to further improve the detection limit of this proposed biosensor.

Acknowledgements

The authors thank Prof. Yogesh Singh, Vice chancellor, Delhi

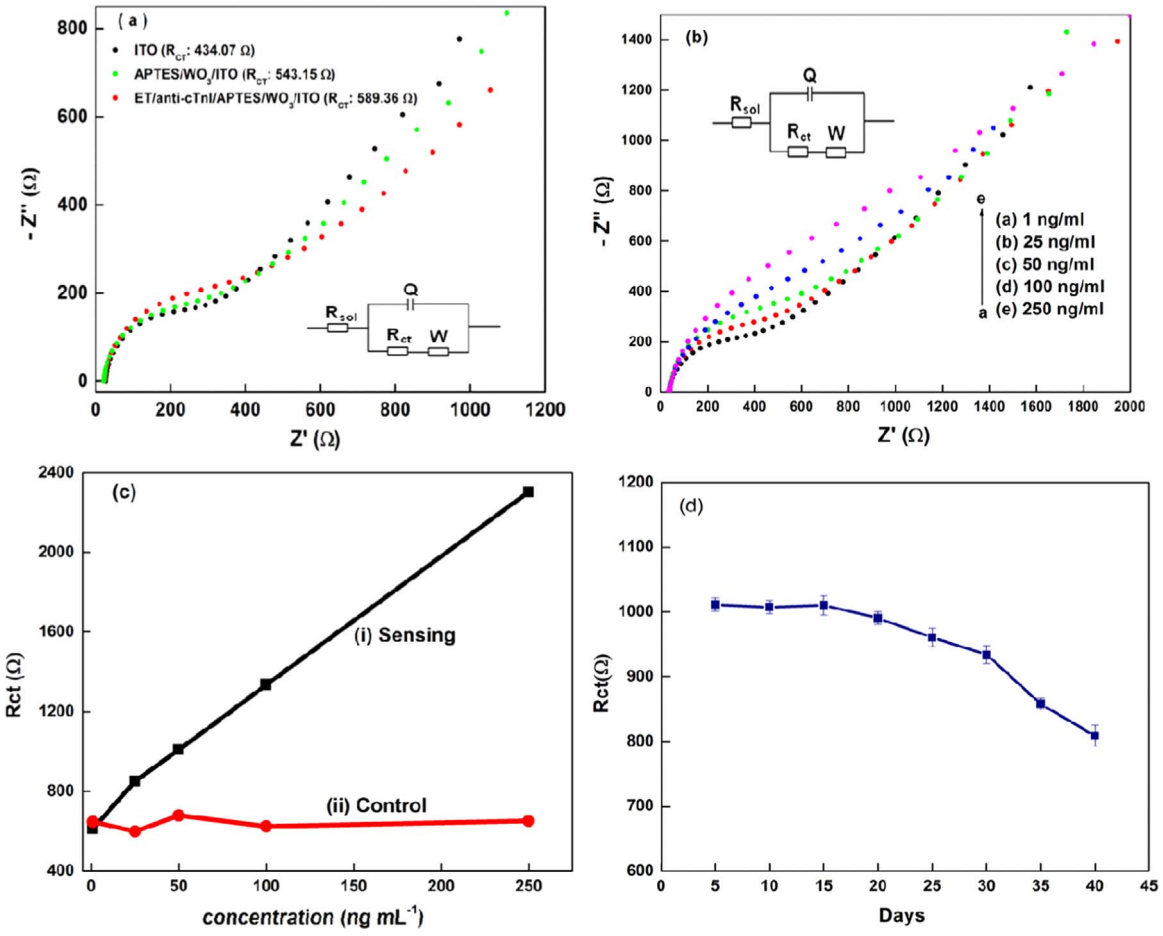

Fig. 3. (a) Shows results of the electrochemical impedance spectroscopy (EIS) studies of the various fabricated electrodes (ITO, APTES/n-WO_3/ITO and anti-cTnI/APTES/n-WO_3/ITO) **(b)** Response studies of the anti-cTnI/APTES/n-WO_3/ITO immunoelectrode as a function of cTnI concentration (1–250 ng/mL) using EIS technique **(c)** Calibration plot obtained between R_{ct} and cTnI concentration with control studies **(d)** Stability studies of the anti-cTnI/APTES/n-WO_3/ITO immunoelectrode.

Technology University, Delhi, India for providing the research facilities. The financial supports received from IUAC sponsored project (Grant No. IUAC/XIII.7/UFR-56324), Department of Atomic Energy - Board of Research in Nuclear Sciences (DAE-BRNS), India and Department of Science and Technology, India (Grant No. DST/INSPIRE/04/2014/002540) are gratefully acknowledged.

Appendix A. Supplementary information

Supplementary information associated with this article can be found in the online version at doi:10.1016/j.matlet.2016.09.107.

References

[1] P.R. Solanki, A. Kaushik, V.V. Agrawal, B.D. Malhotra, Nanostructured metal oxide-based biosensors, NPG Asia Mater. 3 (1) (2011) 17–24.
[2] H. Zheng, J.Z. Ou, M.S. Strano, R.B. Kaner, A. Mitchell, K. Kalantar-zadeh, Nanostructured tungsten oxide–properties, synthesis, and applications, Adv. Funct. Mater. 21 (12) (2011) 2175–2196.
[3] Z. Deng, Y. Gong, Y. Luo, Y. Tian, WO_3 nanostructures facilitate electron transfer of enzyme: application to detection of H_2O_2 with high selectivity, Biosens. Bioelectron. 24 (8) (2009) 2465–2469.
[4] V. Hariharan, S. Radhakrishnan, M. Parthibavarman, R. Dhilipkumar, C. Sekar, Synthesis of polyethylene glycol (PEG) assisted tungsten oxide (WO 3) nanoparticles for L-dopa bio-sensing applications, Talanta 85 (4) (2011) 2166–2174.
[5] Q.-Q. Sun, M. Xu, S.-J. Bao, C.M. Li, pH-controllable synthesis of unique nanostructured tungsten oxide aerogel and its sensitive glucose biosensor, Nanotechnology 26 (11) (2015) 115602.
[6] A. Periyakaruppan, R.P. Gandhiraman, M. Meyyappan, J.E. Koehne, Label-free detection of cardiac troponin-i using carbon nanofiber based nanoelectrode arrays, Anal. Chem. 85 (8) (2013) 3858–3863.
[7] M. Tong, G. Dai, Y. Wu, X. He, D. Gao, WO3 thin film prepared by PECVD technique and its gas sensing properties to NO2, J. Mater. Sci. 36 (10) (2001) 2535–2538.
[8] N. Majoul, S. Aouida, B. Bessaïs, Progress of porous silicon APTES-functionalization by FTIR investigations, Appl. Surf. Sci. 331 (2015) 388–391.
[9] M. Ata, Y. Liu, I. Zhitomirsky, A review of new methods of surface chemical modification, dispersion and electrophoretic deposition of metal oxide particles, RSC Adv. 4 (43) (2014) 22716–22732.
[10] K.K. Jagadeesan, S. Kumar, G. Sumana, Application of conducting paper for selective detection of troponin, Electrochem. Commun. 20 (2012) 71–74.
[11] S. Srivastava, V. Kumar, M.A. Ali, P.R. Solanki, A. Srivastava, G. Sumana, P.S. Saxena, A.G. Joshi, B. Malhotra, Electrophoretically deposited reduced graphene oxide platform for food toxin detection, Nanoscale 5 (7) (2013) 3043–3051.
[12] See Supplementary Information Sheet for the Preparation of n-WO3, its Functionalization, Fabrication of Bioelectrode, UV–vis, Real Sample Analysis, Reproducibility, Selectivity Studies and Comparison Table.

Journal of Alloys and Compounds 763 (2018) 102–110

Contents lists available at ScienceDirect

Journal of Alloys and Compounds

journal homepage: http://www.elsevier.com/locate/jalcom

Biofunctionalized tungsten trioxide-reduced graphene oxide nanocomposites for sensitive electrochemical immunosensing of cardiac biomarker

Deepika Sandil [a, b], Saurabh Srivastava [a], B.D. Malhotra [c], S.C. Sharma [a], Nitin K. Puri [a, *]

[a] Advanced Sensor Laboratory, Department of Applied Physics, Delhi Technological University, Delhi, 110042, India
[b] Department of Applied Physics, Bhagwan Parshuram Institute of Technology, Delhi, 110089, India
[c] Department of Biotechnology, Delhi Technological University, Main Bawana Road, Delhi, 110042, India

ARTICLE INFO

Article history:
Received 12 February 2018
Received in revised form
14 April 2018
Accepted 26 April 2018
Available online 27 April 2018

Keywords:
Reduced graphene oxide
Tungsten trioxide
Cardiac biomarker troponin I
Electrochemical biosensor

ABSTRACT

We demonstrate the fabrication of a facile and efficient biosensing platform for electrochemical detection of human cardiac biomarker Troponin I (cTnI) using Tungsten trioxide-reduced graphene oxide (WO_3-RGO) nanocomposite as a matrix. The *in-situ* hydrothermal method was employed for the synthesis of the WO_3-RGO nanocomposite. Raman spectroscopy, X-ray diffraction (XRD), high-resolution transmission electron microscopy (HRTEM) and field emission scanning electron microscopy (FE-SEM) were employed to investigate structural and morphological behavior. The WO_3-RGO nanocomposite was further functionalized with 3-aminopropyl tri-ethoxy saline (APTES) for the activation of amino groups ($-NH_2$) that can covalently bind to the antibodies of cTnI. This immunosensor was further studied using contact angle measurement, Fourier transform infrared spectroscopy (FT-IR) and electrochemical techniques. The synergistic behavior between RGO and WO_3 nanorods has allowed the immunosensor to exhibit enhanced heterogeneous electron transfer rate constant ($K_o = 2.4 \times 10^{-4}$ cms^{-1}) resulting in improved biosensor efficiency. The immuno-sensor exhibit good sensitivity as 58.24 $\mu A/cm^2$ per decade in an extended linear detection range 0.01–250 ng/mL with the stability up to 30 days. Besides this, the fabricated immuno-sensor exhibits good reproducibility and excellent selectivity towards the detection of the cTnI biomarker. Furthermore, the validation of immunosensor with cardiac patient samples demonstrates the clinical application of this nano-biosensing platform for the detection of other biomarkers too.

1. Introduction

Cardiovascular disease (CVD), a heart and blood vessel disease has become the primary cause of morbidity and mortality across the world. Among different CVDs, Myocardial Infarction (MI), an acute coronary syndrome (ACS) cause adverse cardiac injury in the myocardium such as irreversible damage to tissues. Electrocardiogram (ECG) currently preferred for the measurement and diagnosis of cardiac injuries. However, ECG has some limitations and sensitivity issues which suggests for an alternative approach for the diagnosis purpose [1]. Hence, a sensitive and rapid diagnosis is crucial for the early prognosis of Myocardial Infarction (MI). In clinical research, cardiac biomarkers play an important role in understanding and identification of myocardial infarction concerning other cardiac diseases, which might help in the diagnosis of CVD. Currently, creatine Kinas-MB, myoglobin and cardiac troponin (cTnT and cTnI) considered as remarkable MI diagnostic biomarkers. Among these, cardiac troponin I (cTnI) had highest cardio-specificity and considered as a principal diagnostic biomarker for MI [2]. Cardiac troponin I is a protein found in cardiac muscles and is made up of 209 amino acid residues with a molecular weight as 22.5 kDa [3]. After myocardial infarction, the systemic blood concentration of this protein rises and remains elevated for 8–10 days, hence serving longer window of detection for MI. The level of cTnI in normal blood serum is below 0.6 ng/ml which could potentially rise to 1–4 ng/ml at the onset of AMI. It can increase up to 100 ng/ml or more within 3–6 h and remains elevated for 5–9 days. For the detection of cTnI many conventional methods such as fluoro-

* Corresponding author.
E-mail addresses: nitinpuri2002@yahoo.co.in, nitinkumarpuri@dtu.ac.in (N.K. Puri).

https://doi.org/10.1016/j.jallcom.2018.04.293
0925-8388/

immunoassay, enzyme-linked immunosorbent assay (ELISA), radioimmunoassay and spectrophotometric methods have been used. However, these assays are time-consuming, expensive, laborious and demands small volume of blood for testing [4,5]. Thus for the safe and rapid diagnosis of the AMI, biosensors can be used as a faster and cheaper means for its detection. Among different biosensors, electrochemical biosensors based on immunochemical reactions such as specific antibody-antigen interaction considered as the most sensitive detection tool due to its precise measurement, fast driven analysis and simple preparation [6,7]. Also, they allow automation, miniaturization, development of disposable devices and require very small sample volumes [8–11]. While fabricating an electrochemical immunosensor, biomolecular immobilization is a crucial step to achieve efficient performance. For the successful antibody immobilization, an ideal immunosensor should permit high loading and retain its biological activity for the long term. Nanomaterials in this context can be preferred as a substantial matrix for the immobilization of antibodies [12]. A lot of nanomaterials such as gold, metals, carbon and metal oxides with variable morphology have been utilized to fabricate the biosensing platform owing to their distinctive physiochemical features, good biocompatibility, and large electro-active surface [13]. Among different nanomaterials, nanostructured metal oxides exhibit good catalytic properties, high electron −transfer kinetics and firmed adsorption capability that can provide appropriate microenvironments for the immobilization of biomolecule. Tungsten trioxide nanostructures (n-WO_3) have been considered as a promising material as an immobilized matrix because of its enhanced catalytic activity, chemical stability, simple synthesis and strong adherence to the substrate [14].

The incorporation of semiconducting materials such as carbon nanotubes and graphene with the nanostructured metal oxides provide improved biosensing characteristics [15]. In this context, graphene or chemically reduced graphene oxide (RGO) considered as promising supportive matrix [16]. RGO, an array of carbon atoms are covalently connected via sp^2 bonds to form a two-dimensional honeycomb sheet that contributes toward its exceptional properties such as good electrical conductivity, large surface area, and high electrochemical activity [17].

Herein, we report the synthesis of a WO_3-RGO nanocomposite with simultaneous reduction of GO. And for the first time, the synthesized nanocomposite has been utilized as an immobilized matrix for the fabrication of a facile and label-free electrochemical immuno-sensor for the detection of a cardiac biomarker cTnI. Further, EDC-NHS chemistry was employed for the activation of carboxyl groups of an antibody of cardiac troponin I. The proposed mechanism delivers improved sensitivity, wide detection range, and good stability.

2. Experimental section

2.1. Synthesis of WO_3-RGO nanocomposite and functionalization of electrodes

WO_3-RGO nanocomposite was synthesized by employing the In-situ hydrothermal method. In brief, a defined amount of as-synthesized graphene oxide (GO) [See Supplementary information sheet] was dispersed in 20 mL of DI water and kept for half an hour ultrasonication. Then, 0.1 M of $NaWO_4 \cdot 2H_2O$ and 0.225 g of NaCl were added to the resultant dispersed solution and kept on stirring for one hour. The pH value of the resultant suspension was adjusted to 2 using HCl solution. After this, the suspension was transferred to 50 mL Teflon −lined stainless steel autoclave and placed in a hot air oven at temperature 180° C for 24 h. Latterly, the autoclave was cooled naturally to the room temperature, and the sample was collected through multiple washing with deionized water and ethanol followed by drying at 70° C.

The as-synthesized WO_3-RGO nanocomposite was further functionalized with APTES for providing active amino groups (-NH_2) that can covalently bind to the antibodies. Electrophoretic deposition technique (EPD) was used for deposition of APTES functionalized WO_3-RGO nanocomposite thin films on the pre-hydrolyzed ITO electrode at optimized potential 45 V for 90 s. The fabricated APTES/WO_3-RGO nanocomposite/ITO electrodes were washed with DI water and dried at room temperature.

2.2. Fabrication of the immuno-electrode

Subsequently, the cTnI antibodies were covalently attached to the APTES/WO_3-RGO nanocomposite/ITO electrode using EDC-NHS chemistry. A fresh stock solution (50 μg/mL) of anti-cTnI was prepared in phosphate buffer solution (PBS, pH = 7.4). Prior to immobilization, the carboxyl groups present in antibodies were activated by using EDC-NHS chemistry. EDC (0.2 M) worked as a coupling agent and NHS (0.05 M) as an activator. 15 μL of anti-cTnI was mixed with 7.5 μL of 0.2 M EDC and 7.5 μL of 0.05 M NHS. Subsequently, this solution (30 μL) was uniformly spread onto APTES/WO_3-RGO nanocomposite/ITO electrode by drop-casting. The electrode was kept in a humid chamber at room temperature followed by washing with PBS to remove any unbound antibody molecules. Lastly, ethanolamine (EA) solution (0.1 mg/mL) was used for blocking the non-specific active sites present on the electrode. The fabricated EA/anti-cTnI/APTES/WO_3-RGO nanocomposite/ITO immunoelectrode was washed with PBS solution and stored at 4 °C when not in use.

2.3. Electrochemical measurement procedure

The electrochemical measurements such as electrochemical impedance spectroscopy (EIS) and differential pulse voltammetry (DPV) were performed using an electrochemical Autolab Potentiostat (Netherlands) employing a three-electrode system that consists of the fabricated immuno-electrode as the working electrode, platinum (Pt) as the counter electrode and Ag/AgCl as the reference electrode. The phosphate buffer saline (PBS, 50 mM, pH 7.4) containing 5 mM $[Fe(CN)_6]^{3-/4-}$ as redox couple was used for all the electrochemical measurements. The impedance spectrum was measured in the frequency range of 10^5 to 10^{-1} Hz at a biasing potential of 10 mV. The Nyquist plot was studied in which X-axis and Y-axis represent the real part, and the imaginary part of the impedance and the curve consists of the semi-circle and the straight line. The straight line at low frequency signifies the diffusion process whereas the semicircle at high frequency signifies the charge transfer resistance (R_{CT}). For the differential pulse voltammetry measurements, the response was measured at the scan rate of 50 mV/s in the potential range of −0.8 to 0.8 V.

A step-wise fabrication process of EA/anti-cTnI/APTES/WO_3-RGO nanocomposite/ITO immunoelectrode is shown in Scheme 1.

3. Results and discussion

3.1. Crystallographic and morphological studies

The crystallinity and phase purity analysis of RGO and RGO-WO_3 nanocomposite was examined by powder X-ray diffractometer (XRD) in the range of 5°–80°. The XRD spectrum of graphene oxide (GO) shown in Fig. 1(a) exhibits a characteristic peak at 11.7° corresponding to (002) plane (d_{002} = 7.5 Å), which shifts to 23.4° in the XRD spectrum of RGO (d_{002} = 3.79 Å) (Fig. 1(b)). The reduction in

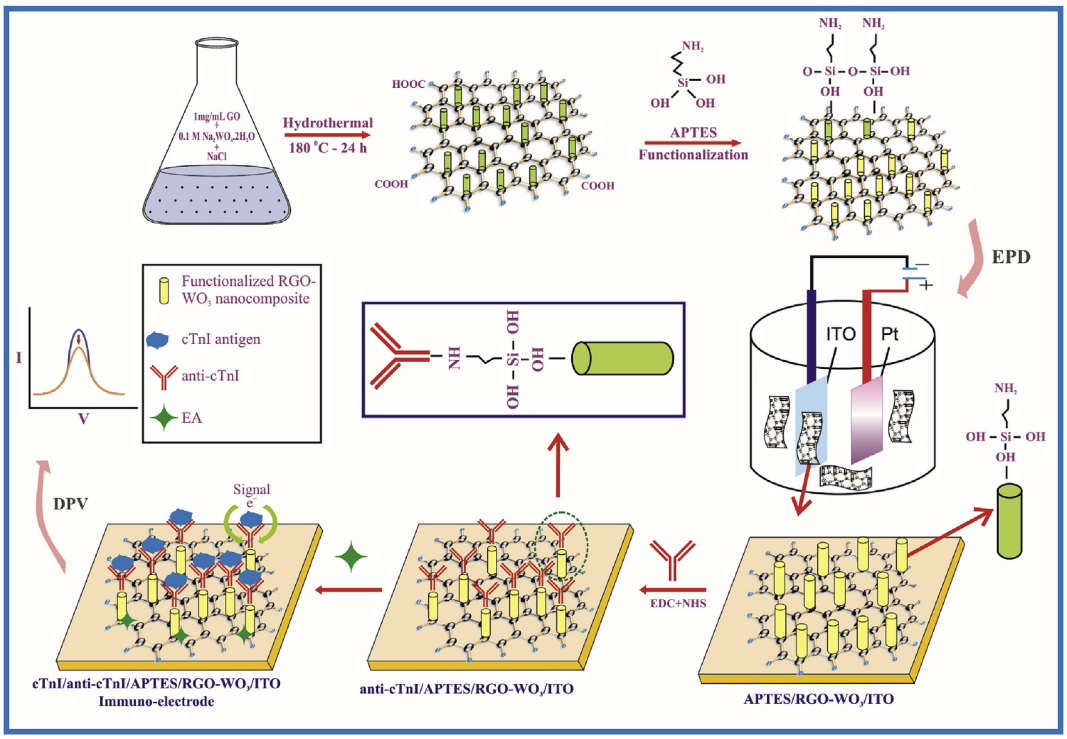

Scheme 1. Fabrication of anti-cTnI/APTES/WO_3-RGO nanocomposite/ITO based immunosensor for cTnI detection.

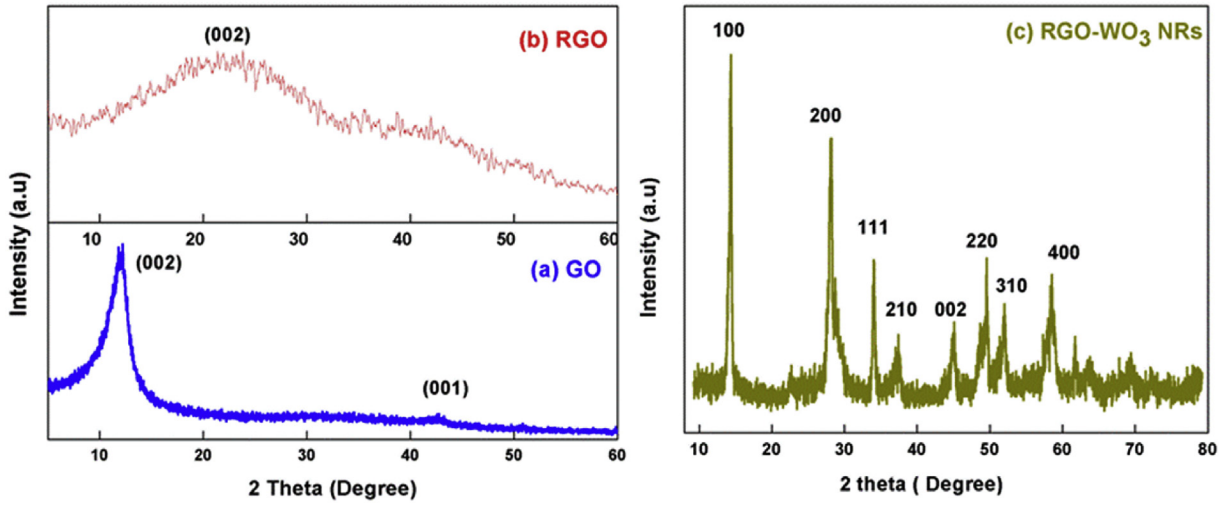

Fig. 1. XRD pattern of (a) GO (b) RGO and (c) WO_3-RGO nanocomposite composite.

the interplanar spacing of RGO as compared to GO is due to the removal of the oxide groups that allow graphene sheets to be tightly packed. The XRD pattern of synthesized RGO-WO_3 nanocomposite (Fig. 1(c)) shows strong diffraction peaks at $2\theta = 14.3°$and $28.1°$ corresponding to (100) and (200) planes respectively. The other peaks are seen at 34.2°, 37°, 44.8°, 49.6°, 52.2° and 59.01° are indexed to (111), (210), (002), (220), (310) and (400) crystal lattice planes, respectively. All these planes are well matched with a hexagonal WO_3 crystal structure (JCPDF 75-2187) without the presence of any undesired phases. The intense high peaks of the nanocomposite indicate good crystallinity of the structure. Additionally, no peak emerges at around $2\theta = 23.4°$ in the XRD spectrum of the nanocomposite, suggesting that the RGO sheets are homogeneously dispersed in the nanocomposite. The average crystallite size of WO_3 nanorods in nanocomposite was found to be 32 nm using Debye-Scherrer's equation.

The morphological and structural analysis of the synthesized WO_3 NRs and RGO-WO_3 nanocomposite have been studied using field-emission scanning electron microscopy (FE-SEM) and Transmission electron microscopy (TEM), respectively, shown in Fig. 2. From Fig. 2 a, it can be seen that the proposed hydrothermal synthesis route has obtained a uniform 1-D nanostructure of WO_3 NRs with a smooth surface and exist in the form of bundles with an average diameter as 54 nm. The average size of the nanorods as estimated by FESEM is in close agreement with the TEM image of the WO_3 NRs (Inset, Fig. 2(a)). However, in the *in-situ* grown RGO-

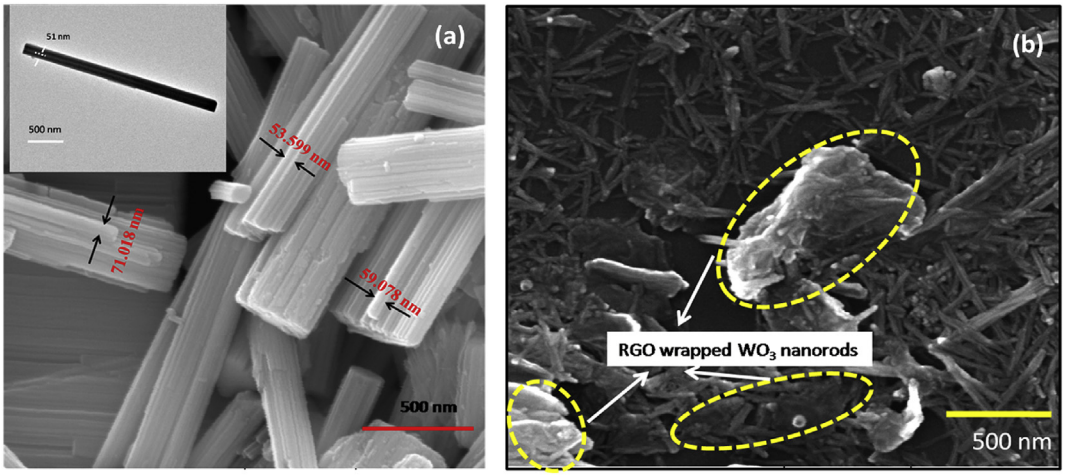

Fig. 2. (a) FESEM image of WO_3 NRs, inset TEM image of WO_3 NRs and (b) FESEM image of WO3-RGO nanocomposite composite.

WO_3 nanocomposite, the RGO affects the width and uniformity of the 1-D structure as can be observed by comparing Fig. 2(a) and b. Instead of bundles, monodispersed WO_3 NRs was observed in this case. Also, the WO_3 NRs are visible on the surface of the graphene sheets while some of these are found to be trapped between the RGO sheets.

3.2. Spectroscopic studies

The grafting of the WO_3-RGO nanocomposite surface through the APTES and antibody immobilization was investigated by studying FT-IR spectrum of the WO_3—RGO nanocomposite, APTES/WO_3-RGO nanocomposite, and anti-cTnI/APTES/WO_3-RGO nanocomposite [Fig. 3(a)]. The FT-IR spectrum of WO_3-RGO nanocomposite (curve (i)) exhibits the two distinctive peaks at 1205 cm^{-1} and at 1724 cm^{-1} which can ascribe to C—OH stretching vibrations of a hydroxyl group and C=O stretching vibration of carboxylic/carbonyl groups respectively present in RGO. The peaks observed at 962 cm^{-1} and 1610 cm^{-1} represents the C—H stretching vibrations and aromatic C=C stretching vibrations, whereas the characteristic peaks of WO_3 seen at 1410 cm^{-1} and 766 cm^{-1} correspond to W—O and W—O—W stretching vibration of the bridging O_2 [18]. The peaks at 3440 cm^{-1} and 1623 cm^{-1} in curve (ii) can be ascribed to asymmetric (N—H) stretching and bending of the NH_2 present in the APTES revealing that APTES has been successfully grafted on the WO_3-RGO nanocomposite surface [19]. The 1408 cm^{-1} peak corresponds to bending vibrations (Si—CH_2) present in APTES. The intensities of IR peaks are found to be suppressed after immobilization of antibody onto the APTES/WO_3-RGO nanocomposite/ITO (curve (iii)). The appearance of the additional band at 3462 cm^{-1}, 1636 cm^{-1} and 705 cm^{-1} indicate the presence of N—H stretching of the amide A, amide I and amide IV, respectively, confirming the successful binding of antibody onto APTES/WO_3-RGO nanocomposite/ITO electrode [20].

The Raman spectroscopy has also investigated the interaction between WO3 NRs and RGO sheets. Fig. 3 (b) represents the Raman spectra of RGO, WO_3 NRs and WO_3-RGO nanocomposite obtained in the range of 200 cm^{-1} to 3000 cm^{-1}. The Raman spectra of RGO (curve (i)) indicates well-defined peaks at 1349 cm^{-1} and at 1598 cm^{-1} respectively that can be attributed to the presence of characteristic D-band and G-band in RGO. The intense peaks centered at 813 cm^{-1}, 760 cm^{-1} and 933 cm^{-1} (curve (ii)) indicate stretching vibrations of W— O, W—O—W, and W=O respectively. Whereas, peaks observed at 242 cm^{-1} and 329 cm^{-1} can be

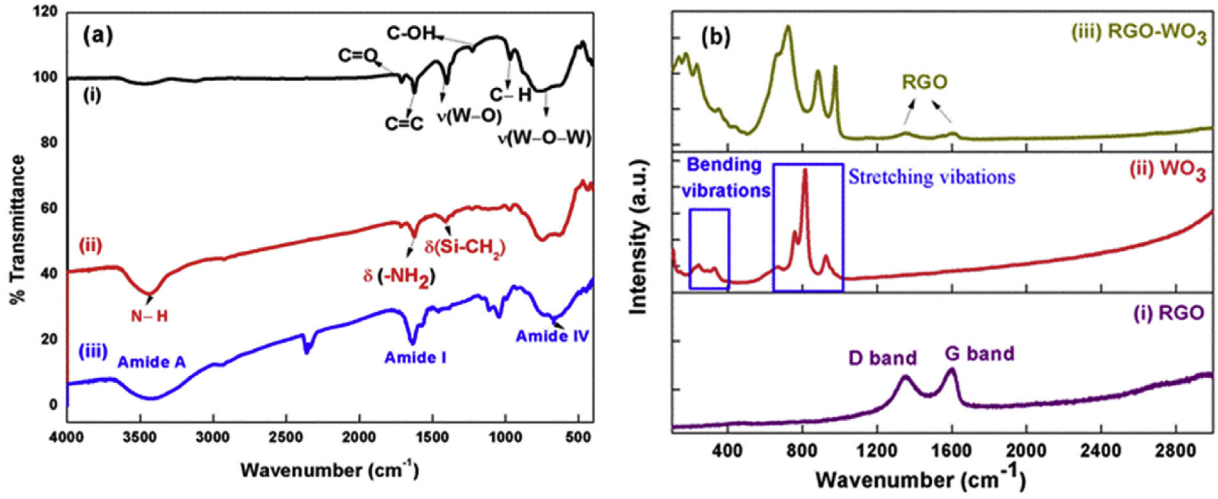

Fig. 3. (a) FT-IR spectra of (i) WO_3-RGO nanocomposite, (ii) APTES/WO_3-RGO nanocomposite and (iii) anti-cTnI/APTES/WO_3-RGO nanocomposite and (b) Raman spectra of (i) RGO, (ii) WO_3 NRs and (iii) WO_3-RGO nanocomposite.

assigned to the bending vibration of O–W–O [21]. It is noteworthy that the peaks observed in WO_3 NRs are shifted and broaden in case of WO_3-RGO nanocomposite composites (curve (iii)) along with the presence of D and G band. The observed change can be attributed to the formation of C–O–W bonds during the hydrothermal treatment, which further confirms the decoration of WO_3 NRs on the RGO sheets surface.

3.3. Contact angle measurement studies

The investigation of the hydrophilic and hydrophobic character of the WO_3-RGO nanocomposite/ITO electrode has been done using contact angle measurement. The static sessile drop method has been employed to determine the contact angle of the electrode at different stages of surface modification. For the study of drop image, an image analysis system is used to calculate the contact angle (θ) value from the shape of the drop. The initial contact angle value of the hydrolyzed ITO glass electrode (66.54°) [Fig. 4(a)] is found to decrease to 31.50° [Fig. 4(b)] on the deposition of WO_3-RGO nanocomposite film due to the presence of oxygenated hydrophilic groups like →OH and →COOH in the WO_3-RGO nanocomposite matrix. However, after functionalization with APTES, the contact angle is found to increase to ~37° [Fig. 4(c)]. This increase of contact angle value indicates the presence of hydrophobic alkyl chains in APTES molecules which imparts a more hydrophobic character to the surface of the matrix. Finally, after covalent immobilization of antibody molecules on the functionalized surface, the contact angle value decreased to 6.03° [Fig. 4(d)] showing the hydrophilicity nature of the antibody molecules. Thus, the successful immobilization of antibody over the functionalized matrix APTES/WO_3-RGO nanocomposite was accomplished.

3.4. Electrochemical characterization

The electrochemical properties of WO_3NRs and in-situ grown WO_3-RGO nanocomposite have been investigated by electrochemical impedance spectroscopy (EIS) studies conducted in the frequency range of 10^5 to 10^{-1} Hz at a biasing potential of 10 mV. The electrochemical system has modeled with an equivalent circuit (Randles circuit) comprising of solution resistance (Rs), charge transfer resistance (R_{CT}), Warburg impedance (W) and double layer capacitance (C_{DL}). The diameter of the semi-circle as shown in the Nyquist plot (Fig. 5(a)) measures the magnitude of charge transfer resistance R_{CT} that depends on the dielectric characteristics at the electrode/electrolyte interface [22]. All these studies have been done using software Nova provided with the Autolab system. The charge transfer resistance value measured for WO_3-RGO nanocomposite ($R_{CT} = 887\ \Omega$) is small as compared to that of WO_3 NRs ($R_{CT} = 1350\ \Omega$). This decrease in resistance can be attributed to the excellent electrical conductivity of the RGO in the nanocomposite matrix that enhances the electron transfer kinetics at the electrode and solution interface.

The heterogeneous electron transfer rate constant (k_o) of the WO_3 NRs/ITO and WO′$_3$-RGO nanocomposite has been calculated using equation (1)

$$K_o = \frac{RT}{n^2 F^2 A R_{CT} S} \quad (1)$$

where R represents as the gas constant, T as absolute temperature (K), F as the Faraday constant, A as the specific electrode area (cm^2), S as the bulk concentration of redox probe (mol cm^{-3}) and n as the number of transferred electrons per molecule of the redox probe. The K_o value of the WO_3-RGO nanocomposite has been estimated as 2.54×10^{-4} cm s^{-1} which is better than that of the WO_3 NRs (1.8×10^{-4} cm s^{-1}). This indicated that the WO_3-RGO nanocomposite exhibits faster charge transfer property as compared to that of WO_3 NRs and can give a superior analytical performance in electrochemical biosensing device.

Further, the electrochemical impedance spectra (EIS) obtained for different modified electrodes is shown in Fig. 5(b). The maximum R_{CT} value is found for WO_3 NRs as 1.35 KΩ. However, the significant reduction in the R_{CT} value is observed in the case of the WO_3-RGO nanocomposite (887 Ω). This can be ascribed to the enhanced electrochemical conductivity of the RGO in the nanocomposite matrix. After antibody immobilization, the

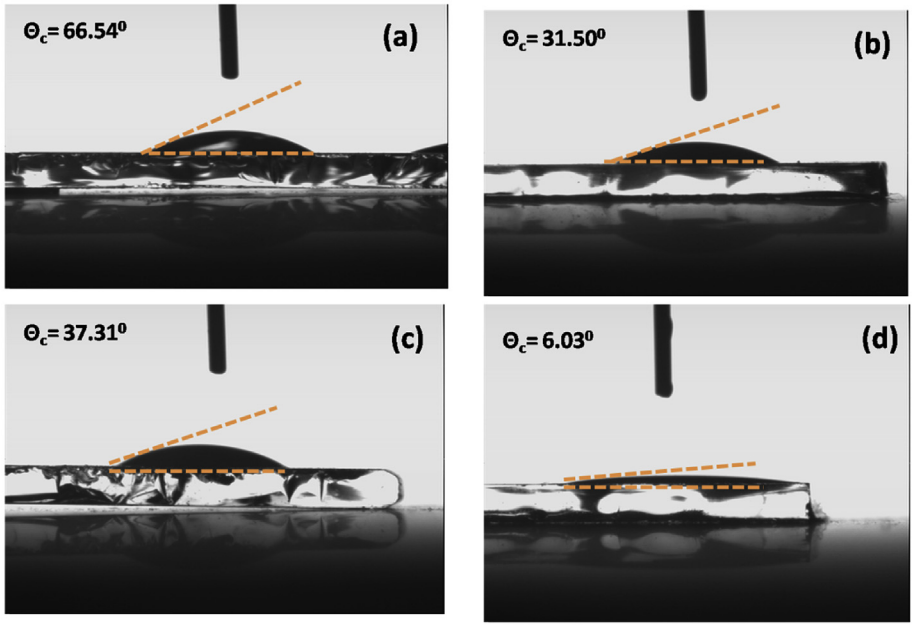

Fig. 4. Contact angle measurement of (a) hydrolyzed ITO glass, (b) WO_3-RGO nanocomposite/ITO, (c) APTES/WO_3-RGO nanocomposite/ITO and (d) anti-cTnI/APTES/WO_3-RGO nanocomposite/ITO.

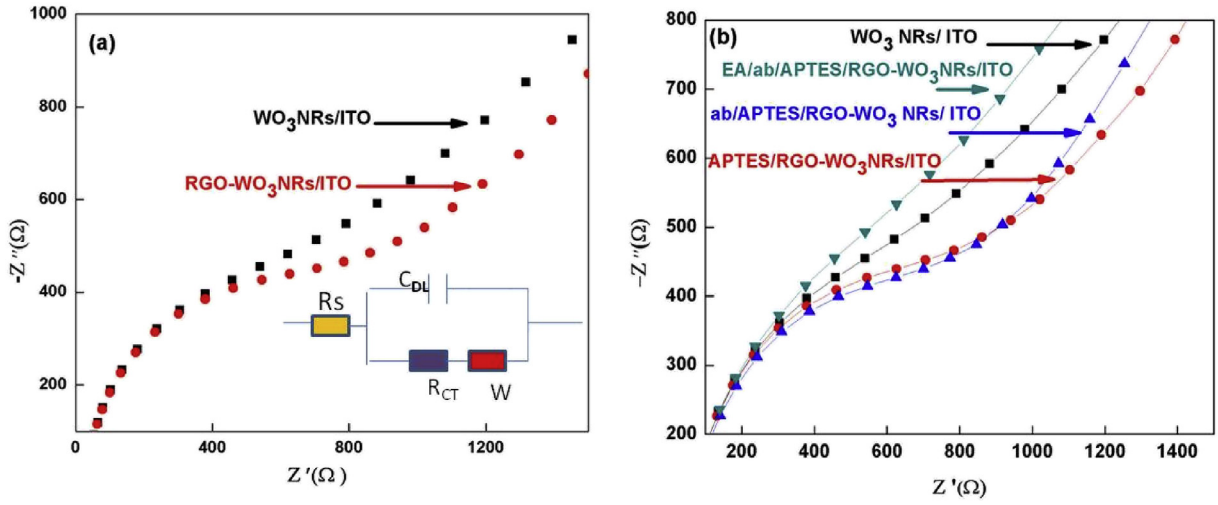

Fig. 5. Electrochemical impedance spectroscopy (EIS) of (a) WO_3 NRs/ITO and WO_3-RGO nanocomposite/ITO electrodes (Inset: Randles circuit) and (b) EIS spectra of different modified electrodes in PBS solution (50 mM, pH 7.4)containing 5 mM $[Fe(CN)_6]^{3-/4-}$

functionalized matrix (anti-cTnI/APTES/RGO-WO_3NRs/ITO) exhibited a higher R_{CT} (905 Ω) as compared to WO_3-RGO nanocomposite which shows the insulating nature of the antibody molecules. Lastly, after attachment of ethanolamine (EA) which covers most of the non-specific active sites of the immunoelectrode surface, the charge transfer process is again hindered, resulting in a higher R_{CT} (1.6 KΩ) of the EA/anti-cTnI/APTES/WO3-RGO nanocomposite electrode.

3.5. Electrochemical sensing studies

The variation in the response current of the immunoelectrode as a function of cTnI concentration (0.01 ng/mL to 250 ng/mL) was studied using differential pulse voltammetry (DPV) technique (Fig. 6(a)). The response study was carried out in phosphate buffer saline (PBS, 50 mM, pH 7.4) containing 5 mM $[Fe(CN)_6]^{3-/4-}$ as redox coupling agent. For each measurement, 20 μL of diluted antigen was added into the electrochemical cell with 10 min of incubation. The response graph shows that the magnitude of the peak current decreases with the increase in cTnI concentration in the detection range 0.01–250 ng/mL. This decrease in response current attribute towards the formation of electrically insulating antigen-antibody complexes produced from the specific interaction of cardiac troponin I antigen and its antibody that might have blocked the electron transfer via $[Fe(CN)_6]^{3-/4-}$ [23]. In Fig. 6(b), calibration plot was obtained between response peak current and different cTnI concentration. It was observed that the DPV peak current varies linearly with a logarithmic cTnI concentration in the linearity range of 0.01–250 ng/mL, obeying equation (2).

$$I = 0.1587\ (mA) - 0.01456\ (mA) * log\left[cTnI\ concentration\left(ng\ mL^{-1}\right)\right] \quad (2)$$

The sensitivity of 58.24 μA/cm^2per decade is estimated from the slope of the calibration curve with regression coefficient as 0.989. Further, this immunosensor can detect cTnI concentration as low as 0.01 ng/mL. A control experiment (inset, Fig. 6 (b)) was performed in the presence of cTnI concentrations (0.01–250 ng/mL), to check for any non-specific adsorption of the antigen molecule to the electrode surface in the absence of antibodies. However, no

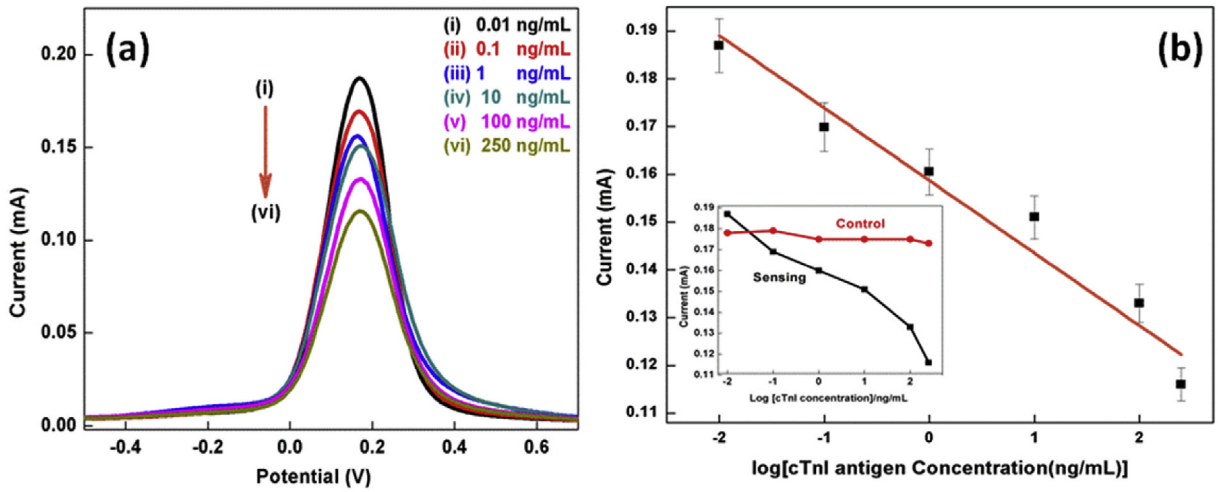

Fig. 6. (a) The differential pulse voltammetry (DPV) responses of the EA/anti-cTnI/APTES/WO_3-RGO nanocomposite/ITO immunoelectrode obtained as a function of cTnI concentrations (0.01–250 ng/mL) and (b) Calibration plot between the DPV peak current and the logarithm of cTnI concentrations (0.01–250 ng/mL); inset: control study.

remarkable change was observed in the current response revealing that cTnI antigen specifically interacts with the EA/anti-cTnI/APTES/WO3-RGO nanocomposite/ITO immunoelectrode.

The reproducibility of the EA/anti-cTnI/APTES/WO_3-RGO nanocomposite/ITO immunosensor was examined by measuring the DPV current response in the presence of cTnI (0.01 ng/mL) on four independently fabricated immunoelectrode prepared under identical conditions (Fig. 7(a)). The relative standard deviation (RSD) was studied to evaluate the reproducibility of the electrodes. It was found that the immunoelectrode shows good reproducibility for four different electrodes with low value of RSD of 4.36% with an average current of 200 μA. The low value of RSD obtained for each electrode comes within the acceptable error range under the tested conditions, suggesting a good reproducibility.

For a clinical purpose, a sensor must possess high specificity for the target biomolecule compared to other interfering protein biomarkers present in the blood serum. Hence, the specificity of the fabricated immunosensor was evaluated using different interferents such as Carcinoembryonic antigen (CEA), Cytokeratin-19 antigen (CYFRA), endotheline one protein (ET), C-reactive protein (CRP) and Myoglobin (Mb) as shown in Fig. 7(b). The magnitude of DPV current response for the EA/anti-cTnI/APTES/WO_3-RGO nanocomposite/ITO immunoelectrode (shown as blank in Fig. 7(b)) has been observed as 0.209 mA. After that, the current response of the immunoelectrode has been taken in the presence of above interferents each of concentration 5 ng/mL with 10 min incubation. Although we observed some signal variation, there was no prominent alteration in the current response in the presence of each interferent as compared to the blank electrode. However, on the addition of cTnI protein, a remarkable reduction of current was observed. This specificity of the immunoelectrode can be attributed to the fact that all other protein biomarkers could not able to bind with anti-cTnI antibody functionalized on the APTES/RGO-WO_3 nanocomposite surface.

Further, for clinical application, the developed immunosensor was utilized to measure cTnI concentration in human serum obtained from pathology laboratory (Dr. Lal path lab, Rohini, Delhi). The DPV current response is recorded for four different real samples and those for standard samples of the same concentrations. The results are shown in Fig. 7(c) reveals a low RSD value for the current responses obtained for real and standard samples. This indicates that the developed detection strategy might be preliminarily applicable for the determination of cTnI in human serum for routine clinical diagnosis.

The shelf life of the proposed immunosensor was also monitored by measuring DPV current response in the presence of 0.01 ng/mL cTnI with a regular interval of 1 week. The immunoelectrode retains its activity up to four weeks with the decrease in

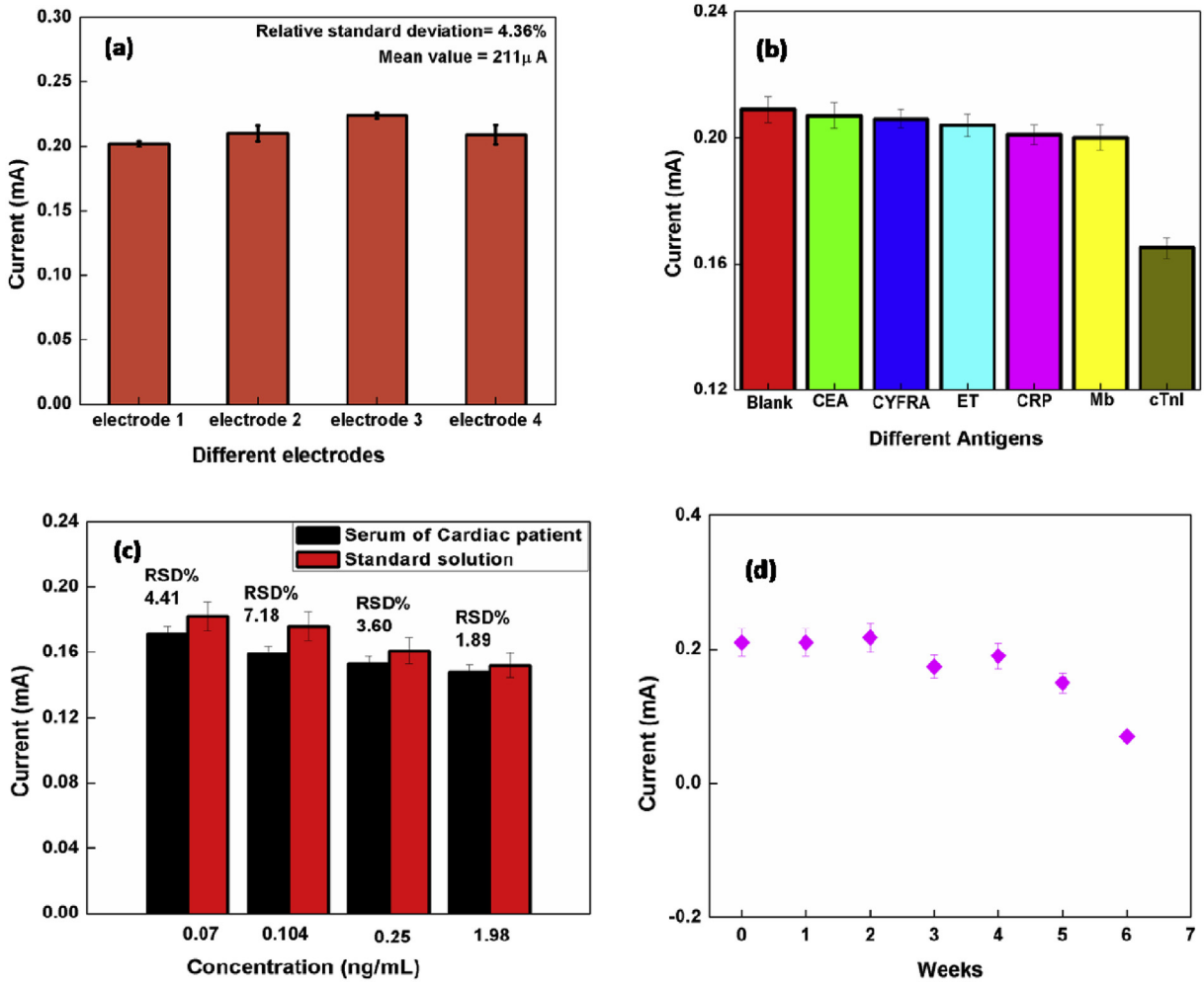

Fig. 7. (a) Electrochemical current response of different EA/anti-cTnI/APTES/WO_3-RGO nanocomposite/ITO immunoelectrode fabricated under identical condition with cTnI (0.01 ng/mL), (b) Electrochemical current response of the immunoelectrode in the presence of different interferent (c) Real sample analysis study and (d) Shelf life studies of EA/anti-cTnI/APTES/WO_3-RGO nanocomposite/ITO immunoelectrode.

Table 1
Comparative analysis of fabricated immunosensor for the detection of cardiac biomarker troponin I along with those reported in the literature.

Sensing platform	Detection technique	Detection range	Sensitivity (S)	Detection limit	Stability	Reference
Conducting paper	CV	1-100 ng/mL	5.5μA/ngmL^{1}cm^{-2}	–	–	[24]
Porous GO/GCE	EIS	0.1–10 ng/mL	–	0.07 ng/mL	–	[25]
Pt/Graphene sheet/GCE	EIS	0.01–10 ng/mL	80 Ω cm^2 per decade	4.2 pg/mL	–	[26]
Au/GO/GCE	Amperometric	0.05–3.0 ng/mL -	–	0.05 ng/mL	30 days	[27]
APTES/WO_3-RGO nanocomposite	**DPV**	**0.01–250 ng/mL**	**58.24μA/cm^{2}per decade**	**0.01 ng/mL**	**30 days**	**Present work**

current as 8% when stored in refrigerated conditions at 4 °C, implying that cTnI antibody has been immobilized on APTES/WO_3-RGO nanocomposite/ITO matrix with its bioactivity well preserved. A comparative analysis of presently fabricated immunoelectrode with previously reported electrode materials has shown in Table 1. The proposed WO_3-RGO nanocomposite based immunosensor exhibits improved linearity and sensitivity as compared to these methods.

4. Conclusions

In summary, a hydrothermally synthesized tungsten trioxide-reduced graphene oxide (WO_3-RGO) nanocomposite based electrochemical immunosensor was fabricated for the cardiac biomarker detection. A thin film of APTES/WO_3-RGO nanocomposite/ITO was obtained using electrophoretic deposition technique, followed by covalent immobilization of antibody of cTnI for the label-free electrochemical detection of cTnI using DPV technique. The heterogeneous electron transfer kinetics of WO_3-RGO nanocomposite found to be superior as compared to that of bare WO_3 resulting in the high performance of the immunosensor. The electrochemical measurements showed that the proposed immunosensor exhibit a good sensitivity of 58.24 μA/cm^2 per decade in a wide detection range of 0.01–250 ng/mL. This superior performance can be attributed to: (i) strong covalent coupling of antibody molecules to WO_3-RGO nanocomposite matrix through APTES which leads to the high stability of the device, (ii) large oxygen moieties present in WO_3 leading to increased antibody loading capacity resulting in wider detection range and lastly, (iii) strong synergistic effect between WO_3-RGO nanocomposite that has enhanced the electron transfer kinetics. The study of real sample analysis has also revealed an excellent correlation between the current response of standard and real samples of cardiac troponin I (cTnI). Thus all these features is responsible for high sensing performance of the proposed electrochemical immunosensor.

Conflicts of interest

There are no conflicts to declare.

Acknowledgements

The authors thank Prof. Yogesh Singh, Vice-chancellor, Delhi Technology University, Delhi, India for providing the research facilities. The financial support received from IUAC sponsored project (Grant No. IUAC/XIII.7/UFR-56324), Department of Atomic Energy -Board of Research in Nuclear Sciences (DAE-BRNS), India and Department of Science and Technology, India (Grant No. IFA14-MS-34) are gratefully acknowledged.

Appendix A. Supplementary data

Supplementary data related to this article can be found at https://doi.org/10.1016/j.jallcom.2018.04.293.

References

[1] M. Fathil, M.M. Arshad, S.C. Gopinath, U. Hashim, R. Adzhri, R. Ayub, A. Ruslinda, A. Azman, M. Zaki, T.-H. Tang, Diagnostics on acute myocardial infarction: cardiac troponin biomarkers, Biosens. Bioelectron. 70 (2015) 209–220.
[2] X. Han, S. Li, Z. Peng, A.M. Othman, R. Leblanc, Recent development of cardiac troponin I detection, ACS Sens. 1 (2016) 106–114.
[3] F.S. Apple, P.O. Collinson, I.T.F.o.C.A.o.C. Biomarkers, Analytical characteristics of high-sensitivity cardiac troponin assays, Clin. Chem. 58 (2012) 54–61.
[4] A.S. Ahammad, Y.-H. Choi, K. Koh, J.-H. Kim, J.-J. Lee, M. Lee, Electrochemical detection of cardiac biomarker troponin I at gold nanoparticle-modified ITO electrode by using open circuit potential, Int. J. Electrochem. Sci. 6 (2011) 1906–1916.
[5] Y. Lin, Q. Zhou, D. Tang, R. Niessner, D. Knopp, Signal-on photoelectrochemical immunoassay for aflatoxin B1 based on enzymatic product-etching MnO2 nanosheets for dissociation of carbon dots, Anal. Chem. 89 (2017) 5637–5645.
[6] K. Zhang, S. Lv, Z. Lin, D. Tang, CdS: Mn quantum dot-functionalized gC 3 N 4 nanohybrids as signal-generation tags for photoelectrochemical immunoassay of prostate specific antigen coupling DNAzyme concatamer with enzymatic biocatalytic precipitation, Biosens. Bioelectron. 95 (2017) 34–40.
[7] Z. Qiu, J. Shu, D. Tang, Near-Infrared-to-Ultraviolet light-mediated photoelectrochemical aptasensing platform for cancer biomarker based on core–shell NaYF4: Yb, Tm@ TiO2 upconversion microrods, Anal. Chem. 90 (2017) 1021–1028.
[8] G. Liu, Y. Lin, Nanomaterial labels in electrochemical immunosensors and immunoassays, Talanta 74 (2007) 308–317.
[9] Q. Xiang, The development and application of electrochemical biosensor, in: International Conference on Information and Management Engineering, Springer, 2011, pp. 215–220.
[10] J. Shu, D. Tang, Current advances in quantum-dots-based photoelectrochemical immunoassays, Chem. An Asian J. 12 (2017) 2780–2789.
[11] J. Shu, Z. Qiu, S. Lv, K. Zhang, D. Tang, Plasmonic enhancement coupling with defect-engineered TiO2–x: a mode for sensitive photoelectrochemical biosensing, Anal. Chem. 90 (2018) 2425–2429.
[12] P.R. Solanki, A. Kaushik, V.V. Agrawal, B.D. Malhotra, Nanostructured metal oxide-based biosensors, NPG Asia Mater. 3 (2011) 17.
[13] Z. Qiu, J. Shu, D. Tang, Bioresponsive release system for visual fluorescence detection of carcinoembryonic antigen from mesoporous silica nanocontainers mediated optical color on quantum dot-enzyme-impregnated paper, Anal. Chem. 89 (2017) 5152–5160.
[14] L. Santos, C.M. Silveira, E. Elangovan, J.P. Neto, D. Nunes, L. Pereira, R. Martins, J. Viegas, J.J. Moura, S. Todorovic, Synthesis of WO 3 nanoparticles for biosensing applications, Sens. Actuators B Chem. 223 (2016) 186–194.
[15] C. Hu, T. Lu, F. Chen, R. Zhang, A brief review of graphene–metal oxide composites synthesis and applications in photocatalysis, J. Chin. Adv. Mater. Soc. 1 (2013) 21–39.
[16] L. Fu, T. Xia, Y. Zheng, J. Yang, A. Wang, Z. Wang, Preparation of WO 3-reduced graphene oxide nanocomposites with enhanced photocatalytic property, Ceram. Int. 41 (2015) 5903–5908.
[17] Q. Zhou, Y. Lin, K. Zhang, M. Li, D. Tang, Reduced graphene oxide/BiFeO3 nanohybrids-based signal-on photoelectrochemical sensing system for prostate-specific antigen detection coupling with magnetic microfluidic device, Biosens. Bioelectron. 101 (2018) 146–152.
[18] X. An, C.Y. Jimmy, Y. Wang, Y. Hu, X. Yu, G. Zhang, WO 3 nanorods/graphene nanocomposites for high-efficiency visible-light-driven photocatalysis and NO 2 gas sensing, J. Mater. Chem. 22 (2012) 8525–8531.
[19] A. Radu, G. Truica, R. Penu, V. Moroeanu, S.C. Litescu, Use of the Fourier transform infrared spectroscopy in characterization of specific samples, UPB Sci. Bull. B Chem. Mater. Sci. 74 (2012) 137–148.
[20] M.A. Ali, C. Singh, K. Mondal, S. Srivastava, A. Sharma, B.D. Malhotra, Mesoporous few-layer graphene platform for affinity biosensing application, ACS Appl. Mater. Interfaces 8 (2016) 7646–7656.
[21] C.I. Vargas-Consuelos, K. Seo, M. Camacho-López, O.A. Graeve, Correlation between particle size and Raman vibrations in WO3 powders, J. Phys. Chem. C 118 (2014) 9531–9537.
[22] M. Cell, Electrochemical Impedance Spectroscopy (EIS): A Powerful and Cost-Effective Tool for Fuel Cell Diagnostics.
[23] S. Kumar, J.G. Sharma, S. Maji, B.D. Malhotra, Nanostructured zirconia decorated reduced graphene oxide based efficient biosensing platform for non-invasive oral cancer detection, Biosens. Bioelectron. 78 (2016) 497–504.

[24] K.K. Jagadeesan, S. Kumar, G. Sumana, Application of conducting paper for selective detection of troponin, Electrochem. Commun. 20 (2012) 71–74.
[25] S.H. Kazemi, E. Ghodsi, S. Abdollahi, S. Nadri, Porous graphene oxide nanostructure as an excellent scaffold for label-free electrochemical biosensor: detection of cardiac troponin I, Mater. Sci. Eng. C 69 (2016) 447–452.
[26] S. Singal, A.K. Srivastava, A.M. Biradar, A. Mulchandani, Pt nanoparticles-chemical vapor deposited graphene composite based immunosensor for the detection of human cardiac troponin I, Sensor. Actuator. B Chem. 205 (2014) 363–370.
[27] G. Liu, M. Qi, Y. Zhang, C. Cao, E.M. Goldys, Nanocomposites of gold nanoparticles and graphene oxide towards an stable label-free electrochemical immunosensor for detection of cardiac marker troponin-I, Anal. Chim. Acta 909 (2016) 1–8.

Journal of MATERIALS RESEARCH

Article
DOI: 10.1557/jmr.2018.481

Protein-functionalized WO_3 nanorods–based impedimetric platform for sensitive and label-free detection of a cardiac biomarker

Deepika Sandil[1], Suresh C. Sharma[2], Nitin K. Puri[2,a)]

[1]Advanced Sensor Laboratory, Department of Applied Physics, Delhi Technological University, Delhi 110042, India; and Department of Applied Physics, Bhagwan Parshuram Institute of Technology, Delhi 110089, India
[2]Advanced Sensor Laboratory, Department of Applied Physics, Delhi Technological University, Delhi 110042, India
[a)]Address all correspondence to this author. e-mail: nitinkumarpuri@dtu.ac.in, nitinpuri2002@yahoo.co.in

Received: 6 September 2018; accepted: 26 November 2018

We report the development of a sensitive and a label-free electrochemical immunosensing platform for the detection of cardiac biomarker troponin I (cTnI) using tungsten trioxide nanorods (WO_3 NRs). The low-temperature hydrothermal technique was employed for the controlled synthesis of WO_3 NRs. Thin films of 3-aminopropyltriethoxy saline (APTES)-functionalized WO_3 NRs were deposited on indium tin oxide (ITO)-coated glass substrate (0.5 cm × 1 cm) using electrophoretic deposition technique. The covalent immobilization of cTnI antibody onto functionalized WO_3 NRs electrode was accomplished using EDC-NHS [1-(3-(dimethylamino)-propyl)-3-ethylcarbodiimide hydrochloride and *N*-hydroxysulfosuccinimide] chemistry. The structural and morphological characterizations of WO_3 NRs and functionalized WO_3 NRs were studied using X-ray diffraction, field emission scanning electron microscopy, transmission electron microscopy, Fourier transform infrared spectroscopy, and electrochemical techniques. The impedimetric response study of the proposed immunosensor demonstrates high sensitivity [6.81 KΩ mL·cm^2)] in a linear detection range of 0.01–10 ng/mL. The excellent selectivity, good reproducibility, and long-term stability of the proposed immunosensing platform indicate WO_3 NRs as a suitable platform for the development of a point-of-care biosensing device for cardiac detection.

Introduction

In recent times, nanotechnology-based research has uncovered a multitude of novel materials suitable for the designing of biosensors. Among the numerous nanomaterials, metal oxide–based nanomaterials have been considered significant due to their great efficacy, nontoxicity, functional biocompatibility, and catalytic behavior [1, 2]. And among different morphologies, one-dimensional (1D) materials such as nanowires, nanorods, and nanofibers possess distinct features, such as enhanced electronic properties, unique catalytic activities, and high surface area. Such excellent properties of 1D material make it a promising platform for the development of biosensors by providing high signal-to-noise ratio, higher sensitivity, large surface area, and shorter response time [3, 4, 5, 6]. Recently, Augustine et al. have developed the 1D metal oxide–based platform for cancer detection [7]. Zhao et al. had developed ZnO nanowire–based electrochemical biosensor for L-lactic acid amperometric detection [8]. All these results indicate that 1D metal oxide–based materials can be ideal candidates for the development of sensitive biosensors.

The nanostructured tungsten trioxide (nWO_3) is an *n*-type semiconductor and has gained increasing attentions due to its potential in various fields such as electrochromic devices, photo-oxidation, solar cell devices, and sensors [9, 10, 11, 12]. It belongs to the family of transition metal oxide with electronic conformations of d^0 and d^{10}, which exhibits stimulating characteristics and steadiness important for the sensing uses. High electroactive surface area, fast electron transfer kinetics, and enhanced electrochemical properties are some of the important characteristics of nWO_3 that makes it an ideal candidate as a sensing electrode [13, 14, 15]. Owing to these exclusive electrochemical properties, nWO_3 can be considered as an ideal platform for sensing applications. Zhou et al. demonstrated the use of Na-doped tungsten trioxide

nanorods (WO_3 NRs) as a sensing platform for the detection of BPA [16]. Santos et al. fabricated nitrite biosensor based on WO_3 nanoparticles [14]. Indeed, the versatile properties of nWO_3, such as high sensitivity, biocompatibility, and reversible kinetics, make nWO_3 as a promising platform for the construction of biosensing electrodes. WO_3 nanostructures, such as nanorods, nanofibers, and nanobelts, have shown remarkable performance by providing high electrical and thermal electron transport kinetics due to the quantum confinement along with flexibility that can enable the physical manipulation of its structure. Also, electrical conductivity of these highly confined structures becomes very sensitive to the presence of ions and other carriers [17]. In this work, we report the synthesis of hexagonal phase WO_3 NRs using a facile hydrothermal method. And as-synthesized WO_3 NRs were used as an immobilized matrix for the fabrication of biosensing platform.

Acute myocardial infarction (AMI) is one of the severe cardiac vascular diseases. Bad cholesterol, saturated fats, trans-fat, and high blood pressure are few of the leading causes of the AMI. Different conventional methods have been in use for the detection of AMI, including enzyme-linked immunosorbent assay (ELISA), radioimmunoassay, and fluoroimmunoassay. However, these methods are complex, expensive, and time-consuming and need experts for the analysis. The biosensor in this regard can be seen as an alternative technique for the detection of AMI diseases as it offers simplicity in processing, low cost, high sensitivity, small sample volume, and portability [18]. It confers the exquisite specificity and sensitiveness of biomolecules in conjunction with a physicochemical transducer, which carries out the biointeraction measurements with real-time, ease, and simple-to-use formats. Among the various studied biosensors, such as optical, electrical, and electrochemical, the electrochemical immunosensors are gaining significant attention as a label-free, fast, portable, and reliable analytical tool for clinical diagnostics and environmental monitoring and in health care [19, 20, 21]. The electrochemical immunosensors are based on specific antigen–antibody interaction and considered as a most sensitive detection tool in diagnosis because of its fast driven analysis, simplicity in its functioning, precise measurement, and ease of fabrication. For successful development of an electrochemical immunosensor, the immobilization of biomolecules and amplification of response signal are the primary requisite [22]. Nanostructured metal oxides in this context have been preferred as an immobilized matrix due to their strong adherence behavior, chemical stability, and high catalytic activity [1, 2, 22].

Cardiac biomarkers are known to play a significant role in the development of biosensors as point-of-care (POC) devices [23]. They are used in the diagnosis of AMI by detecting the myocardial damage in the cells. These cardiac biomarkers are helpful in the diagnosis of the patient with ischemic chest pain not only with diagnostic ECG but also with non-diagnostic ECG. Among different cardiac biomarkers studied, myoglobin (Mb), creatine kinase-MB (CK-MB) isoenzyme, and cardiac troponin I (cTnI) have been found to be specific biomarkers present only in cardiac muscles. However, cardiospecificity of cTnI and long persistence of it in the blood circulation make it a principal biochemical marker of the cardiac injury [24, 25]. cTnI is a protein with a molecular weight of 29 kDa and is one of the subunits of troponin complex present in cardiac muscles. It gets released into the blood serum within 3–5 h after the onset of cardiac injury, crossing the normal limit value of the healthy humans (<0.5 ng/mL) and remains elevated for 6–10 days. The concentration of cTnI in patients ranging from 0.6 to 1 ng/mL indicates minor damage to the cells, whereas more than 1 ng/mL remarks the risk for future heart injuries. Thus, monitoring the concentration of cTnI in serum at an early stage will be clinically significant as the diagnostic tool [26].

Here, we demonstrate the application of WO_3 NR–based immunosensing platform for the label-free electrochemical detection of cardiac biomarker. The structural and electrochemical characteristics of the fabricated platform have been characterized using various spectroscopic techniques. Through this work, the author has strived to present the suitability and applications of nWO_3 in the field of biosensing.

Results and discussions

Microscopic and structural studies

The crystallinity of the hydrothermally synthesized WO_3NRs was studied using X-ray diffraction (XRD) pattern, as shown in Fig. 1. The high-intense diffraction peaks observed at two-theta value 23.1°, 28.22°, 36.75°, 49.8°, and 56.2° correspond to (002), (200), (202), (220), and (204) crystal planes of WO_3 of

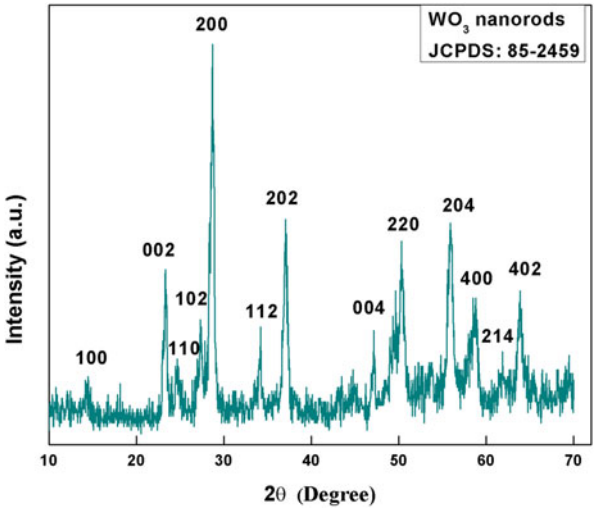

Figure 1: XRD pattern of hydrothermally synthesized nWO_3.

hexagonal phase, respectively. The other major diffraction peaks observed at 14.01°, 24.3°, 27.2°, 33.8°, 47.4°, 58.12°, 61.98°, and 63.45° correspond to (100), (110), (102), (112), (004), (400), (214), and (402) crystal planes, respectively, indicating the formation of pure hexagonal WO_3 phase (JCPDS 85-2459). The average crystallite size of WO_3 NRs was calculated using the Debye–Scherrer's equation given as follows:

$$d = 0.89\lambda/\beta\cos\theta \quad , \tag{1}$$

where λ (1.540 Å) corresponds to X-ray wavelength and β and θ represent full width at half maximum and Bragg's angle, respectively. The calculated crystallite size of WO_3 NRs was found to be 68 nm.

Figure 2 represents the micrographs depicting the morphological structure of the synthesized WO_3 sample, as examined under a field emission scanning electron microscope (FESEM) and transmission electron microscope (TEM). FESEM micrograph observed at low magnification [Fig. 2(a)] revealed that the synthesized sample has a morphological structure of nanorods grown in large scale, and at high magnification [Fig. 2(b)], we observed existence of nanorods bundles with inhomogeneous distribution. The estimated diameter of these nanorods was found as 50 ± 30 nm. The selected area electron diffraction [Fig. 2(c)] pattern showed that the synthesized WO_3 NRs were single crystalline and grown along [002], [112], and [204] directions. These results were in good agreement with the XRD studies. The TEM image [inset, Fig. 2(c)] also revealed the existence of bundles of rods with variable length ranging from hundreds of nanometers to few micrometers and that of diameter in the range of 50–100 nm.

Spectroscopic analysis

Fourier transform infrared (FT-IR) spectroscopic study was performed to investigate the presence of chemical bonds at the different stages of functionalization and immobilization process. Figure 3 represents the FT-IR spectra of the (i) 3-aminopropyltriethoxy saline (APTES)/WO_3 NRs/ITO (indium tin oxide), (ii) cardiac troponin I antibody (anti-cTnI)/APTES/WO_3 NRs/ITO, and (iii) ethanolamine (EA)/anti-cTnI/APTES/WO_3 NRs/ITO. The APTES/WO_3 NRs/ITO electrode exhibited characteristic bands of WO_3 at 1408 cm^{-1} and 823 cm^{-1}, which correspond to ν(W–O) and ν (W–O_{inter}–W) stretching vibration of the oxygen, respectively [27, 28]. The bands observed at 1623 and 3437 cm^{-1} indicate the presence of free –NH_2 groups in APTES molecule [29, 30]. Also, the additional band seen at 2942 cm^{-1} and 1109 cm^{-1} can be assigned to C–H bonds of aldehydes groups present on the APTES molecule surface and stretching mode of Si–O–Si, respectively [31]. After covalent immobilization of anti-cTnI, the bands observed at 1249 and 1384 cm^{-1} indicate the formation of an amide bond (C–N) between amino groups of APTES and –COOH groups of anti-cTnI. Furthermore, the bands observed at 1567 and 1643 cm^{-1} can assign to N–H bending of amide II and amide I of carbonyl stretching mode [32]. Also, few of the bands were found to be shifted on antibody immobilization. All these results indicate successful immobilization of antibody biomolecule on the functionalized matrix. Furthermore, with the incorporation of EA on the immobilized matrix, we observed no changes in the band's position, rather the intensity of the bands get reduced due to the insulating nature of EA.

Electrochemical characterizations

The electrochemical characteristics of the fabricated sensing platform were investigated using cyclic voltammetry (CV) and electrochemical impedance spectroscopic (EIS) techniques. CV has been widely studied in determining the qualitative information of electrochemical kinetics of the fabricated electrode. The cyclic voltammograms of (i) APTES/WO_3NRs/ITO,

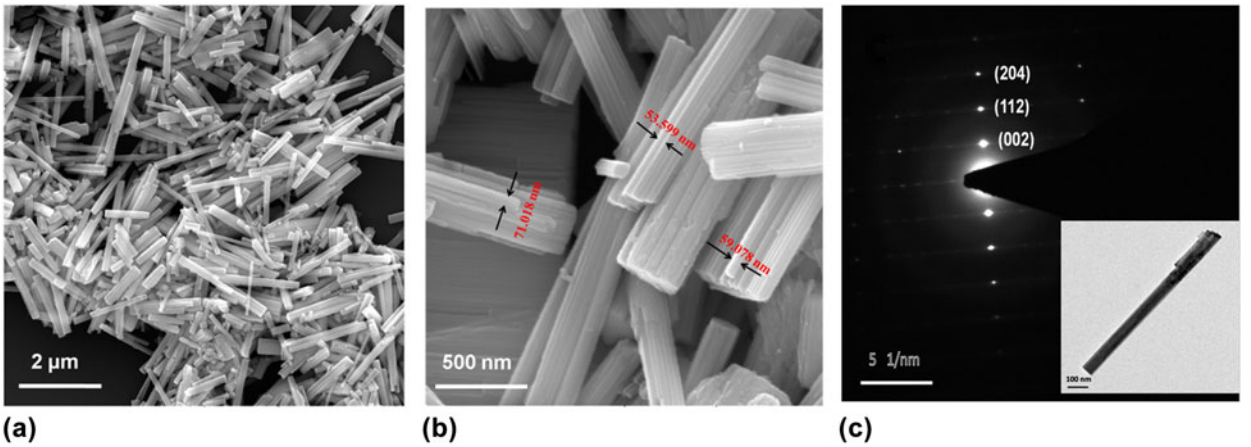

Figure 2: FESEM micrograph of WO_3 NRs (a) at low magnification and (b) at high magnification, and (c) selected area electron diffraction image of WO_3 NRs. Inset: TEM image of WO_3 NRs.

(ii) anti-cTnI/APTES/WO_3NRs/ITO, and (iii) EA/anti-cTnI/APTES/WO_3NRs/ITO, as shown in Fig. 4(a), were obtained at the scan rate of 50 mV/s in a phosphate buffered saline (PBS, pH 7.4) coupled with five millimolar $[Fe(CN)_6]^{3-/4-}$. The magnitude of the oxidation peak current to the reduction peak current (i_a/i_c = 1.05) for APTES/WO_3NRs/ITO electrode showed the reversible process of the redox couple $[Fe(CN)_6]^{3-/4-}$. Furthermore, the anodic peak current for anti-cTnI/APTES/WO_3NRs/ITO immunoelectrode (0.303 mA) was found to be lower than that for APTES/WO_3 NRs/ITO electrode (0.347 mA), indicating decreased in electron transfer at the electrode interface due to the insulating nature of the immobilized antibodies of cTnI. The incorporation of EA on immunoelectrode further decreases the magnitude of the current value to 0.230 mA. This was due to the nonspecific adsorption of EA that blocked the non-specific active sites present on the antibody immobilized surface of the immunoelectrode. All these results indicate the successful fabrication of immunosensing platform.

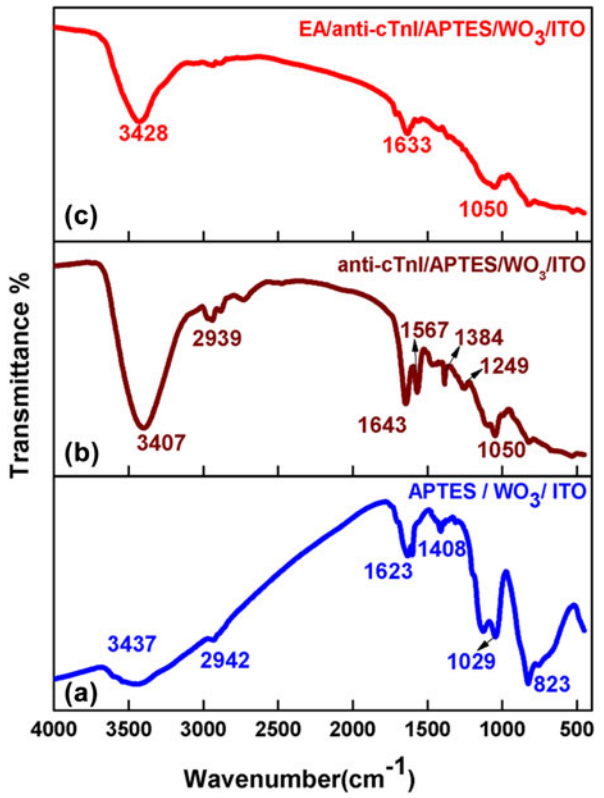

Figure 3: FT-IR spectra of (a) APTES/WO_3 NRs/ITO electrode, (b) anti-cTnI/APTES/WO_3 NRs/ITO immunoelectrode, and (c) EA/anti-cTnI/APTES/WO_3 NRs/ITO immunoelectrode.

Furthermore, the EIS study was also carried out to study the interfacial properties between the fabricated electrode surface and the electrolyte in the frequency range of 0.01–10^5 Hz. The experimental data of EIS were modeled using an equivalent circuit known as Randles circuit. The circuit consisted of Warburg impedance (Z_W), double-layer capacitance (C_{dl}), solution resistance (R_S), and the electron transfer resistance (R_{CT}). Figure 4(b) represents the EIS spectra (Nyquist plot) of the (i) APTES/WO_3NRs/ITO, (ii) anti-cTnI/APTES/WO_3NRs/ITO, and (iii) EA/anti-cTnI/APTES/WO_3 NRs/ITO immunoelectrode that was obtained on an Autolab potentiostat/galvanostat system. From the EIS spectra, the R_{CT} value of APTES/WO_3 NRs/ITO electrode was found to be 2.15 KΩ, which increased to 2.34 KΩ after antibody immobilization. This increased impedance revealed the insulating nature of the antibody. Furthermore, with the incorporation of EA molecules that covered the nonspecific sites of the immunoelectrode, the charge transfer phenomenon again gets hindered, resulting in

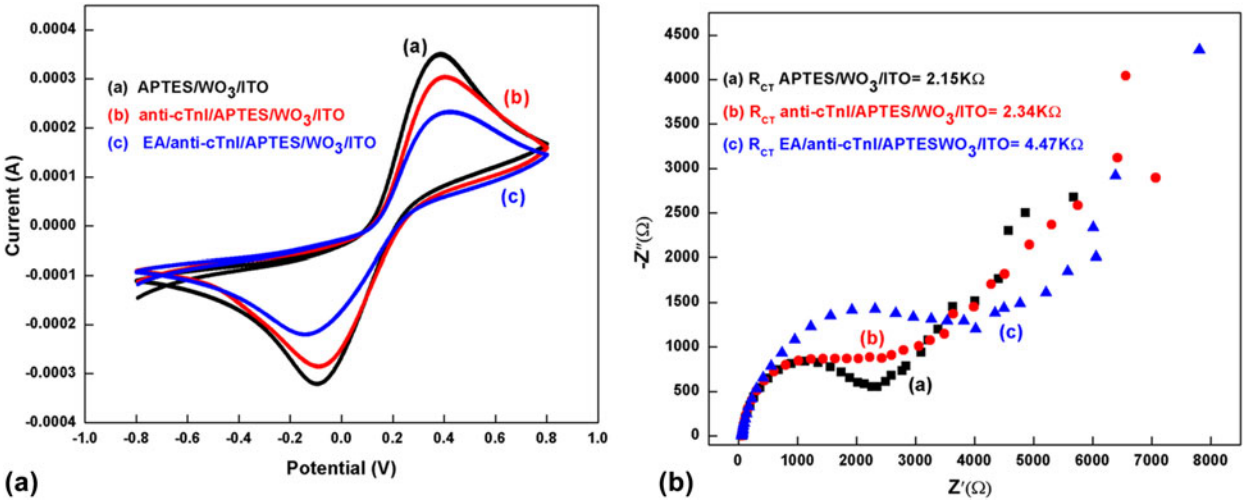

Figure 4: (a) Cyclic voltammogram (CV) of the different modified electrodes in PBS (pH = 7.4) at the scan rate of 50 mV/s. (b) The EIS spectra of the modified electrodes in the frequency range 0.01–10^5 Hz.

increase in R_{CT} value to 4.47 KΩ. Moreover, these electrodes were also characterized by evaluating heterogeneous electron transfer constant (K_O) using Eq. (2):

$$K_O = \frac{RT}{n^2F^2AR_{CT}C} \quad , \tag{2}$$

where T represents temperature, R is the gas constant, n is the total number of electrons transferring constant, F is the Faraday's constant, C is the bulk concentration of the redox couple, and A is the effective area of the electrode. The value of K_O estimated for APTES/WO_3NRs/ITO electrode (9.91×10^{-5} cm/s) was found to be high compared with that of EA/anti-cTnI/APTES/WO_3NRs/ITO immunoelectrode (4.47×10^{-5} cm/s), thus demonstrating faster electron transfer kinetics at the interface of the electrode. The cyclic voltammogram response of EA/anti-cTnI/APTES/WO_3 NRs/ITO immunoelectrode was also studied as a function of scan rate (40–160 mV/s), as shown in Fig. 5(a). The magnitude of both anodic peak current (I_{pa}) and cathodic peak current (I_{pc}) of the response exhibited a linear relationship with the square root of scan rate [Fig. 5(b)], revealing a diffusion-controlled process of the electrochemical reaction [Eqs. (3) and (4)].

$$I_{pa} = 0.022 \text{ mA} + \left[0.0287 \text{ mA(s/mV)} \times (\text{scan rate [mV/s]})^{1/2}\ R^2 = 0.0990\right] \quad , \tag{3}$$

$$I_{pc} = -0.0528 \text{ mA} + \left[-0.0225 \text{ mA(s/mV)} \times (\text{scan rate [mV/s]})^{1/2}\ R^2 = 0.0989\right] \quad . \tag{4}$$

Also, it was observed that with an increase in scan rate, there was a positive shift in the oxidation peak potential (V_{pa}) and negative shift in the reduction peak potential (V_{pc}), and linearity was seen between redox peak potential shifts ($\Delta E = V_{pa} - V_{pc}$) and the square root of the scan rate for the EA/anti-cTnI/APTES/WO_3 NRs/ITO immunoelectrode, satisfying Eq. (5). From Fig. 5(c), we observe an appreciable linear fitting, suggesting a facile electron transport from electrolyte to the electrode surface.

$$\Delta E(\text{V}) = 0.422 \text{ V} + \left[0.025 \text{ V(s/mV)} \times (\text{scan rate [mV/s]})^{1/2}\right], \quad R^2 = 0.997 \quad . \tag{5}$$

Electrochemical response investigations

The investigation of the electrochemical response studies of the fabricated immunoelectrode as a function of cTnI concentration (0.01–10 ng/mL) was performed using the EIS technique. Figure 6(a) represents the Nyquist plot of EIS performed in a PBS solution [pH = 7.4, containing $[Fe(CN)_6]^{3-/4-}$] (inset: Randles circuit). The transportation of electrochemically produced charge at the interface of electrode and electrolyte has been modeled by measuring the change in resistance. The charge transfer resistance (R_{CT}), which corresponds to the diameter of the semicircle of the Nyquist plot, has been measured using NOVA software. The R_{CT} value of the EA/anti-cTnI/APTES/WO_3 NRs/ITO immunoelectrode increased with the increase in cTnI concentration. This increase in impedance revealed the formation of insulating antigen–antibody complex produced due to the specific key–lock interaction of the anti-cTnI and cTnI, which might have hindered the electron motion. The obtained calibration plot between R_{CT} value and the cTnI concentration is shown in Fig. 6(b). The value of R_{CT} varies linearly with the cTnI concentration up to 1 ng/mL and obeys Eq. (6).

$$R_{CT} = 2.12\ (\text{K}\Omega) + 1.723\ (\text{K}\Omega \cdot \text{mL}/(\text{ng} \cdot \text{cm}^2)) \times [\text{concentration (ng/mL)}] \quad , \tag{6}$$

with regression coefficient (R^2) = 0.995.

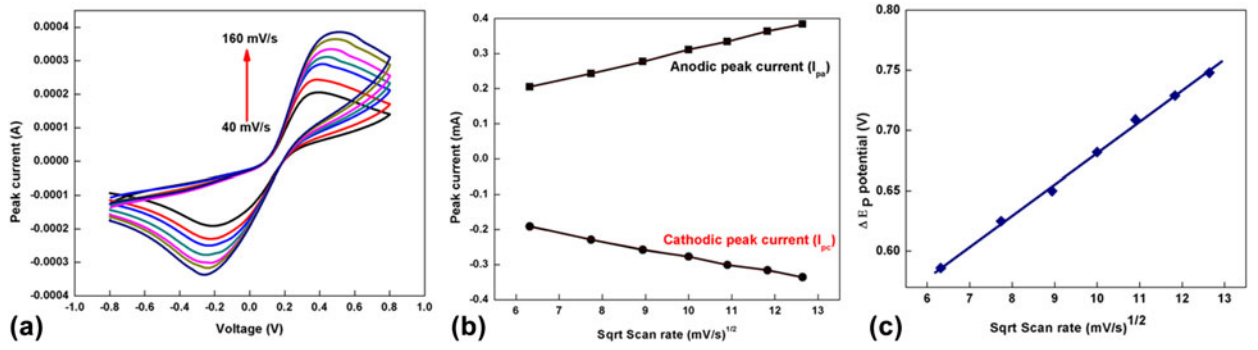

Figure 5: (a) CV response of EA/anti-cTnI/APTES/n-WO_3/ITO immunoelectrode as a function of scan rate (40–160 mV/s). (b) Variation of anodic peak current (I_{pa}) and cathodic peak current (I_{pc}) with respect to square root of the scan rate. (c) Variation of redox peak potential difference with respect to square root of scan rate.

We observed that APTES/WO_3 NRs/ITO–based immunoelectrode exhibits good sensitivity as 6.81 [KΩ·ml/(ng·cm^2)] in a linear detection range of 0.01–1 ng/mL. This high sensitivity exhibited by the immunoelectrode can be attributed to the presence of WO_3 NRs in the matrix that perhaps provided the enhanced charge conduction channel for the electron transfer kinetics. Moreover, a controlled study was conducted to investigate the electrochemical impedance response of APTES/WO_3 NRs/ITO immunoelectrode toward the cTnI antigen without using anti-cTnI [Fig. 6(b), inset]. It was found that there was no significant change in the magnitude of R_{CT} value in response to the different concentration of cTnI antigen. Hence, we can conclude that the fabricated immunosensor response was due to immunoreactions between cTnI antigen and anti-cTnI only.

The reproducibility of the EA/anti-cTnI/APTES/WO_3 NRs/ITO–based immunoelectrode was investigated by measuring the charge transfer resistance (R_{CT}) on four different fabricated immunoelectrodes prepared under ideal conditions in the presence of 0.5 ng/mL cTnI. However, no noticeable change in the R_{CT} value was observed, as seen in Fig. 7(a). The reproducibility of the immunoelectrode was estimated by evaluating relative standard deviation (RSD %). The calculated mean value of R_{CT} for these four electrodes (2.19 KΩ) with RSD of 4.14% was found to be within an acceptable error range, suggesting an excellent reproducibility of the immunoelectrode.

The selectivity study of the fabricated immunoelectrode was investigated in the presence of other interfering biomarkers, such as C-reactive protein, Mb, cytokeratin-19 antigen, and carcinoembryonic antigen, using EIS measurements. Figure 7(b) shows the interference study of the immunoelectrode, where no significant change in the R_{CT} value was observed among different interferents (concentration of each biomarker as 10 ng/mL) concerning blank immunoelectrode. However, after addition of cTnI antigen, there was a remarkable change in the R_{CT} value, which signifies the high specificity of the fabricated immunoelectrode for the cTnI biomarker.

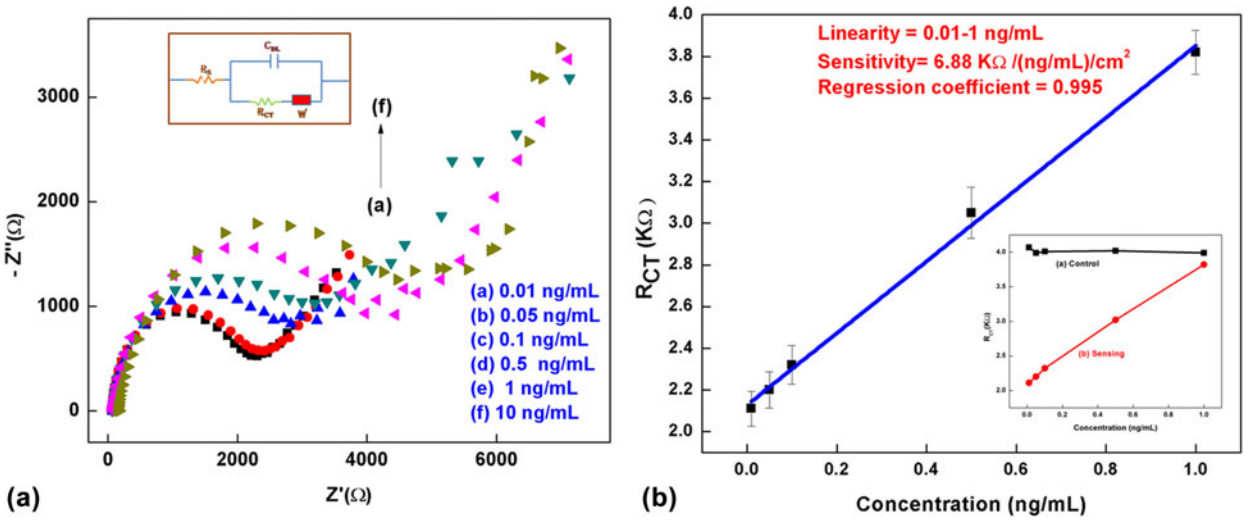

Figure 6: (a) EIS response study of the immunoelectrode as a function of cTnI antigen concentration (0.01–10 ng/mL); inset shows Randles equivalent circuit. (b) A calibration plot obtained between R_{CT} and cTnI antigen concentration; inset shows sensing along with control study.

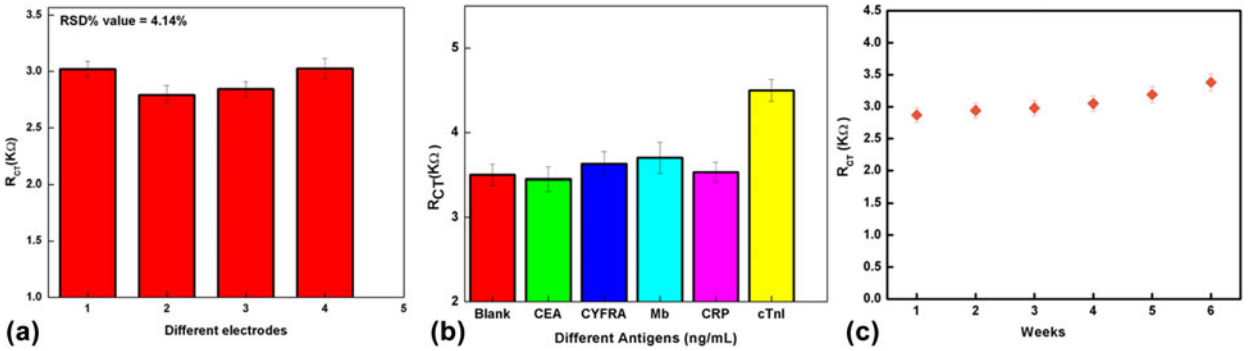

Figure 7: (a) Reproducibility study of the immunoelectrodes fabricated under identical conditions with cTnI (0.5 ng/mL). (b) Interference study of the immunoelectrode in the presence of different interferents. (c) Shelf life study of the EA/anti-cTnI/APTES/nWO_3/ITO immunoelectrode.

Furthermore, the shelf life study of the fabricated immunoelectrode was conducted by measuring R_{CT} value in the presence of 0.5 ng/mL cTnI antigen at the regular interval of 7 days [Fig. 7(c)]. The increase in R_{CT} value was found to be 7.3% up to 5 weeks after which the R_{CT} increased to more than 20% at the end of 6 weeks. Thus, the fabricated immunoelectrode retained its biological activity up to 5 weeks. Hence, all these results indicated that the EIS technique for detection of biomarkers proved to be an efficient, simple, and fast response technique. In Table I, the sensing characteristics of the fabricated immunosensor are compared with those of other reported in the literature.

Conclusion

We have developed an efficient and a label-free electrochemical sensing platform for detection of cardiac biomarker using nWO_3 NRs as an immobilized matrix. The APTES-functionalized WO_3 NRs were deposited on ITO electrode using electrophoretic deposition (EPD) technique, and subsequently, the functionalized WO_3 NRs were used as an immobilized matrix for the covalent binding of anti-cTnI biomolecules. The variation in impedance signal of the fabricated immunosensor was observed on formation of immunocomplex between anti-cTnI and cTnI antigen. The experimental results of the impedimetric studies reveal high sensitivity [6.81 KΩ·ml/(ng·cm^2)] and good reproducibility with long-term stability (5 weeks). The better performance of the proposed immunosensor can be attributed to the enhanced electrochemical and high electrocatalytic activity of WO_3 NRs, which provide high aspect ratio for increased antibody loading onto WO_3 NRs matrix. Hence, these results direct us toward the realization of integrated and portable POC diagnostic tool based on WO_3 NRs matrix.

Experimental

Materials and reagents

Sodium tungstate ($Na_2WO_4{\cdot}2H_2O$), NaCl, and HCl were used as reagents for the synthesis of WO_3 NRs. APTES, water-soluble EDC [1-(3-(dimethylamino)-propyl)-3-ethylcarbodiimide hydrochloride], EA, and *N*-hydroxysulfosuccinimide (NHS) were used for the functionalization and immobilization process and were procured from Sigma–Aldrich and Fisher Scientific. Potassium ferricyanide $K_3[Fe(CN)_6]$ and potassium ferrocyanide $K_4[Fe(CN)_6]{\cdot}3H_2O$ were also procured from Fisher Scientific. cTnI antigen and anti-cTnI were obtained from Ray Biotech, Inc. (India). PBS (pH 7.4) solution was used for the dilution of biomolecules and washing, and it was prepared using sodium monophosphate (NaH_2PO_4, 0.02 mol/L) and sodium diphosphate dihydrate ($Na_2HPO_4{\cdot}2H_2O$, 0.02 mol/L), which were procured from Fisher Scientific. All the reagents and chemicals were used without any further purification. The Milli-Q water having a resistivity of 18.3 MΩ was used for the preparation of all buffers and solutions.

Instrumentation

The crystallography of the as-synthesized material was studied using powder XRD analyzer obtained on a Bruker D-8 Advances equipped with Cu K_α radiation wavelength, λ = 0.154 nm. The morphological and structural studies were investigated using FESEM (TESCAN), TEM (JEOL), and FT-IR spectrometer (PerkinElmer). The CV and EIS studies were carried out at ambient temperature (24 °C) on an Autolab Potentiostat (the Netherlands) using NOVA software. The standard three-electrode cell configuration was used for conducting the electrochemical measurements with the fabricated electrode as the working electrode, platinum (Pt) wire as the counter electrode, and silver/silver chloride (Ag/AgCl) electrode as the reference electrode. PBS solution (50 mM, pH 7.4) containing 5 mM of [$Fe(CN)_6^{3-/4-}$] as redox species was used as an electrolyte.

Synthesis and functionalization of WO_3 NRs

Synthesis of WO_3 NRs

nWO_3 was synthesized using a hydrothermal method. First, 0.5 M sodium tungstate ($Na_2WO_4{\cdot}2H_2O$) solution was prepared in 30 mL of Milli-Q water and was stirred continuously. The pH value of the resultant solution was reduced to "2" with the addition of 6 M HCl dropwise. Further 1.2 g of NaCl was added to the solution and stirred for two hours. After two hours, the resultant solution was transferred to a 50-mL Teflon-lined vessel and placed in a stainless steel autoclave. This autoclave was then placed in an oven at 180 °C for about

TABLE I: Sensing characteristics of the WO_3 NR–based platform compared with those reported in the literature.

Sensing platform	Detection technique	Label	Detection range	Sensitivity (*S*)	Detection limit	Stability	Reference
ZnO n.ps	FET	No	1 ng/mL–10 μg/mL	35.3 nA/(g/mL)	3.24 pg/mL	...	[34]
Gold nanodumbbells	EIS	...	0.05–500 ng/mL	...	8 pg/mL	...	[35]
Carbon nanofibers	EIS	No	0.25–10 ng/mL	...	0.2 ng/mL	...	[36]
ZrO_2 n.ps	CV	No	0.1–100 ng/mL	3.9 μA·mL/(ng·cm^2)	0.1 ng/mL	...	[26]
WO_3 NRs	EIS	No	0.01–10 ng/mL	6.81 [KΩ·mL/(ng·cm^2)]	0.01 ng/mL	5 weeks	Present work

10 h for hydrothermal reaction. After this reaction period, the stainless steel autoclave was allowed to cool naturally to room temperature, and the sample was collected after centrifuging it 4–5 times with Milli-Q water. The as-synthesized sample was used for further characterization and functionalization process.

Functionalization and preparation of electrodes

The as-synthesized nanostructures were chemically modified to activate functional groups on their surfaces for the immobilization of the biomolecules. APTES is an amino-silane compound that customarily provides active amino groups ($-NH_2$) that can covalently bond with carboxyl groups (–COOH) of the antibody biomolecules [33]. APTES was thus used for the functionalization process. In brief, 100 mg of WO_3 NRs was dispersed in 30 mL of 2-propanol and sonicated to obtain a well-dispersed suspension. Next, 250 µL of APTES (98%) was added to the suspended solution and was stirred at 280 rpm for 40 h at room temperature (24 °C). The resultant functionalized WO_3 NRs were filtered and washed thoroughly with Milli-Q water to remove the unbound APTES. EPD technique was employed for the deposition of functionalized WO_3 NRs (APTES/WO_3 NRs) onto ITO glass substrate. Before deposition, a highly dispersed colloidal suspension of functionalized WO_3 NRs (1 mg/mL) was prepared in acetonitrile via ultrasonication. An optimized DC potential (48 V) for 120 s was considered for the deposition of the APTES/WO_3 NRs film onto the hydrolyzed ITO electrode using a two-electrode system, where a hydrolyzed ITO and platinum wire were taken as an anode and a cathode, respectively. Finally, the as-prepared electrode (APTES/WO_3NRs/ITO) was washed with Milli-Q water and kept in a covered Petri dish for further modifications.

Fabrication of immunosensor

For immobilization of anti-cTnI, 20 µL of anti-cTnI solution (see supplementary sheet) was uniformly spread on the surface of the APTES/WO_3 NRs/ITO electrode by drop casting. The prepared electrode was kept in a humid chamber at room temperature for 6–7 h. The $-NH_2$ groups of APTES molecules can be covalently bound with –COOH groups of anti-cTnI that were activated using EDC and NHS chemistry, resulting in the formation of a strong amide bond (OC–NH). Last, EA (0.01 M) was used for blocking the all nonspecific active sites of the fabricated electrode. The resulting EA/anti-cTnI/APTES/WO_3 NRs/ITO immunosensor was kept at 5 °C when not in use. A stepwise fabrication of immunosensor and immobilization of antibodies on the surface of APTES/WO_3 NRs/ITO electrode is shown in Scheme 1.

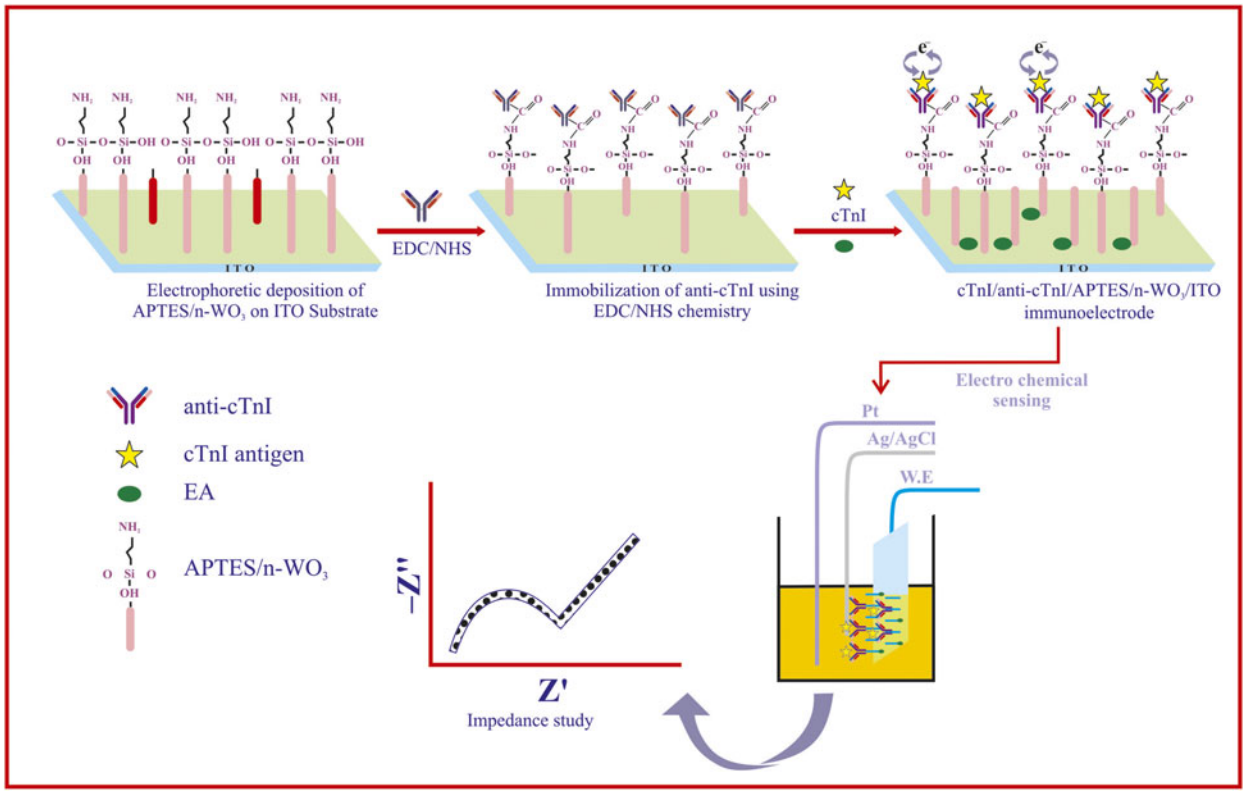

Scheme 1: Schematic representation of fabrication of immunoelectrode for electrochemical biosensing.

References

1. **P.R. Solanki, A. Kaushik, V.V. Agrawal, and B.D. Malhotra**: Nanostructured metal oxide-based biosensors. *NPG Asia Mater.* **3**, 17 (2011).
2. **A. Walcarius, S.D. Minteer, J. Wang, Y. Lin, and A. Merkoçi**: Nanomaterials for bio-functionalized electrodes: Recent trends. *J. Mater. Chem. B* **1**, 4878 (2013).
3. **F. Wang, L. Song, H. Zhang, L. Luo, D. Wang, and J. Tang**: One-dimensional metal-oxide nanostructures for solar photocatalytic water-splitting. *J. Electron. Mater.* **46**, 4716 (2017).
4. **X. Fang, L. Hu, C. Ye, and L. Zhang**: One-dimensional inorganic semiconductor nanostructures: A new carrier for nanosensors. *Pure Appl. Chem.* **82**, 2185 (2010).
5. **P.R. Solanki, J. Singh, B. Rupavali, S. Tiwari, and B.D. Malhotra**: Bismuth oxide nanorods based immunosensor for mycotoxin detection. *Mater. Sci. Eng., C* **70**, 564 (2017).
6. **P. Galvin, N. Padmanathan, K.M. Razeeb, J.F. Rohan, L.C. Nagle, A. Wahl, E. Moore, W. Messina, K. Twomey, and V. Ogurtsov**: Nanoenabling electrochemical sensors for life sciences applications. *J. Mater. Res.* **32**, 2883 (2017).
7. **S. Augustine, A.G. Joshi, B.K. Yadav, A. Mehta, P. Kumar, V. Renugopalakrishanan, and B.D. Malhotra**: An emerging nanostructured molybdenum trioxide-based biocompatible sensor platform for breast cancer biomarker detection. *MRS Commun.* **8**, 668 (2018).
8. **Y. Zhao, X. Yan, Z. Kang, X. Fang, X. Zheng, L. Zhao, H. Du, and Y. Zhang**: Zinc oxide nanowires-based electrochemical biosensor for L-lactic acid amperometric detection. *J. Nanopart. Res.* **16**, 2398 (2014).
9. **C. Yan, W. Kang, J. Wang, M. Cui, X. Wang, C.Y. Foo, K.J. Chee, and P.S. Lee**: Stretchable and wearable electrochromic devices. *ACS Nano* **8**, 316 (2013).
10. **I.M. Szilágyi, B. Fórizs, O. Rosseler, Á. Szegedi, P. Németh, P. Király, G. Tárkányi, B. Vajna, K. Varga-Josepovits, and K. László**: WO_3 photocatalysts: Influence of structure and composition. *J. Catal.* **294**, 119 (2012).
11. **D. Sandil, S. Kumar, K. Arora, S. Srivastava, B. Malhotra, S. Sharma, and N.K. Puri**: Biofunctionalized nanostructured tungsten trioxide based sensor for cardiac biomarker detection. *Mater. Lett.* **186**, 202 (2017).
12. **H. Zheng, Y. Tachibana, and K. Kalantar-zadeh**: Dye-sensitized solar cells based on WO_3. *Langmuir* **26**, 19148 (2010).
13. **J. Shi, G. Hu, Y. Sun, M. Geng, J. Wu, Y. Liu, M. Ge, J. Tao, M. Cao, and N. Dai**: WO_3 nanocrystals: Synthesis and application in highly sensitive detection of acetone. *Sens. Actuators, B* **156**, 820 (2011).
14. **L. Santos, C.M. Silveira, E. Elangovan, J.P. Neto, D. Nunes, L. Pereira, R. Martins, J. Viegas, J.J. Moura, and S. Todorovic**: Synthesis of WO_3 nanoparticles for biosensing applications. *Sens. Actuators, B* **223**, 186 (2016).
15. **Z-X. Cai, H-Y. Li, J-C. Ding, and X. Guo**: Hierarchical flowerlike WO_3 nanostructures assembled by porous nanoflakes for enhanced NO gas sensing. *Sens. Actuators, B* **246**, 225 (2017).
16. **Y. Zhou, L. Yang, S. Li, and Y. Dang**: A novel electrochemical sensor for highly sensitive detection of bisphenol A based on the hydrothermal synthesized Na-doped WO_3 nanorods. *Sens. Actuators, B* **245**, 238 (2017).
17. **J. Liu, O. Margeat, W. Dachraoui, X. Liu, M. Fahlman, and J. Ackermann**: Gram-scale synthesis of ultrathin tungsten oxide nanowires and their aspect ratio-dependent photocatalytic activity. *Adv. Funct. Mater.* **24**, 6029 (2014).
18. **J. Ali, J. Najeeb, M.A. Ali, M.F. Aslam, and A. Raza**: Biosensors: Their fundamentals, designs, types and most recent impactful applications: A review. *J. Biosens. Bioelectron.* **8**, 1 (2017).
19. **S. Ko, B. Kim, S-S. Jo, S.Y. Oh, and J-K. Park**: Electrochemical detection of cardiac troponin I using a microchip with the surface-functionalized poly(dimethylsiloxane) channel. *Biosens. Bioelectron.* **23**, 51 (2007).
20. **M.D. Prakash, S. Singh, C. Sharma, and V.S.R. Krishna**: Electrochemical detection of cardiac biomarkers utilizing electrospun multiwalled carbon nanotubes embedded SU-8 nanofibers. *Electroanalysis* **29**, 380 (2017).
21. **N.J. Ronkainen, H.B. Halsall, and W.R. Heineman**: Electrochemical biosensors. *Chem. Soc. Rev.* **39**, 1747 (2010).
22. **B.D. Malhotra, S. Srivastava, M.A. Ali, and C. Singh**: Nanomaterial-based biosensors for food toxin detection. *Appl. Biochem. Biotechnol.* **174**, 880 (2014).
23. **A. Qureshi, Y. Gurbuz, and J.H. Niazi**: Biosensors for cardiac biomarkers detection: A review. *Sens. Actuators, B* **171**, 62 (2012).
24. **X. Han, S. Li, Z. Peng, A.M. Othman, and R. Leblanc**: Recent development of cardiac troponin I detection. *ACS Sens.* **1**, 106 (2016).
25. **T. Keller, T. Zeller, D. Peetz, S. Tzikas, A. Roth, E. Czyz, C. Bickel, S. Baldus, A. Warnholtz, and M. Fröhlich**: Sensitive troponin I assay in early diagnosis of acute myocardial infarction. *N. Engl. J. Med.* **361**, 868 (2009).
26. **S. Kumar, S. Kumar, S. Augustine, and B.D. Malhotra**: Protein functionalized nanostructured zirconia based electrochemical immunosensor for cardiac troponin I detection. *J. Mater. Res.* **32**, 2966 (2017).
27. **W. Zhao, B. Cui, H. Qiu, P. Chen, and Y. Wang**: Multifunctional Fe_3O_4@WO_3@mSiO_2–APTES nanocarrier for targeted drug delivery and controllable release with microwave irradiation triggered by WO_3. *Mater. Lett.* **169**, 185 (2016).
28. **M. Tong, G. Dai, Y. Wu, X. He, and D. Gao**: WO_3 thin film prepared by PECVD technique and its gas sensing properties to NO_2. *J. Mater. Sci.* **36**, 2535 (2001).
29. **D. Sandil, S. Srivastava, B. Malhotra, S. Sharma, and N.K. Puri**: Biofunctionalized tungsten trioxide-reduced graphene oxide nanocomposites for sensitive electrochemical immunosensing of cardiac biomarker. *J. Alloys Compd.* **763**, 102–110 (2018).

30. **N. Majoul, S. Aouida, and B. Bessaïs**: Progress of porous silicon APTES-functionalization by FTIR investigations. *Appl. Surf. Sci.* **331**, 388 (2015).
31. **M. Ata, Y. Liu, and I. Zhitomirsky**: A review of new methods of surface chemical modification, dispersion and electrophoretic deposition of metal oxide particles. *RSC Adv.* **4**, 22716 (2014).
32. **S. Srivastava, S. Abraham, C. Singh, M.A. Ali, A. Srivastava, G. Sumana, and B.D. Malhotra**: Protein conjugated carboxylated gold@reduced graphene oxide for aflatoxin B_1 detection. *RSC Adv.* **5**, 5406 (2015).
33. **S. Kumar, S. Kumar, S. Tiwari, S. Augustine, S. Srivastava, B.K. Yadav, and B.D. Malhotra**: Highly sensitive protein functionalized nanostructured hafnium oxide based biosensing platform for non-invasive oral cancer detection. *Sens. Actuators, B* **235**, 1 (2016).
34. **M. Fathil, M.M. Arshad, A. Ruslinda, S.C. Gopinath, R. Adzhri, U. Hashim, and H. Lam**: Substrate-gate coupling in ZnO-FET biosensor for cardiac troponin I detection. *Sens. Actuators, B* **242**, 1142 (2017).
35. **M. Negahdary, M. Behjati-Ardakani, N. Sattarahmady, H. Yadegari, and H. Heli**: Electrochemical aptasensing of human cardiac troponin I based on an array of gold nanodumbbells—Applied to early detection of myocardial infarction. *Sens. Actuators, B* **252**, 62 (2017).
36. **A. Periyakaruppan, R.P. Gandhiraman, M. Meyyappan, and J.E. Koehne**: Label-free detection of cardiac troponin-I using carbon nanofiber based nanoelectrode arrays. *Anal. Chem.* **85**, 3858 (2013).